A POPULATION-GUIDED APPROACH TO IDENTIFY GENETIC MODULATORS OF TCDD-ELICITED TOXICITY

By

Peter William Dornbos

A DISSERTATION

Submitted to
Michigan State University
in partial fulfillment of the requirements
for the degree of

Biochemistry and Molecular Biology – Environmental Toxicology – Doctor of Philosophy

2018

ABSTRACT

A POPULATION-GUIDED APPROACH TO IDENTIFY GENETIC MODULATORS OF TCDD-ELICITED TOXICITY

By

Peter William Dornbos

Traditional toxicological studies have not incorporated genetic variability, but rather have focused on homogenous models, such as inbred mouse strains. The lack of incorporation of genetic heterogeneity provides a challenge in defining safe-exposure limits that encompass all individuals within the population. The goal of this dissertation was to use a population-based approach to characterize the impact of genetic heterogeneity within TCDD-induced toxicity. TCDD is a pervasive and persistent environmental contaminant that is associated with a plethora of adverse health effects in humans. TCDD-elicited toxicity is mediated through activation of a ligand-activated transcription factor called the aryl hydrocarbon receptor (AHR). While the *Ahr* gene sequence inherited is known to impact TCDD-induced toxicity, we hypothesize that other genomic factors will impact susceptibility to TCDD-elicited toxicity. To test this hypothesis, a mixture of *in vitro* and *in vivo*-based methods were employed to quantify the variability in response across heterogeneous individuals and to identify genetic modulators of TCDD-induced immunosuppression and alterations in liver homeostasis.

First, an *in vitro*-based approach was used to identify the inherent variability in the human population to TCDD-elicited suppression of B cells. The results showed that there was a wide range of response (>70-fold) at high doses of TCDD. B cells were isolated from a genetically-diverse mouse panel and exposed to TCDD to scan for genetic modulators that may explain the wide-degree of variability across human individuals. Our study implicated *Serpinb2*, which encodes for serine peptidase inhibitor, clade B, member 2, as a modulator of TCDD-elicited suppression of the B cell. Further downstream functional analysis identified that *Serpinb2* plays a protective role against TCDD-elicited suppression of the B cell in mice.

Secondly, an *in vivo* mouse population-based approach was used to scan for genetic modulators of TCDD-elicited alterations in liver homeostasis. Hepatic sequestration of TCDD was found to be dependent on AHR-mediated transcription. Inter-strain differences in expression of AHR-responsive genes implicated *Tgfbr2,* which encodes for transforming growth factor β receptor II (TGFBR2), as a potential modulator of TCDD-elicited liver toxicity. Functional analyses suggested that TGFBR2-activity protects against TCDD-elicited inflammation, but increases hepatic lipid accumulation in the livers of male, but not female, mice.

Finally, TCDD-elicited change in body weight across our mouse panel implicated *Hmgcr*, which encodes the rate-limiting enzyme of cholesterol biosynthesis called HMG-CoA reductase (HMGCR). While reports indicate that TCDD-impacts cholesterol homeostasis in rodents, the phenotype has not been demonstrated in the human population. Multiple linear regression analysis using data derived from the National Health and Nutrition Examination Survey (NHANES) suggests that, like in previous rodent studies, serum TCDD levels are also associated with cholesterol levels in humans in a sex-specific manner. Further functional mouse analyses suggest that HMGCR is a modulator of TCDD-elicited liver phenotypes. More specifically, inhibition of HMGCR was found to protect against AHR-mediated steatosis in both sexes, but increase TCDD-elicited liver injury in males and alters glycogen metabolism in females.

The results outlined in this dissertation indicate the power in using population-based models in characterizing the degree of variability and identifying modulating genes within adverse responses to chemical exposures, such as TCDD. We hope that our data will impact real-world risk assessment in ensuring that safe-exposure guidelines for TCDD reflect population-wide variability. While many of the findings outlined still need confirmation in the human population, our results may be used to identify individuals within the human population that may be more susceptible to TCDD-induced toxicity which, ultimately, has potential to impact public health.

ACKNOWLEDGEMENTS

There are many people that have helped make this dissertation research possible. First, I would like to thank my PhD mentor John LaPres. John is a fantastic and patient mentor that has pushed me to develop new and better skills throughout my time in his lab. John has truly shown that science is more than just a career, but a way of life. John's optimistic outlook on the sciences has made my time and research in his lab truly enjoyable. One of the many highlights was John's willingness to listen to many good and bad proposals for future projects and experiments. These conversations have not only helped me learn about cutting-edge technologies and the process of thoroughly testing a hypothesis, but have helped me (and many others) develop as a scientist. Beyond the lab, John is also always happy to talk about other aspects of his student's lives and does not hesitate to share quality advice on a diverse-set of subjects. As I am looking forward to potentially starting a career in academia, John has set the bar high as to who and what a graduate-student mentor should be. While all good things eventually come to an end, I can honestly say I thoroughly enjoyed my time in his lab and under his quality mentorship.

I also would like to thank the many other members of the LaPres lab during my time at MSU. I would like to thank Steve Proper and HyeJin Hwang who helped train me on a diverse-set of subjects. I would like to thank Michelle Steidemann for all of her advice (especially with western blotting) and her willingness to listen to my many practice talks. I would like to acknowledge Amanda Jurgelewicz who helped me collect a good portion of data which was used in Chapter 5 of my dissertation. I would also like extend a thank you to my many undergraduate students who have come and gone during my time in the LaPres lab; I hope my training helped them develop a greater love for biology and biochemistry. I would like to say a special thank you to David Nava and James Hosner who extracted RNA from a large number of mouse samples during the NanoString gene expression profiling which was included in Chapter 4. Also, I would

like to acknowledge Anooj Aniruddha for his help in developing a graphical user interface for 'IMPUTER,' an automated software program that predicts amino acid sequences based on polymorphism data which we hope to publish in the near future.

I need to extend a huge thank you to Melanie Warren and Dr. David Threadgill for their work dosing mice and providing samples for the mouse B cell and *in vivo* mouse panel projects. I would like thank Dr. Kelly Fader and Dr. Rance Nault of the Zacharewski lab who have not only trained me on many techniques, but also have helped plan and dedicate time to several extensive *in vivo* mouse experiments. I would like to thank the other members of the Zacharewski lab, such as Russell Fling and Claire Doskey, who have helped with long and tedious mouse necropsy days. I would like to give a special thank you to Bob Crawford of the Kaminski lab for his willingness to share reagents with little notice, advice in troubleshooting assays that weren't working, and for his extensive help with FLOW cytometry analysis during the mouse B cell work. I would also like to thank the other members of the Kaminski lab, such as Brian Zhou, Mike Rizzo, and Dr. Joe Henriquez, that have helped in many ways.

I would like thank my thesis committee: 1) Dr. Tim Zacharewski, 2) Dr. Norbert Kaminski, 3) Dr. Bill Henry, and 4) Dr. George Mias. I appreciate their willingness to serve as a member of my committee as I know they have busy schedules. I appreciate all of the thoughtful-feedback which has helped in many ways over my time as PhD student. I want to thank them for taking the time and effort over the past five or so years to read my research updates and listen to my presentations.

Finally, I would like to thank my family. My parents, siblings, and in-laws have always been supportive of my career path, listened to practice talks, double-checked resumes/CVs, and have asked questions and taken interest in my research which I truly appreciate. Foremost, I would like

thank my beautiful wife Darcy who has always been by my side through the ups and, unfortunately, the downs of graduate school that come all too often. She has been incredibly patient throughout my time in graduate school. She has dealt with the '5 minute' trips to the lab which always seem to be longer than an hour, listened to an untold number of horrible and unpolished practice talks, and has always brought optimism to my sometimes pessimistic outlook when results did not bring what I had hoped. Never once has she complained, but rather is always up-lifting and pushes me to be a better scientist and to be a better person in and out of the lab. I could not have accomplished this without her help and support. Finally, I would like to thank my personal fan club, Elyse and Evelyn, who are our two beautiful daughters that were born during my time at MSU. Not only do they mean the world to me, but also have helped keep the importance of things in perspective. I hope that, as they grow older, they will be proud of me and my future endeavors. I know I will always be proud of them.

TABLE OF CONTENTS

LIST OF TABLES

LIST OF FIGURES

KEY TO ABBREVIATIONS

2,4,5-T	2,4,5-trichlorophenoxyacetic acid
A	Alanine
ADI	Acceptable Daily Intake
ADIPOR1	Adiponectin receptor 1
AHR	Aryl hydrocarbon Receptor
AHRR	Aryl hydrocarbon receptor repressor
AIC	Akaike Information Criteria
AIP/ARA9	AHR-interacting protein
ALT	Alanine aminotransferase
ALT	Alanine Aminotransferase
ANOVA	Analysis of Variance
ARNT	Aryl hydrocarbon receptor nuclear translocator
BCR	B cell receptor
BH	Beta-Hydroxybutyrate
bHLH	Basic helix-loop-helix
BMCL	Lower-bound confidence interval in the concentration-response
BMD	Benchmark Dose
BMI	Body Mass Index
CC	Collaborative Cross Mouse Population
CCL2	Chemokine (C-C motif) ligand 2
CCS	HyClone Cosmic Calf Serum
CD	Cluster of Differentiation
CD40	CD40 Ligand

CDKN1A	Cyclin-dependent kinase inhibitor 1
CE	Cholesterol Ester
CI	Confidence Intervals
CO_2	Carbon Dioxide
CYP	Cytochrome P450-dependent monoxygenase
DMEM	Dulbecco's modified Eagle's Medium
DMSO	Dimethyl Sulfoxide
DO	Diversity Outbred Mouse Population
DRE	Dioxin Response Element
DRR	Dose Response Relationship
EC_{10}	Concentration that results in 10% of an effect
ECL	enhanced chemiluminescence
EDTA	Ethylenediamine tetraacetic acid
ELISA	Enzyme-Linked Immunosorbant Assay
ELISPOT	Enzyme-Linked ImmunoSpot Assay
ENTK2	Ethanolamine kinase 2
EPA	U.S. Environmental Protection Agency
FFA	Free Fatty Acids
GC/MS	Gas chromatography-mass spectrometry
GPNMB	Transmembrane glycoprotein neuromedin-B
GYS2	Glycogen Synthase 2
H&E	Hematoxylin and eosin
h^2	Heritability
HBSS	Hank's Balanced Salt Solution
HDL	High-Density Lipoprotein
HEPES	2-[4-(2-hydroxyethyl)piperazin-1-yl] ethanesulfonic acid

HMGCR	3-hydroxyl-3-methylglutaryl (HMG)-CoA reductase
HSP90	Heat shock protein of 90 kDa
I	Isoleucine
IC_{50}	Concentration that results in 50% inhibition
IgG	Immunoglobulin isotype g
IgM	Immunoglobulin isotype m
IL	Interleukin
Indel	Insertion/Deletion
IP	Intraperitoneal
IVIVE	*in vitro*-to-*in vivo* extrapolation
K	Lysine
Kd	Dissociation Constant
kDA	Kilodaltons
KISS1	Metastasis-suppressor 1
KO	Knockout
LA-TCDD	Lipid-adjusted TCDD
LCL	Lymphoblastoid cell line
LCS	Lab control spike
MB	Method blank
LD_{50}	Dose with 50% lethality
LDL	Low-Density Lipoprotein
LOD	Logs of Difference
MACS	Magnetic-activated cell sorting
MAGWAS	Multivariate genome-wide association analysis
Mb	Megabase
MFI	Mean Fluorescence Intensity

MN	Micronucleus
MT2	Metallothionein 2
NAFLD	Non-alcoholic fatty liver disease
NFKB	Nuclear factor-kappa B
NHANES	National Health and Nutrition Examination Survey
NLW	Normalized Liver Weight
NRC	National Research Council
NTP	National Toxicology Program
ORO	Oil Red O
PAI2	Plasminogen activator inhibitor-2
PAS	Per-Arnt-Sim
PAH	polycyclic aromatic hydrocarbon
PAS	Periodic Acid-Schiff Stain
PB	Peripheral blood
PBMC	Peripheral blood mononuclear cells
PBPK	Physiologically-based pharmacokinetic model
PBS	phosphate buffered saline
PBST	Phosphate-buffered saline with 0.1% Tween-20
PCR	Polymerase Chain Reaction
PMM1	Phosphomannomutase 1
PN	post-natal day
PPARA	Peroxisome proliferator-activated receptor alpha
ppt	Part-per-trillion
PYGL	Glycogen Phosphorylase
QTL	Quantitative Trait Locus
QuHAnT	Quantitative Histological Analysis Tool

R	Arginine
RB1	Retinoblastoma protein
RET	Bone marrow
RfD	Reference Dose
RIPA	Radioimmunoprecipitation assay
RPMI	Roswell Park Memorial Institute Medium
S+T	Simvastatin and TCDD Co-Treatment
SDS-PAGE	sodium dodecyl sulfate-polyacrylamide gel electrophoresis
SERPINB2	Serine peptidase inhibitor, clade B, member 2
SLC	Solute Carrier Transporter
SNP	Single Nucleotide Polymorphism
T1	Tertile 1
T2	Tertile 2
T3	Tertile 3
TAD	Transactivation Domain
TBST	Tris-Buffered Saline with 0.05% tween-20
TC	Total Cholesterol
TCA	Trichloroacetic acid
TCDD	2,3,7,8-tetrachlorodibenzo-*p*-dioxin
TCE	Trichloroethylene
TGFB1	Transforming growth factor-beta 1
TGFB2	Transforming growth factor-beta 2
TGFB3	Transforming growth factor-beta 3
TGFBR2	Transforming growth factor-beta receptor, type
TLW	Total Liver Weight
TNF	Tumor necrosis factor

UTR	Untranslated Region
V	Valine
VF_d	Toxicodynamic uncertainty factor
VLDL	Very Low-Density Lipoprotein
µm	micrometer

Chapter 1: Introduction

This chapter contains a portion of a previously published research article in *Toxicology*, Volume 395, pages 1-8 entitled “Incorporating Population-level Genetic Variability within Laboratory Models in Toxicology: From the Individual to the Population.”

Authors: Peter Dornbos[1,2] and John J. LaPres[1,2,3]

Affiliations: [1]Department of Biochemistry and Molecular Biology, [2]Institute for Integrative Toxicology; [3]Center for Mitochondrial Science and Medicine, Michigan State University, East Lansing, Michigan, USA.

1.1. 2,3,7,8-tetrachlordibenzo-p-dioxin (TCDD) Exposure in Humans

2,3,7,8-tetrachlorodibenzo-*p*-dioxin (TCDD) is a pervasive contaminant of environmental concern. With exception of small volumes that are synthesized for academic research, TCDD is primarily created as a byproduct of industrial processes (Gilpin et al. 2003). TCDD is most well-known as a contaminant created during the synthesis of an herbicide called 2,4,5-trichlorophenoxyacetic acid (2,4,5-T or Agent Orange) which was used during the Vietnam war. Other industrial processes that result in TCDD creation include manufacturing of herbicides and pesticides, waste incineration, and chlorine bleaching of paper and pulp. Beyond industrial processes, TCDD is also created during natural processes such as volcanic eruptions and forest fires (Srogi 2008). Once in the environment, TCDD is quite persistent and resistant to degradation in soil. The half life of TCDD is estimated to be between 9 and 15 years for surface soil and up to 100 years for sub-surface soil (Kimbrough et al. 1984; Paustenbach et al. 1992).

TCDD is lipophilic and, thus, can accumulate within the food chain (Gilpin et al. 2003; Jackson et al. 1993). The primary mode of exposure within the general human population is through consumption of high lipid-containing foods, such as fish and dairy products (Gilpin et al. 2003). Typically, background exposures within the human population are low with lipid-adjusted TCDD levels of 1 to 10 ppt in serum (Nault et al. 2016). It must be noted that, while day-to-day exposures are typically low, TCDD bioaccumulates in organisms. As such, the level of TCDD is highly-correlated with age (Chen et al. 2010; Chen et al. 2013). There also have been several unfortunate cases where humans were exposed to TCDD at high-levels. The most famous of these was through use of Agent Orange during the Vietnam war. There have also been other several documented cases of accidental, heavy exposures that have occurred in the human sub-populations including an industrial accident in Seveso, Italy (Cole et al. 2003; Warner et al. 2013) and industrial workers exposed to chemical byproducts. The most unique case of TCDD exposure was the purposeful poisoning of Victor Yushchenko while a presidential-candidate in Ukraine in

2004 (Sorg et al. 2009). Once exposed, the half-life of TCDD has been found to be quite long in humans. Previous reports indicate that elevated levels of TCDD can be found in adipose tissue of humans after over 30 years post-exposure (Schecter and Ryan 1988). In a study of human individuals that were exposed to TCDD, the average half-life of TCDD in the serum of humans (n=36) was found to be 7.1 years (Pirkle et al. 1989).

There is strong epidemiological evidence that TCDD exposures drive adverse health outcomes in humans. The most notable of these is chloracne. TCDD-induced chloracne has been established in multiple exposures, including those exposed in Seveso, in industrial settings, and in the poisoning of Victor Yushchenko (Baccarelli et al. 2002; Kerger et al. 2006; McKee 2009; Sorg et al. 2009). TCDD is also known to induce immune suppression. Previous exposures indicate that sub-populations exposed to high-levels of TCDD have lower-levels of Immunoglobulin G (IgG) in the blood (Baccarelli et al. 2002). Furthermore, *in vitro* work has established that human immune cells are clearly impacted by TCDD (Lu et al. 2010; Lu et al. 2011). Exposures to TCDD and other dioxin-like compounds are known to be associated with increased incidence of metabolic disorders including nonalcoholic fatty-liver disease (NAFLD), diabetes, and metabolic syndrome (Cave et al. 2010; Lee et al. 2007; Taylor et al. 2013). TCDD is also associated with several cancers in humans, including Non-Hodgkins Lymphoma, renal, prostate, testicular, and bladder cancers (Chang et al. 2017; Leng et al. 2014; O'Brien et al. 1991). This association, however, has been somewhat debated as the cancer risk in highly-exposed populations have not been found to much higher than other populations (Boffetta et al. 2011; Cole et al. 2003).

1.2. The Aryl Hydrocarbon Receptor as Mediator of TCDD-induced Toxicity

Most, if not all, of TCDD-mediated toxicity is through activation of the aryl hydrocarbon receptor (AHR). *Ahr* null mouse models indicate that TCDD-mediated toxicity, such as immune

suppression and liver toxicity, is dependent on the AHR (Fernandez-Salguero et al. 1995; Thurmond et al. 1999). The AHR is a transcription factor that falls within the Per-Arnt-Sim (PAS) domain family of environmental sensors. PAS proteins regulate responses to many environmental changes within the cell including hypoxia, xenobiotic exposure, and the light/dark cycles (McIntosh et al. 2010). While there are many differences across the PAS domain protein family in higher-eukaryotes, there are several domains that are consistently found across all PAS members (Gu et al. 2000)(Figure 1.1). In higher organisms, the most unique feature carried by PAS proteins is the PAS domain, consisting of PAS A and PAS B. The PAS A domain mediates homotypic interactions between PAS domain-containing proteins. In comparison to PAS A, the PAS B domain is much more-versatile providing heterotypic interactions between non-PAS containing protein classes as well as natural and non-natural ligands. Most PAS domain proteins also contain a basic helix-loop-helix (bHLH) domain which, as compared to the PAS domains, are located on the N-terminus of the protein (Gu et al. 2000). The bHLH domain mediates dimerization and DNA binding. Finally, PAS domain proteins also contain a transcriptional activation domain (TAD) which, as compared to PAS domains, is located towards the C-terminus and is involved in recruitment and interactions with other transcriptional co-activators. Unlike the PAS and bHLH domains, the TAD has less sequence homology and, thus, has been lesser-conserved across evolution in the PAS family.

The AHR is ligand activated and its prototypical ligand is TCDD. Interestingly enough, the AHR has been strongly conserved through evolution suggesting an endogenous role beyond a xenobiotic response (Hahn 2002). *Ahr* orthologs can be found in species that likely existed millions of years prior to the evolution of the first vertebrate (Hahn 2002). For example, orthologs of the *Ahr* are present in invertebrate species including roundworms (*C. elegens*) and flies (*D. melanogaster*)(Duncan et al. 1998; Powell-Coffman et al. 1998). *Ahr* orthologs have also been

Figure 1.1. General organization of the aryl hydrocarbon receptor. The figure outlines the general positioning and several known functions of four conserved domains found on the AHR (bHLH, PAS-A, PAS-B, and TAD). This figure is an adapted version of Figure 5 from Okey, 2007 (Okey 2007).

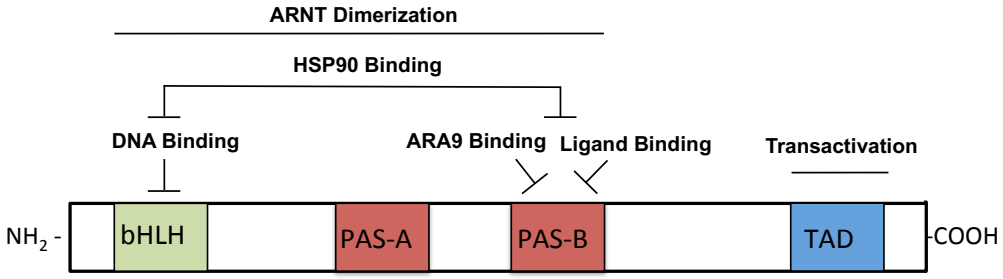

found in several mollusc species, such as the soft shell clam (*M. arenaria*), zebra mussel (*D. polymorpha*), and blue mussel (*M. edulis*)(Butler et al. 2001; Hahn 2002).

For decades, endogenous ligands of the AHR remained elusive. Several studies in the late 1990's and early 2000's identified a diverse set of probable AHR ligands. Such ligands include indoles which are tryptophan break-down products, bilirubin and other tetrapyroles which are likely products of heme break-down, and metabolites of arachidonic acid such as prostaglandins (Bittinger et al. 2003; Denison and Nagy 2003; Rannug and Fritsche 2006; Sinal and Bend 1997). While the ligands are diverse, the AHR clearly plays important roles in several physiological processes beyond the xenobiotic response including hematopoiesis as well as liver and T cell development (Bunger et al. 2008; Gasiewicz et al. 2010; Lahvis et al. 2005; Quintana et al. 2008). The AHR has also been recently found to play a key role within the immune system (Moura-Alves et al. 2014).

The AHR-mediated transcription pathway has been-well characterized (Figure 1.2.). Prior to activation, the majority of the AHR pool is found in the cytoplasm bound to several chaperone proteins including a heat-shock protein 90 (HSP90) homodimer and AH receptor-associated protein (ARA9)(Carver et al. 1998; Heid et al. 2000; Meyer and Perdew 1999). The chaperones have been found to stabilize AHR prior to activation (Petrulis and Perdew 2002). Upon ligation, the AHR separates from chaperones and translocates to the nucleus. Once in the nucleus, the AHR dimerizes with the aryl hydrocarbon receptor nuclear translocator (ARNT) to form a functional transcription factor (Abel and Haarmann-Stemmann 2010; Sorg 2014). The AHR:ARNT complex binds to dioxin response elements (DREs) that are located throughout the genome (Swanson et al. 1995). In the late 1980's, the DREs in the *Cyp1a1* promoter were found to contain the core sequence of 5'-GCGTG-3' with more-variable flanking regions (Denison et al. 1988a, b). Genomic-wide searches and AHR chromatin immunoprecipitation approaches in mouse liver later

identified the presence of DREs located throughout the genome (Dere et al. 2011). Gene expression arrays using both *in vitro* and *in vivo* models later identified that activation of AHR results in aberrant gene expression of many genes which drives the adverse responses to TCDD (Boverhof et al. 2005; Boverhof et al. 2006; Martinez et al. 2002; Puga et al. 2000). Mice carrying mutated-AHR that are unable to translocate to the nucleus are resistant to TCDD-mediated toxicity (Bunger et al. 2003). While technologies are constantly improving to analyze which genes are dysregulated at differing points of time post-exposure, much remains unknown regarding how AHR-mediated aberrant expression leads to the complex diseases associated with TCDD exposures in humans.

1.3. Susceptibility to TCDD-Mediated Toxicity

Differing species have vastly-different sensitivity to TCDD-mediated toxicity with nearly 600-fold differences in the LD_{50} values (Geyer et al. 1990). Guinea pigs have been found to be the most sensitive of mammals that have been exposed to TCDD with an estimated LD_{50} values of ≤ 2 μg TCDD per kg of body weight (μg/kg). Hamsters are on the other side of the spectrum with an estimated LD_{50} values of ≥ 1,157 μg/kg. For reference, non-human primates, such as the rhesus macaque, have an estimated LD_{50} value of 50 μg/kg suggesting that humans, in comparison to some species, are quite sensitive to TCDD-induced toxicity. Beyond the intra-species differences in susceptibility, previous studies with rodents have shown that there are also clear inter-species differences (Chapman and Schiller 1985). For example, C57BL/6J mice that were treated with TCDD for 10-12 weeks had an estimated LD_{50} value of 182 μg/kg. In the same study, however, DBA/2J mice had estimated LD_{50} value of 2,570 μg/kg. As such, there are ≥ 14 fold differences in the estimated LD_{50} values for differing strains of the same species.

Figure 1.2. The aryl hydrocarbon receptor-mediated transcription pathway. The AHR resides in the cytoplasm bound to several chaperone proteins prior to activation. Once activated by a ligand, such as TCDD, the AHR disassociates from the chaperone proteins and translocates to the nucleus. Once in the nucleus, the AHR dimerizes with another PAS protein called the aryl hydrocarbon receptor nuclear translocator (ARNT). The hetereodimer, then, binds to dioxin response elements (DREs) throughout the genome altering gene transcription.

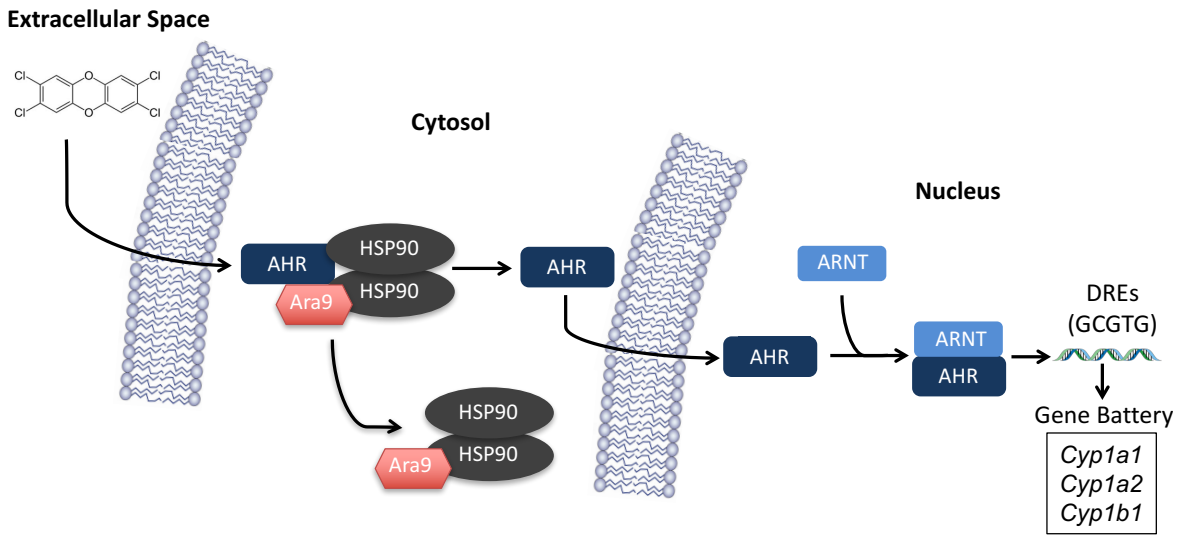

The mouse has been used for decades for toxicological screens. One obvious advantage of the use of rodents is that the vast majority of environmental factors can be controlled. As such, most of the inter-strain differences will be driven by genetic background. Over the past 30 years, the *Ahr* gene has been well-characterized in a large number of mouse strains (Figure 1.3). Previous reports have indicated that mice carry 1 of 4 independent alleles of the *Ahr* which are structurally and functionally unique: 1) Ahr^{b1}, 2) Ahr^{b2}, 3) Ahr^{b3}, and 4) the Ahr^{d} (Poland and Glover 1990; Poland et al. 1994; Thomas et al. 2002). Several nonsynonymous substitutions within the murine *Ahr* are of particular interest. The most influential SNP drives an A375V substitution in strains that carry the Ahr^{d} allele (Poland et al. 1994). Previous radioligand-binding studies have reported that the dissociation constant (Kd) of TCDD for the AHR carried by Ahr^{d} allele mice, such as the DBA/2J, is an estimated 16 nM as compared to 1.8 nM for Ahr^{b1} allele mice, such as the C57BL/6J (Okey et al. 1989; Poland et al. 1994). As such, strains that carry the Ahr^{d} allele are sometimes inaccurately referred to as 'non-responsive' to TCDD. Another SNP of interest induces a premature stop codon unique to the Ahr^{b1} allele which results in a protein that is 95 kilodalton (kDA) as compared to the 104 kDA protein encoded by the Ahr^{b2} and Ahr^{d} allele (Thomas et al. 2002). The Ahr^{b3} allele is only carried by wild-derived strains which tend to be more polymorphic as compared to classical inbred strains. While there is less *Ahr* sequence homology in the strains that carry the Ahr^{b3} allele, these strains carry an alanine at position 375 and, thus, have high affinities for TCDD that are similar to the protein encoded by the Ahr^{b2} allele.

Similar to the rodent models, there are established differences in human responses to TCDD exposures. For example, previous studies using isolated B cells have identified a sub-population of the humans that do not appear to respond TCDD-induced immunosuppression (Lu *et al*., 2010). Previous studies using human placental tissues have indicated that the AHR binding affinity for TCDD in humans can vary up to 10-fold with Kd's that range from ≤ 1 to ≥15 nM in extreme cases (Ema et al. 1994; Harper et al. 2002). Other studies have suggested interindividual

Figure 1.3. Comparison of the general aryl hydrocarbon receptor gene structure across mouse strains and human. Mice have been found to carry 4 independent alleles of the *Ahr*: 1) *Ahr*^{b1}, 2) *Ahr*^{b2}, 3) *Ahr*^{b3}, and 4) the *Ahr*^{d}. While the gene is highly-conserved, an A375V substitution indicated by the '*' in the PAS-B domain of protein encoded by the *Ahr*^{d} allele greatly decreases the affinity for TCDD. The AHR is heavily-conserved across species. While the human AHR is known to have a higher affinity for TCDD as compared to the *Ahr*^{d} allele. The human AHR contains a valine in position 381 which is equivalent to position 375 in the mouse AHR.

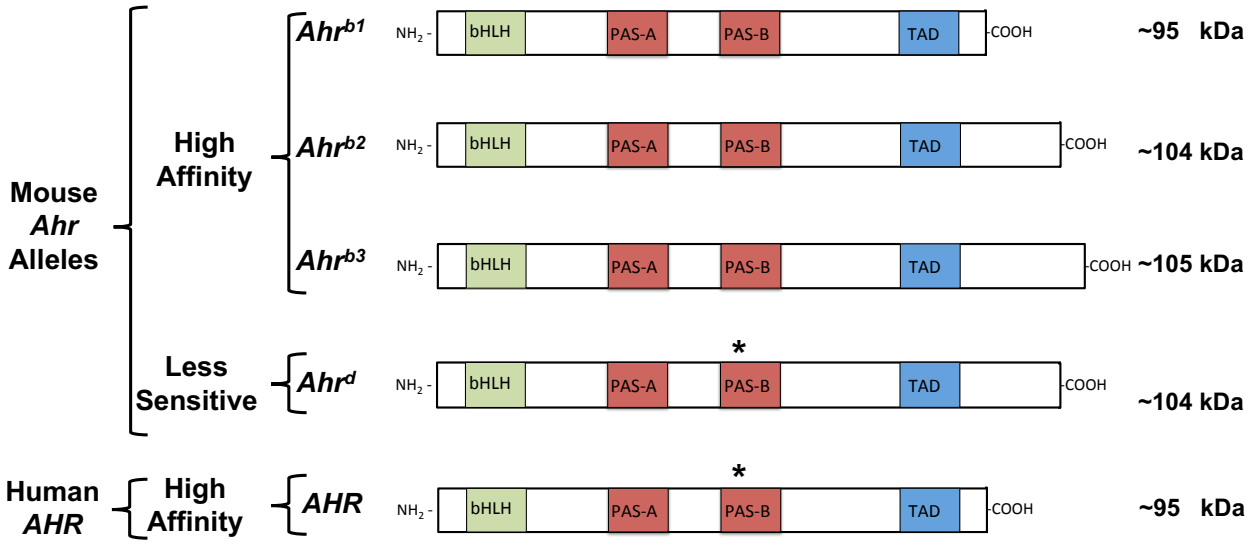

variability in response to another AHR ligands such as polycyclic aromatic hydrocarbons (PAHs)(Smart and Daly 2000) and identified a wide-range in half-life of TCDD in differing individuals (Pirkle et al. 1989). While the average half-life is 7.1 years, the 95% confidence intervals span from 5.8 to 9.6 years across 36 individuals. The variability in the degradation and excretion rate across individuals is likely dependent on many factors. For example, previous reports have established a positive correlation between BMI and increased half-life of TCDD in humans (Kerger et al. 2006). Rodent-based studies indicate that genetics likely plays a major role in driving the interindividual variability in the half-life of TCDD. The half-life of TCDD in mice is quite variable; ranges have been reported that span 11 to 24.4 days depending on the strain (Gasiewicz et al. 1983). Strains that are sensitive to TCDD-mediated toxicity, such as the C57BL/6J (i.e. *Ahr*^{b1} allele mice), were found to have shorter half-lives as compared to less-sensitive strains, such as the DBA/2J (i.e. *Ahr*^{d} allele mice).

Unlike differing mouse strains, polymorphisms in the *AHR* gene assert a modest impact on the human response to TCDD (Harper et al. 2002). There is no AHR sequence variability at position 381 in humans which is equivalent to murine position 375 where the high-impact variant is found. Interestingly enough, human AHRs carry a valine at this position which, as previously mentioned, is most similar to the less sensitive mouse strains (i.e. *Ahr*^{d} allele mice)(Ema et al. 1994). While the valine suggests the human AHR should have a higher Kd for TCDD, the vast majority of the individuals are found to have Kd's that range from 2 and 8 nM (Harper et al. 2002). While carrying the valine, human AHR appears to behave most similarly to the AHR encoded by the mouse *Ahr*^{b} alleles. The valine in position 381, however, was found to be important as a directed substitution to asparagine abolished TCDD binding for the human AHR (Ema et al. 1994). Other SNPs in the human *AHR* gene have been found to impact the response to TCDD. A previous study where AHR constructs with known human *AHR* SNPs were expressed in a liver

cell line indicated that a combined A554K and V570I substitution had less TCDD-induced expression of the AHR-target gene *CYP1A1 (Wong et al. 2001)*. Similarly, expression of constructs containing known human SNPS in a human B cell line indicated that a single R554K substitution can reduce the induction of *CYP1A1* and *CYP1B1* mRNA induction as well as CYP1B1-regulated reporter activity (Kovalova et al. 2016). The same study also showed that a construct containing a combination of SNPs that result in P517S, R554K, and V570I substitutions reduced the sensitivity to TCDD-mediated suppression of secretion of Immunoglobulin-M (IgM). Though several studies suggest that SNPs in the human *AHR* gene impact the response to TCDD, this variation is likely driving a modest impact on downstream TCDD-mediated responses (Okey 2007). Given the interindividual variability in response to TCDD, the modest effect of polymorphisms in the human *AHR* gene, and previous reports indicating that genetic variability can have profound impacts on individual's response to chemicals (Evans and Relling 2004; Kalow et al. 1998), we hypothesize that there are likely other genomic variation beyond the *AHR* sequence that likely impact an individual's response. Understanding of which genetic variants may increase individual's susceptibility to TCDD would have direct impacts on risk assessment in a diverse population.

1.4. Current State of Assessing Exposure Risk in Heterogeneous Populations

The goal of exposure-based risk assessment is to characterize the potential hazardous nature of a chemical within the heterogeneous human population. Knowledge of the dose-response relationship (DRR) between any given chemical, from pharmaceuticals to environmental contaminants, and an adverse physiological response is valuable to accurate risk assessment. Much of the exposure-to-response DRRs have been established using traditional laboratory models. Results from these common models are used to address the level at which an exposure would lead to adverse outcome in the humans. As such, these values derived from

laboratory models are used to calculate safe-exposure limits of the respective chemicals, such as a reference dose (RfD) or an acceptable daily intake (ADI) (IPCS 2005).

In extrapolating exposure from laboratory models to the human population, the World Health Organization's International Programme on Chemical Safety (IPCS) has suggested that acceptable exposure limits be adjusted by a generic total 'uncertainty factor' of 100. This uncertainty factor breaks down into two separate categories each consisting of a 10-fold adjustment: A) interspecies variation that account for physiological differences between animal models and humans and B) interindividual variation that account for differences in susceptibilities across human individuals. The interspecies variation adjustment further breaks down into two categories: A) toxicodynamics (2.5 fold) and B) toxicokinetics (4.0 fold). Similarly, interindividual differences also break down into the same categories, but with slightly different adjustments per category: A) toxicodynamics (3.2 fold) and B) toxicokinetics (3.2 fold) (IPCS 2005). While interspecies variation is a difficult problem to fully-solve without epidemiological data for the chemical exposure and timeline of interest, several aspects that drive interindividual differences can and should be incorporated in toxicological screens.

As the human population is heterogeneous, there are some individuals that are more susceptible to chemically-induced toxicity than others. While uncertainty factors are used to account for these differences in susceptibility, there is certainly a non-zero chance that all individuals are accounted for within the current exposure guidelines. On the contrary, the use of uncertainty factors may also result in exposure-guidelines that are far too conservative and, thus, lead to unnecessary industrial and municipal financial burdens. As such, lack of empirical data in regards to the impact of interindividual variability in DRRs has potential to negatively impact decision-making. A recent report published by the NRC entitled "Science and Decisions: Advancing Risk Assessment" highlights the need for empirical interindividual variability data prior

to risk-assessment decision-making. The report suggested that the incorporation of inter-individual variability present within the human population would effectively linearize the low-dose region of non-cancer DRRs which have, in the past, been considered nonlinear functions (Figure 1.4)(NRC 2009). The proposal by the NRC was based primarily on theoretical evidence and has not been properly tested. If put into practice for risk assessment, the low-dose linearity assumption could lead to unwanted environmental impacts.

1.5. Incorporating Genetic Heterogeneity into Toxicological Screens

Many factors impact individual responses to environmental exposures including concurrent exposures and/or stressors, age, sex, disease-state, and genetic variability. Recent technological advances provided the opportunity to probe the impact of genetic variability in response to chemical exposures. Results have indicated that genetic polymorphisms can have profound impacts on individual responses. In some extreme cases, ≥ 90% of the observed variability in the human population have been attributed to genetic diversity (Evans and Relling 2004; Kalow et al. 1998). As such, there is growing interest in incorporating genetic variability into toxicological screens (Zeise et al. 2013).

The obvious reason for the exclusion of genetic diversity in classical laboratory models is to reduce experimental variability. Inclusion of genetic variability will increase variability and, from an academic standpoint, increase the risk of a poor association within a study. An excellent example of this is the use of knock-out (KO) rodent models to establish the mechanism in which a particular gene is driving a phenotype. From a purely academic standpoint, the results may be noisier when genetic variability is included. It should be noted that we are not arguing for the replacement of isogenic models in toxicology. In many cases, inclusion of genetic variability may not be economically and technically feasible. Isogenic models clearly have a role to play in

Figure 1.4. The National Research Council's (NRC) Low-Dose Linearity Hypothesis. As published in a report in 2009 call "Science and Decisions: Advancing Risk Assessment," the NRC suggest that, in considering population-level genetic variability, the low-dose region of non-cancer dose-response relationships will linearize. As such, the NRC recommends that there are no safe exposures of chemicals that induced adverse, non-cancer endpoints.

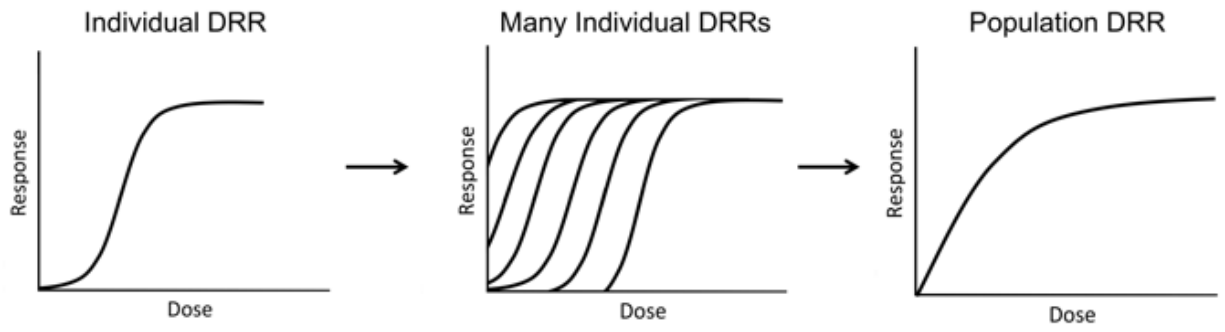

toxicology. However, as highlighted in the studies reviewed below, genetic variability clearly influences dose-response relationships and cannot be ignored.

1.6. Proof of Principle: Advances Driven by Genetically-Diverse Models

As genetic background impacts responses to chemicals, incorporation of genetic diversity into toxicological screens provides an avenue to quantify the influence of genetic diversity within population-level dose-response relationships. Unlike homogenous models, the results from studies using population-based models likely better inform risk assessors of safe-exposure limits that will account for susceptible individuals within the human population. Genetic reference models also have potential to identify genetic variants that may be more susceptible to chemical-induced toxicity (Harrill and McAllister 2017). Genetically diverse populations provide the opportunity to map the differences in responses to areas of the genome that potentially impact susceptibility. As many genetic differences across panels have been analyzed, these models can be used to perform quantitative trait locus analysis that may indicate regions of the genome that are inherited by individuals that were found to be more susceptible to chemical-induced toxicity based on a quantitative phenotype (Figure 1.5). Here, several examples are outlined to indicate the power of incorporating genetic variability into toxicological screens using several distinct laboratory-based models: 1) genetically-diverse cell lines, 2) primary human cells, and 3) genetically-diverse mouse panels.

1.6.1. Genetically Diverse Cell lines

Clonal cell lines have been used in toxicological studies for decades. From an experimental standpoint, these cell lines are excellent in reducing variability in responses to chemical exposures and to gain a mechanistic understanding of chemical-induced toxicity. Furthermore, as cell lines are immortal and can be cryopreserved, they provide a resource that can be studied over long periods of time and can be readily distributed for research purposes.

Figure 1.5. General overview of quantitative trait locus (QTL) analysis. The purpose of QTL analysis is to associate a quantitative trait with a region of the genome. A quantitative trait/phenotype is used to categorize groups of individuals that responded similarly. Software will scan for genetic differences that may indicate a region of the genome that is inherited by individuals that have a similar quantitative phenotype. Such regions may indicate genes or pathways that impact the quantitative trait.

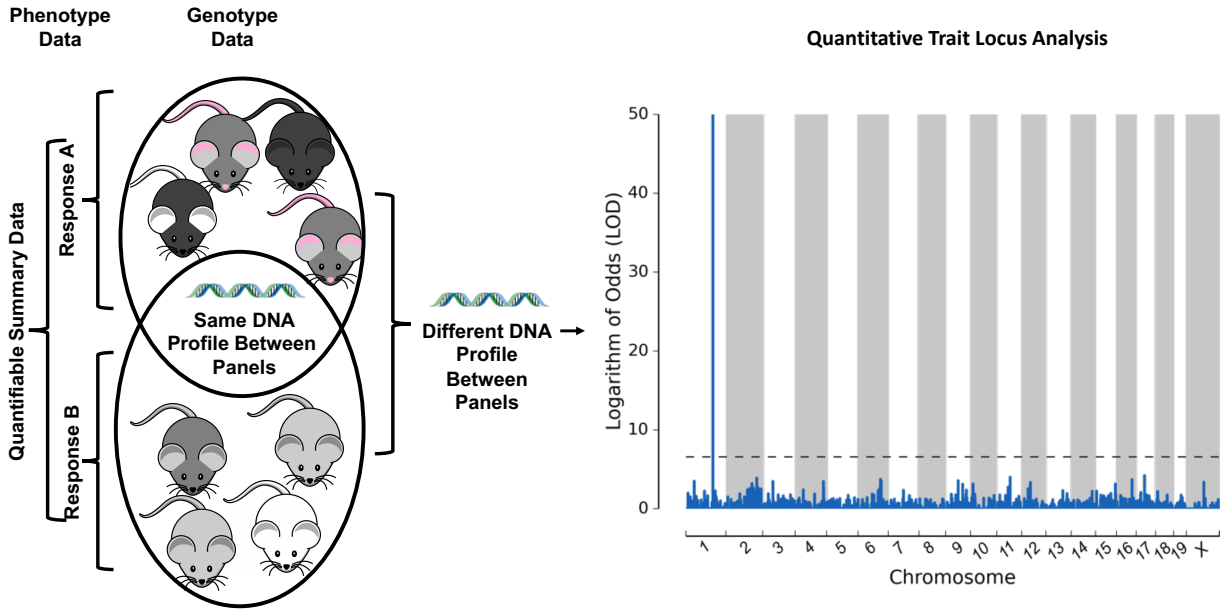

Human lymphoblastoid cell lines (LCLs) can easily and efficiently be derived from a large number of individuals and, by assaying a large number of individual cell lines, can be used to assay population-level variability in responses to exposures (Dolan et al. 2004; Watters et al. 2004). LCLs have been established from individuals of diverse heritages from locations throughout the world. The true power of these LCLs lies in the plethora of genomic and demographic data freely-available, such as through the 1,000 genomes project website, to probe links between genotype and phenotype. Specifically, LCLs can be used to link variant responses to genomic difference amongst cell lines without the need for further genotyping.

Previous studies have shown that LCLs can be successfully used to probe variations in chemicals responses. For example, a recent study indicated that 146 lymphoblastoid cell lines were exposed to multiple concentrations of two separate mixtures of pesticides: 1) a current-use pesticide mixture (n=36 chemicals) and 2) an organic pesticide mixture (n=10 chemicals) (Abdo et al. 2015a). Curve-fitting clearly shows that, within the population of LCLs, there is a large range of susceptibility in the chemically-induced cytotoxic responses. Furthermore, the results were also used to calculate a toxicodynamic uncertainty factor (VF_d) of around 3-fold for each pesticide mixture which, as noted in the report, is analogous to the level of interindividual variability for the pesticide mixtures. Within these individual differences, a polymorphism on chromosome 17 was found to be highly correlated with differences in susceptibility of the cell lines. The polymorphism was found within an open reading frame (i.e. C17orf54) and, in further detail, a major allele (AA) was found to me more sensitive than either the heterozygous genotype (AT) or the minor allele (TT). One of the most innovative aspects of this paper, however, is the use of *in vitro*-to-*in vivo* extrapolation (IVIVE) to estimate the corresponding cumulative oral equivalent dose of the chemical mixtures to reach the EC_{10} in the underlying cytotoxic phenotypes being assayed. Notably, a primary challenge of incorporating *in vitro* data within human risk assessment is

determining the *in vivo* dose required to result in the *in vitro* concentrations at hand (Judson et al. 2011). Results indicated that, with data available for 31 of 36 pesticides in the current-use mixture and 4 of 10 pesticides within the organic mixture, the organic pesticide mixture required significantly less exposure to reach the EC_{10} of the cytotoxic phenotype. Furthermore, the authors estimate that population variability would require a 5-fold margin of safety for the organic pesticide while, in comparison, the current-use pesticide mixture would require less than a 2-fold margin of safety to account for inter-individual differences (Wetmore et al. 2014). While the IVIVE calculations required several assumptions, the methodology provides a method to estimate the chemical exposures required to reach toxicity seen *in vitro* and, furthermore, the influence that population variability plays in defining safe exposure limits (Abdo et al. 2015a).

In a similar study, cytotoxicity of 1,086 LCLs was assayed following exposure to 179 different chemicals found within the National Toxicology Program's (NTP) chemical library (Abdo et al. 2015b). This study also calculated toxicodynamic variability factors (VF_d) for 149 chemicals. In assessing population variability, nearly half of the individual EC_{10} values have interindividual ranges that fall below the generic 3.2-fold adjustment. These results suggest that, in some cases, uncertainty factors can be too conservative. More interestingly, a subset of these chemicals within the study were found to produce EC_{10} value ranges that were much greater than the generic 3.2-fold adjustment indicating the need for chemical-specific data in setting exposure guidelines for the human population. These results also suggest the inherent risks associated with relying on generic uncertainty factors. Furthermore, the authors used multivariate association analysis (MAGWAS) to scan for genetic loci associated with the differences seen in the concentration-responses amongst the individual cell lines for each chemical. The results revealed several patterns and potential key players in chemical-induced cytotoxicity. For example, transmembrane proteins and solute carriers appear to play a key role in mediating chemical-induced cytotoxicity as they are consistently found in the most-significant associated loci. Similarly, a SNP

(rs13120371) in 3' UTR of *SLC7A11* was found to be significantly associated with interindividual differences in 2-Amino-4-methylphenol, methyl mercuric (III) chloride, and N-methyl-p-aminophenol sulfate-induced cytotoxicity. In further detail, the results indicate which alleles appear to be more sensitive to chemical-induced cytotoxicity and, thus, can be used to predict which individuals may be more susceptible to chemical-induced toxicity. For example, a minor allele (AA) was found to be more sensitive to 2-amino-4-methylphenol as compared to the hetereozygous (AT) and major allele (TT) within the 3' UTR of *SLC7A11* (Abdo et al. 2015b).

1.6.2. Primary Human Cells

The 'gold standard' in analyzing human responses to chemical exposure *in vitro* is with primary cells taken from blood or tissue. Human primary cell cultures are more likely to mirror an *in vivo* response than immortalized human cell lines. On the other hand, primary cells typically can only be cultured for a short time and are more sensitive to the freeze-thaw cycles as compared to cell lines. Furthermore, individuals within a study would need to be genotyped to assess genetic variability. The most challenging aspect of working with primary human cells to assess population variability lies with obtaining samples from a large number of individuals. While some methods are quite noninvasive, such as obtaining leukocytes from blood, other tissue samples relevant to toxicological outcomes can be quite invasive, such as the liver. However, such tissues can be obtained through many methods including biopsies, surgical waste products, organ donations, or, in some cases, long-term cultures in cell types less sensitive to cryopreservation.

While resting primary human leukocytes are short-lived and need to be processed within 24 hours of collection, previous studies have indicated that cells obtained from blood donations can be cultured within a few hours preventing the need for a freeze-thaw cycle (Phadnis-Moghe and Kaminski 2017). More specifically, previous reports indicate that B cells can be isolated from whole blood obtained from commercial vendors and activated with CD40-ligand and cytokines to

induced an antibody response (Lu et al. 2009). This model has been used to establish that exposure to 2,3,7,8-tetrachlorodibenzo-*p*-dioxin (TCDD) suppresses the activation and differentiation of human B cells (Lu et al. 2010; Lu et al. 2011; Phadnis-Moghe et al. 2015). Results from these studies have indicated that a subset (~15%) of the human donors do not respond to increasing concentrations of TCDD suggesting this model might be valuable in modeling inter-individual variability in response to immunotoxicants (Lu *et al*., 2010).

Reports have also established that adherent, monolayer primary tissue cells can be used to assay interindividual variability in response to chemicals (den Braver-Sewradj et al. 2016; Martelli et al. 2003; Schuetz et al. 1995). A recent study using both monolayer culture and suspension culture of hepatocytes established a high-level of interindividual variation in phase I- and phase II-mediated metabolism. Their results suggest the presence of up to 3 and 4-fold differences between donors in the cytochrome P450-mediated metabolism of diclofenac in suspension and monolayer culture, respectively. First, the report provides evidence that, even with the same cell type, the level of human interindividual variability measured can be culture model-specific (i.e. suspension vs. adherent cells). Secondly, this article highlights the complexity of human variability as there can be interindividual differences in the rate of metabolism of chemicals (den Braver-Sewradj et al. 2016). Thus, depending on the individual, there can be differences in the rate in which toxic chemicals are metabolized into benign compounds or, differences in the accumulation and excretion rates of toxic metabolites.

1.6.3. Genetically Diverse Mouse Panels

Rodent-based studies provide a financially-reasonable *in vivo* model that can control for many environmental factors and, yet, support complex study design. More importantly, many inbred mouse genomes have been completely sequenced (Adams et al. 2015; Doran et al. 2016; Keane et al. 2011; Morgan et al. 2016). As such, genetically-diverse mouse panels provide an

opportunity to better understand the effect of genetic variation within complex etiologies and identify genetic variants that effect susceptibility to a particular phenotype (e.g. chemical-induced toxicity). The lack of genetic variation within inbred strains provide the opportunity for mice with identical genomes to be assayed over periods of time and differing experimental conditions (Bogue et al. 2015; Rusyn et al. 2010). Most importantly, there is significant diversity across strains. For example, within the *Mus musculus* subspecies it has been estimated that the number and distributions of polymorphisms is greater than found within human population (Ideraabdullah et al. 2004; Rusyn et al. 2010). The creation of genetic diverse reference populations, such as the Collaborative Cross (CC) and the Diversity Outbred (DO) mouse populations, provide the opportunity to assay genetic variability similar to that found in the human population and, to map the differences in responses to places within the genome with high-resolution (CCC 2012; Churchill et al. 2004; Churchill et al. 2012; Logan et al. 2013; Svenson et al. 2012; Threadgill et al. 2011; Threadgill and Churchill 2012; Welsh et al. 2012). The CC is significantly more diverse than previous, commonly used mouse panels, as it was created from 8 diverse founding strains of 3 differing *Mus musculus* subspecies (*M. m. musculus*, *domesticus*, *castaneous*) that encompass 90% of genetic variation in laboratory mice: 1) A/J, 2) C57BL/6J, 3) 129S1/SvImJ, 4) NOD/ShiLtJ, 5) NZO/HILtJ, 6) CAST/EiJ, 7) PWK/PhJ, and 8) WSB/EiJ (Roberts et al. 2007; Threadgill and Churchill 2012). While the statistical power of CC is somewhat limited by the number of fully-inbred strains available, the inbred nature of the panel only requires one round of genotyping per strain (Bogue et al. 2015; Churchill et al. 2004; Threadgill et al. 2011; Threadgill and Churchill 2012). The CC panel has been used to analyze a range of complex traits (Abu-Toamih Atamni et al. 2017; Aylor et al. 2011; Kelada et al. 2012; Kelada 2016; Nashef et al. 2017; Smith et al. 2016; Xue et al. 2016). Similarly, the DO stock was created from early pre-CC strains and, while containing the same level of allelic diversity as the CC, are maintained with a high-level of heterozygosity (Bogue et al. 2015; Chesler 2014; Churchill et al. 2012). While the nature of the DO stock requires genotyping for each mouse, the heterozygosity provides the opportunity

to analyze additivity while the high level of fecundity and large stock population provide an ideal model for high-resolution mapping and selective-breeding studies (Church et al. 2015; Logan et al. 2013; Svenson et al. 2012). These diverse populations of mice provide an *in vivo* method to analyze the impact of population-level genetic variability and to identify variants within populations that may be more or less susceptibility in chemical-induced phenotypes.

Mouse population-based studies have already begun impacting human risk-assessment (Cichocki et al. 2017; French et al. 2015; Harrill et al. 2009; Venkatratnam et al. 2017). For example, a double-blind study in which 49 healthy humans who were exposed to maximum recommended therapeutic range of acetaminophen (4 gram/day for 7 days) found that 31% showed ≥ 2 fold increase of alanine aminotransferase (ALT) serum levels. Thus, within the recommended therapeutic range, some human individuals appear to experience mild liver injury. To identify potential loci associated with increased risk to acetaminophen-induced toxicity, 36 inbred mouse strains were dosed with a range of acetaminophen. Results indicated interstrain differences in several endpoints including the rate of acetaminophen metabolism, ALT levels in the serum, and liver necrosis. The results show that genetic variation amongst the mouse strains profoundly changed the dose-response curves in the degree of necrosis and the level of ALT in the serum. Haplotype-association mapping suggested several genes, such as *Cd44* and *Capn10*, were associated with inter-strain differences in ALT release. These genes were then related to human susceptibility. For example, a nonsynonymous polymorphism in the *CD44* gene was found to be statistically correlated with an individual's level of acetaminophen-induced ALT release. Similarly, a synonymous SNP in *CAPN10* was found to be moderately-associated with an individual's ALT-release. These results demonstrate the usefulness of mouse panels in identifying genes that likely contribute to human population-level variability in response to chemicals (Harrill et al. 2009).

In another study, 50 inbred strains were used to assay the influence of population variability on the toxicokinetics of cytochrome-mediated oxidation of trichloroethylene (TCE) (Venkatratnam et al. 2017). Results indicated that the levels of trichloroacetic acid (TCA), the most abundance metabolite of TCE, varied by an order of magnitude in a strain-specific manner. The results, along with another previous study of perchloroethylene, show the power of the collaborative cross in assaying toxicokinetic population variability (Cichocki et al. 2017). More interestingly, the empirical values measured in the current study were compared to the predicted levels of TCA in tissues by a physiologically-based pharmacokinetic model (PBPK) based on results from 16 inbred mouse strains (Chiu et al. 2014). The CC panel suggests that the PBPK model may be under-estimating the TCA level in tissues highlighting the need for individual-specific data for chemical exposures. More specifically, the 800 mg/kg dose groups in the CC panel were found beyond the PBPK's predicted 95% confidence levels of TCE burden in the liver for more than half of the strains, a third of the strains in the kidney, and nearly half of the strains for the serum. As TCE and TCA are ligands of PPARα, the authors also looked at the expression of two PPARα-inducible genes, *Acox1* and *Cyp4a10*, and found significant induction at the population level of all CC strains with notable interstrain differences as has been previously reported (Bradford et al. 2011). As the expression of *Acox1* was found to be correlated with the level of TCA in the liver, the authors postulate that TCE-mediated effects may be altering TCE metabolism in a strain-specific manner. Furthermore, QTL analysis on the variability in TCA levels in the liver of the differing strains identified a list of potential genes that might explain the response differences. The gene list was narrowed down based on the function of the genes and potential links to TCE-mediated effects. QRTPCR analysis indicated that expression of *Acot8* and *Fitm2* positively correlated with the levels of TCA in the liver and, thus, may be associated with the differences in TCE metabolism and the susceptibility to TCE-mediated toxicity (Venkatratnam et al. 2017).

In a study using DO mice, 600 mice were exposed to varying amounts of benzene via an inhalation chamber (French et al. 2015). The authors used micronucleus (MN) frequency in reticulocytes (RET) derived from the peripheral blood (PB) or bone marrow (BM) to assay the extent of chromosomal damage induced by benzene. The MN frequency was found to be significantly elevated for mice exposed to 100 ppm benzene in PB-RETs and for mice exposed to 1, 10, and 100 ppm for BM-RETs. Interestingly, a large range in the MN frequency in RETs derived from both PB and BM for the 100 ppm dose-group was reported. The most interesting aspect of this report was found in the statistical modeling of the dose-response to estimate the thresholds required to reach toxicity (Crump 1984). The results indicated that 0.205 ppm of benzene could reach the lower-bound confidence interval in the concentration-response (BMCL) found in this stock of DO mice. This BMCL was an order of magnitude lower than found in a previous report using a similar study design in the inbred B6C3F1 mouse strain (Farris et al. 1996). The difference in BMCLs between the studies suggest that incorporation of genetic variability may greatly impact safe-exposure assessments (Farris et al. 1996). In genotyping the mice and running QTL analysis, a locus on chromosome 10 was found to be significantly associated with the MN frequency derived from both the PB and BM within the 100 ppm benzene dose group. More specifically, mice that inherit a gene-duplication event in a region of chromosome 10 from the CAST/EiJ founder strain showed less benzene-induced chromosomal damage. The authors hypothesize that the gene-duplication likely leads to increased expression of several genes in this area, such as *Sult3a1* and *Gm4794*, which are involved in sulfating toxic benzene metabolites. Notably, copy number variation is also found in human population that potentially plays a role in driving interindividual variation in the metabolism of benzene (French et al. 2015; Gaedigk et al. 2012; Yu et al. 2013).

1.7. Overarching Hypothesis and Specific Aims

The impact of genetic variability on individual's susceptibility to TCDD has not been thoroughly addressed. While past reports have established genes and pathways involved in TCDD-induced toxicity, that vast majority have used homogenous models (i.e. single inbred mouse strains and clonal cell lines). Given the complex etiologies associated with disease-states induced by TCDD, homogenous models will likely not encompass the variability in physiological responses seen across diverse human populations. Previous reports on environmental contaminants, such as benzene, have indicated that results are heavily-dependent on the mouse strain chosen (French et al. 2015). The strain-dependence is particular true for the response to TCDD which has been found to be very strain-specific (Chapman and Schiller 1985; French et al. 2015; Shen et al. 1991). In many cases, the response from a differing mouse strain could greatly alter the perceived risk associated with a chemical exposure. Inter-strain differences in response to chemicals and other stressors can also be leveraged to identify genetic determinants that drive differing susceptibilities.

The overall goal of this dissertation was to use several population-based models to assess the impact of genetic variability on the response to TCDD. A mixture of *in vitro*- and *in vivo*-based laboratory models were used to assay the impact that TCDD has on multiple endpoints including the IgM response of B cells and liver homeostasis. **The overarching hypothesis of the project is that a population-guided approach will identify genetic modulators of TCDD-mediated toxicity.** The project consisted of four independent specific aims:

1.7.1. Specific Aim 1. Characterizing the impact of interindividual variability in TCDD-mediated suppression of the human B cell. The primary goal of this aim was to establish the level of interindividual variability in response to TCDD in humans. Previous reports have identified individual differences in response to TCDD, but have not quantified the differences across a large

number of individuals. Furthermore, previous reports have not characterized the impact of interindividual variability on TCDD-mediated dose-response relationships. To address these knowledge gaps, B cells were isolated from 51 unique human donors and exposed to increasing concentrations of TCDD to induce a dose-response. Statistical modeling was used to assess the impact of interindividual variability within the low-dose region of the TCDD-mediated dose-response.

1.7.2. Specific Aim 2. Identifying and characterizing the impact of *Serpinb2* as modulator of TCDD-mediated suppression of the B cell. The vast majority of the mechanistic understanding of TCDD-mediated suppression of the B cell has been characterized using homogenous models. The goal of this aim was to use genetic variability to identify novel genes and/or pathways that impact the immunosuppressive response to TCDD. B cells were isolated and exposed to TCDD from twelve genetically-diverse mouse strains. Quantitative trait locus (QTL) analysis was used to identify genetic regions that are potentially driving differences in sensitivity across the population of mice. A gene called *Serpinb2,* which has previously been shown as dysregulated by TCDD in mouse and human B cells, was found in a genomic region of interest. Further downstream functional analysis was used to assess the role of *Serpinb2* in TCDD-mediated suppression of the B cell.

1.7.3. Specific Aim 3. Characterizing the toxicodynamics of hepatic accumulation of TCDD and identifying *Tgfbr2* as a modulator of TCDD-mediated liver toxicity. The purpose of this aim was three fold. The first goal was to analyze the level of inter-strain variability in the accumulation of TCDD and expression of a subset of the known AHR-responsive genes in the liver. The second goal was to assess whether the accumulation of TCDD is correlated with the AHR-mediated expression. Previous reports have established genes, such as *Cyp1a2*, that are regulated by the AHR and involved in sequestration of TCDD in the liver. However, these studies

have used homogenous mouse models and, thus, potentially have missed other genes and pathways involved. As such, we sought to use QTL analysis to potentially identify modulators of TCDD accumulation and AHR-mediated expression. To address these goals, fourteen mouse strains were dosed with 1 or 100 ng of TCDD / kg of body weight (ng/kg) for 10 consecutive days. Following, the total level of hepatic TCDD was analyzed with GC/MS and TCDD-mediated expression of 9 hepatic AHR-responsive genes were analyzed using NanoString Technology. The results indicate that hepatic accumulation of TCDD is heavily-dependent on genotype and is correlated with AHR-mediated gene expression. QTL analysis identify several genomic regions of interest including an area on Chromosome 9 near a gene called *Tgfbr2*. Further functional analysis was used to identify the role of *Tgfbr2*-related activity in the TCDD-mediated steatohepatitis in the liver of mice that are sensitive to TCDD exposure.

1.7.4. Specific Aim 4. Identifying and characterizing the impact of TCDD-mediated repression of *Hmgcr* in modulating TCDD-mediated liver toxicity. This aim was based primarily on the inter-strain differences in the change in body weights across fourteen genetically-diverse strains following exposure to 100 ng/kg for 10 consecutive days. QTL analysis indicated a strong association in Chromosome 13 near a gene called *Hmgcr*. Previous reports have indicated that the AHR regulates *Hmgcr* mRNA expression and, ultimately, the level of cholesterol in the serum of mice. To assess whether this endpoint is relevant to humans, multiple linear regression models were created using lipid-adjusted levels of TCDD in serum along with total cholesterol data from the Center for Disease Control (CDC) National Health and Nutrition Examination Survey. Models were adjusted for potential confounding variables including age, race, body mass index (BMI), and usage of drugs that impact cholesterol levels. Finally, mice were exposed to TCDD for 10 days in the presence of absence of an HMG-CoA reductase (i.e. the protein encoded by *Hmgcr)* inhibitor called simvastatin to characterize the functional role of *Hmgcr* repression in TCDD-mediated liver pathology.

1.8. Overall Significance

The primary significance of this dissertation lies in proof-of-principle. Previous studies have shown the power of using genetic reference rodent panels to better characterize risk association with environmental exposures (Cichocki et al. 2017; French et al. 2015; Venkatratnam et al. 2017). This is the first population-based approach to assess the impact of genetic variation in response to TCDD exposure. First, a human cell-based *in vitro* model was used to establish a wide-range of interindividual variability in response to TCDD exposure. Secondly, a rodent population-guided approach was used to identify several novel genes that were found to impact the TCDD-mediated suppression of the B cell and liver pathology. This provides proof that a rodent population-based approach has potential to shed light into the mechanism of TCDD-mediated toxicity beyond what has been previously uncovered using homogenous models.

Beyond proof-of-principle, the results clearly show a large-level of interindividual human and inter-mouse strain variation in the response to TCDD. These experiments provide quantitative differences in multiple endpoints across genetically-diverse population of individuals. As current risk assessment relies on the aforementioned 10-fold uncertainty factors to account for interindividual differences, the data from this dissertation have potential to better inform risk assessors of range in responses for a diverse set of phenotypes. Interestingly, several endpoints assayed in this dissertation suggest that a 10-fold adjustment is quite conservative. The results from this set of experiments may be used in future risk assessment to create guidelines that truly encompass the range of responses in the human population. These results could be used to create safe-exposure guidelines grounded in empirical data as opposed to generic uncertainty factors of 10.

Finally, this research provides evidence that genomic factors beyond the *Ahr* allele impact strain specific responses to TCDD. While the *Ahr* allele was found to have significant impact on strain-specific response to TCDD, several others genes were found modulate phenotype-specific responses. Such responses include TCDD-mediated suppression of the IgM response, hepatic accumulation of TCDD, AHR-target gene expression, and several TCDD-induced liver pathologies. While these results need to be confirmed in the human population, we hypothesize that expression- or function-altering variants of these modulating genes may ultimately alter individual human responses to TCDD exposures. As such, the results from these experiments may provide risk assessors with information used to identify individuals or sub-populations of humans that may be more susceptible to TCDD-mediated toxicity.

REFERENCES

REFERENCES

Abdo N, Wetmore BA, Chappell GA, Shea D, Wright FA, Rusyn I. 2015a. In vitro screening for population variability in toxicity of pesticide-containing mixtures. Environ Int 85:147-155.

Abdo N, Xia M, Brown CC, Kosyk O, Huang R, Sakamuru S, et al. 2015b. Population-based in vitro hazard and concentration-response assessment of chemicals: The 1000 genomes high-throughput screening study. Environ Health Perspect 123:458-466.

Abel J, Haarmann-Stemmann T. 2010. An introduction to the molecular basics of aryl hydrocarbon receptor biology. Biol Chem 391:1235-1248.

Abu-Toamih Atamni HJ, Ziner Y, Mott R, Wolf L, Iraqi FA. 2017. Glucose tolerance female-specific qtl mapped in collaborative cross mice. Mamm Genome 28:20-30.

Adams DJ, Doran AG, Lilue J, Keane TM. 2015. The mouse genomes project: A repository of inbred laboratory mouse strain genomes. Mamm Genome 26:403-412.

Aylor DL, Valdar W, Foulds-Mathes W, Buus RJ, Verdugo RA, Baric RS, et al. 2011. Genetic analysis of complex traits in the emerging collaborative cross. Genome Res 21:1213-1222.

Baccarelli A, Mocarelli P, Patterson DG, Jr., Bonzini M, Pesatori AC, Caporaso N, et al. 2002. Immunologic effects of dioxin: New results from seveso and comparison with other studies. Environ Health Perspect 110:1169-1173.

Bittinger MA, Nguyen LP, Bradfield CA. 2003. Aspartate aminotransferase generates proagonists of the aryl hydrocarbon receptor. Mol Pharmacol 64:550-556.

Boffetta P, Mundt KA, Adami HO, Cole P, Mandel JS. 2011. Tcdd and cancer: A critical review of epidemiologic studies. Crit Rev Toxicol 41:622-636.

Bogue MA, Churchill GA, Chesler EJ. 2015. Collaborative cross and diversity outbred data resources in the mouse phenome database. Mamm Genome 26:511-520.

Boverhof DR, Burgoon LD, Tashiro C, Chittim B, Harkema JR, Jump DB, et al. 2005. Temporal and dose-dependent hepatic gene expression patterns in mice provide new insights into tcdd-mediated hepatotoxicity. Toxicol Sci 85:1048-1063.

Boverhof DR, Burgoon LD, Tashiro C, Sharratt B, Chittim B, Harkema JR, et al. 2006. Comparative toxicogenomic analysis of the hepatotoxic effects of tcdd in sprague dawley rats and c57bl/6 mice. Toxicol Sci 94:398-416.

Bradford BU, Lock EF, Kosyk O, Kim S, Uehara T, Harbourt D, et al. 2011. Interstrain differences in the liver effects of trichloroethylene in a multistrain panel of inbred mice. Toxicol Sci 120:206-217.

Bunger MK, Moran SM, Glover E, Thomae TL, Lahvis GP, Lin BC, et al. 2003. Resistance to 2,3,7,8-tetrachlorodibenzo-p-dioxin toxicity and abnormal liver development in mice carrying a

mutation in the nuclear localization sequence of the aryl hydrocarbon receptor. J Biol Chem 278:17767-17774.

Bunger MK, Glover E, Moran SM, Walisser JA, Lahvis GP, Hsu EL, et al. 2008. Abnormal liver development and resistance to 2,3,7,8-tetrachlorodibenzo-p-dioxin toxicity in mice carrying a mutation in the DNA-binding domain of the aryl hydrocarbon receptor. Toxicol Sci 106:83-92.

Butler RA, Kelley ML, Powell WH, Hahn ME, Van Beneden RJ. 2001. An aryl hydrocarbon receptor (ahr) homologue from the soft-shell clam, mya arenaria: Evidence that invertebrate ahr homologues lack 2,3,7,8-tetrachlorodibenzo-p-dioxin and beta-naphthoflavone binding. Gene 278:223-234.

Carver LA, LaPres JJ, Jain S, Dunham EE, Bradfield CA. 1998. Characterization of the ah receptor-associated protein, ara9. J Biol Chem 273:33580-33587.

Cave M, Appana S, Patel M, Falkner KC, McClain CJ, Brock G. 2010. Polychlorinated biphenyls, lead, and mercury are associated with liver disease in american adults: Nhanes 2003-2004. Environ Health Perspect 118:1735-1742.

CCC. 2012. The genome architecture of the collaborative cross mouse genetic reference population. Genetics 190:389-401.

Chang C, Benson M, Fam MM. 2017. A review of agent orange and its associated oncologic risk of genitourinary cancers. Urol Oncol 35:633-639.

Chapman DE, Schiller CM. 1985. Dose-related effects of 2,3,7,8-tetrachlorodibenzo-p-dioxin (tcdd) in c57bl/6j and dba/2j mice. Toxicol Appl Pharmacol 78:147-157.

Chen Q, Garabrant DH, Hedgeman E, Little RJ, Elliott MR, Gillespie B, et al. 2010. Estimation of background serum 2,3,7,8-tcdd concentrations by using quantile regression in the umdes and nhanes populations. Epidemiology 21 Suppl 4:S51-57.

Chen Q, Jiang X, Hedgeman E, Knutson K, Gillespie B, Hong B, et al. 2013. Estimation of age- and sex-specific background human serum concentrations of pcdds, pcdfs, and pcbs in the umdes and nhanes populations. Chemosphere 91:817-823.

Chesler EJ. 2014. Out of the bottleneck: The diversity outcross and collaborative cross mouse populations in behavioral genetics research. Mamm Genome 25:3-11.

Chiu WA, Campbell JL, Jr., Clewell HJ, 3rd, Zhou YH, Wright FA, Guyton KZ, et al. 2014. Physiologically based pharmacokinetic (pbpk) modeling of interstrain variability in trichloroethylene metabolism in the mouse. Environ Health Perspect 122:456-463.

Church RJ, Gatti DM, Urban TJ, Long N, Yang X, Shi Q, et al. 2015. Sensitivity to hepatotoxicity due to epigallocatechin gallate is affected by genetic background in diversity outbred mice. Food Chem Toxicol 76:19-26.

Churchill GA, Airey DC, Allayee H, Angel JM, Attie AD, Beatty J, et al. 2004. The collaborative cross, a community resource for the genetic analysis of complex traits. Nat Genet 36:1133-1137.

Churchill GA, Gatti DM, Munger SC, Svenson KL. 2012. The diversity outbred mouse population. Mamm Genome 23:713-718.

Cichocki JA, Furuya S, Venkatratnam A, McDonald TJ, Knap AH, Wade T, et al. 2017. Characterization of variability in toxicokinetics and toxicodynamics of tetrachloroethylene using the collaborative cross mouse population. Environ Health Perspect 125:057006.

Cole P, Trichopoulos D, Pastides H, Starr T, Mandel JS. 2003. Dioxin and cancer: A critical review. Regul Toxicol Pharmacol 38:378-388.

Crump KS. 1984. A new method for determining allowable daily intakes. Fundam Appl Toxicol 4:854-871.

den Braver-Sewradj SP, den Braver MW, Vermeulen NP, Commandeur JN, Richert L, Vos JC. 2016. Inter-donor variability of phase i/phase ii metabolism of three reference drugs in cryopreserved primary human hepatocytes in suspension and monolayer. Toxicol In Vitro 33:71-79.

Denison MS, Fisher JM, Whitlock JP, Jr. 1988a. The DNA recognition site for the dioxin-ah receptor complex. Nucleotide sequence and functional analysis. J Biol Chem 263:17221-17224.

Denison MS, Fisher JM, Whitlock JP, Jr. 1988b. Inducible, receptor-dependent protein-DNA interactions at a dioxin-responsive transcriptional enhancer. Proc Natl Acad Sci U S A 85:2528-2532.

Denison MS, Nagy SR. 2003. Activation of the aryl hydrocarbon receptor by structurally diverse exogenous and endogenous chemicals. Annu Rev Pharmacol Toxicol 43:309-334.

Dere E, Lo R, Celius T, Matthews J, Zacharewski TR. 2011. Integration of genome-wide computation dre search, ahr chip-chip and gene expression analyses of tcdd-elicited responses in the mouse liver. BMC Genomics 12:365.

Dolan ME, Newbold KG, Nagasubramanian R, Wu X, Ratain MJ, Cook EH, Jr., et al. 2004. Heritability and linkage analysis of sensitivity to cisplatin-induced cytotoxicity. Cancer Res 64:4353-4356.

Doran AG, Wong K, Flint J, Adams DJ, Hunter KW, Keane TM. 2016. Deep genome sequencing and variation analysis of 13 inbred mouse strains defines candidate phenotypic alleles, private variation and homozygous truncating mutations. Genome Biol 17:167.

Duncan DM, Burgess EA, Duncan I. 1998. Control of distal antennal identity and tarsal development in drosophila by spineless-aristapedia, a homolog of the mammalian dioxin receptor. Genes Dev 12:1290-1303.

Ema M, Ohe N, Suzuki M, Mimura J, Sogawa K, Ikawa S, et al. 1994. Dioxin binding activities of polymorphic forms of mouse and human arylhydrocarbon receptors. J Biol Chem 269:27337-27343.

Evans WE, Relling MV. 2004. Moving towards individualized medicine with pharmacogenomics. Nature 429:464-468.

Farris GM, Wong VA, Wong BA, Janszen DB, Shah RS. 1996. Benzene-induced micronuclei in erythrocytes: An inhalation concentration-response study in b6c3f1 mice. Mutagenesis 11:455-462.

Fernandez-Salguero P, Pineau T, Hilbert DM, McPhail T, Lee SS, Kimura S, et al. 1995. Immune system impairment and hepatic fibrosis in mice lacking the dioxin-binding ah receptor. Science 268:722-726.

French JE, Gatti DM, Morgan DL, Kissling GE, Shockley KR, Knudsen GA, et al. 2015. Diversity outbred mice identify population-based exposure thresholds and genetic factors that influence benzene-induced genotoxicity. Environ Health Perspect 123:237-245.

Gaedigk A, Twist GP, Leeder JS. 2012. Cyp2d6, sult1a1 and ugt2b17 copy number variation: Quantitative detection by multiplex pcr. Pharmacogenomics 13:91-111.

Gasiewicz TA, Geiger LE, Rucci G, Neal RA. 1983. Distribution, excretion, and metabolism of 2,3,7,8-tetrachlorodibenzo-p-dioxin in c57bl/6j, dba/2j, and b6d2f1/j mice. Drug Metab Dispos 11:397-403.

Gasiewicz TA, Singh KP, Casado FL. 2010. The aryl hydrocarbon receptor has an important role in the regulation of hematopoiesis: Implications for benzene-induced hematopoietic toxicity. Chem Biol Interact 184:246-251.

Geyer HJ, Scheuntert I, Rapp K, Kettrup A, Korte F, Greim H, et al. 1990. Correlation between acute toxicity of 2,3,7,8-tetrachlorodibenzo-p-dioxin (tcdd) and total body fat content in mammals. Toxicology 65:97-107.

Gilpin **RK**, Wagel DJ, Solch JG. 2003. Production, distribution, and fate of polychlorinated dibenzo-p-dioxins, dibenzofurans, and related organohalogens in the environment. In: Dioxins and health, (Schecter A, Gasiewicz TA, eds). Hoboken, NJ:Wiley, 89-136.

Gu YZ, Hogenesch JB, Bradfield CA. 2000. The pas superfamily: Sensors of environmental and developmental signals. Annu Rev Pharmacol Toxicol 40:519-561.

Hahn ME. 2002. Aryl hydrocarbon receptors: Diversity and evolution. Chem Biol Interact 141:131-160.

Harper PA, Wong J, Lam MS, Okey AB. 2002. Polymorphisms in the human ah receptor. Chem Biol Interact 141:161-187.

Harrill AH, Watkins PB, Su S, Ross PK, Harbourt DE, Stylianou IM, et al. 2009. Mouse population-guided resequencing reveals that variants in cd44 contribute to acetaminophen-induced liver injury in humans. Genome Res 19:1507-1515.

Harrill AH, McAllister KA. 2017. New rodent population models may inform human health risk assessment and identification of genetic susceptibility to environmental exposures. Environ Health Perspect 125:086002.

Heid SE, Pollenz RS, Swanson HI. 2000. Role of heat shock protein 90 dissociation in mediating agonist-induced activation of the aryl hydrocarbon receptor. Mol Pharmacol 57:82-92.

Ideraabdullah FY, de la Casa-Esperon E, Bell TA, Detwiler DA, Magnuson T, Sapienza C, et al. 2004. Genetic and haplotype diversity among wild-derived mouse inbred strains. Genome Res 14:1880-1887.

IPCS. 2005. Chemical-specific adjustment factors for interspecies differences in human variability: Guidance document for use of data in dose/concentration–response assessment. Harmonization project document no. 2. . Geneva:World Health Organization.

Jackson JA, Diliberto JJ, Birnbaum LS. 1993. Estimation of octanol-water partition coefficients and correlation with dermal absorption for several polyhalogenated aromatic hydrocarbons. Fundam Appl Toxicol 21:334-344.

Judson RS, Kavlock RJ, Setzer RW, Hubal EA, Martin MT, Knudsen TB, et al. 2011. Estimating toxicity-related biological pathway altering doses for high-throughput chemical risk assessment. Chem Res Toxicol 24:451-462.

Kalow W, Tang BK, Endrenyi L. 1998. Hypothesis: Comparisons of inter- and intra-individual variations can substitute for twin studies in drug research. Pharmacogenetics 8:283-289.

Keane TM, Goodstadt L, Danecek P, White MA, Wong K, Yalcin B, et al. 2011. Mouse genomic variation and its effect on phenotypes and gene regulation. Nature 477:289-294.

Kelada SN, Aylor DL, Peck BC, Ryan JF, Tavarez U, Buus RJ, et al. 2012. Genetic analysis of hematological parameters in incipient lines of the collaborative cross. G3 (Bethesda) 2:157-165.

Kelada SN. 2016. Plethysmography phenotype qtl in mice before and after allergen sensitization and challenge. G3 (Bethesda) 6:2857-2865.

Kerger BD, Leung HW, Scott P, Paustenbach DJ, Needham LL, Patterson DG, Jr., et al. 2006. Age- and concentration-dependent elimination half-life of 2,3,7,8-tetrachlorodibenzo-p-dioxin in seveso children. Environ Health Perspect 114:1596-1602.

Kimbrough RD, Falk H, Stehr P, Fries G. 1984. Health implications of 2,3,7,8-tetrachlorodibenzodioxin (tcdd) contamination of residential soil. J Toxicol Environ Health 14:47-93.

Kovalova N, Manzan M, Crawford R, Kaminski N. 2016. Role of aryl hydrocarbon receptor polymorphisms on tcdd-mediated cyp1b1 induction and igm suppression by human b cells. Toxicol Appl Pharmacol 309:15-23.

Lahvis GP, Pyzalski RW, Glover E, Pitot HC, McElwee MK, Bradfield CA. 2005. The aryl hydrocarbon receptor is required for developmental closure of the ductus venosus in the neonatal mouse. Mol Pharmacol 67:714-720.

Lee DH, Lee IK, Porta M, Steffes M, Jacobs DR, Jr. 2007. Relationship between serum concentrations of persistent organic pollutants and the prevalence of metabolic syndrome among non-diabetic adults: Results from the national health and nutrition examination survey 1999-2002. Diabetologia 50:1841-1851.

Leng L, Chen X, Li CP, Luo XY, Tang NJ. 2014. 2,3,7,8-tetrachlorodibezo-p-dioxin exposure and prostate cancer: A meta-analysis of cohort studies. Public Health 128:207-213.

Logan RW, Robledo RF, Recla JM, Philip VM, Bubier JA, Jay JJ, et al. 2013. High-precision genetic mapping of behavioral traits in the diversity outbred mouse population. Genes Brain Behav 12:424-437.

Lu H, Crawford RB, North CM, Kaplan BL, Kaminski NE. 2009. Establishment of an immunoglobulin m antibody-forming cell response model for characterizing immunotoxicity in primary human b cells. Toxicol Sci 112:363-373.

Lu H, Crawford RB, Suarez-Martinez JE, Kaplan BL, Kaminski NE. 2010. Induction of the aryl hydrocarbon receptor-responsive genes and modulation of the immunoglobulin m response by 2,3,7,8-tetrachlorodibenzo-p-dioxin in primary human b cells. Toxicol Sci 118:86-97.

Lu H, Crawford RB, Kaplan BL, Kaminski NE. 2011. 2,3,7,8-tetrachlorodibenzo-p-dioxin-mediated disruption of the cd40 ligand-induced activation of primary human b cells. Toxicol Appl Pharmacol 255:251-260.

Martelli A, Mattioli F, Angiola M, Reimann R, Brambilla G. 2003. Species, sex and inter-individual differences in DNA repair induced by nine sex steroids in primary cultures of rat and human hepatocytes. Mutat Res 536:69-78.

Martinez JM, Afshari CA, Bushel PR, Masuda A, Takahashi T, Walker NJ. 2002. Differential toxicogenomic responses to 2,3,7,8-tetrachlorodibenzo-p-dioxin in malignant and nonmalignant human airway epithelial cells. Toxicol Sci 69:409-423.

McIntosh BE, Hogenesch JB, Bradfield CA. 2010. Mammalian per-arnt-sim proteins in environmental adaptation. Annu Rev Physiol 72:625-645.

McKee M. 2009. The poisoning of victor yushchenko. Lancet 374:1131-1132.

Meyer BK, Perdew GH. 1999. Characterization of the ahr-hsp90-xap2 core complex and the role of the immunophilin-related protein xap2 in ahr stabilization. Biochemistry 38:8907-8917.

Morgan AP, Didion JP, Doran AG, Holt JM, McMillan L, Keane TM, et al. 2016. Whole genome sequence of two wild-derived mus musculus domesticus inbred strains, lewes/eij and zalende/eij, with different diploid numbers. G3 (Bethesda) 6:4211-4216.

Moura-Alves P, Fae K, Houthuys E, Dorhoi A, Kreuchwig A, Furkert J, et al. 2014. Ahr sensing of bacterial pigments regulates antibacterial defence. Nature 512:387-392.

Nashef A, Abu-Toamih Atamni HJ, Buchnik Y, Hasturk H, Kantarci A, Stephens D, et al. 2017. Collaborative cross mouse population for studying the alveolar bone changes and impaired glucose tolerance comorbidity after high fat diet consumption. J Periodontol:1-14.

Nault R, Fader KA, Ammendolia DA, Dornbos P, Potter D, Sharratt B, et al. 2016. Dose-dependent metabolic reprogramming and differential gene expression in tcdd-elicited hepatic fibrosis. Toxicol Sci 154:253-266.

NRC. 2009. Science and decisions: Advancing risk assessment. In: Science and decisions: Advancing risk assessment. Washington DC:2009 by the National Academy of Sciences.

O'Brien TR, Decoufle P, Boyle CA. 1991. Non-hodgkin's lymphoma in a cohort of vietnam veterans. Am J Public Health 81:758-760.

Okey AB, Vella LM, Harper PA. 1989. Detection and characterization of a low affinity form of cytosolic ah receptor in livers of mice nonresponsive to induction of cytochrome p1-450 by 3-methylcholanthrene. Mol Pharmacol 35:823-830.

Okey AB. 2007. An aryl hydrocarbon receptor odyssey to the shores of toxicology: The deichmann lecture, international congress of toxicology-xi. Toxicol Sci 98:5-38.

Paustenbach DJ, Wenning RJ, Lau V, Harrington NW, Rennix DK, Parsons AH. 1992. Recent developments on the hazards posed by 2,3,7,8-tetrachlorodibenzo-p-dioxin in soil: Implications for setting risk-based cleanup levels at residential and industrial sites. J Toxicol Environ Health 36:103-149.

Petrulis JR, Perdew GH. 2002. The role of chaperone proteins in the aryl hydrocarbon receptor core complex. Chem Biol Interact 141:25-40.

Phadnis-Moghe AS, Crawford RB, Kaminski NE. 2015. Suppression of human b cell activation by 2,3,7,8-tetrachlorodibenzo-p-dioxin involves altered regulation of b cell lymphoma-6. Toxicol Sci 144:39-50.

Phadnis-Moghe AS, Kaminski NE. 2017. Immunotoxicity testing using human primary leukocytes: An adjunct approach for the evaluation of human risk. Current Opinion in Toxicology 3:25-29.

Pirkle JL, Wolfe WH, Patterson DG, Needham LL, Michalek JE, Miner JC, et al. 1989. Estimates of the half-life of 2,3,7,8-tetrachlorodibenzo-p-dioxin in vietnam veterans of operation ranch hand. J Toxicol Environ Health 27:165-171.

Poland A, Glover E. 1990. Characterization and strain distribution pattern of the murine ah receptor specified by the ahd and ahb-3 alleles. Mol Pharmacol 38:306-312.

Poland A, Palen D, Glover E. 1994. Analysis of the four alleles of the murine aryl hydrocarbon receptor. Mol Pharmacol 46:915-921.

Powell-Coffman JA, Bradfield CA, Wood WB. 1998. Caenorhabditis elegans orthologs of the aryl hydrocarbon receptor and its heterodimerization partner the aryl hydrocarbon receptor nuclear translocator. Proc Natl Acad Sci U S A 95:2844-2849.

Puga A, Maier A, Medvedovic M. 2000. The transcriptional signature of dioxin in human hepatoma hepg2 cells. Biochem Pharmacol 60:1129-1142.

Quintana FJ, Basso AS, Iglesias AH, Korn T, Farez MF, Bettelli E, et al. 2008. Control of t(reg) and t(h)17 cell differentiation by the aryl hydrocarbon receptor. Nature 453:65-71.

Rannug A, Fritsche E. 2006. The aryl hydrocarbon receptor and light. Biol Chem 387:1149-1157.

Roberts A, Pardo-Manuel de Villena F, Wang W, McMillan L, Threadgill DW. 2007. The polymorphism architecture of mouse genetic resources elucidated using genome-wide resequencing data: Implications for qtl discovery and systems genetics. Mamm Genome 18:473-481.

Rusyn I, Gatti DM, Wiltshire T, Kleeberger SR, Threadgill DW. 2010. Toxicogenetics: Population-based testing of drug and chemical safety in mouse models. Pharmacogenomics 11:1127-1136.

Schecter A, Ryan JJ. 1988. Polychlorinated dibenzo-para-dioxin and dibenzofuran levels in human adipose tissues from workers 32 years after occupational exposure to 2,3,7,8-tcdd. Chemosphere 17:915-920.

Schuetz EG, Schuetz JD, Thompson MT, Fisher RA, Madariage JR, Strom SC. 1995. Phenotypic variability in induction of p-glycoprotein mrna by aromatic hydrocarbons in primary human hepatocytes. Mol Carcinog 12:61-65.

Shen ES, Gutman SI, Olson JR. 1991. Comparison of 2,3,7,8-tetrachlorodibenzo-p-dioxin-mediated hepatotoxicity in c57bl/6j and dba/2j mice. J Toxicol Environ Health 32:367-381.

Sinal CJ, Bend JR. 1997. Aryl hydrocarbon receptor-dependent induction of cyp1a1 by bilirubin in mouse hepatoma hepa 1c1c7 cells. Mol Pharmacol 52:590-599.

Smart J, Daly AK. 2000. Variation in induced cyp1a1 levels: Relationship to cyp1a1, ah receptor and gstm1 polymorphisms. Pharmacogenetics 10:11-24.

Smith CM, Proulx MK, Olive AJ, Laddy D, Mishra BB, Moss C, et al. 2016. Tuberculosis susceptibility and vaccine protection are independently controlled by host genotype. MBio 7.

Sorg O, Zennegg M, Schmid P, Fedosyuk R, Valikhnovskyi R, Gaide O, et al. 2009. 2,3,7,8-tetrachlorodibenzo-p-dioxin (tcdd) poisoning in victor yushchenko: Identification and measurement of tcdd metabolites. Lancet 374:1179-1185.

Sorg O. 2014. Ahr signalling and dioxin toxicity. Toxicol Lett 230:225-233.

Srogi K. 2008. Levels and congener distributions of pcdds, pcdfs and dioxin-like pcbs in environmental and human samples: A review. Environ Chem Lett 6:1-28.

Svenson KL, Gatti DM, Valdar W, Welsh CE, Cheng R, Chesler EJ, et al. 2012. High-resolution genetic mapping using the mouse diversity outbred population. Genetics 190:437-447.

Swanson HI, Chan WK, Bradfield CA. 1995. DNA binding specificities and pairing rules of the ah receptor, arnt, and sim proteins. J Biol Chem 270:26292-26302.

Taylor KW, Novak RF, Anderson HA, Birnbaum LS, Blystone C, Devito M, et al. 2013. Evaluation of the association between persistent organic pollutants (pops) and diabetes in epidemiological studies: A national toxicology program workshop review. Environ Health Perspect 121:774-783.

Thomas RS, Penn SG, Holden K, Bradfield CA, Rank DR. 2002. Sequence variation and phylogenetic history of the mouse ahr gene. Pharmacogenetics 12:151-163.

Threadgill DW, Miller DR, Churchill GA, de Villena FP. 2011. The collaborative cross: A recombinant inbred mouse population for the systems genetic era. Ilar j 52:24-31.

Threadgill DW, Churchill GA. 2012. Ten years of the collaborative cross. G3 (Bethesda) 2:153-156.

Thurmond TS, Silverstone AE, Baggs RB, Quimby FW, Staples JE, Gasiewicz TA. 1999. A chimeric aryl hydrocarbon receptor knockout mouse model indicates that aryl hydrocarbon receptor activation in hematopoietic cells contributes to the hepatic lesions induced by 2,3,7, 8-tetrachlorodibenzo-p-dioxin. Toxicol Appl Pharmacol 158:33-40.

Venkatratnam A, Furuya S, Kosyk O, Gold A, Bodnar W, Konganti K, et al. 2017. Collaborative cross mouse population enables refinements to characterization of the variability in toxicokinetics of trichloroethylene and provides genetic evidence for the role of ppar pathway in its oxidative metabolism. Toxicol Sci.

Warner M, Mocarelli P, Brambilla P, Wesselink A, Samuels S, Signorini S, et al. 2013. Diabetes, metabolic syndrome, and obesity in relation to serum dioxin concentrations: The seveso women's health study. Environ Health Perspect 121:906-911.

Watters JW, Kraja A, Meucci MA, Province MA, McLeod HL. 2004. Genome-wide discovery of loci influencing chemotherapy cytotoxicity. Proc Natl Acad Sci U S A 101:11809-11814.

Welsh CE, Miller DR, Manly KF, Wang J, McMillan L, Morahan G, et al. 2012. Status and access to the collaborative cross population. Mamm Genome 23:706-712.

Wetmore BA, Allen B, Clewell HJ, 3rd, Parker T, Wambaugh JF, Almond LM, et al. 2014. Incorporating population variability and susceptible subpopulations into dosimetry for high-throughput toxicity testing. Toxicol Sci 142:210-224.

Wong JM, Okey AB, Harper PA. 2001. Human aryl hydrocarbon receptor polymorphisms that result in loss of cyp1a1 induction. Biochem Biophys Res Commun 288:990-996.

Xue J, Schoenrock SA, Valdar W, Tarantino LM, Ideraabdullah FY. 2016. Maternal vitamin d depletion alters DNA methylation at imprinted loci in multiple generations. Clin Epigenetics 8:107.

Yu X, Kubota T, Dhakal I, Hasegawa S, Williams S, Ozawa S, et al. 2013. Copy number variation in sulfotransferase isoform 1a1 (sult1a1) is significantly associated with enzymatic activity in japanese subjects. Pharmgenomics Pers Med 6:19-24.

Zeise L, Bois FY, Chiu WA, Hattis D, Rusyn I, Guyton KZ. 2013. Addressing human variability in next-generation human health risk assessments of environmental chemicals. Environ Health Perspect 121:23-31.

Chapter 2: The Influence of Human Interindividual Variability on the Low-dose Region of Dose-Response Curve Induced by 2,3,7,8-Tetrachlorodibenzo-*p*-dioxin in Primary B Cells

This chapter is an edited version of a previously published research article in *Toxicological Sciences*, Volume 153, No. 2: pages 352-360.

Authors: Peter Dornbos[1,2], Robert B. Crawford[3], Norbert E. Kaminski[2,3], Sarah L. Hession[4], and John J. LaPres[1,2]

Affiliations: [1]Department of Biochemistry and Molecular Biology; [2]Institute for Integrative Toxicology; [3]Department of Pharmacology and Toxicology; [4]Center for Statistical Training and Consulting, Michigan State University, East Lansing, MI 48824

2.1. Abstract

The influence of interindividual variability is not typically assessed in traditional toxicological studies. Given that chemical exposures occur in heterogeneous populations, this knowledge gap has the potential to cause undue harm within the realms of public health and industrial and municipal finances. A recent report from the National Research Council (NRC) suggests that, when accounting for interindividual variation in responses, traditionally assumed nonlinear dose-response relationships (DRRs) for non-cancer causing endpoints would better be explained with a linear relationship within the low-dose region. To directly test the NRC's assumption, this study focused on assessing the DRR between 2,3,7,8-tetracholorodibenzo-*p*-dioxin (TCDD) exposure and immune suppression in a cohort of unique human donors. Human B cells were isolated from 51 individual donors and treated with increasing concentrations of TCDD (0 through 30 nM TCDD). Two endpoints sensitive to TCDD were assessed: 1) number of Immunoglobulin-M (IgM) secreting B cells and 2) quantity of IgM secreted. The results show that TCDD significantly suppressed both the number of IgM secreting cells and the quantity of IgM secreted. Statistical model comparisons indicate that the low-dose region of the two DRRs is best explained with a nonlinear relationship. Rather than assuming low-dose linearity for all non-cancer causing DRRs, our study suggests the need to consider the specific mode-of-action of toxicants and pharmaceuticals during risk-management decision-making.

2.2. Introduction

The B cell has been well-established as a sensitive target of TCDD-induced toxicity. Briefly, the mammalian immune system consists of two branches: 1) the innate immune system and 2) the adaptive immune system. The primary difference between these branches are within specificity of response; the innate response is a non-specific defense while the adaptive response is specific against an antigen presented. The specificity of the adaptive immune response relies on the production of antibodies, known as immunoglobulins (Ig), which are produced by the B cell.

B cell antibody secretion is initiated through ligation with surface proteins, including the B cell, CD40, and various cytokine receptors. Ligation of these receptors drive the B cell to proliferate and differentiate into an antibody secreting plasma cell. While there are five independent Ig isotypes in mammals, the first wave of the humoral antibody response is release of IgM. TCDD exposures have been found to directly suppress the Immunoglobulin-M (IgM) response of the B cell. More specifically, *in vitro* exposures have shown that, with increasing concentrations of TCDD, there are significant reductions in the number of B cells that secrete IgM and the concentrations of IgM secreted into culture media (Crawford et al. 2003; Sulentic et al. 1998). While much of the current understanding of TCDD-induced B cell dysfunction has been derived from mouse studies and murine cell lines, recent publications using primary cells have confirmed that TCDD suppresses the activation and differentiation of human B cells *in vitro* (Lu et al. 2010; Lu et al. 2011; Phadnis-Moghe et al. 2015).

The level of TCDD-mediated impairment of the IgM response in human B cells has been shown to vary across individuals. More specifically, previous reports have shown that a subset of the human population's B cell response is non-responsive to increasing concentrations of TCDD (Lu *et al*., 2010). However, much remains unknown in regards to range of interindividual

responses to TCDD as well as the influence that interindividual variability plays within the population-level dose response. The primary aim of this study was to better characterize the influence of human interindividual variability within the TCDD-mediated suppression of the B cell. B cells were isolated from a large number of human donors (n=51) and activated with CD40-ligand in the presence of increasing concentrations of TCDD. Two TCDD-sensitive endpoints were analyzed: 1) the number cells secreting IgM and 2) the amount of IgM secreted during the period of culture (Lu *et al.*, 2010; Crawford *et al.*, 2003). The results from the endpoints were statistically modeled at the individual level and as an averaged population to address the influence of increasing interindividual variability in the shape of a DRR. As receptor-mediated processes contain thresholds prior to receptor saturation (Kenakin 2004), an AHR-mediated response serves as an excellent platform in assessing whether variation within individual DRRs will linearize the low-dose region of a population-level DRR. Study results were found to directly address the NRC's 'low-dose linearity assumption'.

2.3. Results

2.3.1. TCDD-induced suppression of IgM secretion in human primary B cells

Results from the population of donors assayed indicate a significant reduction in both endpoints tested: a) the number of IgM-secreting cells as determined by ELISPOT ($p \leq 0.05$, n=51; Figure 2.1A) and b) the quantity of secreted IgM in the supernatant at the end of the culture period as determined by ELISA ($p \leq 0.05$, n=49; Figure 2.1B). Notably, statistically significant suppression was found at TCDD levels ≥ 0.3 nM for the number of cells secreting IgM (Figure 2.1A, $p \leq 0.05$, effect size (η^2) = 0.14) and at ≥ 0.01 nM for the quantity of IgM present in the culture supernatant (Figure 2.1B, $p \leq 0.05$, effect size (η^2) = 0.10). There were no significant differences between non-treated CD40 ligand-activated B cells (i.e naïve) and the vehicle (i.e. DMSO-treated) controls for either endpoint.

2.3.2. Variability in IgM response across individuals

A high-degree of interindividual variability was found across individual's response to increasing [TCDD] (Figure 2.2). At 30 nM of TCDD, differences across donors were found to be ≥ 70 fold in the number of cells secreting IgM and ≥ 16 fold for the concentration of IgM in the culture media (Figure 2.2A and 2.2B). Interestingly, 11% (6 of 51) of the donors appeared nonresponsive to TCDD-induced decrease in the number of B cells secreting IgM. This is similar to previously published research (Lu et al. 2010). In contrast to "responsive" donors whose B cells displayed significant suppression at ≥ 0.1 nM, the 'nonresponsive' donors displayed no significant change in response at any TCDD concentration. There is a significant difference in the number of B cell secreting IgM when comparing the 'nonresponsive' and 'responsive' cohorts following exposure to the vehicle control ($p \leq 0.05$)(Figure 2.3A). Such results suggest that the 'nonresponsive' cohort's B cells activate to a lesser degree in the presence of CD40 ligand. In analyzing the concentration of IgM secreted into the media, the number of donors deemed 'nonresponsive' dropped to approximately 8% (4 of 49)(Figure 2.3B). Again, the concentration of

Figure 2.1. TCDD-induced suppression of IgM response in primary human B cells. Increasing levels of TCDD induces a dose-dependent decrease in the number of IgM secreting cells (**A**; n=51) and the concentration of IgM secreted into culture medium (**B**; n=49). Stars (*) indicate a p≤0.05 as compared to the vehicle and error bars indicate standard error of the mean response.

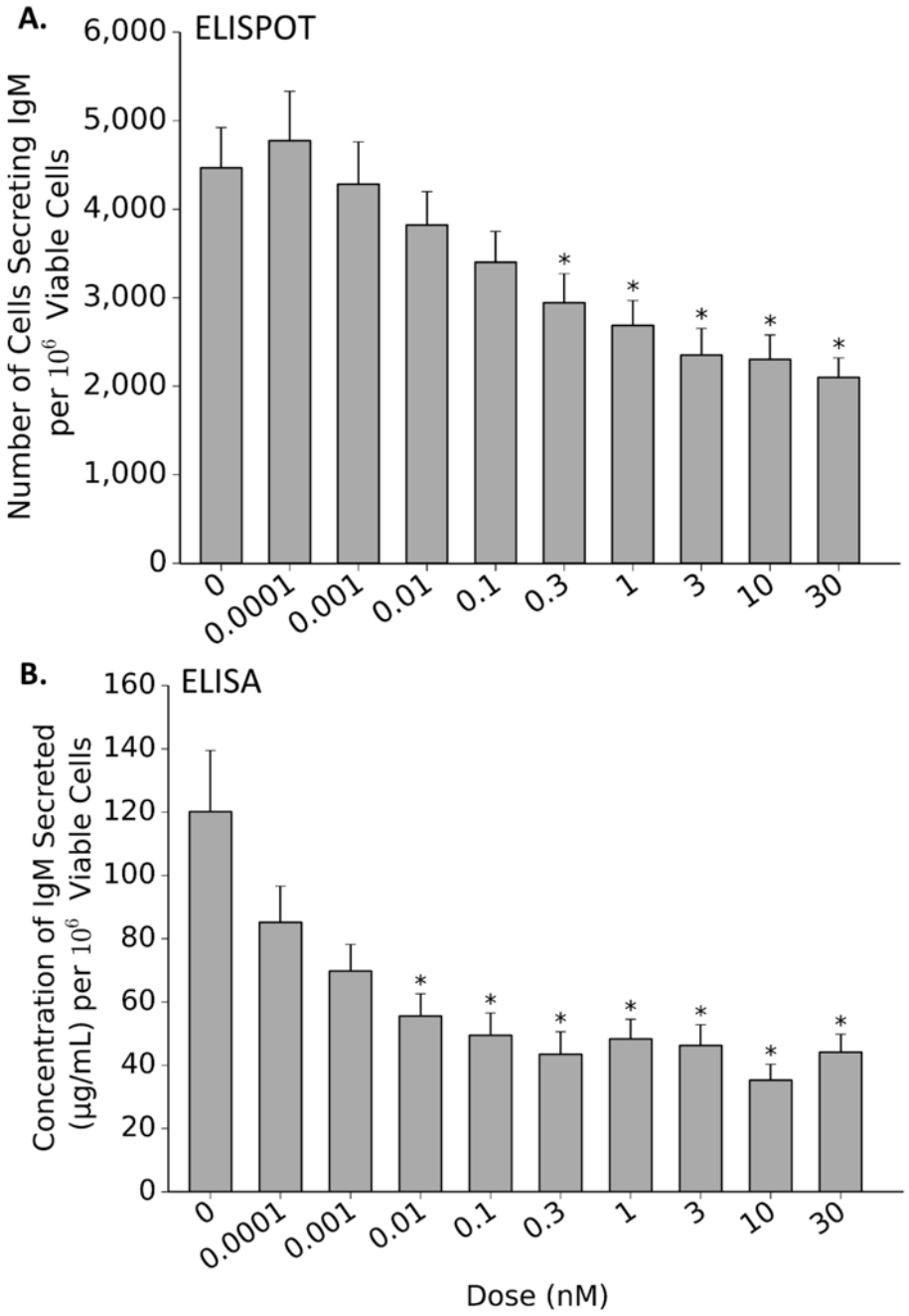

Figure 2.2. Interindividual variability in response to TCDD-induced suppression of IgM secretion. Percent inhibition for each individual donor was calculated by normalizing results from each dose to that individual's vehicle control (100%). The black line indicates the mean response of all donors. Results indicate a large degree of differences amongst individual donor's B cells response to increasing concentrations of TCDD within the number of cells secreting IgM (**A**; ELISPOT data) and the concentration of IgM secreted into the culture media (**B**; ELISA data).

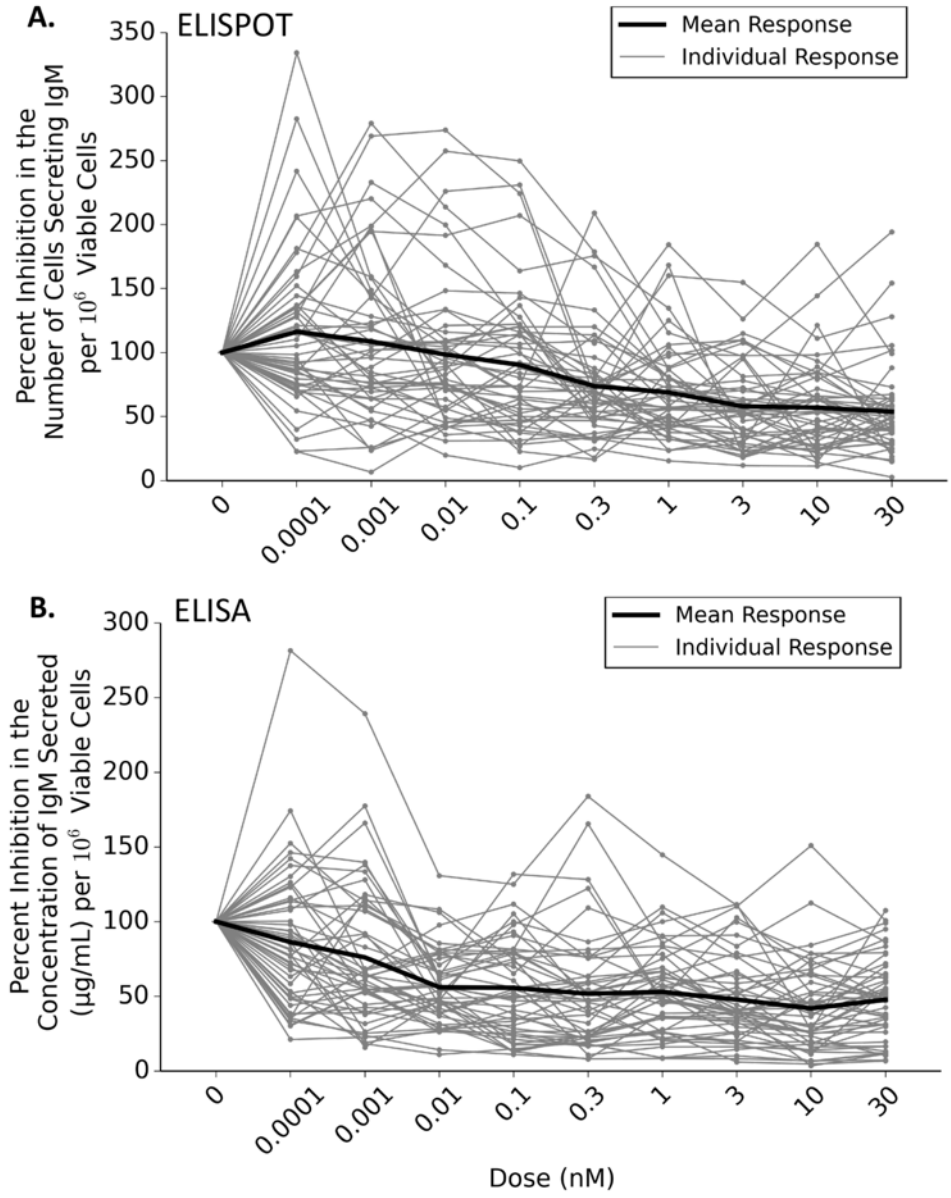

Figure 2.3. Responsive and nonresponsive donors to increasing concentrations of TCDD. Six donors were found to be nonresponsive to TCDD in enumerating the number of cells secreting IgM (**A**; ELISPOT). Nonresponsive donors displayed a significantly decreased number of IgM expressing cells when compared to the mean response of the responsive donors exposed to vehicle control (* indicates a p≤0.05). Four of the six nonresponsive donors identified in the ELISPOT were confirmed in the concentration of IgM secreted (**B**; ELISA). These four nonresponsive donors did not display a significantly decreased IgM in the media when compared to responsive donors exposed to DMSO.

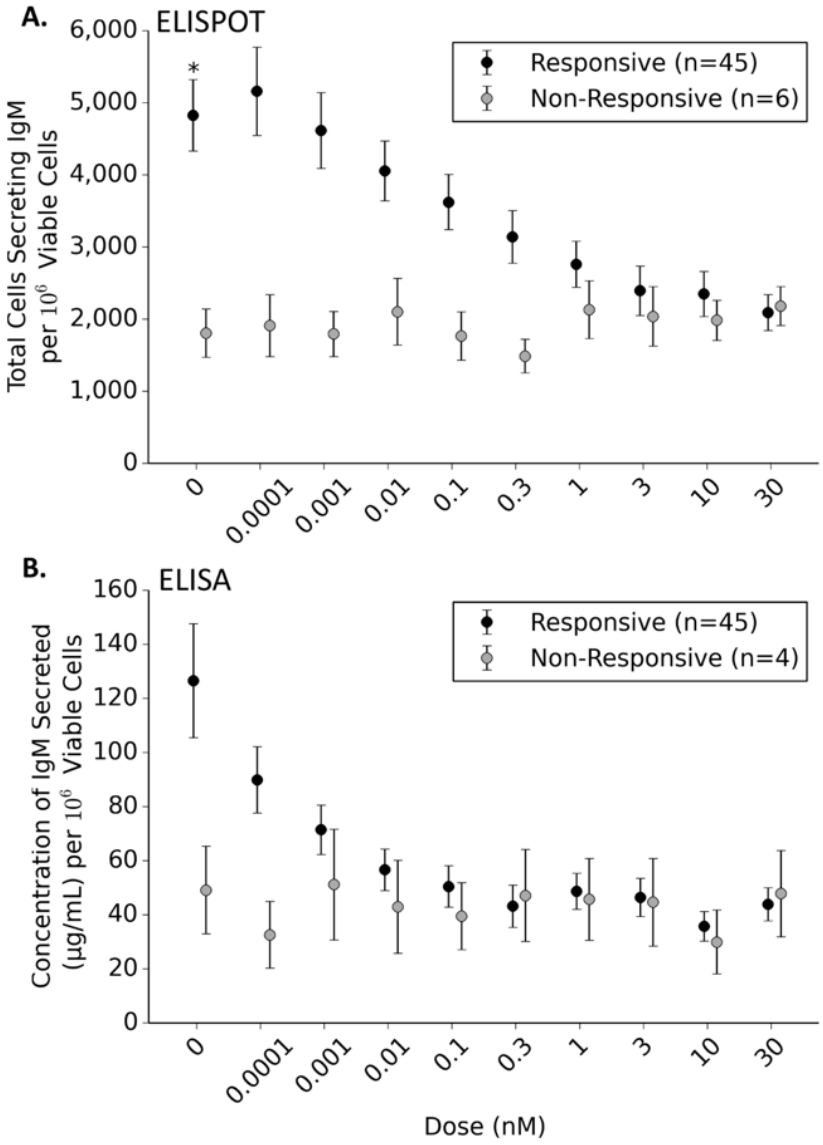

IgM secreted in 'responsive' cohort was found to be statistically lower at [TCDD] ≥ 0.01 while the 'nonresponsive' cohort was not statistically affected by TCDD. Unlike the previous endpoint that showed a statistical difference between the mean numbers of cells secreting IgM exposed to the vehicle control, this endpoint did not have statistical differences in comparing the 'responsive' and 'nonresponsive' cohort. The lack of statistical difference is likely due to lack of statistical power in the 'nonresponsive' cohort (n=4) for this particular endpoint.

2.3.3. Modeling the DRRs of the individual donors

Individual responses for both endpoints were fit to the models available in the BMD software. In all cases during modeling of the individual responses, the best fitting model was chosen by the lowest Akaike Index Criterion (AIC) value (Akaike 1974). For the number of cells secreting IgM (ELISPOT data), most of the individual responses best fit to the Exponential 4 model (29.4% Table 2.1) with a small percentage of donors that were best fit to the linear model (3.9%, Table 2.1). For the quantity of IgM secreted (ELISA data), an equal percentage of individuals best fit to the Hill and Power model (30.6%, Table 2.1) while only a small number of individual donors fit to the linear model (2.0%, Table 2.1). The donors that best fit to linear models were all within the 'nonresponsive' cohorts previously noted. Thus, as expected for a TCDD-induced receptor-mediated response, the vast majority of the individual responses best fit to nonlinear models.

2.3.4. Determining low-dose regions of dose-response relationships

The goal of this study is to determine the shape of the DRR in the low-dose region of a non-cancer DRR. In defining the low-dose region, the DRR of the number of IgM secreting B cells (ELISPOT) and the quantity of IgM secreted (ELISA) data were first fit to a 4-parameter logistic model using maximum likelihood estimation with R code written in-lab (Prentice 1976). Results indicate that the TCDD-induced IC_{50} of the ELISPOT and ELISA data were 0.533 ± 0.954 and

Table 2.1. Results of modeling the individual donor DRRs. Results indicate the majority of the donors fit best to nonlinear models as opposed to the linear model. The results were acquired via the BMD software and were confirmed via maximum likelihood estimation R code written in-lab.

Model Type	Percentage of Individuals	
	ELISPOT (n=51)	ELISA (n=49)
Exponential 4	29.4%	16.3%
Power	17.6%	30.6%
Exponential 2	17.6%	6.1%
Hill	15.7%	30.6%
Polynomial 2°	11.8%	14.3%
Linear	3.9%	2.0%
Exponential 5	3.9%	0%
Exponential 3	0%	0%

0.003 ± 0.007 nM, respectively (Table 2.2). The IC_{50} values were further confirmed by the coefficient estimations from the fitting of the endpoints of interest to the Hill function using the BMD software (Table 2.2). Results were confirmed by visual inspection of a graphical representation of the models overlaying the log-transformed data (Figure 2.4A and 2.4B). The calculated IC_{50} values were used to define the cut-off point for the low-dose region of the DRR. Specifically, all doses below the next available dose of the IC_{50} were considered part of the low-dose region of the curve.

2.3.5. Statistical modeling the low-dose region of a DRR

The low-dose region of the number of B cells secreting IgM (ELISPOT) and the concentration of IgM secreted (ELISA) datasets were fit to the models available in the BMD software to determine the best fitting statistical model. In comparing linear and nonlinear models, our results suggest that the low-dose region of both DRRs were best explained by the power model (Table 2.3). Based on the AIC values of the models available in the BMD software, the linear model was the least adequate in explaining the data (Table 2.4). Results are also presented by overlaying the graphical representation of best-fitting power model and the linear model over the log-transformed response variable further suggesting that the power model fits better to the observed data (Figure 2.5A and 2.5B). The results from the power and linear model of both DRRs were also reverse-transformed to visualize the shape within the low-dose region on a continuous, non-transformed scale (Figure 2.6A and 2.6B).

Table 2.2. Maximum-likelihood estimates of coefficients for the 4-Parameter Logistic and Hill models fit to the log-transformed TCDD-induced DRRs. Results indicate the IC_{50} values for both endpoints measured: 1) the number of cells secreting IgM (ELISPOT) and 2) the concentration of IgM secreted in the culture media (ELISA).

Model Type	Coefficient	ELISPOT Results (n=51)		ELISA Results (n=49)	
		Estimate	Standard Error	Estimate	Standard Error
4-Parameter Logistic $f(x) = d + \frac{a - d}{1 + (\frac{x}{c})^b}$	Upper (d)	3.555	0.037	1.860	0.061
	Lower (a)	3.131	0.137	1.375	0.132
	Slope (b)	-0.409	0.229	-0.275	0.185
	IC_{50} (c)	0.533	0.954	0.004	0.010
Hill Model $f(x) = y + \frac{v * d^n}{k^n + d^n}$	Intercept (y)	3.558	0.036	1.863	0.060
	Slope (v)	-0.431	0.158	-0.477	0.122
	Hill Coefficient (n)	0.415	0.227	0.286	0.165
	IC_{50} (k)	0.555	0.984	0.003	0.006

Figure 2.4. Graphical representation of the statistical models used to calculate the IC_{50}. Graphs indicate the 4-parameter and hill model estimations used to calculate the IC_{50} for two endpoints of interest adequately fit the observed means of the number of cells secreting IgM (**A**; ELISPOT data) and the concentration of IgM secreted into the culture media (**B**; ELISA data). Graphed models and observed means are plotted as an overlay over a scatterplot of the raw log-transformed data for each individual.

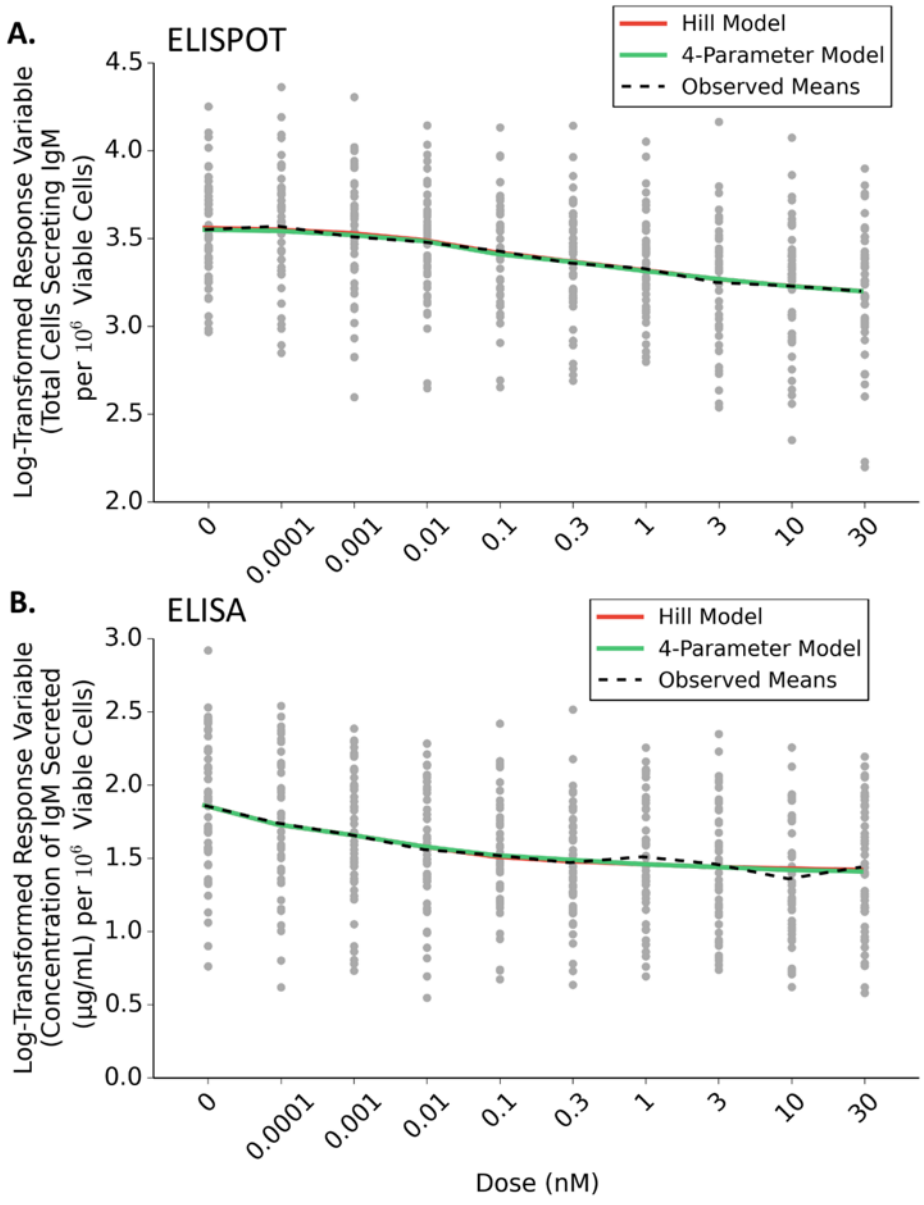

Table 2.3. Coefficient estimates and Akaike Criterion results of the low-dose regions of the log-transformed response variables. Table indicates the model fit, coefficient estimates, and the AIC values of the TCDD-induced DRRs of interest suggest that power model best explains the low-dose region of the DRRs of interest: 1) number of B cells secreting IgM (ELISPOT) and 2) the concentration of IgM secreted into culture media (ELISA). All results were derived using the BMD software. All coefficient estimates were confirmed via maximum likelihood estimation R code written in-lab.

Model Type	Coefficient	ELISPOT Results (n=51)		ELISA Results (n=49)	
		Estimate	Standard Error	Estimate	Standard Error
Linear Model $f(x) = \beta_0 + (\beta_1 * x)$	Intercept	3.502	0.019	1.763	0.038
	Slope	-0.199	0.049	-20.912	7.544
	Akaike Criterion	-463.96		-117.1	
Power Model $f(x) = \beta_0 + (\beta_1 * x^n)$	Intercept	3.565	0.036	1.860	0.062
	Slope	-0.245	0.049	-0.704	0.435
	Power	-0.242	0.103	0.186	0.118
	Akaike Criterion	-470.6		-119.8	

Table 2.4. The AIC values from fitting dataset to all available models in the BMD software. Table indicates the AIC values of fitting each model available in the BMD software to the low-dose regions of the two endpoints of interest: 1) number of B cells secreting IgM and the (ELISPOT data) and 2) the concentration of IgM secreted during the period of culture (ELISA data). Results suggest that the power model best fits the data.

Model Type	ELISPOT (n=51)	ELISA (n=49)
Power	-470.36	-119.82
Exponential 4	-469.56	-118.54
Exponential 5	-469.56	-118.57
Polynomial 2	-468.83	-118.33
Hill	-467.33	-117.82
Exponential 2	-464.10	-117.64
Exponential 3	-464.10	-117.64
Linear	-463.96	-117.62

Figure 2.5. Statistical models fit to the low-dose region of TCDD-induced dose-response relationship. Graphs indicate the estimated fit of the power model better explains the low-dose region of the DRRs as opposed to the linear model of the two endpoints of interest: the number of B cells secreting IgM (**A**) and the concentration of IgM secreted during the period of culture (**B**). Graphed models along with the observed means were plotted as an overlay over a scatterplot of the raw log-transformed data for each individual.

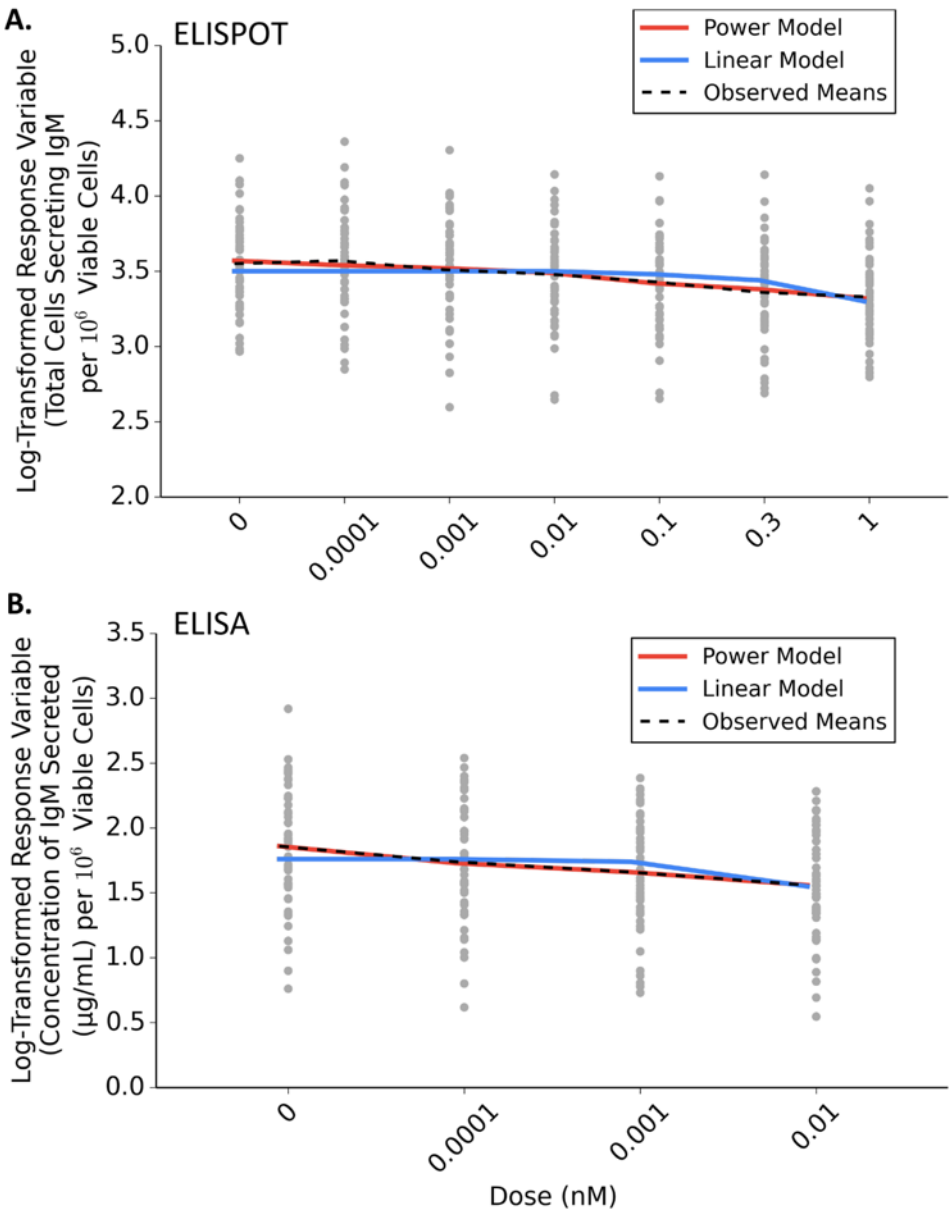

Figure 2.6. Reverse Log-transformed Model Results on Continuous, Non-transformed Scale. Graphs indicate that the observed means are best fit by a nonlinear model as compared to a linear model for the TCDD-induced DRRs of interest: the number of cells secreting IgM (**A**; ELISPOT data) and the concentration of IgM secreted into the culture media (**B**; ELISA data).

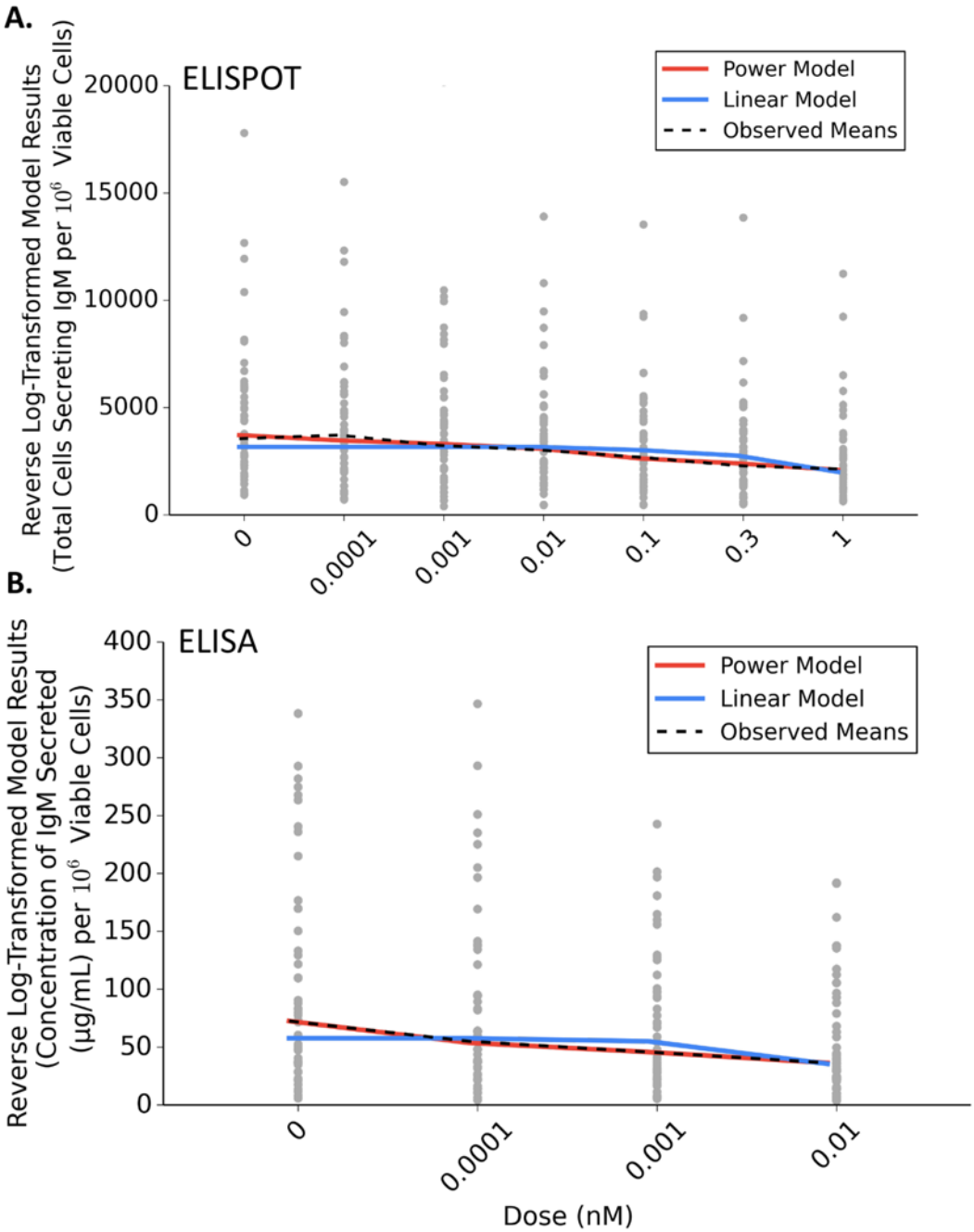

2.4. Discussion

In a recent report entitled “Science and Decisions: Advancing Risk Assessment,” the NRC suggested that, during risk-management decision-making, the low-dose region of non-cancer DRRs should be assumed as linear without the presence of thresholds. As reviewed by Rhomberg et al. in 2011, the NRC has based their assumption on three primary arguments: 1) the ‘additivity to background argument’ that indicates that increasing exposure to chemicals will lead to linear increases of response over the spontaneous background levels in a population; 2) the ‘population heterogeneity argument’ that suggests that, regardless of the shape of the individual DRRs, the dose-response curve will linearize when incorporating the interindividual variability of the human population; and 3) the ‘epidemiological evidence argument’ which cites epidemiological studies that have suggested a no-threshold response to increasing exposures (NRC 2009; Rhomberg 2011; White et al. 2009). The focus of this report is on the argument regarding population heterogeneity. Notably, as toxicological studies often focus on mechanistic details in single cell lines or inbred mouse strains, there is little data to inform on the influence of population heterogeneity on the shape of DRRs (Rhomberg 2011). The NRC did not evaluate the potential effect of population heterogeneity with adequate peer-reviewed datasets (NRC 2009). Foremost, the NRC’s assumption generalizes the shape of the low-dose region for all chemical exposures; however, as chemicals have different modes of action, it is unlikely that all chemically affected biological processes, such as receptor-mediated events, will result in a linear low-dose region (Bogen 2015). Given the potential risks associated with invalid assumptions in regards to the low-dose regions of non-cancer DRRs, such as unsafe exposures in susceptible individuals and financial burden associated with the chemical monitoring and cleanup, the NRC’s assumption warrants further scrutiny and evaluation.

Receptor mediated responses, from a biochemical standpoint, are a nonlinear signaling process that contain thresholds (i.e. receptor saturation); such processes are traditionally

modeled with a sigmoidal, Hill model (Kenakin 2004). The nonlinear nature of receptor-mediated events provides an excellent platform to determine whether individual nonlinear responses will linearize in the low-dose region of a DRR when human interindividual variability is considered. In this study, we used AHR-mediated suppression of the IgM response of CD40L-activated human primary B cells to model the effect of increasing interindividual variability. Two endpoints of interest were measured following a 7-day exposure period: 1) the number of IgM secreting cells and 2) the quantity of IgM secreted into the culture media. These two endpoints displayed concentration-dependent suppression of B cell function following TCDD treatment ($p \leq 0.05$)(Figure 2.1A and 2.1B). The results are in accordance with a previous report showing that TCDD significantly suppresses the number of cells secreting IgM (Lu et al. 2011). As determined by maximum likelihood-estimation, the IC_{50} for TCDD was found to differ over 150 fold between the two endpoints: 1) 0.533 ± 0.954 nM for the number of B cells secreting IgM and 2) 0.003 ± 0.007 nM for the quantity of IgM secreted (Table 2.2). Such results suggest that the endpoint measuring TCDD-induced suppression of IgM secreted by human B cells is more sensitive when compared to the decrease in IgM-secreting B cells. Notably, the disassociation constant (K_d) of the human AHR with TCDD is estimated between 1 and 12 nM and is dependent on the individual donor's AHRs that were tested (Ema et al. 1994; Harper et al. 2002; Lorenzen and Okey 1991). The IC_{50} found for the concentration of IgM secreted into culture media in this study is well below the K_d of the human AHR. Such results suggest that very little AHR activation is required to see a robust response in the concentration of IgM secreted from human B cells.

As previously mentioned, variability in the sensitivity of individual's AHR-induction by TCDD suggest that some individuals are more susceptible to TCDD-induced toxicity (Harper et al. 2002; Lorenzen and Okey 1991). Given that the AHR mediates most of the TCDD-induced toxic responses and as polymorphisms in differing mouse strains affect sensitivity to TCDD, polymorphisms in the human AHR gene have been postulated to play a role in the interindividual

variability in responses to TCDD (Okey et al. 2005; Okey 2007). A previous report suggested that some human donors did not have B cells that responded to increasing concentrations of TCDD and this might be due to polymorphisms found in the transactivation domain of the AHR of these 'nonresponsive' individuals (Harper et al. 2002; Lu et al. 2010). Similarly, a cohort of 6 'nonresponsive' donors appears to be activated to a lesser degree than the cohort of 'responsive' donors in the present study (Figure 2.3A). We hypothesize that the lack of response in the number of cells secreting IgM to TCDD is due to a lesser degree of CD40L-mediated activation of the B cells from these individuals as the number of cells secreting IgM was significantly decreased in these donors. Differences in CD40L-activation amongst our cohort of donors may be due to a plethora of reasons including polymorphisms within CD40 receptor gene, previous and present exposures, infections, inflammation, and many other factors of which we are unable to gather information due to the anonymity of blood donation (Blanco-Kelly et al. 2010; Jacobson et al. 2005; Orozco et al. 2010; Raychaudhuri et al. 2008; Teruel et al. 2012). Surprisingly, 2 of the 6 'nonresponsive' donors were deemed 'responsive' in assaying the concentration of IgM secreted into the media (i.e. ELISA; Figure 2.3B). Thus, even with a seemingly lesser number of cells secreting IgM, the concentration of IgM secreted is still affected by increasing [TCDD]. Such results may be confounded as the ELISA is measuring the concentration of IgM being secreted over the seven-day period of exposure while the ELISPOT enumerates the absolute number of cells secreting IgM at a specific time following exposure. Furthermore, these results suggest that, along with the IC_{50} values, the colorimetric ELISA is a more sensitive measure of the IgM response from activated B cells as compared to enumerating the number of IgM secreting cells by ELISPOT.

The low-dose regions of the two dose response curves were fit to all models available in the BMD software and comparison metrics were used to assess goodness of fit. Our results indicate that the low-dose region of the TCDD-induced DRR for both endpoints of interest fit better

to the power model as compared to the linear model (Table 3.3, Figure 3.5A and 3.5B). As such, a nonlinear relationship best describes the low-dose region. To our knowledge, this is the largest study using unique donors to assess the effect of human interindividual variability within the low-dose region of a DRR. Based on the DRR data collected from this cohort, our statistical models of best fit to the low-dose region of these DRRs are contrary to the assumptions made by the NRC (NRC 2009). However, we do acknowledge that our sample set of 51 unique donors does not model the genetic diversity in the human population and further studies are needed to definitively test the NRC's assumption. This present study, however, makes significant steps towards better risk-management decision-making in regards to the effect of interindividual variability within TCDD-mediated endpoints as well as other receptor-mediated responses. The results of this study are also contrary to the adoption of a generalized model for linear low-dose effects in all non-cancer endpoints as suggested by the NRC. Our results provide evidence that some chemical exposures, such as receptor-mediated toxicants, elicit non-linear responses in the low-dose region of DRRs. Finally, the results from this study indicate a large range in individual's susceptibility to TCDD-induced toxicity.

REFERENCES

REFERENCES

Akaike H. 1974. A new look at the statistical model identification. Automatic Control, IEEE Transactions on 19:716-723.

Blanco-Kelly F, Matesanz F, Alcina A, Teruel M, Diaz-Gallo LM, Gomez-Garcia M, et al. 2010. Cd40: Novel association with crohn's disease and replication in multiple sclerosis susceptibility. PLoS One 5:e11520.

Bogen KT. 2015. Linear-no-threshold default assumptions for noncancer and nongenotoxic cancer risks: A mathematical and biological critique. Risk Anal.

Crawford RB, Sulentic CE, Yoo BS, Kaminski NE. 2003. 2,3,7,8-tetrachlorodibenzo-p-dioxin (tcdd) alters the regulation and posttranslational modification of p27kip1 in lipopolysaccharide-activated b cells. Toxicol Sci 75:333-342.

Ema M, Ohe N, Suzuki M, Mimura J, Sogawa K, Ikawa S, et al. 1994. Dioxin binding activities of polymorphic forms of mouse and human arylhydrocarbon receptors. J Biol Chem 269:27337-27343.

Harper PA, Wong J, Lam MS, Okey AB. 2002. Polymorphisms in the human ah receptor. Chem Biol Interact 141:161-187.

Jacobson EM, Concepcion E, Oashi T, Tomer Y. 2005. A graves' disease-associated kozak sequence single-nucleotide polymorphism enhances the efficiency of cd40 gene translation: A case for translational pathophysiology. Endocrinology 146:2684-2691.

Kenakin T. 2004. Principles: Receptor theory in pharmacology. Trends Pharmacol Sci 25:186-192.

Lorenzen A, Okey AB. 1991. Detection and characterization of ah receptor in tissue and cells from human tonsils. Toxicol Appl Pharmacol 107:203-214.

Lu H, Crawford RB, Suarez-Martinez JE, Kaplan BL, Kaminski NE. 2010. Induction of the aryl hydrocarbon receptor-responsive genes and modulation of the immunoglobulin m response by 2,3,7,8-tetrachlorodibenzo-p-dioxin in primary human b cells. Toxicol Sci 118:86-97.

Lu H, Crawford RB, Kaplan BL, Kaminski NE. 2011. 2,3,7,8-tetrachlorodibenzo-p-dioxin-mediated disruption of the cd40 ligand-induced activation of primary human b cells. Toxicol Appl Pharmacol 255:251-260.

NRC. 2009. Science and decisions: Advancing risk assessment. In: Science and decisions: Advancing risk assessment. Washington DC:2009 by the National Academy of Sciences.

Okey AB, Franc MA, Moffat ID, Tijet N, Boutros PC, Korkalainen M, et al. 2005. Toxicological implications of polymorphisms in receptors for xenobiotic chemicals: The case of the aryl hydrocarbon receptor. Toxicol Appl Pharmacol 207:43-51.

Okey AB. 2007. An aryl hydrocarbon receptor odyssey to the shores of toxicology: The deichmann lecture, international congress of toxicology-xi. Toxicol Sci 98:5-38.

Orozco G, Eyre S, Hinks A, Ke X, Wilson AG, Bax DE, et al. 2010. Association of cd40 with rheumatoid arthritis confirmed in a large uk case-control study. Ann Rheum Dis 69:813-816.

Phadnis-Moghe AS, Crawford RB, Kaminski NE. 2015. Suppression of human b cell activation by 2,3,7,8-tetrachlorodibenzo-p-dioxin involves altered regulation of b cell lymphoma-6. Toxicol Sci 144:39-50.

Prentice RL. 1976. A generalization of the probit and logit methods for dose response curves. Biometrics 32:761-768.

Raychaudhuri S, Remmers EF, Lee AT, Hackett R, Guiducci C, Burtt NP, et al. 2008. Common variants at cd40 and other loci confer risk of rheumatoid arthritis. Nat Genet 40:1216-1223.

Rhomberg LR. 2011. Practical risk assessment and management issues arising were we to adopt low-dose linearity for all endpoints. Dose Response 9:144-157.

Sulentic CE, Holsapple MP, Kaminski NE. 1998. Aryl hydrocarbon receptor-dependent suppression by 2,3,7, 8-tetrachlorodibenzo-p-dioxin of igm secretion in activated b cells. Mol Pharmacol 53:623-629.

Teruel M, Simeon CP, Broen J, Vonk MC, Carreira P, Camps MT, et al. 2012. Analysis of the association between cd40 and cd40 ligand polymorphisms and systemic sclerosis. Arthritis Res Ther 14:R154.

White RH, Cote I, Zeise L, Fox M, Dominici F, Burke TA, et al. 2009. State-of-the-science workshop report: Issues and approaches in low-dose-response extrapolation for environmental health risk assessment. Environ Health Perspect 117:283-287.

Chapter 3: *Serpinb2* as a genetic modulator of TCDD-mediated suppression of the B cell.

This chapter is an edited version of an article currently under review at *Chemical Research in Toxicology.*

Authors: Peter Dornbos[1,2], Melanie Warren[3], Robert B. Crawford[4], Norbert E. Kaminski[2,4], David W. Threadgill[3], John J. LaPres[1,2]

Affiliations: [1]Department of Biochemistry and Molecular Biology, Michigan State University, East Lansing, MI 48824, [2]Institute for Integrative Toxicology, Michigan State University, East Lansing, MI 48824, [3]Interdisciplinary Program in Toxicology, Texas A&M University, College Station, TX 77843, [4]Department of Pharmacology and Toxicology, Michigan State University, East Lansing, MI 48824

3.1. Abstract

Recent technological advances have indicated that genetic variability can greatly impact interindividual responses to chemical exposures. Previous studies have identified a profound amount of interindividual variability in the 2,3,7,8-tetrachlordibenzo-p-dioxin (TCDD)-mediated immunosuppression in CD40 ligand-activated human B cells. To identify genetic modulators of TCDD response, B cells were isolated from 12 genetically diverse mouse strains, activated with CD40-ligand, and dosed with increasing concentrations of TCDD. Quantitative trait locus analysis implicated a region of mouse Chromosome 1 to be associated with inter-strain differences in TCDD-mediated suppression of the Immunoglobulin-M (IgM) response. Within this locus, *Serpinb2,* which encodes for the serine peptidase inhibitor, clade B, member 2 whose human ortholog is plasminogen activator inhibitor 2 (PAI2), was found to be dysregulated by TCDD at the gene and protein expression level. Furthermore, *Serpinb2*$^{-/-}$ mice were found to be significantly more sensitive to TCDD-mediated suppression in the number of cells secreting IgM as compared to littermate controls. As such, this study not only suggests a protective role of human PAI2 within TCDD-mediated immunosuppression, but also implicates a role for PAI2 in regulating B cell function.

3.2 Introduction

The goal of this aim was to follow-up on the wide-range of responses seen in the study outlined in Chapter 2. In the previous study, CD40L-activated human primary B cells were used to identify up to 71-fold differences across individual's responses at the highest dose of TCDD (30 nM)(Dornbos et al. 2016). While interindividual variability in toxicant-induced signaling can be driven by many factors, genetic background has been found to have profound impacts on individual responses. Advances in technologies for genetic analysis have not only improved our understanding of complex etiologies associated with diseases, but have shown that sub-populations with specific genetic variants may be more susceptible to stressor-induced injury. The use of population-based models, such as genetically-diverse panels of inbred mouse strains, have provided the means to effectively pinpoint genes and pathways that impact susceptibility to environmental exposures (Dornbos and LaPres 2017; Harrill and McAllister 2017).

To address whether there are genetic factors that may be impacting individual responses, a mouse population-guided approach was used to scan for potential genetic modulators that may impact susceptibility to TCDD-mediated suppression of the B cell. As CD40 signaling is highly conserved across mouse and human (Spriggs et al. 1992), the same human-CD40 ligand model was used to expose B cells isolated from 12 genetically-diverse mouse strains. Analysis of the inter-strain differences suggested that genomic factors beyond the *Ahr* allele impact strain-specific responses. More specifically, a gene called *Serpinb2,* which encodes the ortholog of the human plasminogen activator inhibitor-2 (PAI2), was found within a genomic region that was implicated by QTL analysis. Further downstream analysis confirmed that *Serpinb2*-related activity has a significant impact on TCDD-mediated suppression of the B cell. While *Serpinb2* has been shown to play a role within the immune system, this is the first report linking its activity to a phenotype within the B cell (Schroder et al. 2011).

3.3 Results

3.3.1. Inter-strain Differences in Response to TCDD

All 12 strains had a decrease in the number of cells secreting IgM at the high dose of TCDD (30 nM), each mouse strain displayed a unique dose-dependent response to TCDD (Figure 3.1A). Comparison between the percent inhibition induced at the high dose of TCDD (30 nM) within the mice included in the current study with a previous study with TCDD-induced suppression of human B cells from 51 unique human donors, an overlapping histogram suggests the interindividual differences between the two datasets are comparable (Figure 3.1B)(Dornbos et al. 2016). Of the 12 strains, 2 were found to contain a statistically significant decrease as indicated with ANOVA and Dunnett's posthoc with the log-transformed response: 1) C57BL/6J ($n=6$; $p<0.05$) and 2) FVB/nJ ($n=5$; $p<0.05$) (Figure 3.1C and 3.1D, respectively). There was also a 10-fold difference in the number of cells secreting IgM at the highest dose of TCDD for the most- and least-suppressed mice. As such, results show that mice within the genetic screen have a wide-range in sensitivities to TCDD.

3.3.2. Differences amongst *Ahr* allelic categories

A linear regression model with individual strains as the independent variables and the percent inhibition of the IgM response at [30nM] TCDD as the dependent variable was used to estimate the observed variance that is due to inter-strain differences (Table 3.1). The multiple R^2 value was 0.33 with 95% confidence intervals that span from 0.20 to 0.40. As such, we estimate that ~33% of the observed variance is due to genetic differences across strains. Previous reports have established that mouse strains carry one of four different *Ahr* alleles that encode for receptors with differing binding affinities for TCDD (Poland and Glover 1990; Poland et al. 1994; Thomas et al. 2002). A multiple global sequence alignment indicates that the strains in this panel carry 3 different *Ahr* alleles: 1) Ahr^{b1} (n=1; grey), 2) Ahr^{b2} (n=5; blue), and 3) Ahr^{d} (n=6; green)(Figure 3.2A). Allelic clustering was used to group mice of the same allele together to

Figure 3.1. Inter-strain differences in the response to TCDD-mediated immunosuppression. B cells isolated from 12 genetically-diverse strains of mice were exposed to increasing concentrations of TCDD (0 to 30 nM) for 6 days and the percentage of cells secreting IgM was determined by ELISPOT. Each strain was normalized to its own vehicle control to compare TCDD-mediated effects within the IgM response across strains (**A**). The distributions of the percentage of cells secreting IgM at the high dose of TCDD (30 nM) as normalized to the vehicle control for all mice (blue) and humans (red) was created to visualize overlap (maroon) between the mouse and previous human study (**B**). The dose-response analysis for the C57BL/6J (**C**, n=6) and FVB/nJ (**D**, n=5) strains indicate statistically significant, concentration-dependent decreases in the number of cells secreting IgM as compared to the vehicle control as indicated with an ANOVA with a Dunnett's posthoc. Stars (*) indicate a $p<0.05$ and error bars indicate standard error.

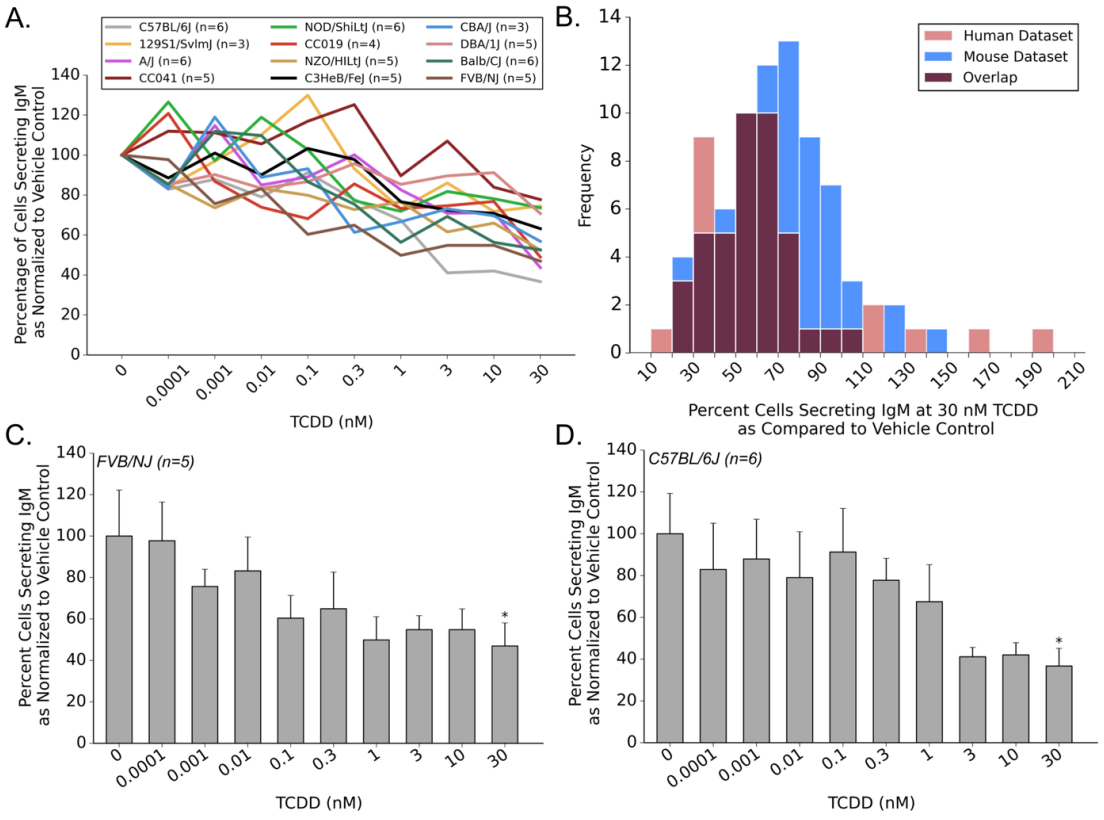

Figure 3.2. The *Ahr* allele does not drive all inter-strain differences to TCDD-mediated suppression of the IgM response. Genomic data was used to predict the AHR amino acid sequence for each mouse strain included in the study. A multiple sequence alignment of the AHR protein sequences from the 12 mouse strains assayed indicates that 3 unique alleles are present in this panel: 1) Ahr^{b1} (grey), 2) Ahr^{b2} (blue), and 3) Ahr^{d} (green) (**A**). The average percent decrease in IgM secreting B cells at 30 nM TCDD as normalized to the vehicles control was determined from all the mice within their respective *Ahr* allele (**B**). Comparison of the TCDD-induced suppression of IgM secretion in B cells from the individual strains (Ahr^{b1} (grey), Ahr^{b2} (blue), and Ahr^{d} (green)) indicates that some strains do not respond like strains within their respective AHR allelic categories (**C**). Stars (*) indicate a $p<0.05$ and error bars indicate standard error.

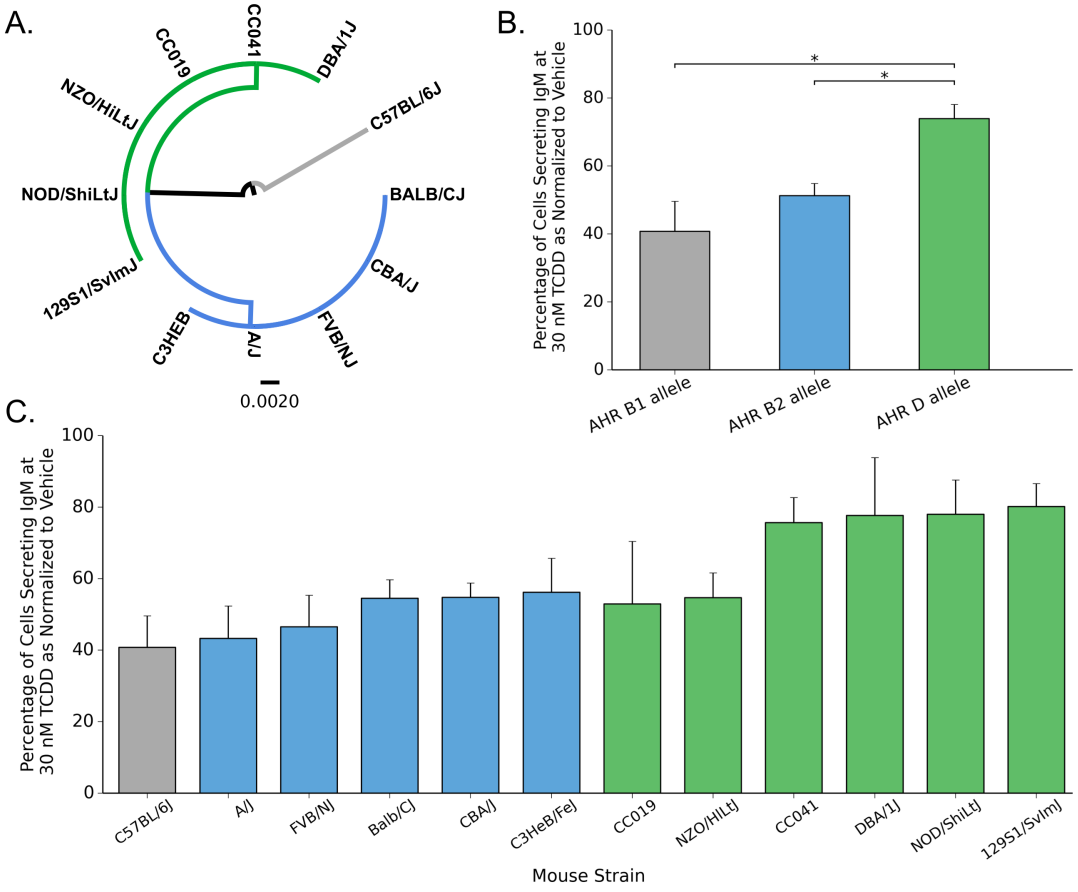

Table 3.1 The *Ahr* allele does not drive all inter-strain differences to TCDD-mediated suppression of the IgM response. All estimates are relative to the TCDD-mediated inhibition in 129S1/SvImJ (i.e. the least affected strain). Stars (*) indicate significant differences.

Coefficient	Estimate	Standard Error	t value	Pr (>|t|)
Intercept	80.222	12.739	6.297	<0.001*
A/J	-36.909	15.602	-2.366	0.022*
BALB/cJ	-25.666	15.602	-1.645	0.107
C3HeB/FeJ	-24.068	16.114	-1.494	0.142
C57BL/6J	-39.417	15.602	-2.526	0.015*
CBA/J	-25.840	18.015	-1.414	0.164
CC019	-27.320	16.852	-1.621	0.112
CC041	-4.568	16.114	-0.283	0.778
DBA/1J	-2.534	16.114	-0.157	0.876
FVB/NJ	-33.709	16.114	-2.092	0.042*
NOD/ShiLtJ	-2.232	15.602	-0.143	0.887
NZO/HILTJ	-25.527	16.114	-1.584	0.120

Residual Standard Error: 22.06 on 47 degrees of freedom.

Multiple R^2: 0.313; Adjusted R^2: 0.175

F Statistic: 2.118 on 11 of 47 degrees of freedom; p = 0.0374

compare the percentage of cells secreting IgM at 30 nM TCDD across the 3 *Ahr* alleles. The results indicate that mice carrying the Ahr^{b1} and Ahr^{b2} alleles have a significantly lower percentage of cells secreting IgM as compared to the Ahr^{d} mice ($p<0.05$; Figure 3.2B). There was no significant difference when comparing the of Ahr^{b1} and Ahr^{b2} allelic categories. These results agree with previous reports (Poland et al. 1994). In comparing percentage of cells secreting IgM across the individual strains at the 30 nM treatment of TCDD, several strains were found to behave differently than what might be predicted based on the *Ahr* allele carried (Figure 3.2C). For example, the NZO/HILTJ and CC019 strains, which both carry the Ahr^{d} allele, appear to respond similarly to the majority of Ahr^{b2} mice. Similarly, the A/J strain, which carries the Ahr^{b2} allele, appear to respond quite similarly to the C57BL/6J strain which carry Ahr^{b1} allele.

3.3.3. QTL Analysis of Percent Inhibition Identifies Significant Association

Exploratory QTL analysis was performed using the percent inhibition at the high dose of TCDD (30 nM) where statistical significant inhibition was present amongst several mouse strains. The genome-wide scan indicated a significant association with Chromosome 1 (LOD=5.61; $p<0.05$)(Figure 3.3). Genes within 1 Mb of the marker with the maximal LOD score were compiled into lists of potential candidates that may be modulating the TCDD-induced suppression in the number of antibody secreting cells (Table 3.2). While several candidate genes near the interval identified may contribute TCDD-mediated immunosuppression, only one, *Serpinb2,* is dysregulated by TCDD at the level of mRNA expression in both mouse and human B cells (Kovalova et al. 2017). Furthermore, the *Serpinb2* gene is located within 60 kb of the marker significantly associated with the B cell phenotype. As such, *Serpinb2* was selected for further confirmatory analysis and to evaluate potential roles in modulating inter-strain differences in susceptibility to TCDD-mediated suppression of the immune response.

Figure 3.3. Quantitative Trait Loci (QTL) analysis indicates a significant association within Chromosome 1. The TCDD-mediated percent suppression in the number of cells secreting IgM at 30 nM TCDD as normalized to the vehicle control was determined with an ELISPOT assay. The percent suppression was used to scan the genome for quantitative trait loci (QTLs) that potentially drive inter-strain differences using the WebQTL software from GeneNetwork. A significant association was identified on chromosome 1 at a marker located at 107.584 Mb (LOD = 5.611; p=0.031). The horizontal black-dotted line indicates the threshold of significance based on a permutation test (n=1000).

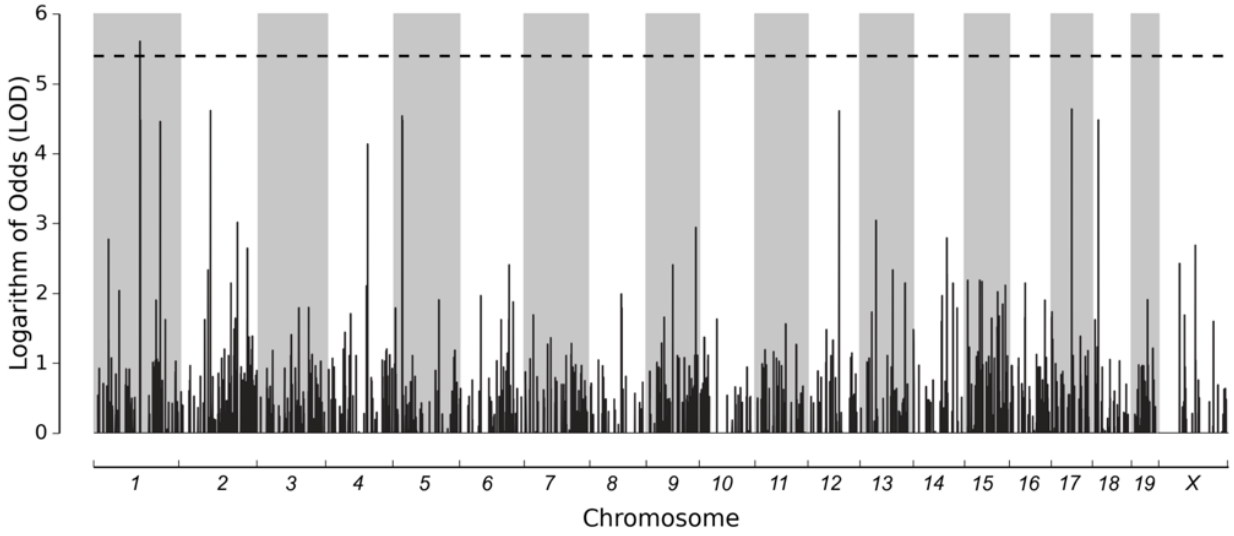

Table 3.2. Candidate genes associated with TCDD-induced suppression of the B cell. Genes located within 1 Mb upstream or downstream of the statistically significant association on chromosome 1 were considered. A literature search indicated that *Serpinb2* (bolded), which is located from 107.500-107.526 Mb on Chromosome 1 (i.e. within 59,000 bp of the significant marker), is dysregulated by TCDD within pokeweed mitogen-activated mouse and human B cells.

Chromosome	Location (Mb)	Logs of Difference (LOD)	P-value	Genes Within Region
Chr 1	107.584	5.611	0.031	*Bcl2, Kdsr, Vps4d, Serpinb5, Pou2f3-rs1, Serpinb12, Serpinb13, Serpinb3a, Serpinb3d, Serpinb3b, Serpinb3c, Serpinb11, Serpinb7,* ***Serpinb2****, Serpinb10, Serpinb8*

3.3.4. Time course of TCDD-mediated *Serpinb2* Expression

B cells were compared from a sensitive (C57BL/6J; Ahr^{b1} allele) and a less-sensitive strain (DBA/1J; Ahr^{d} allele) to TCDD-mediated immunosuppression to investigate for the presence of inter-strain differences in *Serpinb2* mRNA expression. Results indicated a significant increase in *Serpinb2* expression following 2 days of exposure to TCDD in DBA/1J mice ($p<0.05$), but not C57BL/6J mice (Figure 3.4A). More notably, *Serpinb2* expression was found to be significantly higher in DBA/1J as compared to C57BL/6J ($p<0.05$, Figure 3.4A). In addition, *Cyp1a1* expression was also assessed as a biomarker for AHR activation. Expression of *Cyp1a1* mRNA was significantly increased at day 2 in DBA/1J ($p<0.05$) and at day 2, 3, and 4 for C57BL/6J ($p<0.05$; Figure 3.4B). Interestingly, DBA/1J mice were found to have a significantly higher TCDD-induced fold change in *Cyp1a1* expression on day 2 as compared to C57BL/6J strain ($p<0.05$), but the upregulation dissipates by day 3 (Figure 3.4B). In contrast, C57BL/6J had significantly more *Cyp1a1* expression induced by TCDD as compared DBA/1J at day 3 and day 4 ($p<0.05$; Figure 3.4B). As such, results indicate statistically significant inter-strain differences in TCDD-mediated expression of *Serpinb2* and *Cyp1a1* within B cells.

3.3.5. Time-course of TCDD-dysregulated Intracellular SERPINB2 and IgM Expression

To assess whether the differential *Serpinb2* gene expression is also found at the protein level, SERPINB2 protein expression was analyzed over a 4-day time-course with a focus on the time-points where expression of *Serpinb2* and *Cyp1a1* mRNA was dysregulated. Results indicated significant TCDD-induced increases in the fold change of the percentage of $SERPINB2^{+}$ cells after TCDD treatment as compared to the vehicle control for DBA/1J mice at day 3 and 4 ($p<0.05$; Figure 3.5A). Similarly, there was a significant increase in mean fluorescent intensity (MFI) of SERPINB2 in DBA/1J at day 3 and day 4 following TCDD treatment ($p<0.05$; Figure 3.5B). In contrast, there were no significant changes in the percentage $SERPINB2^{+}$ cells or the

Figure 3.4. *Serpinb2* gene expression was found to be dysregulated by TCDD in the DBA/1J and not in the C57BL/6J. Total RNA was extracted from B cells isolated from C57BL/6J (*Ahr*^{b1} allele) and DBA/1J (*Ahr*^{d} allele) mice that were exposed to TCDD (30 nM) for 0.33, 1, 2, 3, 4, 5, and 6 days. QRTPCR was used to assess whether expression of *Serpinb2* mRNA is affected by TCDD exposure in the both strains (**A**). QRTPCR was also used to analyze *Cyp1a1* mRNA induction as a biomarker of AHR activation (**B**). All fold changes are reported for TCDD-treated cells that are normalized to the vehicle control (not shown). Stars (*) indicate a $p<0.05$; stars directly over bars indicate differences in the TCDD treatment as compared to the vehicle control or, when over bracket, indicate a comparison of TCDD treatments across strains. Error bars indicate standard error.

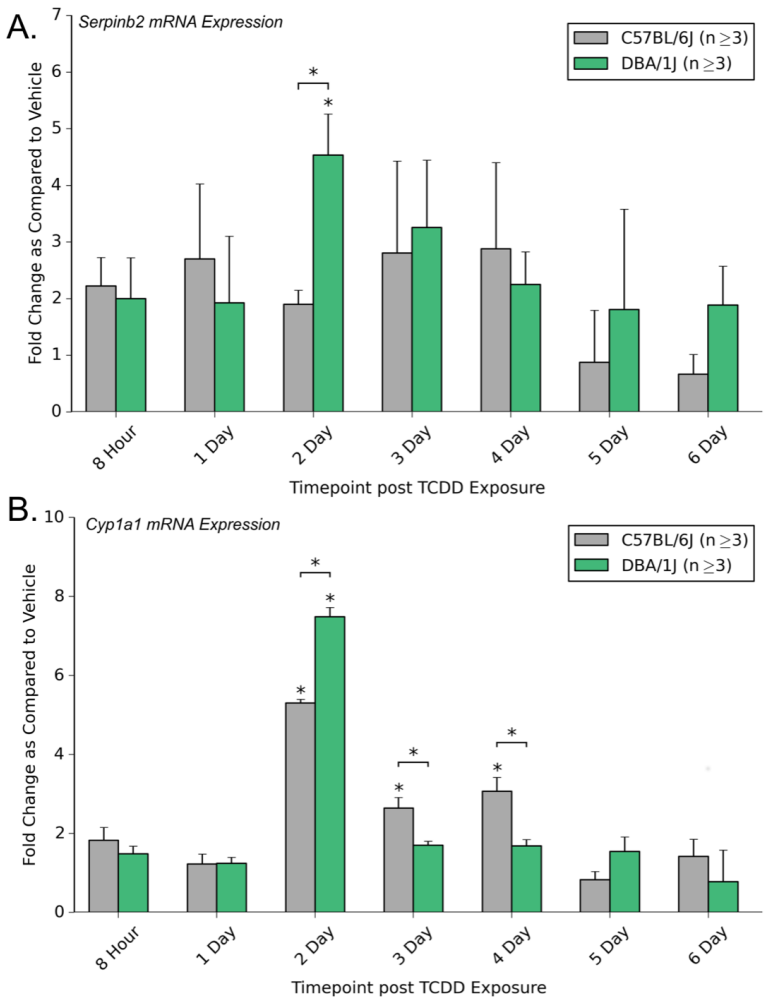

Figure 3.5. TCDD exposure increased the percentage of SERPINB2$^+$ and level of intracellular SERPINB2 expression in DBA/1J, but not C57BL/6J mice. B cells isolated from a C57BL/6J and DBA/1J mice were exposed to TCDD (30 nM) for 2, 3, 4, and 5 days. Flow cytometry was used to assess the level of intracellular SERPINB2 protein expression. The percentage of cells that are SERPINB2$^+$ were assessed at each timepoint (**A**). Similarly, mean fluorescence intensity for the SERPINB2 antibody was used to assess the level of SERPINB2 expression at each timepoint (**B**). A representative sample for DBA/1J (**C**) and C57BL/6J (**D**) was chosen to visualize the shift of SERPINB2 expression in the population of B cells treated with TCDD as compared to the vehicle. All fold changes are reported for TCDD-treated cells that are normalized to the vehicle control (not shown). Stars (*) indicate a $p<0.05$; stars directly over bars indicate differences in the TCDD treatment as compared to the vehicle control or, when over bracket, indicate a comparison of TCDD treatments across strains. Error bars indicate standard error.

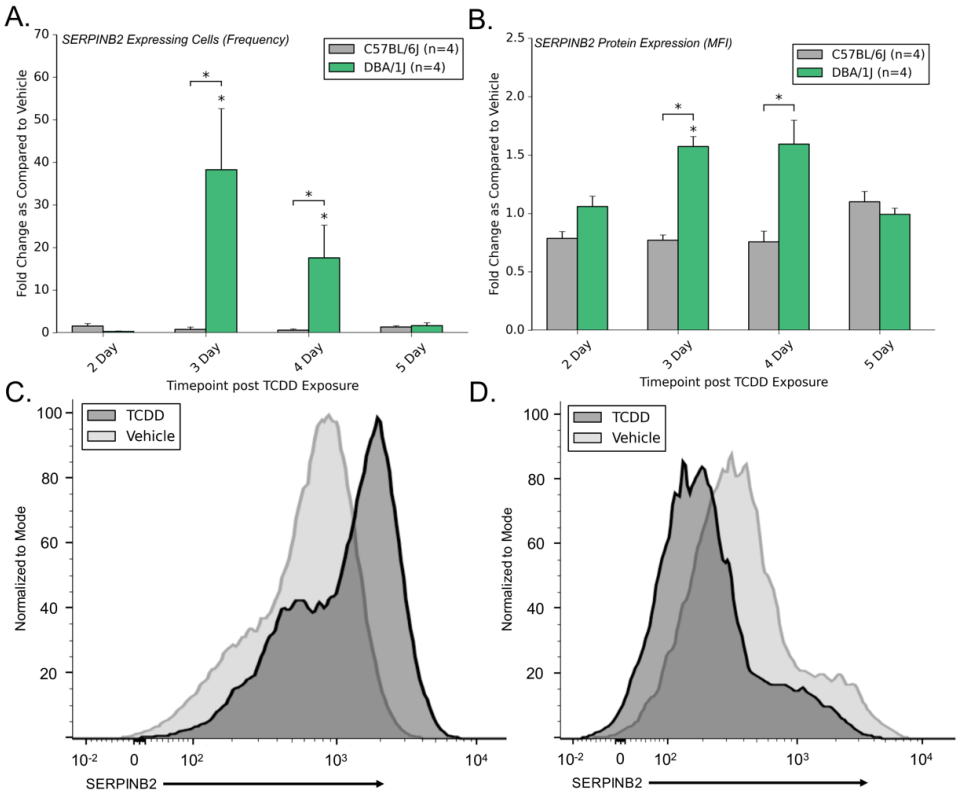

SERPINB2 MFI for C57BL/6J mice (Figure 3.5A and 5B). In comparing the strains, the percentage of SERPINB2$^+$ cells were significantly higher in the DBA/1J at day 2 and day 3 ($p<0.05$, respectively; Figure 3.5A). Similarly, DBA/1J also had significantly higher TCDD-induced SERPINB2 expression as indicated by the SERPINB2 MFI at day 3 and day 4 ($p<0.05$; Figure 3.5B). A representative sample for each strain was chosen to visualize the increase in the expression of SERPINB2 in DBA/1J as compared to the slight decrease seen within C57BL/6J (Figure 3.5C and 5D, respectively). Results suggest that, along with the mRNA expression data, the protein expression data also suggests inter-strain differences in the levels of intracellular SERPINB2.

As the QTL analyses were based on TCDD-induced inter-strain differences in the number of cells secreting IgM, intracellular IgM expression was also assessed to potentially identify a correlation with SERPINB2 expression. The TCDD-induced fold change in the frequency of SERPINB2$^+$, SERPINB2$^-$, IgM$^+$, and IgM$^-$ cells were compared at each timepoint across the two strains. Results indicate that on day 2 post-TCDD exposure, there is a significantly smaller fold change in the number of cells that are SERPINB2$^+$/IgM$^+$ induced by TCDD in DBA/1J as compared to C57BL/6J ($p<0.05$; Figure 3.6A). However, on day 3 post-exposure, TCDD-induced a significantly higher fold change of SERPINB2$^+$/IgM$^+$ cells in DBA/1J as compared to C57BL/6J ($p<0.05$; Figure 3.6B). Notably, while TCDD-induced an increase in SERPINB2$^+$/IgM$^+$ DBA/1J mice on day 3, the C57BL/6J was found to have a decrease (i.e. > 6 fold difference between mice). As such, there appears to be a time-dependent correlation between SERPINB2 expression and higher levels of intracellular IgM in the DBA/1J. This trend continues on Day 4 as DBA/1J was found to have a significantly higher fold change in SERPINB2$^+$/IgM$^+$ as compared to SERPINB2$^+$/IgM$^+$ in C57BL/6J ($p<0.05$; Figure 3.6C). However, the TCDD-induced frequency of SERPINB2$^+$/IgM$^-$ cells in the DBA/1J also increases on day 4 as compared to the C57BL/6J

Figure 3.6. Intracellular SERPINB2 expression correlates with high level of intracellular IgM in a time-dependent manner. B cells isolated from C57BL/6J and DBA/1J mice were exposed to TCDD (30 nM) for 2, 3, 4, and 5 days. Flow cytometry was used to assess the TCDD-induced fold change in the frequency of cells that are SERPINB2^{+} and high IgM^{+} on day 2 (**A**), day 3 (**B**), day 4 (**C**), and day 5 (**D**). All fold changes are reported for TCDD-treated cells that are normalized to the vehicle control (not shown). Stars (*) indicate a $p<0.05$; stars directly over bars indicate differences in the TCDD treatment as compared to the vehicle control or, when over bracket, indicate a comparison of TCDD treatments across strains. Error bars indicate standard error.

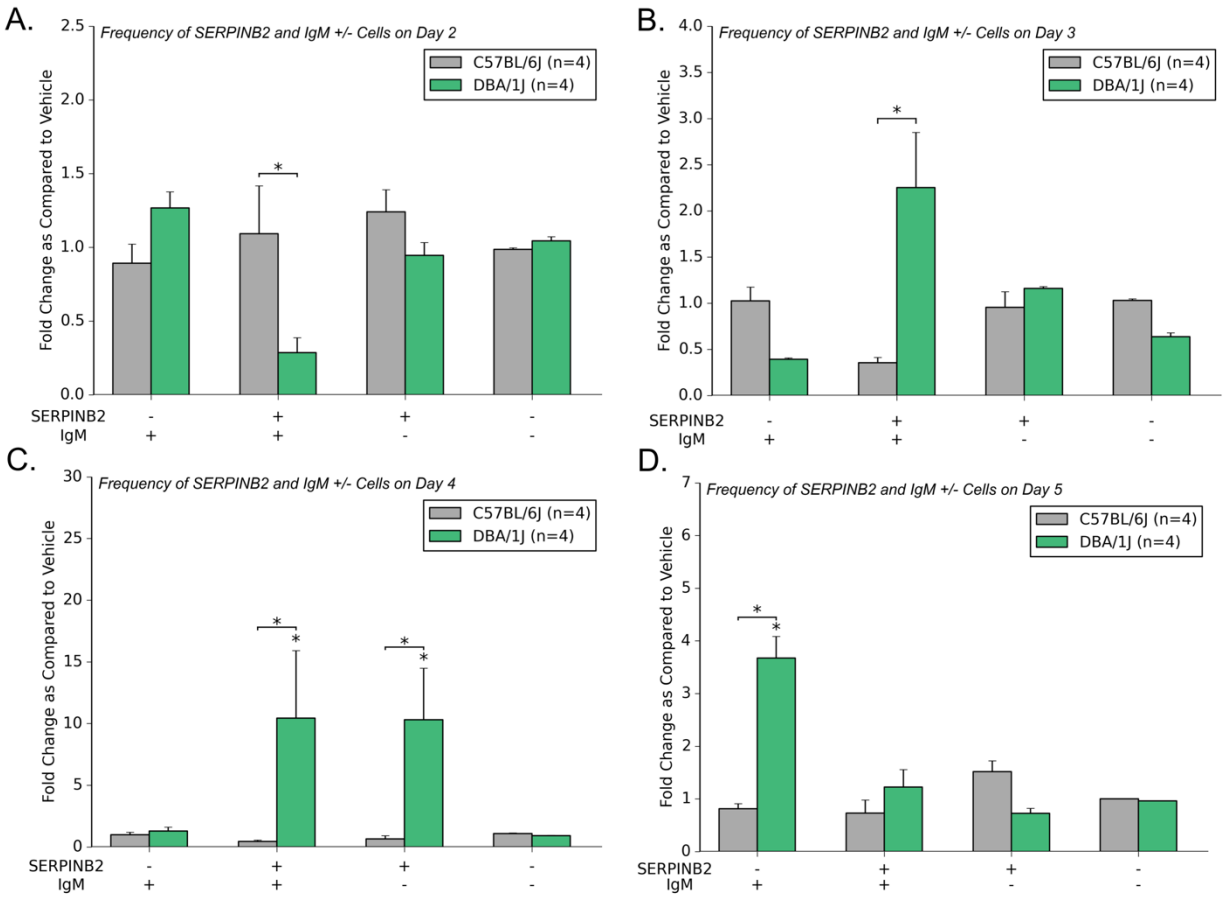

(p<0.05; Figure 3.6C). Finally, on day 5, where the TCDD-induced increase in SERPINB2 levels has dissipated, there was a significantly larger TCDD-induced fold change in $SERPINB2^{-}/IgM^{+}$ cells in DBA/1J compared to the C57BL/6J (p<0.05). Consequently, there appears to be a correlation with TCDD-induced expression of intracellular SERPINB2 and IgM on day 3 in DBA/1J, but not C57BL/6J.

3.3.6. *Serpinb2*$^{-/-}$ mice are more sensitive to TCDD-induced Immunosuppression

While the above comparison suggests the *Serpinb2* gene and SERPINB2 protein expression display significant inter-strain variation, the results do not provide a functional relationship for SERPINB2 in TCDD-induced suppression of the IgM response. To test this relationship directly, a SERPINB2 knockout mouse on a C57BL/6J background was used. B cells from *Serpinb2*$^{-/-}$ mice along with wild type controls were isolated and treated with TCDD using the same model as for the genomic screen (i.e. 6 total days of culture). Results indicated that both *Serpinb2*$^{-/-}$ mice and wild type controls had significant decreases in the percentage of cells secreting IgM (p<0.05; Figure 3.7A). More notably, *Serpinb2*$^{-/-}$ mice were significantly more sensitive to TCDD-mediated suppression with significantly lower percentages of cells secreting IgM as compared to wild type controls (p<0.05; Figure 3.7A). The *Serpinb2*$^{-/-}$ and wild type mice both were found to significantly induce *Cyp1a1* mRNA expression on day 2 (p<0.05; Figure 3.7B). The expression of *Cyp1a1* mRNA for the TCDD treatments were not different between strains suggesting that, while the AHR is activated in both strains, the difference in sensitivity between the *Serpinb2*$^{-/-}$ and wild type mice is likely not due to differing levels of AHR activity (Figure 3.7B).

3.3.7. *Serpine1*$^{-/-}$ mice are not more susceptible to TCDD-induced Immunosuppression

To determine if the above results were specific to SERPINB2 activity, B cells were also analyzed from SERPINE1 null mice. Similar to the results from the *Serpinb2*$^{-/-}$ study, there was a significant TCDD-induced decrease in the percentage of cells secreting IgM in *Serpine1*$^{-/-}$ and wild

Figure 3.7. *Serpinb2*$^{-/-}$ mice, but not *Serpine1*$^{-/-}$ mice, are more sensitive to TCDD-induced immunosuppression. B cells isolated from *Serpinb2*$^{-/-}$ and *Serpine1*$^{-/-}$ mice along with the respective wild type controls were exposed to TCDD (30 nM) for 6 days. An ELISPOT assay was used to assess for TCDD-mediated percent suppression as normalized to the vehicle control in the *Serpinb2*$^{-/-}$ and wild type controls (**A**). RNA was isolated from *Serpinb2*$^{-/-}$ and wild type controls that were exposed to TCDD (30 nM) for 2 days. QRTPCR was used to assess the level of TCDD-mediated *Cyp1a1* induction in both strains as a marker of AHR activation (**B**). An ELISPOT was also used to assess the percentage of cells secreting IgM as normalized to the vehicle control in the *Serpine1*$^{-/-}$ mice and wild type controls (**C**). RNA was isolated from *Serpine1*$^{-/-}$ and wild type controls that were exposed to TCDD (30 nM) for 2 days. QRTPCR was used to assess the level of TCDD-mediated *Cyp1a1* induction in both strains (**D**).

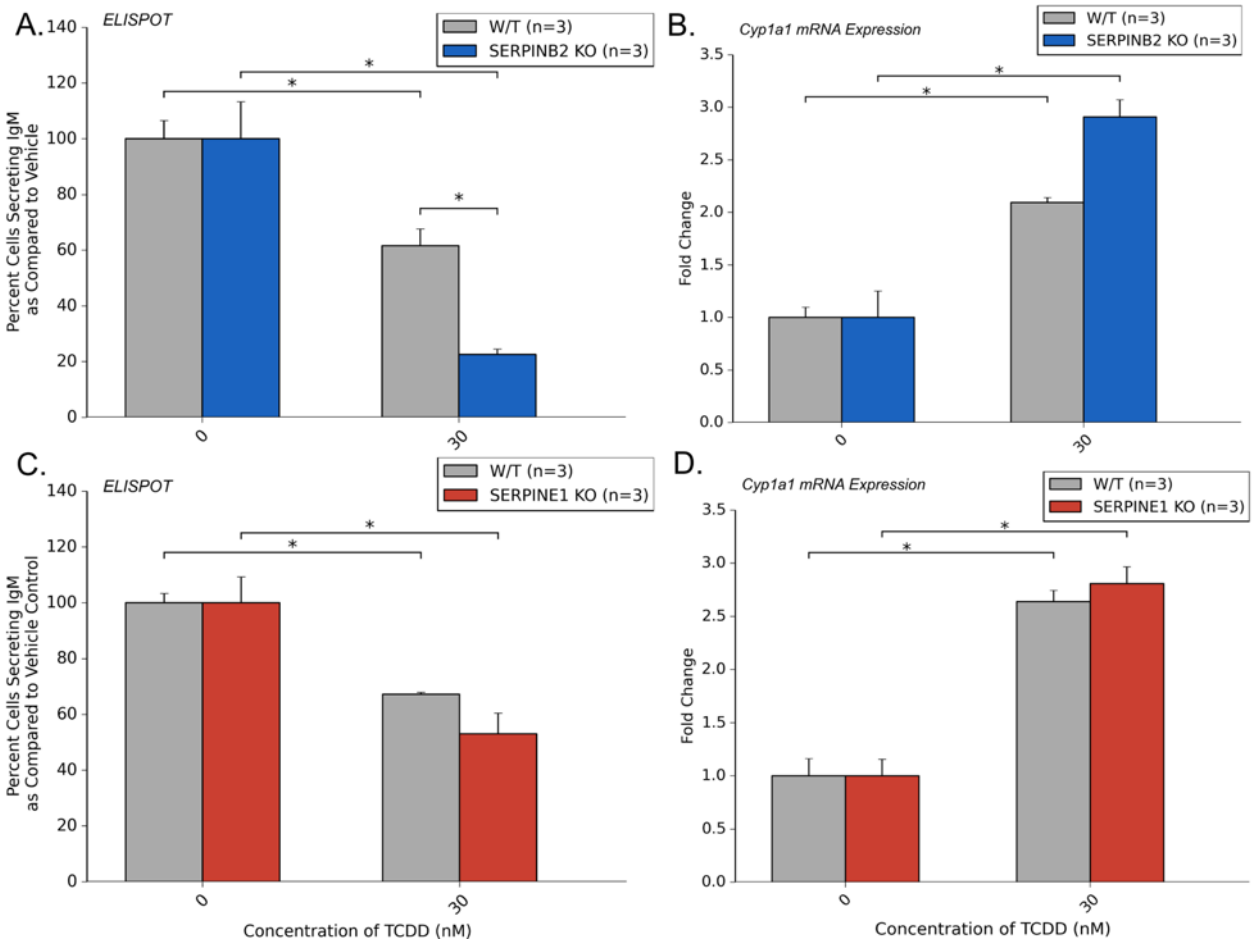

type controls ($p<0.05$; Figure 3.7C). Significant increases in TCDD-induced *Cyp1a1* mRNA expression were found in both strains as well ($p<0.05$; respectively; Figure 3.7D). However, in comparing the TCDD treatments between the *Serpine1*$^{-/-}$ mice with wild type controls, there was no significant differences in either the percentage of cells secreting IgM or in the induction of *Cyp1a1* mRNA (Figure 3.7C and 7D). As such, the loss of SERPINE1 did not appear to affect sensitivity to TCDD-induced suppression in the number of antibody-secreting cells with similar levels of AHR activation between the *Serpine1*$^{-/-}$ and wild type controls. Thus, the aforementioned differences in sensitivity appear to be specific to the activity of SERPINB2.

3.4. Discussion

Traditional toxicological studies focused on environmental contaminants have rarely considered the influence of genetic variability when assessing risk associated with exposures. As genetic background has been shown to play an important role in influencing individual's responses to chemicals, this lack of population-level testing provides a challenge for risk assessment. With the use of population-based models, genetic information can be leveraged to better understand which sub-populations may be more at-risk for adverse health outcomes following chemical exposures. In this study, we used to a mouse population-guided approach to scan for potential genetic modifiers that impact the interindividual variability in TCDD-mediated immunosuppression observed in human B cells (Dornbos et al. 2016),

Results from this study indicated, similar to our human B cell study, a wide-range in response to TCDD-induced B cell suppression (Figure 3.1A and 1B). Furthermore, QTL analysis identified a region of the genome that was significantly correlated with inter-strain differences (Figure 3.2C and Figure 3). A gene within this region, *Serpinb2,* had previously been reported to be influenced at the level of mRNA expression by TCDD in mouse and human B cells (Kovalova et al. 2017). The TCDD-inducible expression results were confirmed at the mRNA and protein level with our CD40 ligand-activation model in the DBA/1J strain, but not in the C57BL/6J strain (Figure 3.4A, Figure 3.5A and 5B). Furthermore, a *Serpinb2*$^{-/-}$ mouse strain was found to be more sensitive to TCDD-mediated suppression in the percentage of cells secreting IgM, suggesting that SERPINB2 plays a protective role in TCDD-mediated immunosuppression of the B cell (Figure 3.7A). The induction of SERPINB2 in DBA/1J was found to correlate with a higher level of intracellular IgM on day 3, but not on day 4, which may suggest some time-dependence as to when the protection of TCDD-mediated suppression may occur (Figure 3.6B and 6C). Finally, this

response was found to be specific to *Serpinb2*, as the same phenotype was not observed in *Serpine1*$^{-/-}$ mice (Figure 3.7C).

Based on the expression patterns of PAI2, the human ortholog of *Serpinb2*, during infection and inflammatory stimuli (i.e. cytokines), PAI2 has been suggested to play an important role within the immune response (Schroder et al. 2010; Zhao et al. 2013). Previous reports, however, have primarily focused on the role of *Serpinb2* in the macrophage where, after activation, SERPINB2 is one of the most abundant proteins (Costelloe et al. 1999; Gan et al. 2008; Kruithof et al. 1995; Losick and Isberg 2006; Medcalf and Stasinopoulos 2005; Schroder et al. 2010; Sekine et al. 2009). While TCDD-induced *Serpinb2* mRNA expression has been reported in human and mouse B cells activated with pokeweed mitogen (Kovalova et al. 2017), this is the first report indicating a TCDD-elicited increase in *Serpinb2* mRNA and SERPINB2 protein expression in CD40 ligand-activated B cells. As such, these findings suggest a novel role of *Serpinb2* in B cell function and further confirms that *Serpinb2* plays a key role within multiple-levels of immune function.

While SERPINB2/PAI2 has been extensively studied, its role in immune function still remains elusive (Medcalf and Stasinopoulos 2005). Here, we have shown that loss of the gene results in a greater sensitivity to TCDD-mediated immune suppression in mice. In speculating on the potential mechanism to explain this suppressed immunity, previous reports have identified that human PAI2 binds directly to proteasome subunit β1 which may provide some insight into the phenotype we observed (Fan et al. 2004). Past studies have also shown that CD40 signaling activates and promotes translocation of NFKB into the nucleus (Berberich et al. 1994). As the proteasome has been shown to play a key role in regulating NFKB signaling in several cell types, including human B cells, previous reports have suggested that PAI2's association with the proteasome may be involved in regulation of NFKB signaling (Berberich et al. 1994; Karin and

Ben-Neriah 2000; Kosaka et al. 1999; Schroder et al. 2010; Schroder et al. 2011). Similarly, *Serpinb2*$^{-/-}$ mice have also been reported to have enhanced levels of NFKB activity (Schroder et al. 2010). Interestingly, the AHR and NFKB have been previously reported to interact both physically and via downstream signaling cascades (Tian et al. 1999; Tian 2009; Vogel and Matsumura 2009). Furthermore, a recent paper has shown that, upon TCDD treatment, altered expression of NFKB/REL members may, along with AHR activation, mediate a decrease in Ig expression (Salisbury and Sulentic 2015). Increased PAI2 expression may provide protection to less-sensitive strains via regulation of NFKB/REL signaling. Human PAI2 has also been reported to bind and protect retinoblastoma protein (RB1) from calpain cleavage ultimately leading to increase RB1 levels within the cell leading to increased cell survival (Tonnetti et al. 2008). A physical interaction between AHR and RB1 has also been reported and this interaction might modulate the cell cycle (Murray et al. 2014; Puga et al. 2000). The increase in the PAI2 pool within activated B cells may promote cell survival in an RB1-dependent manner. Finally, human PAI2 has been shown to bind and stabilize CDKN1A in human fibroblasts (Hsieh et al. 2017). Previous reports have noted B cells accumulate CDKN1A upon CD40 ligation (Mullins et al. 1998). While CDKN1A is known to promote cell senescence, it also has been found to be necessary for the assembly and nuclear localization of cyclin D/CDK4 and, thus, progression to G1 phase of replication (LaBaer et al. 1997; Zhang et al. 1994). Increased PAI2 expression, therefore, might increase the pool of CDKN1A to a level high-enough in the nucleus to move to the G1 phase contributing to the separation seen between the number of IgM secreting cells of sensitive and less-sensitive strains (Mullins et al. 1998).

Mouse population-based studies have been used to inform human-based risk assessment in the past (Chiu et al. 2014; Cichocki et al. 2017; Harrill et al. 2009). Here, a genetically-diverse mouse panel was used to characterize the functional role of *Serpinb2* in TCDD-mediated suppression of the mouse B cell. The results from this study suggest that human PAI2 plays a

role in mediating the IgM response. Notably, a number of *Serpinb2* polymorphisms within the human population have been identified that impact a plethora of disease-states (Andraweera et al. 2014; Buyru et al. 2003; Corsetti et al. 2016; Palafox-Sanchez et al. 2009; Vazquez-Del Mercado et al. 2007). While further research is needed, we speculate that polymorphisms that impact human PAI2 activity will alter individual's susceptibility to TCDD-mediated immunosuppression and, more broadly, the CD40-mediated IgM response.

REFERENCES

REFERENCES

Andraweera PH, Dekker GA, Thompson SD, Nowak RC, Jayasekara RW, Dissanayake VH, et al. 2014. Polymorphisms in the fibrinolytic pathway genes and the risk of recurrent spontaneous abortion. Reprod Biomed Online 29:745-751.

Berberich I, Shu GL, Clark EA. 1994. Cross-linking cd40 on b cells rapidly activates nuclear factor-kappa b. J Immunol 153:4357-4366.

Buyru N, Altinisik J, Gurel CB, Ulutin T. 2003. Pcr-rflp detection of pai-2 variants in myocardial infarction. Clin Appl Thromb Hemost 9:333-336.

Chiu WA, Campbell JL, Jr., Clewell HJ, 3rd, Zhou YH, Wright FA, Guyton KZ, et al. 2014. Physiologically based pharmacokinetic (pbpk) modeling of interstrain variability in trichloroethylene metabolism in the mouse. Environ Health Perspect 122:456-463.

Cichocki JA, Furuya S, Venkatratnam A, McDonald TJ, Knap AH, Wade T, et al. 2017. Characterization of variability in toxicokinetics and toxicodynamics of tetrachloroethylene using the collaborative cross mouse population. Environ Health Perspect 125:057006.

Corsetti JP, Salzman P, Ryan D, Moss AJ, Zareba W, Sparks CE. 2016. Influences on plasminogen activator inhibitor-2 polymorphism-associated recurrent cardiovascular disease risk in patients with high hdl cholesterol and inflammation. Atherosclerosis 250:1-8.

Costelloe EO, Stacey KJ, Antalis TM, Hume DA. 1999. Regulation of the plasminogen activator inhibitor-2 (pai-2) gene in murine macrophages. Demonstration of a novel pattern of responsiveness to bacterial endotoxin. J Leukoc Biol 66:172-182.

Dornbos P, Crawford RB, Kaminski NE, Hession SL, LaPres JJ. 2016. The influence of human interindividual variability on the low-dose region of dose-response curve induced by 2,3,7,8-tetrachlorodibenzo-p-dioxin in primary b cells. Toxicol Sci 153:352-360.

Dornbos P, LaPres JJ. 2017. Incorporating population-level genetic variability within laboratory models in toxicology: From the individual to the population. Toxicology.

Fan J, Zhang YQ, Li P, Hou M, Tan L, Wang X, et al. 2004. Interaction of plasminogen activator inhibitor-2 and proteasome subunit, beta type 1. Acta Biochim Biophys Sin (Shanghai) 36:42-46.

Gan H, Lee J, Ren F, Chen M, Kornfeld H, Remold HG. 2008. Mycobacterium tuberculosis blocks crosslinking of annexin-1 and apoptotic envelope formation on infected macrophages to maintain virulence. Nat Immunol 9:1189-1197.

Harrill AH, Watkins PB, Su S, Ross PK, Harbourt DE, Stylianou IM, et al. 2009. Mouse population-guided resequencing reveals that variants in cd44 contribute to acetaminophen-induced liver injury in humans. Genome Res 19:1507-1515.

Harrill AH, McAllister KA. 2017. New rodent population models may inform human health risk assessment and identification of genetic susceptibility to environmental exposures. Environ Health Perspect 125:086002.

Hsieh HH, Chen YC, Jhan JR, Lin JJ. 2017. The serine protease inhibitor serpinb2 binds and stabilizes p21 in senescent cells. J Cell Sci 130:3272-3281.

Karin M, Ben-Neriah Y. 2000. Phosphorylation meets ubiquitination: The control of nf-[kappa]b activity. Annu Rev Immunol 18:621-663.

Kosaka Y, Calderhead DM, Manning EM, Hambor JE, Black A, Geleziunas R, et al. 1999. Activation and regulation of the ikappab kinase in human b cells by cd40 signaling. Eur J Immunol 29:1353-1362.

Kovalova N, Nault R, Crawford R, Zacharewski TR, Kaminski NE. 2017. Comparative analysis of tcdd-induced ahr-mediated gene expression in human, mouse and rat primary b cells. Toxicol Appl Pharmacol 316:95-106.

Kruithof EK, Baker MS, Bunn CL. 1995. Biological and clinical aspects of plasminogen activator inhibitor type 2. Blood 86:4007-4024.

LaBaer J, Garrett MD, Stevenson LF, Slingerland JM, Sandhu C, Chou HS, et al. 1997. New functional activities for the p21 family of cdk inhibitors. Genes Dev 11:847-862.

Losick VP, Isberg RR. 2006. Nf-kappab translocation prevents host cell death after low-dose challenge by legionella pneumophila. J Exp Med 203:2177-2189.

Medcalf RL, Stasinopoulos SJ. 2005. The undecided serpin. The ins and outs of plasminogen activator inhibitor type 2. Febs j 272:4858-4867.

Mullins MW, Pittner BT, Snow EC. 1998. Cd40-mediated induction of p21 accumulation in resting and cycling b cells. Mol Immunol 35:567-580.

Murray IA, Patterson AD, Perdew GH. 2014. Aryl hydrocarbon receptor ligands in cancer: Friend and foe. Nat Rev Cancer 14:801-814.

Palafox-Sanchez CA, Vazquez-Del Mercado M, Orozco-Barocio G, Garcia-De la Torre I, Torres-Carrillo N, Torres-Carrillo NM, et al. 2009. A functional ser(413)/ser(413) pai-2 polymorphism is associated with susceptibility and damage index score in systemic lupus erythematosus. Clin Appl Thromb Hemost 15:233-238.

Poland A, Glover E. 1990. Characterization and strain distribution pattern of the murine ah receptor specified by the ahd and ahb-3 alleles. Mol Pharmacol 38:306-312.

Poland A, Palen D, Glover E. 1994. Analysis of the four alleles of the murine aryl hydrocarbon receptor. Mol Pharmacol 46:915-921.

Puga A, Barnes SJ, Dalton TP, Chang C, Knudsen ES, Maier MA. 2000. Aromatic hydrocarbon receptor interaction with the retinoblastoma protein potentiates repression of e2f-dependent transcription and cell cycle arrest. J Biol Chem 275:2943-2950.

Salisbury RL, Sulentic CE. 2015. The ahr and nf-kappab/rel proteins mediate the inhibitory effect of 2,3,7,8-tetrachlorodibenzo-p-dioxin on the 3' immunoglobulin heavy chain regulatory region. Toxicol Sci 148:443-459.

Schroder WA, Le TT, Major L, Street S, Gardner J, Lambley E, et al. 2010. A physiological function of inflammation-associated serpinb2 is regulation of adaptive immunity. J Immunol 184:2663-2670.

Schroder WA, Major L, Suhrbier A. 2011. The role of serpinb2 in immunity. Crit Rev Immunol 31:15-30.

Sekine H, Mimura J, Oshima M, Okawa H, Kanno J, Igarashi K, et al. 2009. Hypersensitivity of aryl hydrocarbon receptor-deficient mice to lipopolysaccharide-induced septic shock. Mol Cell Biol 29:6391-6400.

Spriggs MK, Armitage RJ, Strockbine L, Clifford KN, Macduff BM, Sato TA, et al. 1992. Recombinant human cd40 ligand stimulates b cell proliferation and immunoglobulin e secretion. J Exp Med 176:1543-1550.

Thomas RS, Penn SG, Holden K, Bradfield CA, Rank DR. 2002. Sequence variation and phylogenetic history of the mouse ahr gene. Pharmacogenetics 12:151-163.

Tian Y, Ke S, Denison MS, Rabson AB, Gallo MA. 1999. Ah receptor and nf-kappab interactions, a potential mechanism for dioxin toxicity. J Biol Chem 274:510-515.

Tian Y. 2009. Ah receptor and nf-kappab interplay on the stage of epigenome. Biochem Pharmacol 77:670-680.

Tonnetti L, Netzel-Arnett S, Darnell GA, Hayes T, Buzza MS, Anglin IE, et al. 2008. Serpinb2 protection of retinoblastoma protein from calpain enhances tumor cell survival. Cancer Res 68:5648-5657.

Vazquez-Del Mercado M, Garcia-Cobian TA, Munoz Valle JF, Torres-Carrillo N, Martin-Marquez BT, Arana-Argaez VE, et al. 2007. Genotype ser413/ser of pai-2 polymorphism ser413/cys is associated with anti-phospholipid syndrome and systemic lupus erythematosus in a familial case: Comparison with healthy controls. Scand J Rheumatol 36:206-210.

Vogel CF, Matsumura F. 2009. A new cross-talk between the aryl hydrocarbon receptor and relb, a member of the nf-kappab family. Biochem Pharmacol 77:734-745.

Zhang H, Hannon GJ, Beach D. 1994. P21-containing cyclin kinases exist in both active and inactive states. Genes Dev 8:1750-1758.

Zhao A, Yang Z, Sun R, Grinchuk V, Netzel-Arnett S, Anglin IE, et al. 2013. Serpinb2 is critical to th2 immunity against enteric nematode infection. J Immunol 190:5779-5787.

Chapter 4: Characterization of the Impact of Genetic Heterogeneity in Accumulation of TCDD and Identification of *Tgfbr2* as a Modulator of TCDD-induced Liver Injury

This chapter is an edited version of an article that is submitted to *Toxicology and Applied Pharmacology*.

Authors: Peter Dornbos[1,2], Melanie Warren[3], Kelly A. Fader[1,2], David Nava[1], James Hosner[1], Rance Nault[1,2], Senem Aykul[1], Jack Harkema[2,4], Eric Martinez-Hackert[1], Tim Zacharewski[1,2], Hui Lin[5], David Threadgill[3], John J. LaPres[1,2]

Affiliations: [1]Department of Biochemistry and Molecular Biology, Michigan State University, East Lansing, MI 48824, [2]Institute for Integrative Toxicology, Michigan State University, East Lansing, MI 48824, [3]Interdisciplinary Program in Toxicology, Texas A&M University, College Station, TX 77843, [4]Department of Pathobiology and Diagnostic Investigation, Michigan State University, East Lansing, MI 48824, [5]The Dow Chemical Company, Environmental Technology Center, Midland, MI, 48674

4.1. Abstract

As traditional toxicology studies typically use homogenous models, we used a genetically-diverse mouse population-based approach to scan for novel genetic modulators that impact hepatic sequestration of TCDD and TCDD-elicited hepatotoxicity. A panel of 14 strains of mice were treated with 1 or 100 ng/kg TCDD for 10 days. Significant inter-strain differences in hepatic TCDD burden appear heavily-driven by genetic background. Of 9 AHR-responsive genes analyzed, the TCDD-induced gene dysregulation of 4 genes were found to correlate with TCDD burden. Three of these genes are classical AHR-battery genes suggesting that AHR-mediated transcription drives hepatic TCDD sequestration. TCDD burden and TCDD-induced gene expression were used to scan for genetic modulators of TCDD-induced toxicity. Quantitative trait loci (QTL) analysis identified several novel genomic regions that potentially modulate TCDD-induced gene dysregulation. *Tgfbr2*, which encodes for transforming growth factor β receptor II (TGFBR2), was found within one genomic region of interest. Inhibiting TGFBR2 activity decreased TCDD-elicited inflammation, but increased lipid accumulation, in the livers of male, but not female, C57BL/6 mice. Our results suggest that TGFBR2 activity modulates TCDD-elicited liver toxicity in male mice. These results, while providing further understanding of AHR biology, have the potential to identify sub-populations more susceptible to TCDD-induced toxicity.

4.2 Introduction

Previous studies indicate that the liver is a sensitive target of TCDD-induced toxicity. TCDD exposures in mice lead to increased levels of alanine aminotransferase (ALT) in the serum, inflammation, and liver weight (Boverhof et al. 2005; Kopec et al. 2013; Pierre et al. 2014). TCDD-elicited increase in liver weight is likely driven, at least in part, by induction of fatty liver disease. Previous reports show that a single, bolus dose of TCDD (30 μg/kg) results in an increased deposition of fatty acids in the liver of mice that are sensitive to TCDD (Boverhof et al. 2005). If exposure to TCDD is prolonged, the increased fatty acid uptake in the liver has been shown to progress to steatohepatitis with fibrosis (Nault et al. 2016a; Nault et al. 2016c; Nault et al. 2017; Pierre et al. 2014). Epidemiological studies indicate that exposures to TCDD and other dioxin-like compounds are associated with increased incidence of liver disease in humans as well. More specifically, exposures to TCDD and other dioxin-like chemicals are associated with increased levels of liver enzymes, diabetes and metabolic syndrome (Cave et al. 2010; Dietrich and Hellerbrand 2014; Lee et al. 2007; Taylor et al. 2013).

Previous rodent-based studies show that TCDD accumulates in the liver in a dose-dependent manner (Nault et al. 2016a). Furthermore, genes that are regulated by the AHR are involved in the hepatic sequestration of TCDD. For example, CYP1A2, which is a part of the AHR gene-battery, is known to bind the contaminant (Voorman and Aust 1989). Hepatic sequestration of TCDD is greatly reduced following a single dose of TCDD in *Cyp1a2*$^{-/-}$ mice (Diliberto et al. 1997; Hakk et al. 2009). Notably, hepatic TCDD sequestration has not been addressed using heterogeneous models that mirror the variability in the human population. Similarly, TCDD-induced gene expression has been heavily-studied in mice using homogenous models. The impact of incorporating genetic variability has not yet been characterized for either the accumulation of TCDD or AHR-mediated transcription.

To address this knowledge gap, 14 genetically-diverse mouse strains were exposed to vehicle control, 1, or 100 ng/kg/day of TCDD for 10 consecutive days. Following exposure, gas chromatography-mass spectrometry (GC/MS) was used to analyze the level of hepatic TCDD accumulation. Expression of 9 AHR-responsive genes were also analyzed in the liver. These results were used to further characterize the toxicodynamics of AHR-mediated sequestration. QTL analysis implicated a region on mouse Chromosome 9 that has potential to modulate TCDD-induced toxicity in the liver. Amongst the genes within this region, *Tgfbr2*, which encodes for transforming growth factor β receptor type II, was found to modulate the level of inflammation and fat accumulation in the liver of TCDD-exposed C57BL/6 mice. While a ligand of TGFBR2 called TGFB1 is altered by TCDD, this is the first report with functional data that suggests TGFBR2 activity plays a role in TCDD-induced liver pathology.

4.3 Results

4.3.1. Inter-strain variability in TCDD liver burden

There is wide variability in the level of TCDD burden in the liver of mice that received TCDD. Within the 1 ng/kg/day dose group, the population mean level of TCDD was 22.7 ng/kg of liver with 95% confidence intervals that range from 6.0 to 39.4 ng/ kg of liver (Figure 4.1). Notably, there is a > 40-fold difference in the accumulation of TCDD in the livers in the 1 ng/kg/day group with the lowest levels in NZO/HlLtJ (2.8 ng/kg liver) and highest in DBA/1J (119.5 ng/kg liver)(Figure 4.1). Within the 100 ng/kg/day dose group, the population mean level of TCDD was 1909.7 ng/kg of liver with the 95% confidence interval ranging from 955.1 to 2864.2 ng/kg of liver (Figure 4.1). The mean level of TCDD accumulation is > 84-fold higher in mice that received 100 ng/kg/day dose group as compared to the 1 ng/kg/day mice. Within the higher dose group, there is > 30-fold difference in the mean levels of TCDD in the livers across strains with the lowest in NOD/ShiLtJ (159.2 ng/kg liver) and highest in BXD91 (5286.7 ng/kg liver; Figure 4.1). The heritability estimate (h^2) for accumulation of TCDD within the 100 ng/kg/day dose group is 0.94 with 95% confidence intervals that span from 0.90 to 0.96 (Table 4.1). The h^2 estimate suggests that genetic variance in this mouse panel drives roughly 15 times more of the observed variance as compared to environmental factors. These results suggest that accumulation of TCDD in the liver of mice is highly genotype-dependent. In comparison with serum lipid adjusted toxic equivalent factors (TEQs) for TCDD and dioxin-like compounds previously reported, the levels of hepatic TCDD measured in this study suggest that the dosing scheme provided environmentally relevant physiological levels of TCDD for the 1 and 100 ng/kg/day dose groups (Nault et al. 2016a). The mean level of TCDD in the vehicle control group was 2.8 ng/kg of liver and is not genotype-dependent.

As inbred mouse strains are known to carry one of four distinct *Ahr* alleles that impact affinity for AHR-ligands, an AHR amino acid sequence alignment was performed to determine the

Figure 4.1. Mean hepatic TCDD levels in 14 genetically-diverse mouse strains. GC/MS was used to assess the hepatic TCDD burden in mice (n=3) treated with 1 ng/kg or 100 ng/kg of TCDD for 10 consecutive days. Levels are reported as ng of TCDD per kg of liver (ng/kg). Bars indicate mean level of TCDD; error bars indicate standard error. Orange and blue box indicates the 95% confidence intervals of population-level mean TCDD levels for the 1 ng/kg/day and 100 ng/kg/day dose group, respectively. White dotted lines within colored boxes indicate the population-level means for respective dose group.

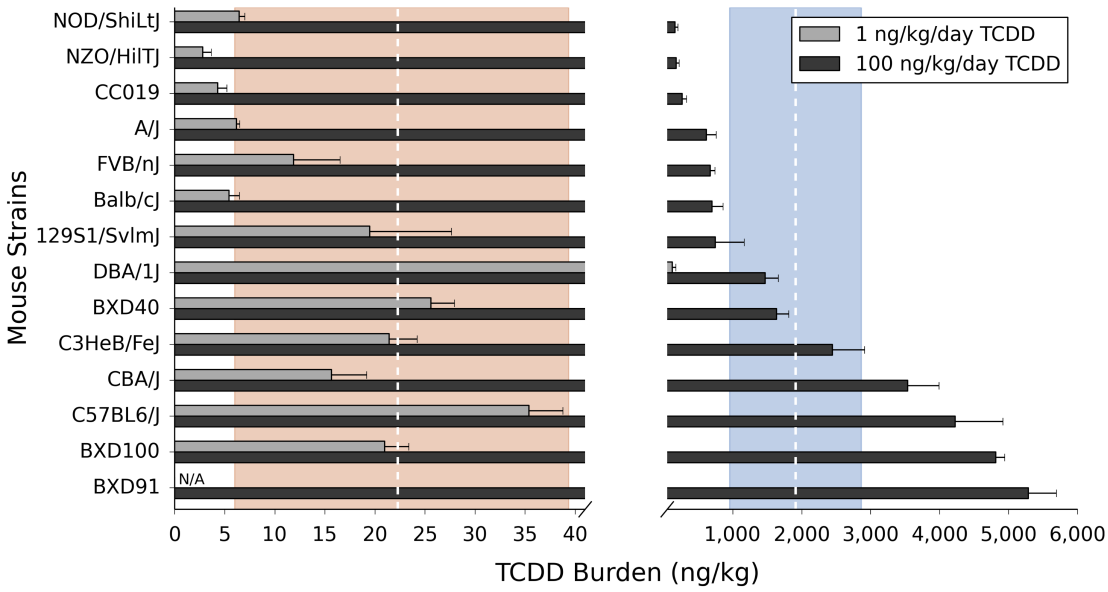

Table 4.1. Coeffecient estimates for regression model comparing inter-strain differences in hepatic TCDD accumulation for the 100 ng/kg/day dose group. All coefficient estimates are relative to the NOD/ShiLtJ which had the lowest mean level of hepatic TCDD across the 14 mouse strains. Stars (*) indicate a p <0.05.

Coefficient	Estimate	Standard Error	t value	Pr (>|t|)
Intercept	159.27	315.46	0.505	0.618
129S1/Svlmj	588.07	446.13	1.318	0.198
A/J	457.07	446.13	1.025	0.314
BALB/cJ	536.93	446.13	1.204	0.239
BXD100	4653.15	446.13	10.430	<0.001*
BXD40	1474.07	446.13	3.304	0.002*
BXD91	5127.40	446.13	11.493	<0.001*
C3HeB/FeJ	2284.07	446.13	5.120	<0.001*
C57BL/6J	4064.07	446.13	9.110	<0.001*
CBA/J	3374.07	446.13	7.563	<0.001*
CC019	104.73	446.13	0.235	0.816
DBA/1J	1307.40	446.13	2.931	0.006*
FVB/NJ	514.40	446.13	1.153	0.259
NZO/HILTJ	20.17	446.13	0.045	0.964

Residual Standard Error: 22.06 on 47 degrees of freedom.

Multiple R^2: 0.939; Adjusted R^2: 0.911

F Statistic: 33.37 on 13 of 28 degrees of freedom; p = <0.001*

Ahr allele carried by each strain (Poland and Glover 1990; Poland et al. 1994; Thomas et al. 2002). Phylogenetic analysis indicates that mice in this study carry one of three distinct *Ahr* alleles: 1) Ahr^{b1} (grey), 2) Ahr^{b2} (blue), and 3) Ahr^{d} (green)(Figure 4.2A). On average, the level of TCDD sequestered in the liver is impacted by the *Ahr* allele carried by the mouse strain (Figure 4.2B). The mean level of TCDD in Ahr^{b1} mice is significantly higher than the mean levels found in Ahr^{b2} and Ahr^{d} mice ($p<0.05$). Similarly, Ahr^{b2} mice sequester more TCDD than Ahr^{d} mice ($p<0.05$). Notably, allelic differences in TCDD burden were only present in mice treated with 100 ng/kg/day TCDD and not at the lower dose of TCDD.

While there are significant differences in the mean levels of TCDD across *Ahr* alleles in the 100 ng/kg/day dose group, there is clearly intra-allelic variability (Figure 4.2C). For example, DBA/1J and BXD40 were found to have significantly higher TCDD burdens than other Ahr^{d} mice such as NOD/ShiLtJ, NZO/HlLtJ, and CC019 ($p<0.05$). Similarly, CBA/J had significantly higher TCDD burden than all the other Ahr^{b2} mice ($p<0.05$). C3HeB/FeJ were found to accumulate significantly higher levels of TCDD as compared to A/J ($p<0.05$). Notably, in comparing individual strains across allelic categories, several Ahr^{d} allele mice, such as the 129S1/SvImJ, DBA/1J, and BXD40, were found to accumulate higher levels of TCDD than Ahr^{b2} mice, such as A/J, FVB/NJ, and BALB/cJ. These results suggest that, while the *Ahr* allele affects the sequestration of TCDD, other genomic factors likely also impact accumulation.

4.3.2. TCDD-induced expression of nine AHR-responsive genes

TCDD-induced expression (i.e. relative to vehicle control) of nine AHR-responsive genes were assessed with a customized NanoString PlexSet. Of the 243 total gene expression vs. dose group vs. mouse strain combinations, 36 combinations were found to have statistically significant increases in expression as compared to the strain's respective vehicle control ($p<0.05$; Table 4.2). A sensitive (i.e. expressing the Ahr^{b1} allele, BXD100) and less-sensitive strain (i.e. expressing the

Figure 4.2. Genotype-dependent differences in accumulation of TCDD in the liver. AHR amino acid sequence alignment was used to identify the allele carried by each strain: 1) *Ahr*^{b1} (grey), 2) *Ahr*^{b2} (blue), and 3) *Ahr*^{d} (green)(**A**). TCDD concentrations in the liver for each strain were used to calculate the mean level of TCDD found to accumulate within each *Ahr* allelic category. Results were used to compare mean TCDD levels across *Ahr* alleles (**B**); asterisk (*) indicates $p<0.05$. Mean TCDD levels in each strain were also compared within *Ahr* allelic categories (**C**). Letters over bars indicate significant differences ($p<0.05$) with the mean of: [a]NOD/ShiLtJ, [b]NZO/HlLtJ, [c]CC019, [d]A/J, [e]FVB/NJ; [f]BALB/cJ, [g]C3HeB/FeJ ($p<0.05$). In all cases, grey indicates an *Ahr*^{b1} allele (very high affinity), blue indicates an *Ahr*^{b2} allele (high affinity), and green indicates an *Ahr*^{d} allele (low affinity). Bars indicate means and error bars indicate standard error.

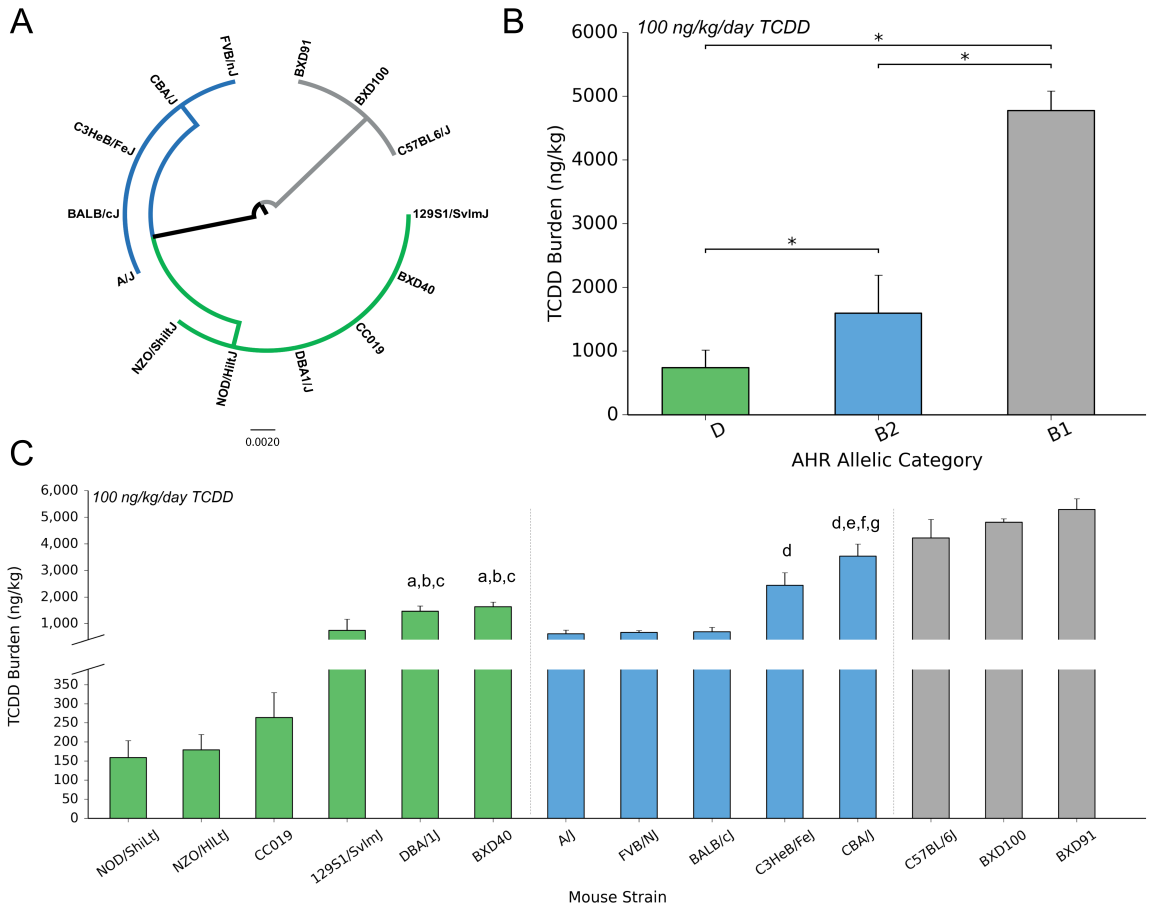

Table 4.2. TCDD-induced fold changes of 9 AHR-responsive hepatic genes in 14 genetically-diverse mice relative to the intra-strain vehicle control. Yellow highlights genes differentially expressed compared to the intra-strain vehicle control (Fold change ≥ 1.5; p ≤ 0.05). Grey indicates an *Ahr*^{b1} allele (very high affinity), blue indicates an *Ahr*^{b2} allele (high affinity), and green indicates an *Ahr*^{d} allele (low affinity).

Ahr Allele	Strain	Dose (ng/kg/day)	Ahrr	Cyp1a1	Cyp1a2	Cyp1b1	Gpnmb	Mt2	Pmm1	Serpinb2	Slc15a2
Ahr ^{b1}	BXD91	100	1.5	1,693.91	15.59	1.15	2.48	1.05	2.52	1.04	3.74
	C57BL6/J	1	1.59	1.43	1.65	1.28	1.43	1.1	1	3.15	1.09
		100	1.74	988.86	13.3	3.31	3.17	1	1.73	4.07	3
	BXD100	1	-1.38	3.5	1.35	1.11	-1.08	-1.5	1.01	1.67	-3.25
		100	-1.47	1,678.36	11.17	1.44	1.75	1.18	1.9	5.32	1.29
Ahr ^{b2}	A/J	1	-2.13	1.04	1.09	-1.81	-4.7	-1.11	-1.11	-3.13	1.5
		100	-1.95	20.34	6.34	-1.39	-2.03	-1.13	1.28	1.01	1.42
	Balb/cJ	1	-1.29	2.17	1.39	2.04	2.4	1.28	-1.01	2.54	1.49
		100	1.03	260.56	8.12	1.4	1.42	-1.12	1.5	3.21	1.36
	FVB/nJ	1	1.62	1.36	1.51	1.49	-1.06	1.37	-1.14	-2	1.06
		100	1.96	34.21	5.48	1.33	1.41	1.41	1.12	-3.31	1.65
	C3HeB/FeJ	1	1.67	1.45	2.09	1.69	-1.16	1.03	-1.09	-1.04	1.48
		100	1.52	373.63	11.53	2.88	1.71	-1.08	1.49	2.14	2.51
	CBA/J	1	1.11	1.81	1.14	1.49	1.79	-1.33	1.38	1.53	-2.57
		100	1.41	636.5	12.72	2.61	4.37	-1.11	1.98	2.25	1.37
Ahr ^{d}	CC019	1	1.57	1.13	-1.04	-1.17	1.37	1.34	-1.32	1.29	4.05
		100	-1.42	1.43	1.75	-1.01	1.11	1.32	-1.32	1.87	1.17
	DBA/1J	1	1.3	-1.85	1.28	1.49	-1.04	1.36	1.22	-5.57	1.41
		100	-1.2	2.27	3.4	1.54	1.19	1.02	1.18	-5.87	2.08
	BXD40	1	1.15	1.24	1.22	-1.09	1.8	-1.59	1.01	4.25	1.1
		100	1.33	4.57	2.73	-1.08	2.15	-1.14	-1.05	4.79	-1.21
	NOD/ShiLtJ	1	-1.04	1.08	1.08	-1.41	1.3	-1.14	-1.15	2.54	-2.01
		100	-1.25	-1.73	1.4	-1.95	-1.21	-1.62	1.08	-1.29	-1.09
	NZO/HiltJ	1	1.36	2.04	-1.01	1.28	-2.3	-1.6	1.06	8.96	1.43
		100	-1.05	1.3	1.09	1.58	-2.38	-1.91	1	2.35	1.49
	129S1/SvImJ	1	-1.24	1.54	1.06	1.33	-1.38	-1.27	1.04	1.09	-1.53
		100	1.82	3.29	3.12	-1.03	-1.28	-1.47	-1.1	-1.62	1.45

Ahr^{d} allele, NOD/ShiLtJ) were chosen to confirm NanoString Technology PlexSet results using QRTPCR. Both technologies indicate a significant induction of *Cyp1a1* expression in BXD100 at 100 ng/kg/day dose group ($p<0.05$; Figure 4.3A). Similarly, both technologies indicate repression in the expression of *Cyp1a1* at 100 ng/kg/day in NOD/ShiLtJ (Figure 4.3B). There were no significant differences in comparing technologies at either dose group for either the BXD100 and NOD/ShiLtJ.

The greatest TCDD-induced changes were found in *Cyp1a1* expression with up to 1,694-fold increases (Table 4.2). The largest number of statistically significant changes were found in *Cyp1a2* expression across strains ($p<0.05$; $n=10$; Table 4.2). All genes were found to contain at least one strain that had a significant change in gene expression with the exception of *Mt2* ($p<0.05$; Table 4.2). The vast majority of significantly dysregulated fold changes were found at the higher-dose (100 ng/kg/day) of TCDD ($p<0.05$: Table 4.2). The greatest percentage of significantly TCDD-dysregulated genes were found in *Ahr*^{b1} mice; of 45 gene expression vs. TCDD dose vs. strain combinations, 15 genes were significantly dysregulated by TCDD (33.3% of total; $p<0.05$; Table 4.2). Within the *Ahr*^{b2} mice, 16 of 90 combinations were significantly dysregulated (17.8% of total; $p<0.05$; Table 4.2). Within the *Ahr*^{d} mice, 5 of 108 combinations were found significantly dysregulated (4.6% of total $p<0.05$; Table 4.2). The mean fold changes of *Cyp1a1* and *Cyp1a2* expression in 100 ng/kg/day dose group were chosen to directly compare the TCDD-induced gene expression across alleles. Results indicate that, for both genes, there are significant differences across *Ahr* alleles that adhere to previously published reports (Figure 4.4A and 4B)(Poland et al. 1994). In both cases, TCDD induced significantly more expression in *Ahr*^{b1} and *Ahr*^{b2} as compared to *Ahr*^{d} mice ($p<0.05$; Figure 4.4A and 4B). Similarly, *Ahr*^{b1} mice were found have significantly higher induction as compared to the *Ahr*^{b2} mice ($p<0.05$; Figure 4.4A and 4.4B).

Figure 4.3. Nanostring Technology-based PlexSet confirmation with QRTPCR. TaqMan-based QRTPCR was used to confirm the results acquired from the Nanostring PlexSet (n≥4). An ANOVA was used to compare TCDD-induced expression of *Cyp1a1* for a strain that is sensitive (BXD100; **A**) and a strain that is less-sensitive (NOD/ShiLtJ; **B**) to TCDD. Asterisks (*) indicate a significant difference ($p<0.05$) compared to the vehicle control for that respective technology. Black bars indicate QRTPCR data and grey bars indicate Nanostring data; error bars indicate standard error.

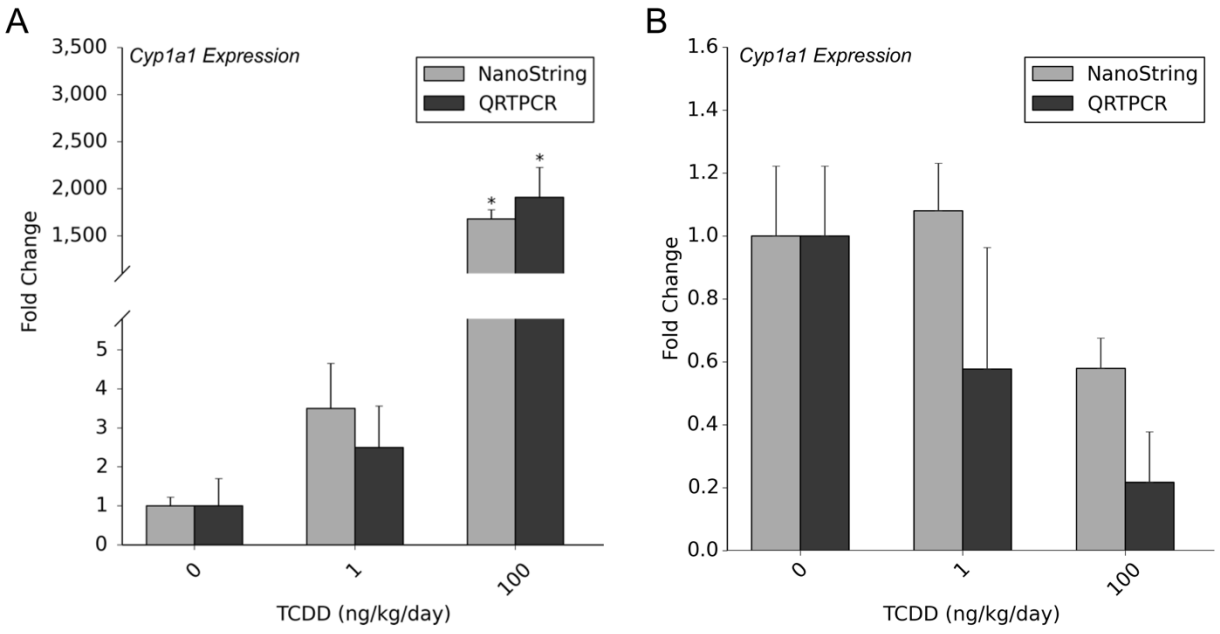

Figure 4.4. Genotype-dependent differences in TCDD-induced expression of hepatic *Cyp1a1* and *Cyp1a2* in 14-genetically diverse mouse strains. TCDD-induced fold change in *Cyp1a1* (**A**) and *Cyp1a2* (**B**) expression within *Ahr* allelic categories. Mean TCDD-induced fold changes in the expression of *Cyp1a1* (**C**) and *Cyp1a2* (**D**) for each strain compared to *Ahr* allelic category. Asterisk (*) indicates a significant difference ($p<0.05$) compared to the vehicle control and, if over bracket, indicates a comparison across alleles. Letters over bars indicate significant differences ($p<0.05$) as compared to means of: [a]NOD/ShiLtJ, [b]NZO/HiLtJ, [c]CC019, [d]DBA/1J, [e]A/J, [f]FVB/NJ; [g]BALB/cJ, [h]C57BL/6J, [i]BXD100, [j]BXD91 ($p<0.05$). In all cases, grey indicates an Ahr^{b1} allele, blue indicates an Ahr^{b2} allele, and green indicates an Ahr^{d} allele. In all cases, bars indicate means and error bars indicate standard error.

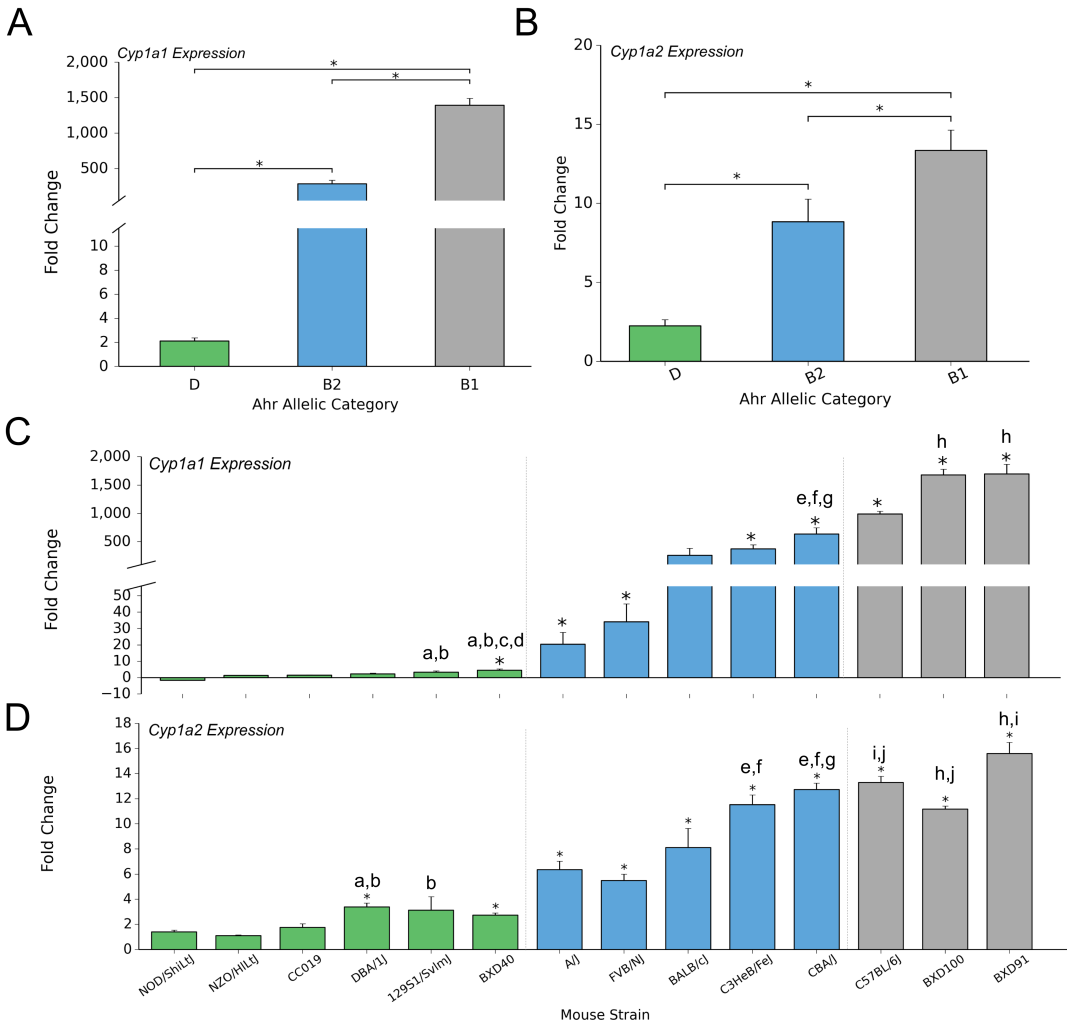

While there are significant differences across *Ahr* alleles in TCDD-induced *Cyp1a1* and *Cyp1a2* expression, there are also intra-allelic differences across strains as well (Figure 4.4C and 4.4D). For example, 129S1/SvlmJ and BXD40 were found to have more TCDD-induced *Cyp1a1* expression than several other Ahr^{d} mice ($p<0.05$; Figure 4.4C). CBA/J mice were found to have significantly higher TCDD-induced *Cyp1a1* expression than several other Ahr^{b2} mice ($p<0.05$; Figure 4.4C). Similarly, BXD100 and BXD91, which carry the Ahr^{b1} allele, were found to have significantly higher TCDD-induced *Cyp1a1* expression as compared to the C57BL/6J ($p<0.05$; Figure 4.4C). TCDD-induced *Cyp1a2* expression was found to having differing patterns of intra-allelic variability. For example, Ahr^{d} mice, such DBA/1J, have significantly more TCDD-induced expression as compared to NOD/ShiLtJ and NZO/HlLtJ ($p<0.05$; Figure 4.4D). Similarly, 129S1/SvlmJ had significantly more TCDD-induced *Cyp1a2* expression as compared to the NZO/HlLtJ, but not NOD/ShiLtJ which was seen in the *Cyp1a1* expression profile ($p<0.05$; Figure 4.4D). For Ahr^{b2} mice, C3HeB/FeJ was found to have significantly more TCDD-induced *Cyp1a2* expression to other Ahr^{b2} mice ($p<0.05$; Figure 4.4D). Finally, all three Ahr^{b1} mice have significantly different levels of TCDD-induced expression of *Cyp1a2* ($p<0.05$; Figure 4.4D). Most notably, several Ahr^{b1} mice, such as C57BL/6J and BXD100, have very similar or less TCDD-induced expression of *Cyp1a2* as compared to mouse strains that carry the Ahr^{b2} allele, such as the C3HeB/FeJ and the CBA/J. These results suggest that other genomic factors that are independent of the inherited *Ahr* allele likely impact TCDD-induced expression of AHR-responsive genes.

4.3.3. Dynamics of TCDD burden and AHR-mediated expression in the liver

The mean hepatic TCDD burden and the mean number of probe counts (i.e. transcripts) as normalized to 3 house-keeping genes for each AHR-responsive gene was used to analyze the dynamics of TCDD-induced gene expression for each dose group. In the 1 ng/kg/day TCDD dose group, no significant correlations between gene expression and hepatic TCDD burden were

identified. For the higher-dose of TCDD, however, 4 of the 9 AHR-target genes were found to correlate with the hepatic levels of TCDD in a statistically significant and positive manner (Figure 4.5). The strongest correlation with hepatic TCDD burden was with *Cyp1a1* expression ($p<0.05$, $r=0.951$; Figure 4.5A). *Cyp1a2* expression was the second-highest correlation found with TCDD burden ($p<0.05$, $r=0.899$; Figure 4.5B). Expression of *Cyp1b1* and *Pmm1* were also significantly-associated with hepatic TCDD burden ($p<0.05$; $r=0.805$ and $r=0.612$, respectively; Figure 4.5C and 4.5D). The correlations of hepatic TCDD burden and expression of *Ahrr* and *Serpinb2* were trending towards significance (Figure 4.5E and 4.5F). Expression of *Ahrr*, *Gpnmb*, and *Mt2* were not associated with hepatic TCDD burden which is most likely due to the limited TCDD-induced changes (Figure 4.5G, 4.5H, and 4.5I). Thus, Pearson correlation analysis indicates that, amongst the 9 AHR-target genes assessed, higher levels of TCDD-induced activation of AHR-battery genes tend to positively correlate with the levels of TCDD in the liver. This is further confirmed by the lack of correlation at the lower dose where minimal numbers of significant differences in TCDD-induced expression were present.

4.3.4. Quantitative trait locus analysis

QTL analysis was used to identify potential genes and pathways associated with the inter-strain differences in TCDD accumulation in the liver. For the lower-dose group of TCDD, four significant QTL peaks were identified in the 1 ng/kg/day TCDD dose group ($p<0.05$). More interestingly, in scanning for QTLs that may drive inter-strain differences in accumulation of TCDD within the 100 ng/kg/day dose group of TCDD, a strong, statistically significant association was identified in mouse Chromosome 1 ($p<0.001$). As this region may be involved in modulating inter-strain differences in TCDD accumulation, genes within 1.5 Mb of the significant peak were compiled into a candidate gene list for further analyses (Table 4.3). QTL analysis was also used to identify potential genetic modifiers that drive inter-strain differences in TCDD-induced gene dysregulation. As very few of the genes were significantly dysregulated at the lower-dose of TCDD

Figure 4.5. Correlation between TCDD-induced gene dysregulation and TCDD burden in the liver of 14 genetically-diverse mouse strains. Pearson's correlation (*r*) analysis between log-transformed hepatic TCDD levels of and TCDD-induced gene expression for: 1) *Cyp1a1* (**A**), 2) *Cyp1a2* (**B**), 3) *Cyp1b1* (**C**), 4) *Pmm1* (**D**), 5) *Serpinb2* (**E**), 6) *Slc15a2* (**F**), 7) *Ahrr* (**G**), 8) *Gpnmb* (**H**), and 9) *Mt2* (**I**). In all cases, p values and r values for the respective gene are reported within the graph.

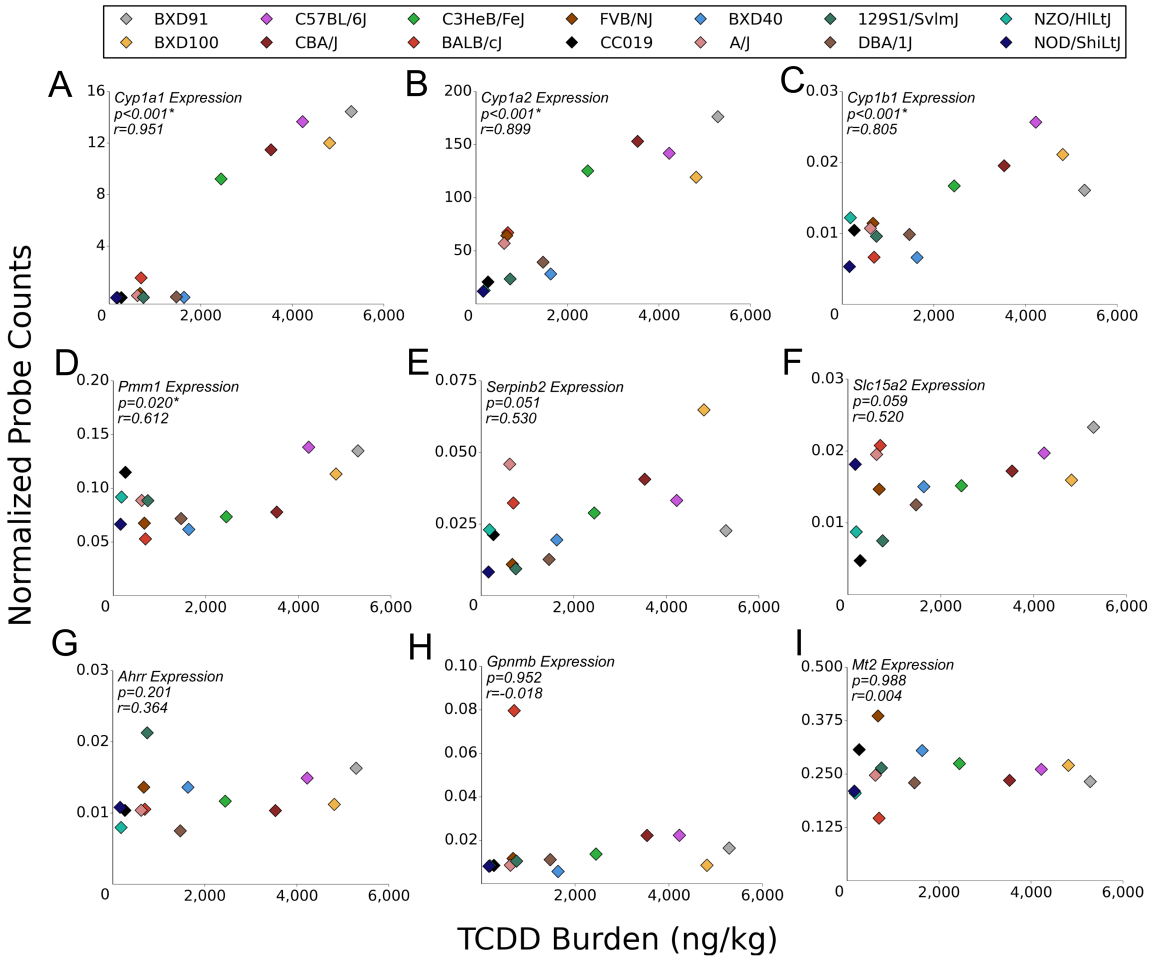

Table 4.3. Candidate genes associated with inter-strain differences in TCDD-induced endpoints. Genes located within 1.5 Mb of all significantly associated markers are lists. Grey highlighting indicates genomic regions associated with multiple TCDD-induced endpoints in this study. Bolded genes were prioritized for further analysis.

Endpoint	Chromosome	Location (Mb)	Logs of Difference (LOD)	P-value	Genes Within Region
Liver Burden of TCDD	1	133.189	>50	<0.001	*Rab7b, Slc26a9, Slc41a1, Rab29, Nucks1, Slc34a3, Elk4, Mfsd4a, Cdk18, Lemd1, Mir135b, Klhdc8a, Nuak2, Tmcc2, Dstyk, Rbbp5, Tmem81, Cntn2, Nfasc, Lrm2, Mdm4, Pik3c2b, Ppp1r15b, Plekha6, Golt1a, Ren2,* ***Kiss1****, Sox13,* ***Etnk2****, Zc3h11a, Zbed6, Lax1, Atp2b4, Optc, Prelp, Fmod, Btg2, Chit1, Chil1, Mybph, Adora1, Ppfia4, Tmem183a, Myog,* ***Adipor1****, Klhl12, Rabif, Kdm5b, Syt2*
Slc15a2	1	133.189	>50	<0.001	
Cyp1a2	1	133.189	>50	<0.001	
Ahrr	1	133.189	>50	<0.001	
Pmm1	9	117.389	>50	<0.001	*Gad11,* ***Tgfbr2****, Rbms3, Zcwpw2, Azi2, Cmc1, Platr11, Eomes, Golga4, Itga9*
Ahrr	9	117.389	>50	<0.001	
Cyp1a1	11	69.478	6.119	0.022	*Ntn1, Myh10, Ndel1, Aurkb, Vamp2, Per1 Hes7, Alox8, Kdm6b, Efnb2, Trp53, Atp1b2, Cd68, Eif4a1, Tnfsf13, Tnfsf12, Polr2a, Nlgn2, Slc2a4, Dvl2, Acadvl, Dlg4, Asgr1, Alox12, Alox15, Arrb2, Cxcl16, Pld2, Chrne, Gp1ba, Pfn1*
Pmm1	X	139.214	>50	<0.001	*Tex13a, Il1rapl2, Nrk, Serpina7, Mum1l1, Platr21, Trap1a, Rnf128, Tbc1d8b, Ripply1, Cldn2, Morc4, Rbm41, Nup62cl, Pih1h3b, Mir3475, Frmpb3, Prps1, Tsc22d3, Mid2*

(3.4% of total; Table 4.3), QTL analysis was focused on the data from the higher-dose group where significant gene dysregulation was more prevalent (Table 4.3). Furthermore, *Mt2* data was not included in QTL analysis due to lack of statistically significant changes induced by TCDD. QTL analysis of inter-strain differences in TCDD-induced dysregulation of 9 AHR-responsive genes identified 9 statistically significant QTL peaks (Table 4.3). There are 3 statistically significant associations in Chromosome 1, 2 associations in Chromosome 9, and 1 association in Chromosome 11 and X. Candidate gene lists of genes within 1.5 Mb of the significant marker were compiled for each dose group (Table 4.3). Interestingly, several significantly associated markers were identified for ≥ 2 endpoints. For example, a region of Chromosome 1 was identified while scanning for modulators of hepatic TCDD accumulation and expression of 3 AHR-responsive genes: *Slc15a2*, *Cyp1a2*, and *Ahrr* (Table 4.3). Similarly, QTL analysis also identified a marker on mouse Chromosome 9 that potentially impacts TCDD-induced *Pmm1* and *Ahrr* expression (Table 4.3).

4.3.5. Potential genetic modulators of TCDD burden and TCDD-induced gene expression

Genomic regions where ≥ 2 significant associations were identified by QTL analysis were prioritized for further investigation. Several genes within these regions have previously been associated with TCDD-induced gene dysregulation or phenotypes seen with TCDD exposures. Within the region of Chromosome 1, *Kiss1* and *Entk2* expression have been reported as dysregulated by TCDD (Table 4.3)(Forgacs et al. 2012; Mueller and Heger 2014). Similarly, while *Adipor1* has not been shown to be dysregulated by TCDD, the adiponectin pathway has been previously implicated in TCDD-induced phenotypes (Table 4.3)(Angrish et al. 2013). In this mouse panel, TCDD was not found to dysregulate mRNA expression of these genes in a subset of strains that were analyzed (Table 4.4). Similarly, polymorphisms in coding regions were not found to be associated with inter-strain differences in response to TCDD. Another of gene interest is *Tgfbr2* which resides in the overlapping associations found on mouse Chromosome 9 (Table 4.3).

Table 4.4. TCDD-induced fold changes of the expression of genes within genomic regions identified with QTL analysis. Mean fold changes (n=5) are reported with standard error in parenthesis. Grey indicates an *Ahr*^{b1} allele (very high affinity) and green indicates an *Ahr*^{d} allele (low affinity).

Strain	TCDD (ng/kg/day)	Tgfbr2 Fold Change (SE)	Kiss1 Fold Change (SE)	Etnk2 Fold Change (SE)	Adipor1 Fold Change (SE)
C57BL/6	0	1.00 (0.08)	1.00 (0.33)	1.00 (0.29)	1.00 (0.21)
	1	0.56 (0.02)	1.58 (0.33)	1.14 (0.33)	0.80 (0.09)
	100	0.80 (0.02)	0.85 (0.23)	1.10 (0.22)	0.99 (0.07)
BXD100	0	1.00 (0.21)	1.00 (0.21)	1.00 (0.11)	1.00 (0.04)
	1	1.01 (0.09)	2.46 (0.68)	1.70 (0.23)	1.08 (0.12)
	100	0.98 (0.22)	2.10 (0.57)	1.14 (0.19)	1.05 (0.12)
NOD/ShiLtJ	0	1.00 (0.11)	1.00 (0.24)	1.00 (0.12)	1.00 (0.05)
	1	0.64 (0.08)	2.20 (0.57)	1.16 (0.11)	0.74 (0.08)
	100	0.34 (0.15)	1.27 (0.53)	1.10 (0.21)	0.81 (0.19)
NZO/HlLtJ	0	1.00 (0.21)	1.00 (0.45)	1.00 (0.19)	1.00 (0.16)
	1	1.14 (0.25)	0.80 (0.22)	1.02 (0.42)	1.49 (0.12)
	100	0.77 (0.13)	0.69 (0.15)	0.85 (0.21)	0.88 (0.10)

Previous reports indicate that this gene is dysregulated by TCDD (Fraser et al. 2002; Gaido et al. 1992). In this study, the coding regions of *Tgfbr2* were found to be highly-conserved. While there were not differences in TCDD-induced fold changes of *Tgfbr2* mRNA found across a subset of strains, there were clear differences in basal expression of *Tgfbr2* mRNA expression (Table 4.4). Furthermore, previous literature has implicated the TGF-β pathway in TCDD-induced toxicity. Given the collective evidence, *Tgfbr2* was selected for further analysis.

4.3.6. *Tgfbr2* modulates TCDD-induced inflammation and lipid deposition in the liver

To test whether *Tgfbr2* is modulating TCDD-induced liver toxicity, a TGFBR2-Fc fusion protein previously shown to trap TGFBR2 ligands (i.e. TGFB1 and TGFB3) was used to inhibit TGFBR2 activity *in vivo* (Yung et al. 2016). Male and female C57BL/6 mice (i.e. Ahr^{b1} allele mice) were gavaged with either vehicle or 10 µg/kg/day of TCDD in the presence or absence of the TGFBR2-Fc fusion protein over 10 days. The hepatic expression of AHR-battery genes, such as *Cyp1a1*, *Cyp1a2*, and *Cyp1b1*, were significantly induced in all groups treated with TCDD. The TGFBR2 inhibitor did not affect the induction of *Cyp1a1*, *Cyp1a2*, and *Cyp1b1* by TCDD (Figure 4.6). As indicated by H&E staining of liver sections, male mice that received TCDD alone (i.e. without the TGFBR2-Fc protein) exhibited higher levels of infiltrating cells as compared to females using this dosing scheme (Figure 4.7A). Oil red O staining indicates that, for both males and females, TCDD induced significant increases in the lipid deposited in the liver which adheres to previously published reports (Figure 4.7A, 4.7B, and 4.7C)(Kopec et al. 2013; Nault et al. 2016a; Pierre et al. 2014). In comparison across treatment groups, treatment with a TGFBR2-Fc protein reduces the level of infiltrating immune cells in the liver of male, but not female, C57BL/6 mice treated with TCDD (Figure 4.6A). Interestingly, males that received TCDD and TGFBR2-Fc protein accumulate significantly more lipid in the liver as compared to TCDD alone (Figure 4.7A and 4.7B). While not significant, female mice also accumulated higher levels of lipid (Figure 4.7C).

Figure 4.6. TCDD-induced expression of AHR-target genes in the liver. QRTPCR was used to analyze the impact of TCDD, TGFBR2-FC fusion protein, and TCDD + TGFBR-Fc fusion protein co-treatment on expression of AHR-target genes for females (*Cyp1a1* (**A**), *Cyp1a2* (**B**) *Cyp1b1* (**C**)) and males (*Cyp1a1* (**D**), *Cyp1a2* (**E**) *Cyp1b1* (**F**)). Sample size (n) is ≥ 4 for all groups. Asterisk (*) indicates a $p<0.05$ as compared to the respective vehicle control: sesame oil vs. TCDD or sesame oil + TGFBR2-FC fusion protein vs. TCDD + TGFBR2-FC fusion protein.

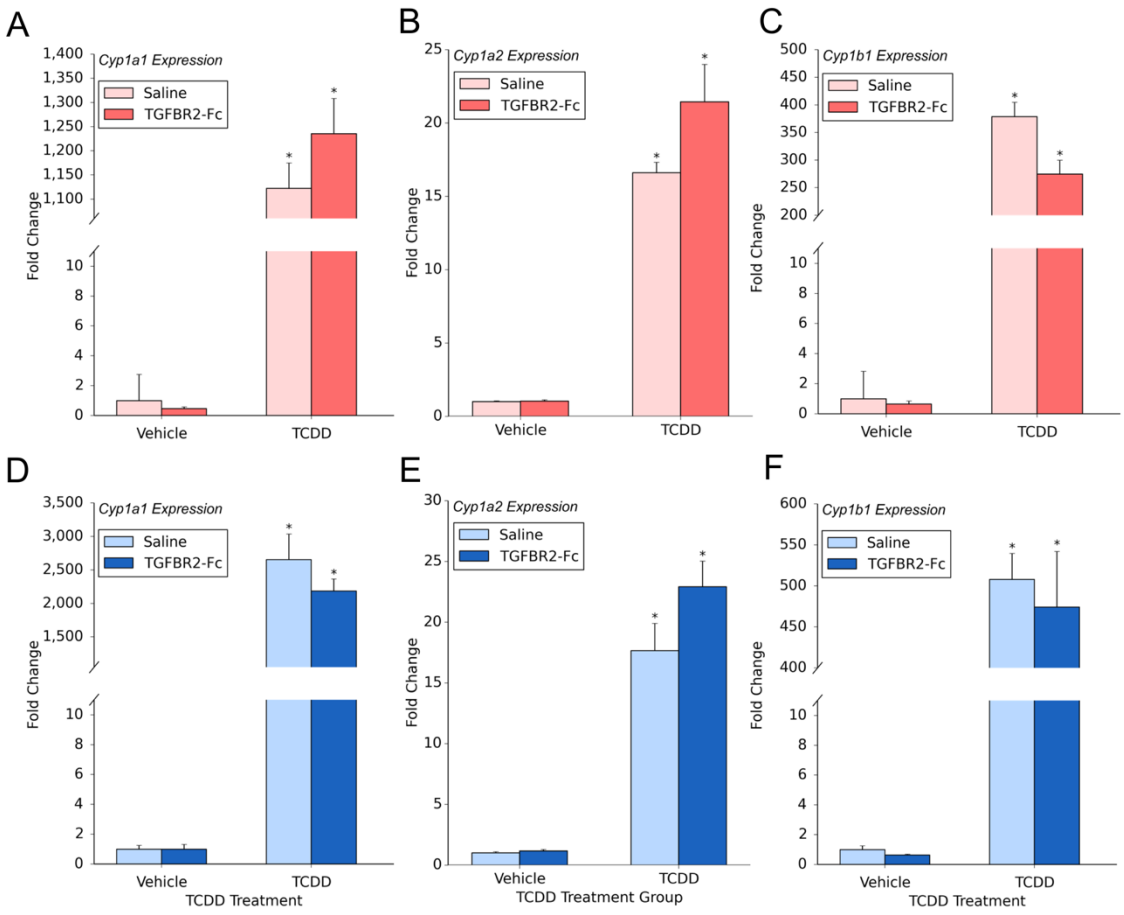

Figure 4.7. Hepatic histological effects of TCDD and TGFBR2 inhibitor co-treatment in C57BL/6 mice liver. Male and female C57BL/6 mice were treated with vehicle (sesame oil) or 10 µg/kg/day of TCDD for 10 consecutive days, along with an interperitoneal (IP) injection of vehicle (saline) or 15 mg/kg of an inhibitor of TGFBR2 activity every three days. Hematoxylin and eosin (H&E) staining was used to assess infiltrating immune cells and general tissue morphology and oil red O (ORO) was used to quantify lipid deposition. Representative samples were chosen for each treatment group (**A**). Scale bar represents 100 µm for H&E and 50 µm for ORO. Arrows indicate infiltrating immune cells in the H&E stain. Percent area stained with ORO was quantified using the Quantitative Histological Analysis Tool (QuHAnT) for males (**B**) and females (**C**)(Nault et al. 2015). All groups had sample sizes ≥ 4. Stars (*) indicate a $p<0.05$; stars directly over bars indicate differences in the TCDD treatment as compared to the vehicle control or, when over bracket, indicate a comparison of TCDD treatments across strains. Error bars indicate standard error.

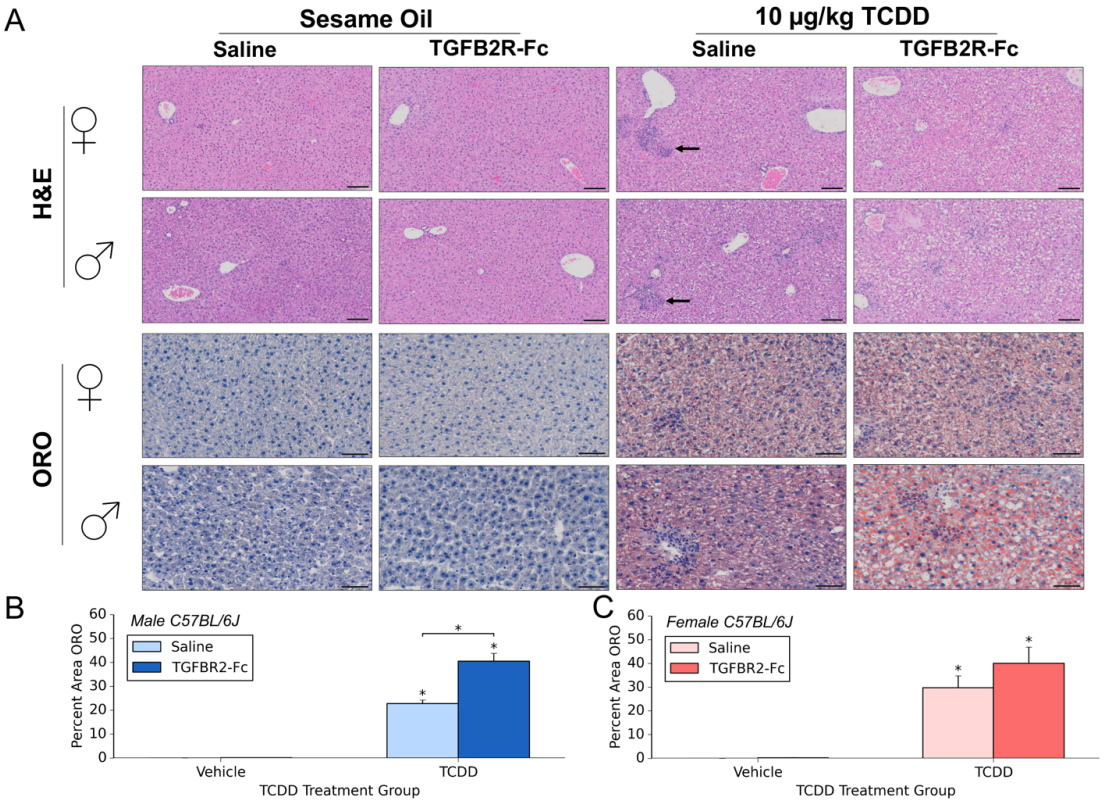

The impact of the TGFBR2-Fc protein on TCDD-induced gene expression was assessed with QRTPCR. In the absence of the TGFBR2-Fc protein, TCDD induce hepatic *Tgfbr2* levels in male C57BL/6 mice ($p<0.05$; Figure 4.8A). Similarly, TCDD-induced a significant increase in *Tgfb1* expression as previously reported ($p<0.05$; Figure 4.8B)(Pierre et al. 2014). In comparing across treatment groups, TCDD-induced expression of *Tgfbr2* and *Tgfb1* were found to be significantly lower in the liver of male mice that received TCDD and the TGFBR2-Fc protein as compared to TCDD alone ($p<0.05$; Figure 4.7A and 4.8B). While TCDD-induced expression of *Tgfb3*, another ligand of TGFBR2, was found to be significantly higher in male mice that received TCDD and the TGFBR2-Fc protein, the basal expression of *Tgfb3* was >250 fold lower as compared to the other ligand of TGFBR2, *Tgfb1* (Figure 4.8C). The increase in *Tgfb3* expression induced by TCDD is likely negligible in comparison to the decrease in *Tgfb1* expression. TCDD-induced expression of several pro-inflammatory genes, such as *Tnf*, *Il6*, and *Ccl2*, were also lower in the male mice found to have less immune cell infiltration ($p<0.05$; Figure 4.8D, 4.8E, and 4.8F). The inflammatory mRNA expression data further confirms that the TGFBR2-Fc protein decreases TCDD-induced hepatic inflammation in males. In contrast to the male C57BL/6J mice, the TGFBR2-Fc protein did not impact the TCDD-induced expression of *Tgfbr2*, TGF-β ligands, or pro-inflammatory cytokines in females.

Figure 4.8. Altered TCDD-induced mRNA expression in the liver by inhibition of TGF-β receptor type II (TGFBR2) activity. QRTPCR was used to analyze the effect of inhibiting TGFBR2 activity on TCDD-induced expression of *Tgfbr2* (**A**), *Tgfb1* (**B**) *Tgfb3* (**C**), *Tnf* (**D**), *Il6* (**E**), and *Ccl2* (**F**). All groups had sample sizes ≥ 4. Asterisk (*) indicates a $p<0.05$; stars directly over bars indicate differences in the TCDD treatment as compared to the vehicle control or, when over bracket, indicate difference between treatment group. Error bars indicate standard error.

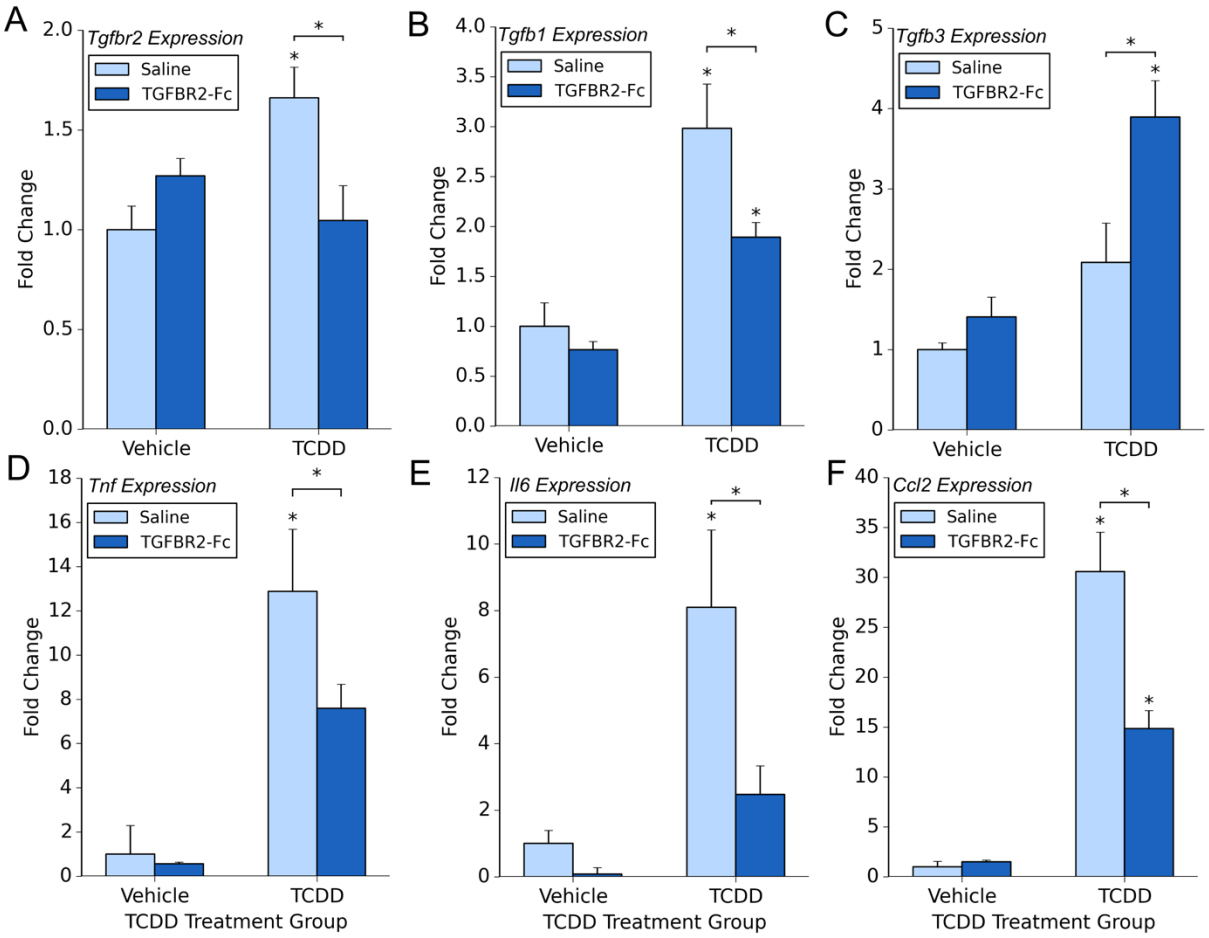

4.4. Discussion

In this study, a mouse population-based study was used to characterize the dynamics of TCDD accumulation and AHR-mediated transcription in the liver of pregnant mice. The results indicate > 40-fold differences in the mean level of hepatic TCDD burden across strains (Figure 4.1). Both TCDD burden and TCDD-induced transcription of AHR-responsive genes appear to be highly-dependent on genotype (Figure 4.3B; Figure 4.4A and 4.4B). On average, strains which are more susceptible to TCDD-induced toxicity, such as Ahr^{b1} and Ahr^{b2} mice, accumulate significantly higher levels of TCDD in the liver over 10 days of consecutive exposure (Figure 4.3B). Overall, higher levels of TCDD-induced transcription of AHR-responsive genes correlate with higher levels of TCDD burden in the liver (Figure 4.5). The results suggest that the TCDD-induced gene dysregulation likely drives hepatic sequestration during repeated TCDD exposure.

These results build upon previous studies that have indicated that AHR-mediated transcription of *Cyp1a2* drives sequestration of TCDD (Diliberto et al. 1997; Hakk et al. 2009; Voorman and Aust 1989). Our study further confirms these findings as *Cyp1a2* expression is highly-correlated with hepatic TCDD burden over repeated TCDD exposure (Figure 4.5B). However, several strains, such as BXD40 and BXD100, appear to be exceptions, as they accumulate higher levels of TCDD in the liver than can be explained by *Cyp1a2* expression alone (Figure 4.3C, Figure 4.4D, Figure 4.5B). Exceptions were also found in correlations of hepatic TCDD burden with other TCDD-induced expression of AHR-responsive genes, such as *Cyp1a1*, *Cyp1b1*, and *Pmm1* (Figure 4.5A, 4.5C, and 4.5D). Such exceptions suggest that other genomic factors impact AHR-signaling beyond the *Ahr* allele inherited by the strain.

QTL analysis was used to scan for genetic modifiers that may impact inter-strain differences in TCDD accumulation and AHR-mediated expression across the mouse panel. Several regions of the mouse genome, such as Chromosome 1 and 9, were found to be

associated with the inter-strain differences seen in multiple endpoints (Table 4.2). A region of Chromosome 1 was associated with the inter-strain differences in TCDD accumulation and TCDD-induced expression of 3 AHR-target genes: *Slc15a2*, *Cyp1a2*, and *Ahrr*. Several genes within this region are of particular interest: 1) *Etnk2*, 2) *Kiss1*, and 3) *Adipor1*. *Etnk2,* which encodes for ethanolamine kinase 2, has been previously reported to be dysregulated following TCDD exposure within mouse liver (Forgacs et al. 2012). This gene is expressed highly in the liver and has been shown to be involved in catalyzing the first step of cytidine diphosphate (CDP)-ethanolamine pathway that results in phosphatidylethanolamine, a common phospholipid within the mammalian cell membrane (Tian et al. 2006; Vance and Vance 2004). *Kiss1*, which encodes for Metastasis-suppressor 1 (aka Kisspeptin1) is also dysregulated by TCDD (Mueller and Heger 2014). While KISS1 has been found to be a key regulator of Gonadotropin-releasing hormone (GnRH) in humans, a recent rodent study has suggested that hepatic *Kiss1* is involved in regulating insulin secretion (Skorupskaite et al. 2014; Song et al. 2014). Previous reports have associated TCDD exposures with hyperinsulinemia in humans exposed to TCDD (Cranmer et al. 2000). *Adipor1*, which encodes for adiponectin receptor 1, is involved in the adiponectin pathway which has been previously implicated in toxicity induced by TCDD and other dioxin-like compounds (Angrish et al. 2013; Wahlang et al. 2013). Adipokines and their associated signaling cascades play important roles in pathologies that are associated with TCDD exposures in humans, such as metabolic syndrome and diabetes (Combs and Marliss 2014; Lopez-Jaramillo et al. 2014). In a subset of mouse strains analyzed in this study, TCDD did not alter the expression of these genes. Genetic sequence analysis did not indicate any causative polymorphisms that appear to drive differing phenotypes. Further analysis is required to elucidate the significance of these genes in modulating TCDD-induced toxicity.

A region of Chromosome 9 was also of particular interest where overlapping associations were identified for TCDD-induced *Pmm1* and *Ahrr* expression (Table 4.2). *Tgfbr2*, which was

located near the significant marker, was of particular interest as the TGF-β pathway has previously been implicated within TCDD-elicited liver toxicity (Pierre et al. 2014). The AHR is likely involved in regulating the TGF-β pathway as *Ahr*$^{-/-}$ mice secrete higher levels of TGF-β ligands (Guo et al. 2004; Zaher et al. 1998). Furthermore, TGF-β signaling has been implicated in promoting liver steatohepatisis and fibrosis, which are phenotypes observed in rodents following TCDD exposure (Bernasconi et al. 1995; Border and Noble 1994; Friedman 1993; Yang et al. 2014). Previously published datasets also indicate the presence of putative DREs with bound AHR (i.e ChIP peaks) near the *Tgfbr2* promoter region (Fader et al. 2017; Nault et al. 2016b). To investigate the role of TGFBR2 within TCDD-induced liver toxicity, C57BL/6 mice (i.e. *Ahr*^{b1} allele) were treated with TCDD along with a TGFBR2-Fc protein that traps TGFBR2 ligands (Yung et al. 2016). Results suggest that upon repeated exposure to 10 μg/kg of TCDD for 10 days, TGFBR2 activity is involved in modulating TCDD-elicited liver toxicity in male, but not female, C57BL/6 mice. Male mice that received TCDD along with TGFBR2 inhibitor, as compared to TCDD alone, have less infiltrating immune cells (Figure 4.7A) and lower levels of expression of pro-inflammatory genes ($p<0.05$; Figure 4.8D, 4.8E, and 4.8F). The TGFBR2 pathway is likely involved in increasing TCDD-induced inflammation in the liver of male C57BL/6 mice. This trend was not present in females (Figure 4.7A). Notably, females that received TCDD alone had mild inflammation and, while TGFBR2 inhibitor slightly decreased the level of inflammatory cells, the difference was not statistically significant. We hypothesize that, with exposure to higher levels of TCDD, females would display a similar phenotype to males upon inhibition of TGFBR2 activity. Interestingly, hepatic lipid accumulation is higher in mice that received TCDD and the TGFBR2 inhibitor ($p<0.05$; Figure 4.7A and 4.7B). Female mice, while not significant, also have higher lipid levels following co-treated with TCDD and the TGFBR2 ligand trap (Figure 4.7A and 4.7C). Our results suggest, upon TCDD exposure, TGFBR2-mediated activity is, along with driving increases in the level of inflammation, protecting against lipid accumulation in the liver of male C57BL/6. The

mechanism behind the TGFBR2-mediated modulation of TCDD-induced inflammation and lipid accumulation requires further investigation. These results, along with further characterization of AHR biology, have potential to impact real-world risk assessment in identifying genetic variants within the human population that may be more susceptible to TCDD-induced toxicity.

REFERENCES

REFERENCES

Angrish MM, Dominici CY, Zacharewski TR. 2013. Tcdd-elicited effects on liver, serum, and adipose lipid composition in c57bl/6 mice. Toxicol Sci 131:108-115.

Bernasconi P, Torchiana E, Confalonieri P, Brugnoni R, Barresi R, Mora M, et al. 1995. Expression of transforming growth factor-beta 1 in dystrophic patient muscles correlates with fibrosis. Pathogenetic role of a fibrogenic cytokine. J Clin Invest 96:1137-1144.

Border WA, Noble NA. 1994. Transforming growth factor beta in tissue fibrosis. N Engl J Med 331:1286-1292.

Boverhof DR, Burgoon LD, Tashiro C, Chittim B, Harkema JR, Jump DB, et al. 2005. Temporal and dose-dependent hepatic gene expression patterns in mice provide new insights into tcdd-mediated hepatotoxicity. Toxicol Sci 85:1048-1063.

Cave M, Appana S, Patel M, Falkner KC, McClain CJ, Brock G. 2010. Polychlorinated biphenyls, lead, and mercury are associated with liver disease in american adults: Nhanes 2003-2004. Environ Health Perspect 118:1735-1742.

Combs TP, Marliss EB. 2014. Adiponectin signaling in the liver. Rev Endocr Metab Disord 15:137-147.

Cranmer M, Louie S, Kennedy RH, Kern PA, Fonseca VA. 2000. Exposure to 2,3,7,8-tetrachlorodibenzo-p-dioxin (tcdd) is associated with hyperinsulinemia and insulin resistance. Toxicol Sci 56:431-436.

Dietrich P, Hellerbrand C. 2014. Non-alcoholic fatty liver disease, obesity and the metabolic syndrome. Best Pract Res Clin Gastroenterol 28:637-653.

Diliberto JJ, Burgin D, Birnbaum LS. 1997. Role of cyp1a2 in hepatic sequestration of dioxin: Studies using cyp1a2 knock-out mice. Biochem Biophys Res Commun 236:431-433.

Fader KA, Nault R, Kirby MP, Markous G, Matthews J, Zacharewski TR. 2017. Convergence of hepcidin deficiency, systemic iron overloading, heme accumulation, and rev-erbalpha/beta activation in aryl hydrocarbon receptor-elicited hepatotoxicity. Toxicol Appl Pharmacol 321:1-17.

Forgacs AL, Kent MN, Makley MK, Mets B, DelRaso N, Jahns GL, et al. 2012. Comparative metabolomic and genomic analyses of tcdd-elicited metabolic disruption in mouse and rat liver. Toxicol Sci 125:41-55.

Fraser D, Wakefield L, Phillips A. 2002. Independent regulation of transforming growth factor-beta1 transcription and translation by glucose and platelet-derived growth factor. Am J Pathol 161:1039-1049.

Friedman SL. 1993. Seminars in medicine of the beth israel hospital, boston. The cellular basis of hepatic fibrosis. Mechanisms and treatment strategies. N Engl J Med 328:1828-1835.

Gaido KW, Maness SC, Leonard LS, Greenlee WF. 1992. 2,3,7,8-tetrachlorodibenzo-p-dioxin-dependent regulation of transforming growth factors-alpha and -beta 2 expression in a human keratinocyte cell line involves both transcriptional and post-transcriptional control. J Biol Chem 267:24591-24595.

Guo J, Sartor M, Karyala S, Medvedovic M, Kann S, Puga A, et al. 2004. Expression of genes in the tgf-beta signaling pathway is significantly deregulated in smooth muscle cells from aorta of aryl hydrocarbon receptor knockout mice. Toxicol Appl Pharmacol 194:79-89.

Hakk H, Diliberto JJ, Birnbaum LS. 2009. The effect of dose on 2,3,7,8-tcdd tissue distribution, metabolism and elimination in cyp1a2 (-/-) knockout and c57bl/6n parental strains of mice. Toxicol Appl Pharmacol 241:119-126.

Kopec AK, Boverhof DR, Nault R, Harkema JR, Tashiro C, Potter D, et al. 2013. Toxicogenomic evaluation of long-term hepatic effects of tcdd in immature, ovariectomized c57bl/6 mice. Toxicol Sci 135:465-475.

Lee DH, Lee IK, Porta M, Steffes M, Jacobs DR, Jr. 2007. Relationship between serum concentrations of persistent organic pollutants and the prevalence of metabolic syndrome among non-diabetic adults: Results from the national health and nutrition examination survey 1999-2002. Diabetologia 50:1841-1851.

Lopez-Jaramillo P, Gomez-Arbelaez D, Lopez-Lopez J, Lopez-Lopez C, Martinez-Ortega J, Gomez-Rodriguez A, et al. 2014. The role of leptin/adiponectin ratio in metabolic syndrome and diabetes. Horm Mol Biol Clin Investig 18:37-45.

Mueller JK, Heger S. 2014. Endocrine disrupting chemicals affect the gonadotropin releasing hormone neuronal network. Reprod Toxicol 44:73-84.

Nault R, Colbry D, Brandenberger C, Harkema JR, Zacharewski TR. 2015. Development of a computational high-throughput tool for the quantitative examination of dose-dependent histological features. Toxicol Pathol 43:366-375.

Nault R, Fader KA, Ammendolia DA, Dornbos P, Potter D, Sharratt B, et al. 2016a. Dose-dependent metabolic reprogramming and differential gene expression in tcdd-elicited hepatic fibrosis. Toxicol Sci 154:253-266.

Nault R, Fader KA, Kirby MP, Ahmed S, Matthews J, Jones AD, et al. 2016b. Pyruvate kinase isoform switching and hepatic metabolic reprogramming by the environmental contaminant 2,3,7,8-tetrachlorodibenzo-p-dioxin. Toxicol Sci 149:358-371.

Nault R, Fader KA, Kopec AK, Harkema JR, Zacharewski TR, Luyendyk JP. 2016c. From the cover: Coagulation-driven hepatic fibrosis requires protease activated receptor-1 (par-1) in a mouse model of tcdd-elicited steatohepatitis. Toxicol Sci 154:381-391.

Nault R, Fader KA, Lydic TA, Zacharewski TR. 2017. Lipidomic evaluation of aryl hydrocarbon receptor-mediated hepatic steatosis in male and female mice elicited by 2,3,7,8-tetrachlorodibenzo-p-dioxin. Chem Res Toxicol 30:1060-1075.

Pierre S, Chevallier A, Teixeira-Clerc F, Ambolet-Camoit A, Bui LC, Bats AS, et al. 2014. Aryl hydrocarbon receptor-dependent induction of liver fibrosis by dioxin. Toxicol Sci 137:114-124.

Poland A, Glover E. 1990. Characterization and strain distribution pattern of the murine ah receptor specified by the ahd and ahb-3 alleles. Mol Pharmacol 38:306-312.

Poland A, Palen D, Glover E. 1994. Analysis of the four alleles of the murine aryl hydrocarbon receptor. Mol Pharmacol 46:915-921.

Skorupskaite K, George JT, Anderson RA. 2014. The kisspeptin-gnrh pathway in human reproductive health and disease. Hum Reprod Update 20:485-500.

Song WJ, Mondal P, Wolfe A, Alonso LC, Stamateris R, Ong BW, et al. 2014. Glucagon regulates hepatic kisspeptin to impair insulin secretion. Cell Metab 19:667-681.

Taylor KW, Novak RF, Anderson HA, Birnbaum LS, Blystone C, Devito M, et al. 2013. Evaluation of the association between persistent organic pollutants (pops) and diabetes in epidemiological studies: A national toxicology program workshop review. Environ Health Perspect 121:774-783.

Thomas RS, Penn SG, Holden K, Bradfield CA, Rank DR. 2002. Sequence variation and phylogenetic history of the mouse ahr gene. Pharmacogenetics 12:151-163.

Tian Y, Jackson P, Gunter C, Wang J, Rock CO, Jackowski S. 2006. Placental thrombosis and spontaneous fetal death in mice deficient in ethanolamine kinase 2. J Biol Chem 281:28438-28449.

Vance JE, Vance DE. 2004. Phospholipid biosynthesis in mammalian cells. Biochem Cell Biol 82:113-128.

Voorman R, Aust SD. 1989. Tcdd (2,3,7,8-tetrachlorodibenzo-p-dioxin) is a tight binding inhibitor of cytochrome p-450d. J Biochem Toxicol 4:105-109.

Wahlang B, Falkner KC, Gregory B, Ansert D, Young D, Conklin DJ, et al. 2013. Polychlorinated biphenyl 153 is a diet-dependent obesogen that worsens nonalcoholic fatty liver disease in male c57bl6/j mice. J Nutr Biochem 24:1587-1595.

Yang L, Roh YS, Song J, Zhang B, Liu C, Loomba R, et al. 2014. Transforming growth factor beta signaling in hepatocytes participates in steatohepatitis through regulation of cell death and lipid metabolism in mice. Hepatology 59:483-495.

Yung LM, Nikolic I, Paskin-Flerlage SD, Pearsall RS, Kumar R, Yu PB. 2016. A selective transforming growth factor-beta ligand trap attenuates pulmonary hypertension. Am J Respir Crit Care Med 194:1140-1151.

Zaher H, Fernandez-Salguero PM, Letterio J, Sheikh MS, Fornace AJ, Jr., Roberts AB, et al. 1998. The involvement of aryl hydrocarbon receptor in the activation of transforming growth factor-beta and apoptosis. Mol Pharmacol 54:313-321.

Chapter 5: TCDD is Associated with Serum Cholesterol in American Adults and HMG-CoA Reductase Modulates AHR-mediated Liver Toxicity

This chapter is an edited version of an article that will be submitted for publication (expected 2019).

Authors: Peter Dornbos[1,2], Amanda Jurgelewicz[3], Kelly Fader[1,2], Courtney Carignan[4], Tim Zacharewski[1,2], John LaPres[1,2]

Affiliations: [1]Department of Biochemistry and Molecular Biology, Michigan State University, East Lansing, MI 48824, [2]Institute for Integrative Toxicology, Michigan State University, East Lansing, MI 48824, [3]Department of Pharmacology and Toxicology, Michigan State University, East Lansing, MI 48824, [4]Department of Food Science and Nutrition, Michigan State University, East Lansing, MI, USA

5.1. Abstract

Previous rodent-based studies have shown that AHR-ligand exposure represses expression of genes involved in cholesterol homeostasis, including *Hmgcr* which encodes the rate-limiting enzyme called 3-hydroxyl-3-methylglutaryl (HMG)-CoA reductase. QTL analysis of the TCDD-induced change in body weight across 14 genetically-diverse mouse strains mapped to an area of Chromosome 13 within 1 Mb of *Hmgcr* ($p<0.001$). We hypothesized, therefore, that AHR-mediated repression of cholesterol biogenesis might play a role in TCDD-induced injury. The first goal of this study was to use data from the 2003-2004 National Health and Nutrition Examination Survey (NHANES) to test for an association between lipid-adjusted TCDD and cholesterol in humans. Results identified a reduction in total cholesterol with increasing serum TCDD in the male-stratified cohort that reached statistical significance upon adjusting for age, body mass index, and race. Low-density lipoprotein (LDL) levels were also negatively associated with increasing TCDD levels in the serum of the full cohort and did not appear to be sex-specific. The second goal was to determine if AHR-mediated modulation of cholesterol biogenesis could impact TCDD-elicited liver injury. C57BL/6 mice were exposed to TCDD in the presence or absence of simvastatin, a competitive inhibitor of HMG-CoA reductase. Simvastatin exposure was found to decrease hepatic TCDD-induced lipid accumulation in a non-sex-specific manner. However, simvastatin and TCDD co-treatment increased AHR-battery gene expression and liver inflammation in a male-specific manner ($p<0.05$). In addition, the simvastatin and TCDD co-treatment led to a significant increase in hepatic glycogen content that coincides with heavier liver in a female-specific manner ($p<0.05$). While further research is needed to better understand the mechanistic details, our results suggest that statins, which are amongst the most prescribed pharmaceuticals, may protect from AHR-mediated steatosis, but increase risk of TCDD-elicited liver damage and inflammation and altered glycogen metabolism in a sex-specific manner.

5.2. Introduction

Several rodent-based studies have indicated that the AHR regulates cholesterol biosynthesis. Exposure to an AHR-ligand called β-naphthoflavone suppresses expression of genes involved in cholesterol synthesis in mice and human hepatocytes, including *Hmgcr* which encodes the rate-limiting enzyme 3-hydroxyl-3-methylglutaryl-CoA Reductase (HMGCR)(Tanos et al. 2012). TCDD-treatment also suppresses expression of genes involved in cholesterol biosynthesis leading to marked-reductions in total cholesterol (TC), high-density lipoprotein (HDL), and low-density lipoprotein (LDL) in the serum in mice (Angrish et al. 2013). Another study reported that, while hepatic cholesterol biosynthesis is repressed in the liver, prolonged exposure to TCDD drives significant increases in hepatic cholesterol ester (CE) accumulation in mice (Nault et al. 2017). The CE accumulation has been suggested to be due to TCDD-mediated repression of genes involved in VLDL secretion and a decrease of bile acid secretion (Fader et al. 2017; Nault et al. 2017).

While the vast-majority of evidence has been collected via culture- or rodent-based models, there is compelling evidence that the AHR regulates cholesterol homeostasis. Given the complex regulation of cholesterol biosynthesis and important functions of cholesterol in organisms, we sought to establish whether cholesterol levels are impacted by TCDD exposures in the human population. Growing evidence suggests that TCDD and other dioxin-like chemicals are associated with increased incidence of metabolic disorders in the human population, such as nonalcoholic fatty-liver disease (NAFLD) (Cave et al. 2010; Lee et al. 2007). In rodents, TCDD exposures leads to accumulation of lipids in the liver and, ultimately, steatohepatitis and fibrosis (Nault et al. 2016a; Nault et al. 2016b; Nault et al. 2017; Pierre et al. 2014). Notably, cholesterol accumulation in the liver has been shown to impact NAFLD (Arguello et al. 2015). As such, TCDD-induced alterations in cholesterol homeostasis may be playing a role in AHR-mediated NAFLD in humans.

To test for human relevance to TCDD-induced alterations in cholesterol homeostasis, data from the National Health and Nutrition Examination Survey (NHANES), a nationally-representative cross-sectional epidemiological survey, were used to test for an association between TCDD and cholesterol levels. Based on regression models created for TC, LDL, and HDL, TC and LDL appear to be negatively correlated with lipid-adjusted TCDD levels in serum of American adults in a significant manner. As such, the results suggest that environmentally-relevant TCDD exposures may impact cholesterol homeostasis in the human population. Following, C57BL/6 mice were co-treated with TCDD and simvastatin, a competitive inhibitor of HMGCR, to characterize a potential functional role of HMGCR in modulating TCDD-mediated NAFLD. Results indicate that TCDD-induced repression of HMGCR appears to protect against hepatic lipid accumulation in both males and females. However, the simvastatin and TCDD co-exposure appears to increase susceptibility to TCDD-mediated liver injury in a male-specific manner and alter glycogen metabolism in a female-specific manner.

5.3. Results

5.3.1. Inter-strain differences in TCDD-induced change in body weight implicates *Hmgcr*

In the study outlined in Chapter 4 where female mice from 14 genetically-diverse strains were treated with TCDD (100 ng/kg/day) for 10 days, the change in weight in comparing TCDD-treated and vehicle mice was quite variable across strains (Figure 5.1A). While some strains were found to have a decrease in body weight, such as FVB/NJ and DBA/1J, other strains, such as CC019 and C3HeB/FeJ, were found to gain weight. A multiple sequence alignment of the *Ahr* gene outlined in Chapter 4 established that 3 independent alleles of the *Ahr* are found within the panel of 14 strains. As sequence-variation in the murine *Ahr* impacts susceptibility to TCDD (Poland et al. 1994), the mean change in weight across *Ahr* alleles were compared (Figure 5.1B). Results indicated that, unlike many TCDD-mediated responses in the mouse, the *Ahr* allele inherited does not have a significant impact on the change in weight in this mouse panel suggesting that other genomic factors may be impacting the response. The inter-strain differences in weight change over the dosing period were used to scan for potential genomic regions that might explain the variability. The results indicate a strong association in Chromosome 13 within 1 Mb of *Hmgcr* ($p<0.001$; Figure 5.1C). These results suggest that *Hmgcr* may be modulating inter-strain susceptibility to TCDD-mediated weight loss amongst our mouse panel.

5.3.2. TCDD and cholesterol levels in serum of the 1999-2004 NHANES cohort

To test for an association between serum lipid-adjusted TCDD and cholesterol in humans, 3 independent analytical datasets were created for a) TC (n=1,094), b) HDL (n=1,094), and c) LDL (n=520) using data from the 2003-2004 NHANES. TC and HDL were measured in the same subjects and, thus, are the same datasets with differing response variables. The TCDD detection frequency in the TC and HDL cohorts was 43.0% while the LDL cohort was 44.3% (Table 5.1). The NHANES imputed values were used for samples that fell below detection limits. The weighted

Figure 5.1. QTL analysis of the inter-strain variability in TCDD-mediated change in body weight. The average change in body weights induced by a 100 ng/kg/day TCDD exposure for each strain (n=14) are layered over a boxplot which indicates the median and interquartile range across all strains (**A**). The mean change in weight response of all mice within each *Ahr* allelic were averaged to indicate the impact of the *Ahr* allele on the change in body weight (**B**). QTL analysis indicated a significant association within Chromosome 13 (p<0.001)(**C**). The dotted line indicates the threshold of genome-wide significance which was determined with permutation testing (n=10,000).

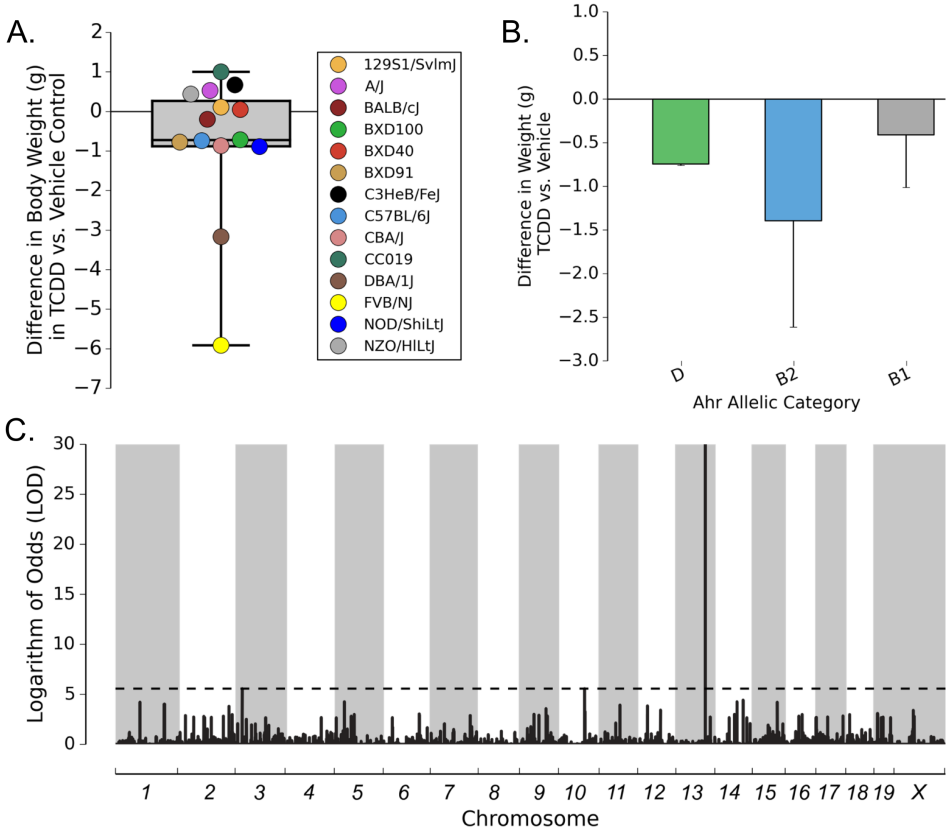

Table 5.1. Detection frequency and levels of serum TCDD and lipid-adjusted serum TCDD. All data were derived from the 2003-2004 nationally-representative and cross-sectional U.S. National Health and Nutrition Examination Survey (NHANES). Analytical datasets were created for total cholesterol (TC; n=1,094), high-density lipoprotein (HDL; n=1,094), and low-density lipoprotein (LDL; n=520). Weighted means, standard error, and percentiles are reported for the full and sex-stratified cohorts.

TCDD	Statistic	TCDD Level in Serum								
		TC Cohort			HDL Cohort			LDL Cohort		
		Full	Male	Female	Full	Male	Female	Full	Male	Female
	Detection Frequency	43.0	35.6	49.5	43.0	35.6	49.5	44.3	40.4	47.5
Total TCDD (fg/g)	Mean	11.69	10.22	13.00	11.69	10.22	13.00	12.00	10.77	13.00
	St. Error	0.35	0.46	0.51	0.35	0.46	0.51	0.55	0.77	0.77
	Minumum	2.76	3.11	2.76	2.76	3.11	2.76	2.83	3.25	2.83
	5%	3.46	3.68	3.39	3.46	3.68	3.39	3.46	3.68	3.32
	10%	3.75	3.96	3.68	3.75	3.96	3.68	3.82	4.03	3.68
	25%	4.38	4.52	4.24	4.38	4.52	4.24	4.46	4.60	4.17
	50%	6.08	5.59	7.70	6.08	5.59	7.70	6.44	6.01	7.14
	75%	16.30	13.90	19.20	16.30	13.90	19.20	16.90	15.90	19.10
	90%	26.70	22.20	29.80	26.70	22.20	29.80	26.90	24.80	28.60
	95%	31.80	28.20	36.40	31.80	28.20	36.40	32.70	28.00	38.10
	Maximum	235.80	235.80	128.20	235.80	235.80	128.20	235.80	235.80	128.20
Lipid-Adjusted TCDD (pg/g)	Mean	1.78	1.55	1.98	1.78	1.55	1.98	1.89	1.73	2.03
	St. Error	0.05	0.06	0.07	0.05	0.06	0.07	0.08	0.11	0.11
	Minumum	0.30	0.30	0.30	0.30	0.30	0.30	0.40	0.40	0.40
	5%	0.50	0.50	0.50	0.50	0.50	0.50	0.50	0.60	0.50
	10%	0.60	0.60	0.60	0.60	0.60	0.60	0.60	0.60	0.60
	25%	0.70	0.70	0.70	0.70	0.70	0.70	0.80	0.80	0.70
	50%	1.10	1.00	1.30	1.10	1.00	1.30	1.10	1.10	1.20
	75%	2.50	1.90	2.90	2.50	1.90	2.90	2.70	2.30	3.00
	90%	3.80	3.40	4.20	3.80	3.40	4.20	4.00	3.60	4.20
	95%	4.70	4.30	5.10	4.70	4.30	5.10	5.00	4.50	5.20
	Maximum	27.00	27.00	12.50	27.00	27.00	12.50	27.00	27.00	12.50

mean ± standard error for serum TCDD (fg/g) and lipid-adjusted serum TCDD (LA-TCDD; pg/g) in the TC and HDL datasets were found to be 12.00 ± 0.55 and 1.89 ± 0.08, respectively, while the LDL dataset was found to be 11.69 ± 0.35 and 1.78 ± 0.05, respectively.

In comparing sexes across the TC, HDL, and LDL cohorts, the full samples were found to have similar proportions of male and females (Table 5.2). Each cohort was found to have a significantly-greater proportion of non-Mexican White individuals ($p<0.05$). Given the detection frequency of TCDD, the continuous LA-TCDD variable was split into sample-weighted tertiles based on increasing TCDD levels (T1 as low-TCDD, T2 as mid-TCDD, and T3 as high-TCDD) prior to regression analysis ($p<0.05$; Table 5.2). While there were not differences in HDL or LDL across tertiles, T2 was found to have significantly lower levels of TC as compared to T1 and T3 ($p<0.05$). T3 was found to contain individuals with a significantly higher ages as compared to T1 and T2 in all 3 datasets ($p<0.05$). BMI is significantly higher in T3 as compared to T1 and T2 in TC and HDL cohorts ($p<0.05$), but not the LDL cohort. In comparing sample-weighted proportions across tertiles, all tertiles had a significantly higher proportion of non-Hispanic white individuals which was consistent with the full sample in each cohort ($p<0.05$). T3, but not T1 or T2, was found to have a significantly-lower proportion of Mexican-American individuals within the LDL cohort ($p<0.05$). In comparing proportions of sexes across tertiles, T2 contains significantly more males while T3 contains significantly less males in the TC and HDL cohorts ($p<0.05$). In the LDL cohort, T3 contains a significantly-lower proportion of males ($p<0.05$).

Each dataset was also stratified by sex. Females were found to have significantly higher levels of HDL as compared to males ($p<0.05$; Table 5.3). There were no differences in comparing TC or LDL levels across sexes. In the TC and HDL cohort, females were found to have significantly higher levels of LA-TCDD. Females in the TC and HDL cohorts were also found to have a significantly higher age as compared to males ($p<0.05$). There were no differences in age

Table 5.2. Demographic statistics for NHANES-derived analytical datasets. All data was derived from the 2003-2004 nationally-representative and cross-sectional U.S. National Health and Nutrition Examination Survey (NHANES). Data were used to created 3 independent and balanced analytical datasets: total cholesterol (TC; n=1,094), high-density lipoprotein (HDL; n=1,094), and low-density lipoprotein (LDL; n=520). Weighted median and interquartile range (IQR) in parenthesis are reported for each continuous variable. Sample size (n) and weighted percentage in parenthesis are reported for the categorical variables. Superscript letters indicate significant differences ($p<0.05$) as indicated by a kruskal wallice test: [a]Tertile 1, [b]Tertile 2, [c]Tertile 3. Asterisks (*) indicate greater while number signs ([#]) indicate a smaller weighted proportion than expected as indicated with a chi-squared test.

Independent Variable	Total Cholesterol (mg/dL)				LDL (mg/dL)				HDL (mg/dL)			
	Weighted Median (IQR) or Sample Size (Weighted %)				Weighted Median (IQR) or Sample Size (Weighted %)				Weighted Median (IQR) or Sample Size (Weighted %)			
	Full Cohort	Tertile 1	Tertile 2	Tertile 3	Full Cohort	Tertile 1	Tertile 2	Tertile 3	Full Cohort	Tertile 1	Tertile 2	Tertile 3
Total Cholesterol, HDL, or LDL	200 (55)	204 (51)	186 (54)[a,c]	207 (58)	117 (47)	119 (46)	110 (43)	120 (44)	52 (20)	52 (19)	51 (19)	55 (23)
Lipid-Adjusted TCDD (pg/g)	1.1 (1.8)	0.7 (0.2)	1.2 (0.4)[a]	3.3 (1.7)[a,b]	1.1 (1.9)	0.7 (0.2)	1.2 (0.7)[a]	3.5 (1.5)[a,b]	1.1 (1.8)	0.7 (0.2)	1.2 (0.4)[a]	3.3 (1.7)[a,b]
Age (months)	516 (275)	451 (222)	434 (218)	649 (240)[a,b]	529 (302)	424 (218)	485 (254)	693 (234)[a,b]	516 (275)	451 (222)	434 (218)	649 (240)[a,b]
Body Mass Index	26.8 (7.6)	26.7 (7.2)	26.2 (7.6)	27.7 (7.8)[a,b]	27.1 (7.3)	26.5 (7.2)	27.1 (7.2)	28.3 (8.2)	26.8 (7.6)	26.7 (7.2)	26.2 (7.6)	27.7 (7.8)[a,b]
Race												
Non-Hispanic White	575 (70.0)*	207 (69.6)*	140 (64.6)*	228 (74.4)*	297 (74.1)*	98 (70.5)*	88 (72.2)*	111 (80.4)*	575 (70.0)*	207 (69.6)*	140 (64.6)*	228 (74.4)*
African American	205 (10.9)	60 (8.4)	58 (11.9)	87 (12.9)	84 (9.6)	30 (9.0)	26 (10.0)	28 (9.9)	205 (10.9)	60 (8.4)	58 (11.9)	87 (12.9)
Mexican American	217 (8.4)	93 (10.8)	68 (11.9)	56 (3.6)	98 (6.7)	45 (9.5)	30 (7.8)	23 (2.3)[#]	217 (8.4)	93 (10.8)	68 (11.9)	56 (3.6)
Other	97 (10.8)	40 (11.2)	29 (12.4)	28 (9.02)	41 (9.6)	20 (11.0)	13 (10.0)	8 (7.4)	97 (10.8)	40 (11.2)	29 (12.4)	28 (9.02)
Sex												
Male	520 (47.3)	200 (51.1)	166 (57.0)*	154 (35.3)	235 (44.6)	87 (43.4)	83 (53.9)	65 (36.1)	520 (47.3)	200 (51.1)	166 (57.0)*	154 (35.3)
Female	574 (52.7)	200 (48.9)	129 (43.0)	245 (64.7)*	285 (55.4)	106 (56.6)	74 (46.1)	105 (63.9)*	574 (52.7)	200 (48.9)	129 (43.0)	245 (64.7)*

Table 5.3. Sex-stratified demographic statistics. All data was derived from the 2003-2004 nationally-representative and cross-sectional U.S. National Health and Nutrition Examination Survey (NHANES). Stratification data is reported for 3 independent analytical datasets: total cholesterol (TC; n=1,094), high-density lipoprotein (HDL; n=1,094), and low-density lipoprotein (LDL; n=520). Weighted median and interquartile range (IQR) in parenthesis are reported for each continuous variable. Sample size (n) and weighted percentage in parenthesis are reported for the categorical variables. An asterisk (*) indicates a significant difference ($p<0.05$) as compared to males as indicated by a T-test. For categorical data, asterisks (*) indicate greater weighted proportion than expected as indicated with a chi-squared test.

Independent Variable	Total Cholesterol (mg/dL) Weighted Median (IQR) or Sample Size (Weighted %)		LDL (mg/dL) Weighted Median (IQR) or Sample Size (Weighted %)		HDL (mg/dL) Weighted Median (IQR) or Sample Size (Weighted %)	
	male (n=520)	female (n=574)	male (n=235)	female (n=285)	male (n=520)	female (n=574)
Total Cholesterol, HDL, or LDL	200 (50)	201 (57)	120 (46)	112 (46)	47 (16)	58 (23)*
Lipid-Adjusted TCDD (pg/g)	1.0 (1.2)	1.3 (2.0)*	1.1 (1.5)	1.2 (2.3)	1.0 (1.2)	1.3 (2.0)*
Age (months)	501 (270)	529 (283)*	519 (294)	538 (317)	501 (270)	529 (283)*
Body Mass Index	27.4 (6.8)	26.3 (8.7)	27.6 (6.5)	26.8 (8.5)	27.4 (6.8)	26.3 (8.7)
Race						
Non-Hispanic White	270 (67.6)*	305 (72.0)*	133 (72.4)*	164 (75.4)*	270 (67.6)*	305 (72.0)*
African American	97 (10.3)	108 (11.4)	39 (9.0)	45 (10.0)	97 (10.3)	108 (11.4)
Mexican American	98 (9.4)	119 (7.6)	42 (7.7)	56 (6.0)	98 (9.4)	119 (7.6)
Other	55 (12.7)	42 (9.1)	21 (10.9)	20 (8.5)	55 (12.7)	42 (9.1)

between sexes in the LDL cohort. There was not a statistical difference in LA-TCDD between sexes in the LDL cohort. There were no differences across sexes in comparing BMI in any cohort. Male- and female-stratification results in a significantly-higher proportion of non-Hispanic White individuals in all datasets ($p<0.05$).

5.3.3. Association of serum TCDD and total cholesterol in humans

In testing for potential associations between LA-TCDD and TC, HDL, or LDL levels, we created 3 crude models followed by final models which were adjusted for age, BMI, and race. Each model was used to assess the full and sex-stratified cohorts for each dependent variable. In analyzing the TC levels, crude regression models estimate that the T2 (mid-TCDD) category has lower levels of TC as compared to T1 (low-TCDD; $p<0.05$; Table 5.4) for the full and sex-stratified cohorts with statistical significance that was robust to adjustment ($p<0.05$; Table 5.5, Figure 5.2A). Adjusted models estimate 8.9%, 9.7%, and 9.1% reductions in TC in comparing T2 with T1 for the full, male-, and female-stratified cohorts, respectively. In comparing T3 (high-TCDD) to T1 (low-TCDD), the male-stratified cohort had a reduction in TC that was near statistical significance in the crude model ($p=0.16$). Adjustment for confounding variables pushed the male-specific 6.2% reduction in TC into statistical significance as compared to T1 ($p<0.05$; Table 5.5; Figure 5.2A). The crude model also estimated a female-specific increase in TC in comparing T3 with T1 ($p<0.05$; Table 5.4). Similarly, an increase in TC from T3 to T1 in the full cohort was near conventional significance ($p=0.17$; Table 5.4). The increase in TC, however, dissipated in both the female-stratified and the full cohort when adjusting for confounding variables (Table 5.5; Figure 5.2A).

In comparing the LDL levels across TCDD tertiles, crude models suggest that the male-stratified cohort has a significant reduction ($p<0.05$) and full cohort has a reduction close to significance ($p=0.06$) in comparing T2 to T1 (Table 5.4). Adjustment for confounding variables

Table 5.4. Crude associations of lipid-adjusted serum TCDD levels with total cholesterol (TC), high-density lipoprotein (HDL), and low-density lipoprotein (LDL) levels. Regression coefficient estimates and 95% confidence intervals (CI) are reported for each model. Coefficient estimates are relative to tertile 1 (low-TCDD). Asterisks (*) indicate statistically significant association ($p<0.05$).

Model	Independent Variable	Total Cohort			Males			Females		
		Estimate (St. Error)	95% CI		Estimate (St. Error)	95% CI		Estimate (St. Error)	95% CI	
			Lower	Upper		Lower	Upper		Lower	Upper
TC Cohort	**Intercept**	205.60 (2.62)*	200.01	211.19	210.90 (3.60)*	203.22	218.58	200.06 (3.56)*	192.47	207.66
	Lipid-Adjusted TCDD (pg/g)									
	Tertile 2 (Mid-TCDD)	-15.85 (4.28)*	-24.97	-6.73	-18.25 (6.44)*	-31.97	-4.53	-14.15 (3.39)*	-21.38	-6.91
	Tertile 3 (High-TCDD)	5.76 (3.98)	-2.72	14.23	-6.20 (4.34)	-15.44	3.04	14.92 (5.07)*	4.11	25.74
LDL Cohort	**Intercept**	120.69 (3.16)*	113.95	127.43	129.09 (5.06)*	118.30	139.87	114.25 (3.07)*	107.69	120.82
	Lipid-Adjusted TCDD (pg/g)									
	Tertile 2 (Mid-TCDD)	-9.13 (4.46)	-18.64	0.38	-15.11 (7.27)*	-30.59	0.38	-5.52 (5.78)	-17.83	6.80
	Tertile 3 (High-TCDD)	2.10 (5.03)	-8.63	12.83	-8.53 (5.10)	-19.40	2.32	9.80 (6.19)	-3.40	23.00
HDL Cohort	**Intercept**	54.18 (1.00)*	52.06	56.31	49.21 (0.76)*	47.60	50.82	59.38 (1.45)*	56.30	207.66
	Lipid-Adjusted TCDD (pg/g)									
	Tertile 2 (Mid-TCDD)	-0.74 (1.80)	-4.57	3.08	0.01 (1.23)	-2.62	2.63	-0.34 (3.63)	-8.09	-6.91
	Tertile 3 (High-TCDD)	3.14 (1.47)*	0.02	6.28	0.09 (1.62)	-3.38	3.56	2.32 (2.08)	-2.10	25.74

Table 5.5. Adjusted associations of lipid-adjusted serum TCDD levels with total cholesterol (TC), high-density lipoprotein (HDL), and low-density lipoprotein (LDL) levels. Final regression coefficient estimates and 95% confidence intervals (CI) are adjusted for age in months, body mass index, and race. Categorical coefficient estimates are relative to tertile 1 (low-TCDD) for TCDD tertiles and to non-Hispanic White category for race. Asterisks (*) indicate statistically significant association ($p<0.05$).

Model	Independent Variable	Total Cohort			Males			Females		
		Estimate (St. Error)	95% CI		Estimate (St. Error)	95% CI		Estimate (St. Error)	95% CI	
			Lower	Upper		Lower	Upper		Lower	Upper
TC Cohort	**Intercept**	163.92 (6.83)*	149.36	178.48	173.86 (11.31)*	149.75	197.98	152.22 (6.33)*	138.74	165.72
	Lipid-Adjusted TCDD (pg/g)									
	Tertile 2 (Mid-TCDD)	-14.61 (4.82)*	-24.89	-4.33	-16.90 (6.66)*	-31.08	-2.71	-13.84 (3.97)*	-22.30	-5.37
	Tertile 3 (High-TCDD)	-4.95 (3.95)	-13.37	3.48	-10.85 (4.37)*	-20.17	-1.53	-2.61 (5.39)	-14.11	8.89
	Age (Months)	0.06 (0.01)*	0.041	0.074	0.03 (0.01)*	0.005	0.054	0.08 (0.01)*	0.058	0.101
	Body Mass Index	0.54 (0.19)*	0.13	0.95	0.77 (0.44)	-0.15	1.70	0.50 (0.21)*	0.05	0.95
	Race									
	African American	-1.86 (3.67)	-9.67	5.95	5.51 (5.07)	-5.30	16.33	-7.85 (4.68)	-17.83	2.12
	Mexican American	-1.67 (2.86)	-7.77	4.43	0.35 (3.37)	-6.84	7.54	-4.05 (4.62)	-13.90	5.80
	Other	-1.61 (8.97)	-20.72	17.50	3.94 (6.19)	-9.25	17.13	-8.24 (12.64)	-35.19	18.71
LDL Cohort	**Intercept**	74.41 (6.08)*	61.45	87.36	96.12 (11.41)*	72.09	120.74	55.95 (7.34)*	40.31	71.59
	Lipid-Adjusted TCDD (pg/g)									
	Tertile 2 (Mid-TCDD)	-10.52 (4.72)*	-20.59	-0.46	-14.98 (7.17)	-30.26	0.30	-9.85 (5.86)	-22.34	2.64
	Tertile 3 (High-TCDD)	-9.67 (4.46)*	-19.18	-0.17	-11.87 (6.33)	-25.36	1.62	-10.65 (5.26)	-21.87	0.57
	Age (Months)	0.04 (0.01)*	0.02	0.06	0.01 (0.02)	-0.03	0.04	0.07 (0.01)*	0.05	0.09
	Body Mass Index	0.94 (0.18)*	0.55	1.32	1.02 (0.40)*	0.17	1.88	0.96 (0.23)*	0.46	1.45
	Race									
	African American	-0.97 (3.19)	-7.77	5.84	2.01 (6.50)	-11.83	15.86	-4.15 (4.85)	-14.48	6.19
	Mexican American	0.24 (4.84)	-10.08	10.57	0.64 (4.94)	-9.89	11.17	-3.00 (6.53)	-16.92	10.93
	Other	-3.24 (15.84)	-37.00	30.51	6.01 (15.51)	-27.06	39.08	-39.2 (6.80)*	-53.68	-24.70
HDL Cohort	**Intercept**	75.86 (4.29)*	66.71	85.02	70.58 (4.96)*	60.01	81.16	77.70 (4.90)*	67.25	88.14
	Lipid-Adjusted TCDD (pg/g)									
	Tertile 2 (Mid-TCDD)	-1.24 (1.82)	-5.13	2.65	-0.67 (1.39)	-3.63	2.28	-0.61 (3.45)	-7.96	6.74
	Tertile 3 (High-TCDD)	2.66 (1.68)	-0.92	6.24	0.80 (1.63)	-2.68	4.27	0.05 (2.39)	-5.05	5.15
	Age (Months)	0.005 (0.004)	-0.003	0.013	0.001 (0.002)	-0.005	0.006	0.01 (0.005)	-0.001	0.024
	Body Mass Index	-0.87 (0.11)*	-1.11	-0.62	-0.79 (0.15)*	-1.11	-0.47	-0.85 (0.11)*	-1.09	-0.62
	Race									
	African American	3.64 (0.86)*	1.80	5.49	4.93 (1.47)*	1.81	8.06	2.48 (1.35)	-0.40	5.36
	Mexican American	-1.70 (1.09)	-4.03	0.62	-0.94 (1.82)	-4.81	2.94	-1.99 (2.15)	-6.57	2.59
	Other	-0.55 (3.11)	-7.18	6.08	0.02 (4.13)	-8.79	8.82	-0.71 (3.14)	-5.99	7.40

Figure 5.2. Association of lipid-adjusted TCDD tertiles with total cholesterol (TC), low-density lipoprotein (LDL), and high-density lipoprotein (HDL). Regression estimates from models adjusted for age, BMI, and race are presented for tertile 1 (low-TCDD), tertile 2 (mid-TCDD), and tertile 3 (high-TCDD). Model estimates are reported for the full cohort and male- and female-stratified cohorts for all 3 datasets: TC (**A**), LDL (**B**), and HDL (**C**). Asterisks (*) indicate a significant difference ($p \leq 0.05$) relative to the Tertile 1.

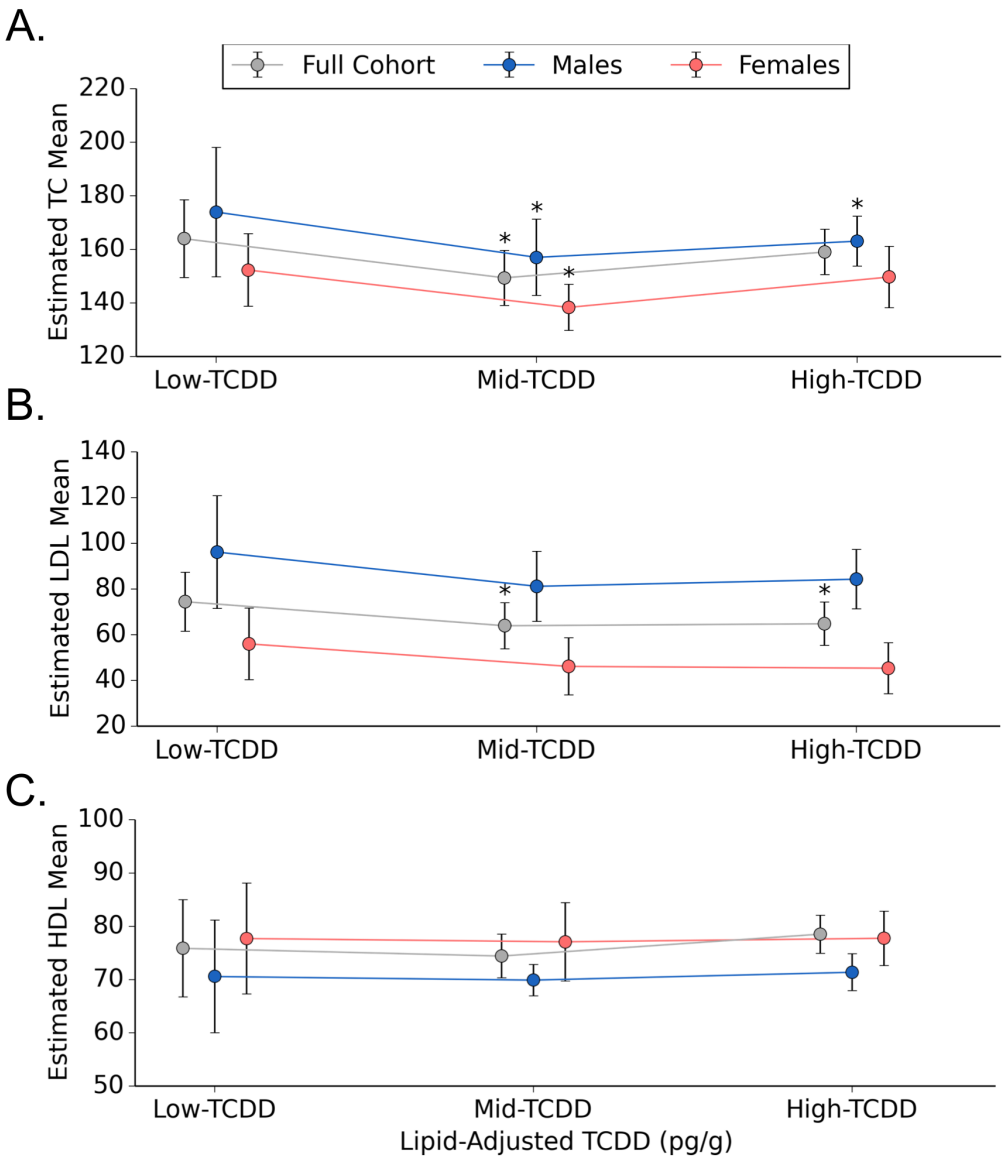

pushed the male-specific trend just above the threshold of significance (p=0.054). Adjustment, on the other hand, pushed the 14.1% reduction in LDL below the threshold of statistical significance for the full cohort (p<0.05; Table 5.5; Figure 5.2B). In comparing T3 with T1, a reduction in LDL was found to be near statistical significance (p=0.11) in the male-stratified cohort, but not the female-stratified or full cohort (Table 5.4). Upon adjustment for confounding variables, the male-specific trended closer to significance (p=0.08) (Table 5.5; Figure 5.2B). In comparing T3 to T1 in the full cohort, adjustment for confounding variables drove the 13.0% reduction in LDL into statistical significance (p<0.05; Table 5.5; Figure 5.2B). While the crude models did not suggest an association between TCDD and LDL in the female-stratified cohort, the adjusted models suggest reductions in LDL from T2 to T1 (p=0.11) and T3 to T1 (p=0.06) were close to the threshold of significance (Table 5.5; Figure 5.2B).

In testing for an association between TCDD and HDL levels, there were no significant associations in HDL levels when comparing T2 and T1. In comparing T3 with T1, the crude model estimated an increase in HDL levels in the full cohort (p<0.05; Table 5.4). The statistical significance dissipated upon adjusted for confounding variables (Table 5.5; Figure 5.2B). There were no significant trends in the crude or adjusted models in comparing T3 and T1 for the male- or female-stratified cohorts.

5.3.4. Impact of TCDD exposure and HMGCR inhibition on cholesterol synthesis in mice

To characterize a potential role of *Hmgcr* activity in TCDD-elicited toxicity, C57BL/6 mice (i.e. Ahr^{b1} allele) were treated with either sesame oil (i.e. vehicle) or 10 μg/kg/day of TCDD for 10 consecutive days in the presence of absence of chow containing simvastatin (500 mg simvastatin per kildogram chow), a competitive inhibitor of HMGCR. In this study, TCDD exposure repressed expression of hepatic *Hmgcr* mRNA for male and female mice fed standard or simvastatin-laced chow, but not in a statistically significant manner (Figure 5.3A and 5.3B). Western blot

Figure 5.3. Simvastatin and TCDD-mediated effects of the expression of HMG-CoA reductase. Expression of *Hmgcr* was analyzed by QRTPCR for females (**A**) and males (**B**). For QRTPCR analysis, all samples are reported as fold changes which are relative to vehicle control (i.e. sesame oil); in all cases, sample sizes (n) were ≥ 7 for gene expression analysis. Western blot analysis was used to assess protein expression of HMGCR (**C**). Densitometry analysis of western blots was used to assess relative protein expression of HMGCR for males (**D**) and females (**E**). Densitometry analysis is reported as fold changes relative to vehicle control (i.e. sesame oil); in all cases, sample sizes (n) were 5 for densitometry analysis. Asterisks (*) indicate statistically significant differences ($p \leq 0.05$).

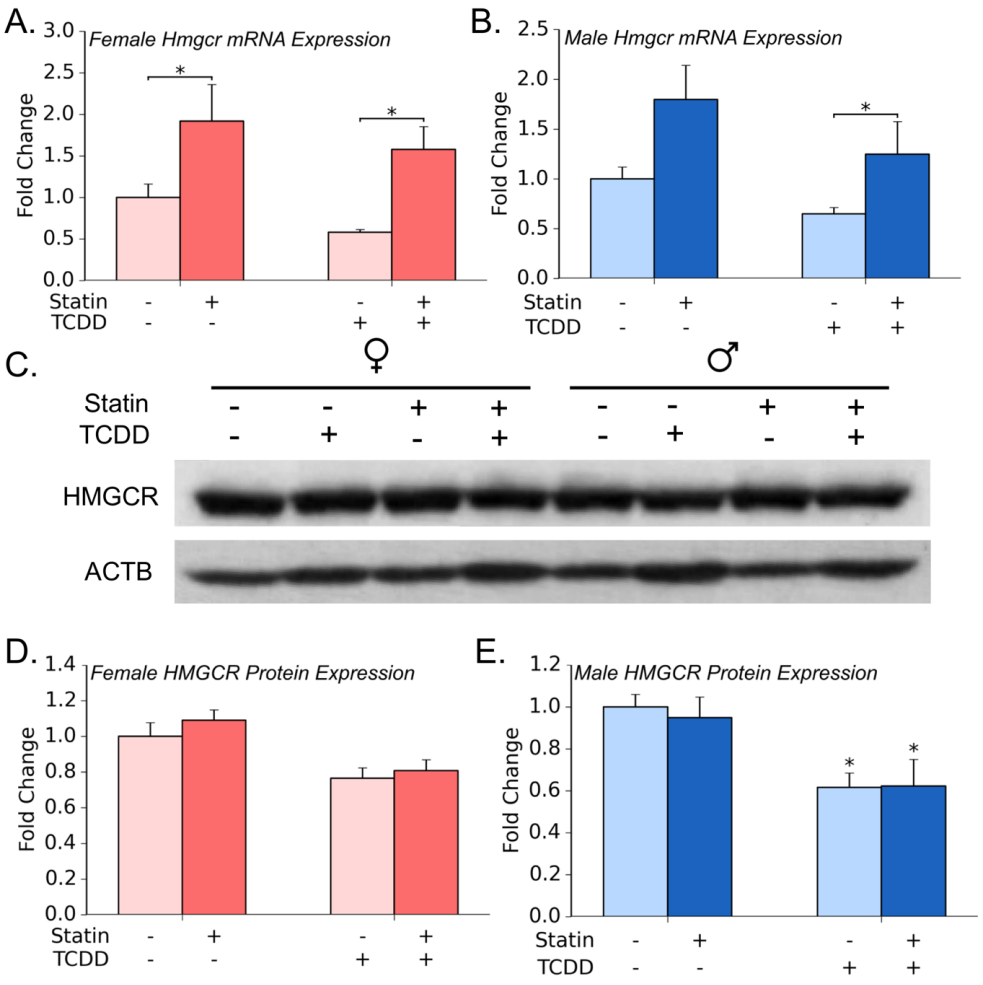

densitometry analysis confirmed TCDD-mediated repression of HMGCR at the protein-level, but was only found statistically significant in males ($p<0.05$; Figure 5.3C, 5.3D, and 5.3E). In comparing standard and simvastatin-laced chow groups, simvastatin and simvastatin + TCDD co-treatment (S+T) increased hepatic *Hmgcr* mRNA expression as compared to vehicle or TCDD-treatment, respectively ($p<0.05$; Figure 5.3A). The *Hmgcr* mRNA expression in males was significantly higher in the S+T group as compared to TCDD alone ($p<0.05$; Figure 5.3B). However, densitometry analysis did not confirm the simvastatin-mediated increased expression of HMGCR at the protein level (Figure 5.3C, 5.3D, and 5.3E).

Female and male serum total cholesterol levels were impacted by TCDD exposure. TCDD and S+T co-treatment led to significantly less TC as compared to either vehicle or simvastatin-treated mice ($p<0.05$, Table 5.6). There were no differences in TC levels across TCDD treatments. Serum LDL, while slightly increased by simvastatin, was not significantly impacted in females (Table 5.6). In males, LDL was significant lower in comparing S+T co-treatment with simvastatin alone ($p<0.05$; Figure 4F). Along these lines, hepatic gene expression of the LDL receptor (*Ldlr*) was not altered by any treatments in males or females (Table 5.7). The most dramatic changes were found in the serum HDL levels. TCDD treatment led to significant reductions in HDL levels in both sexes ($p<0.05$, Table 5.6). Interestingly, simvastatin alone led to a significant decrease the level of HDL in females, but not males ($p<0.05$ Table 5.6). As such, the HDL:LDL ratio (~2.1) in the standard chow fed females was nearly double the HDL:LDL ratio (~1.1) in simvastatin-treated females. HDL:LDL ratios did not change in simvastatin-treated males. Expression of the scavenger receptor class B type 1 gene (*Scarb1*) which serves as the HDL receptor was not altered in the liver by any treatment in females (Table 5.7). While HDL levels were lower in TCDD-treated males, *Scarb1* was found significantly repressed by TCDD ($p<0.05$), but not different across TCDD-treatment groups (Table 5.7). Expression of the apolipoprotein gene A1 (*Apoa1*)

Table 5.6. Cholesterol levels, organ weights, and serum clinical chemistry data for TCDD and simvastatin co-treatment study. Results are presented as mean weights with standard error in parenthesis. In all cases, sample size (n) ≥ 5 in all groups. Superscript letters indicate significant differences ($p<0.05$) as indicated by an ANOVA in comparison to: [a]vehicle (sesame oil), [b]TCDD treatment, or [c]simvastatin treatment. Statistical comparisons were not made across sexes.

Group	Measurement	Females				Males			
		Standard Chow		Statin Chow		Standard Chow		Statin Chow	
		Sesame Oil	TCDD	Sesame Oil	TCDD	Sesame Oil	TCDD	Sesame Oil	TCDD
Cholesterol	Low-Density Lipoprotein (mg/dL)	38.1 (1.5)	34.8 (1.0)	52.7 (3.2)	35.6 (1.0)	40.4 (0.7)	33.1 (0.5)	43.2 (0.8)	29.3 (1.6)[c]
	High-Density Lipoprotein (mg/dL)	80.0 (3.8)	43.7 (1.5)[a]	58.1 (2.1)[a]	37.9 (0.9)[c]	63.2 (2.3)	35.1 (1.2)[a]	70.2 (2.1)	39.1 (2.5)[c]
	Total Cholesterol (mg/dL)	136.7 (1.9)	120.4 (1.5)[a]	137.3 (1.3)	120.5 (0.9)[c]	151.7 (1.5)	122.9 (1.7)[a]	170.0 (1.0)	133.6 (2.7)[c]
	Hepatic Free Cholesterol (mg/g)	2.3 (0.1)	3.9 (0.1)[a]	2.2 (0.1)	3.2 (0.2)[b,c]	2.1 (0.1)	3.2 (0.1)[a]	2.1 (0.1)	2.8 (0.1)[b,c]
Gross Pathology	Liver Weight (g)	0.76 (0.02)	0.99 (0.02)[a]	0.80 (0.02)	1.12 (0.04)[b,c]	1.13 (0.04)	1.27 (0.07)	1.18 (0.03)	1.31 (0.05)
	Normalized Liver Weight (mg/kg)	48.48 (0.86)	65.89 (0.63)[a]	50.83 (0.45)	73.47 (1.83)[b,c]	58.58 (1.39)	71.27 (2.67)[a]	59.38 (1.33)	73.80 (1.69)[c]
	Body Weight (g)	15.6 (0.3)	15.1 (0.3)	15.7 (0.3)	15.2 (0.3)	19.5 (0.3)	17.8 (0.4)[a]	19.9 (0.2)	17.7 (0.5)[c]
	GWAT Weight (g)	0.12 (0.02)	0.1 (0.01)	0.10 (0.009)	0.10 (0.01)	0.23 (0.01)	0.22 (0.01)	0.25 (0.005)	0.22 (0.01)
	Normalized GWAT Weight (mg/kg)	7.7 (1.39)	7.09 (0.57)	6.17 (0.60)	6.85 (2.08)	11.79 (0.76)	12.39 (0.24)	12.39 (0.24)	12.65 (0.42)
Clinical Chemistry	Alanine Aminotransferase (mg/dL)	44.3 (2.2)	335.1 (21.0)	34.6 (0.6)	345.6 (19.5)	34.0 (1.4)	1844.5 (91.5)	94.2 (3.1)	3010.9 (256.9)
	Free Fatty Acids (mmol/mL)	662.7 (19.5)	591.0 (14.4)	470.3 (26.2)	266.6 (25.6)	437.4 (8.1)	472.9 (33.2)	325.4 (20.6)	397.0 (32.4)
	Ketone Bodies (mg/dL)	300.6 (11.3)	208.2 (11.2)	263.7 (11.6)	72.2 (2.0)	85.6 (3.2)	145.5 (3.8)	83.6 (2.4)	130.0 (5.1)
	Glucose (mg/dL)	165.4 (2.2)	153.7 (3.9)	165.2 (2.4)	142.0 (3.3)	223.7 (4.1)	158.8 (2.7)	221.9 (3.4)	156.6 (3.0)
	Triglycerides (mg/dL)	99.9 (1.3)	107.5 (0.7)	99.0 (1.2)	104.7 (1.8)	115.6 (1.5)	108.4 (1.2)	108.4 (1.3)	101.5 (1.3)

Table 5.7. Simvastatin and TCDD-mediated changes in gene expression. Results are presented as fold changes with standard error in parentheses which are relative to vehicle control mice. In all cases, sample size (n) ≥ 7 in all groups for gene expression analysis. Superscript letters indicate significant differences ($p<0.05$) as indicated by an ANOVA in comparison to: [a]vehicle (sesame oil), [b]TCDD treatment, or [c]simvastatin treatment. Statistical comparisons were not made across sexes.

Gene	Females				Males			
	Standard Chow		Statin Chow		Standard Chow		Statin Chow	
	Sesame Oil	TCDD	Sesame Oil		Sesame Oil	TCDD	Sesame Oil	TCDD
Apoa1	1.00 (0.11)	0.26 (0.02)[a]	0.97 (0.12)	0.22 (0.02)[c]	1.00 (0.14)	0.33 (0.05)[a]	1.93 (0.05)[b]	0.36 (0.07)[c]
Cyp1a1	1.00 (0.26)	2959.93 (104.63)[a]	1.08 (0.86)	2625.40 (315.80)[c]	1.00 (0.13)	2514.14 (343.20)[a]	1.46 (0.15)	4070.06 (405.41)[b,c]
Cyp1a2	1.00 (0.04)	16.51 (1.13)[a]	0.76 (0.11)	14.44 (1.19)[c]	1.00 (0.06)	12.85 (2.00)[a]	0.98 (0.06)	17.56 (1.99)[b,c]
Cyp1b1	1.00 (0.21)	505.86 (60.38)[a]	0.81 (0.19)	377 (20.43)[c]	1.00 (0.10)	701.56 (95.72)[a]	0.99 (0.09)	1320.70 (167.30)[b,c]
Cyp4a10	1.00 (0.15)	0.36 (0.04)[a]	0.51 (0.08)[b]	0.19 (0.03)[b,c]	1.00 (0.22)	0.32 (0.06)[a]	1.11 (0.14)	0.78 (0.14)[b]
Cyp4a14	1.00 (0.24)	0.57 (0.08)[a]	0.71 (0.12)	0.27 (0.03)[b,c]	1.00 (0.29)	0.11 (0.02)[a]	1.4 (0.20)	0.35 (0.08)[b,c]
Gys2	1.00 (0.15)	0.49 (0.04)[a]	0.78 (0.10)	0.28 (0.03)[b,c]	1.00 (0.18)	0.24 (0.04)[a]	1.05 (0.16)	0.36 (0.08)[c]
Lcat	1.00 (0.31)	0.70 (0.05)	0.63 (0.04)	0.57 (0.06)	1.00 (0.11)	1.19 (0.14)	1.42 (0.14)	1.48 (0.24)
Ldlr	1.00 (0.11)	0.87 (0.05)	0.97 (0.11)	1.26 (0.14)	1.00 (0.15)	0.75 (0.06)	0.95 (0.10)	0.92 (0.23)
Ppara	1.00 (0.20)	0.54 (0.05)[a]	0.63 (0.08)	0.32 (0.05)[b,c]	1.00 (0.16)	0.44 (0.04)[a]	0.96 (0.11)	0.85 (0.10)[b]
Pygl	1.00 (0.14)	0.32 (0.03)[a]	0.53 (0.05)[b]	0.24 (0.02)[c]	1.00 (0.11)	0.37 (0.10)[a]	1.01 (0.15)	0.39 (0.05)[c]
Scarb1	1.00 (0.09)	0.75 (0.11)	1.01 (0.14)	0.81 (0.16)	1.00 (0.09)	0.48 (0.10)[a]	1.06 (0.11)	0.63 (0.10)[c]

was repressed by TCDD in males and females regardless of simvastatin treatment ($p<0.05$; Table 5). Interestingly, *Apoa1* was found to induced by simvastatin treatment as compared to vehicle in males, but not females ($p<0.05$; Table 5.7). Repression of lecithin cholesterol acyltransferase (*Lcat*) gene expression, which is involved in maturation of HDL, was trending-towards statistical significance in the females, but not males ($p=0.06$; Table 5.7). Hepatic total cholesterol levels were also significantly impacted by TCDD. TCDD and S+T co-treatment led to significantly more hepatic cholesterol as compared to vehicle and simvastatin-treated mice, respectively ($p<0.05$; Table 5.6). Interestingly, S+T co-treatment resulted in significantly less hepatic cholesterol accumulation as compared to TCDD-treated male and female mice ($p<0.05$; Table 5.6).

5.3.5. The effect of TCDD and statin co-treatment on TCDD-elicited pathology

In assessing gross pathology, TCDD and S+T co-treatment led to significantly higher total liver weight (TLW) and body-weight normalized liver weights (NLW) in females as compared to the respective controls ($p<0.05$; Table 5.6). While TLW was not affected in males, TCDD and S+T co-treatment led to significantly-heavier NLWs ($p<0.05$; Table 5.6). The S+T co-treatment led to significantly-heavier TLWs and NLWs as compared to TCDD alone in females, but not males ($p<0.05$, Table 5.6).

Hematoxylin and eosin (H&E) stain was used to visualize liver morphology. In comparing across groups, TCDD exposure led to infiltration of immune cells and to vacuolization (Figure 5.4A). TCDD-mediated liver damage was confirmed by increases in serum alanine aminotransferase (ALT) levels ($p<0.05$; Table 5.6). The S+T co-treated males were found to have more infiltrating cells as compared to TCDD alone, along with higher serum ALT ($p<0.05$, Table 5.6). The increase in ALT correlates with significantly more expression of AHR-battery genes in S+T co-treated male mice as compared to TCDD-treatment, such as *Cyp1a1*, *Cyp1a2*, and *Cyp1b1* ($p<0.05$; Table 5.7). The most notable morphological difference across TCDD groups,

Figure 5.4. Impact of simvastatin and TCDD co-exposure on hepatic lipid accumulation. Hematoxylin and eosin (H&E) staining of liver was used to assess general morphology and oil red O (ORO) staining was used to assess neutral lipid. Representative samples for each stain were chosen for each treatment group (**A**). Scale bars represents 100 µm for H&E and 50 µm for ORO. Percent area of tissue stained with ORO was quantified with QuHAnT software for females (**B**) and males (**C**). Triglycerides levels in hepatic lipid extracts were quantified with commercially-available reagents in females (**D**) and males (**E**). Triglyceride results are reported as fold changes relative to vehicle control (i.e. sesame oil). In all cases, sample sizes (n) were ≥ 5. Asterisks (*) over bars indicate statistically significant differences ($p \leq 0.05$) as compared to the respective vehicle control (i.e. sesame oil vs. TCDD treatment or simvastatin-treatment vs. simvastatin + TCDD co-treatment) or between means indicated by brackets.

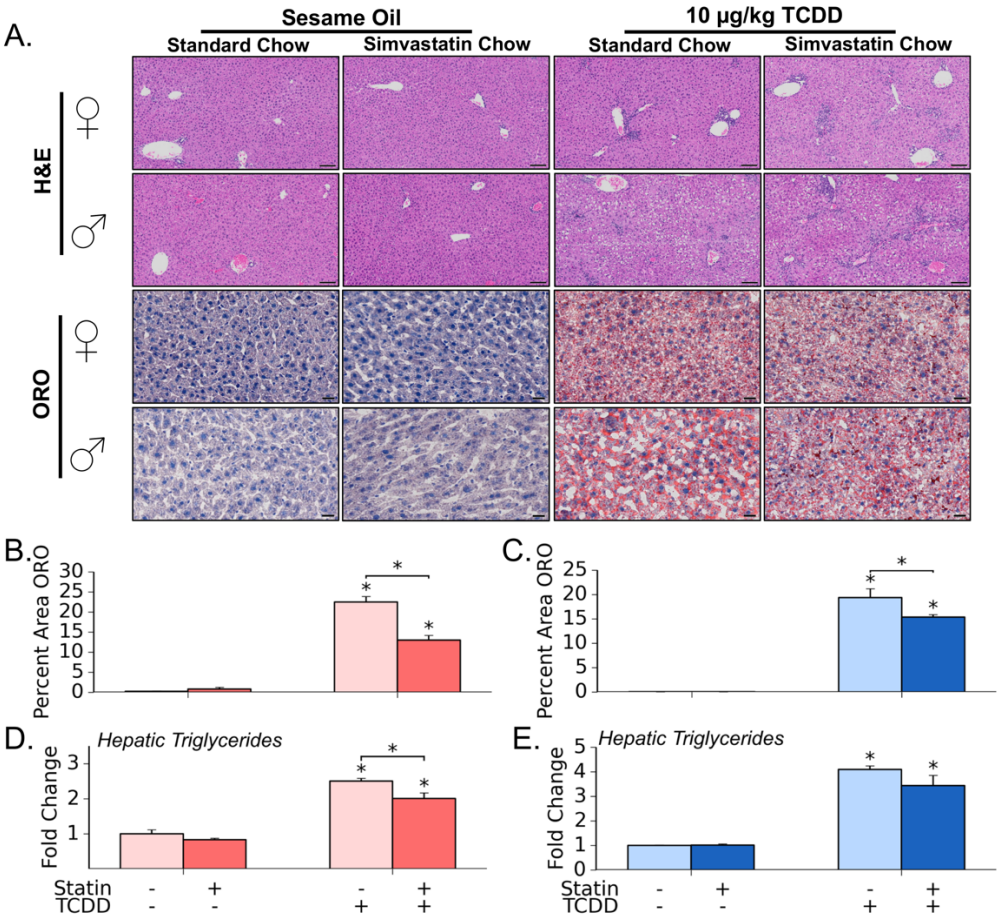

however, was an increase in vacuolization in S+T co-treated females, but not males, as compared to TCDD-treatment alone (Figure 5.4A).

Given that TCDD exposure mediates increase in hepatic lipid accumulation in mice, we hypothesized that the differences in hepatic weight and vacuolization in the S+T co-treated females was due to discrepancies in lipid accumulation. While there were no differences in serum triglyceride levels across exposures (Table 5.6), hepatic oil red O (ORO) staining suggests differences in neutral lipid accumulation across treatments (Figure 5.4A). Quantification of percent area stained with ORO confirmed that, as seen in previous studies, TCDD exposure increased lipids in the liver for both sexes regardless of simvastatin exposure ($p<0.05$; Figure 5.4B and 5.4C)(Nault et al. 2015). These results were confirmed in quantifying triglyceride content in hepatic lipid extract ($p<0.05$, Figure 5.4D and 5.4E). However, in comparing across TCDD treatments, livers from S+T co-treated males and females have significantly less ORO-stained tissue as compared to TCDD-treatment alone ($p<0.05$, Figure 5.4B and 5.4C). The S+T-mediated decrease in lipid accumulation was confirmed in females in quantifying triglycerides in hepatic lipid extracts ($p<0.05$; Figure 5.4D). While not statistically significant, results suggest that S+T co-treatment likely also reduces triglyceride content in males ($p=0.19$; Figure 5.4E).

Serum free fatty acids (FFA), ketone body (i.e. beta-hydroxybutyrate; BH) levels, and expression of hepatic peroxisome proliferator-activator alpha (*Ppara*) were assayed to investigate whether lipids are being utilized for energy production. While male FFA levels were unaffected by treatments, the S+T co-treatment led to significantly lower levels of free fatty acids in the serum as compared to simvastatin and TCDD alone in females ($p<0.05$; Table 5.6). For females, serum BH levels were also lower in S+T co-treatment as compared to simvastatin and TCDD-treatment ($p<0.05$, Table 5.6). The BH levels in males, however, were significantly increased in TCDD and S+T co-treated groups as compared to their respective controls ($p<0.05$), but not different across

TCDD-treated groups (Table 5.6). Hepatic expression of the peroxisome proliferator-activator alpha (*Ppara*) gene was repressed by TCDD regardless of simvastatin treatment ($p<0.05$; Table 5.7). Interestingly, S+T co-treated females, but not males, were found to have significantly more repression of *Ppara* expression as compared to TCDD alone ($p<0.05$; Table 5.7). Expression of genes exclusively regulated by PPAR-alpha, such as *Cyp4a10* and *Cyp4a14*, follow a similar pattern suggesting that PPAR-alpha activity is also further repressed in S+T co-treated females as compared to TCDD treatment ($p<0.05$; Table 5.7). For males, however, S+T co-treatment led to less repression of PPAR-alpha target genes as compared to TCDD alone ($p<0.05$; Table 5.7).

5.3.6. TCDD and simvastatin co-treatment-mediated increases in hepatic glycogen

As the increased hepatic weight and histological differences between TCDD and S+T co-treated females was not due to lipid accumulation, we sought to analyze the hepatic glycogen levels in each group. As compared to TCDD alone, we found significantly more hepatic glycogen in the female S+T co-treatment group ($p<0.05$; Figure 5.5A). While TCDD treatment alone did not impact hepatic glucose, S+T co-treatment led to significantly less hepatic glucose as compared simvastatin-treated female mice ($p<0.05$; Figure 5.5B). As such, the glycogen:glucose ratio is > 2 fold higher in S+T co-treated females as compared to TCDD-treated females. In the male mice, TCDD-treatment led to a significant drop in hepatic glycogen ($p<0.05$; Figure 5.5C). Furthermore, TCDD and S+T co-treatment both led to significant reductions in hepatic glucose in males ($p<0.05$; Figure 5.5D). While the difference between TCDD and S+T co-treatment was not significant for males, the glycogen:glucose ratio is ~1.5 fold higher in S+T co-treated males as compared to TCDD alone. A periodic acid-Schiff stain, which stains polysaccharides such as glycogen, confirmed that S+T co-treatment in females, but not males, led to a notable increase in hepatic glycogen levels as compared to TCDD alone (Figure 5.5E). Hepatic expression of glycogen synthase (*Gys2*) which is involved in glycogen anabolism was found to be significantly

Figure 5.5. Impact of simvastatin and TCDD co-exposure on hepatic glycogen metabolism. Hepatic glycogen was inferred based on background glucose in females (**A** and **B**) and males (**C** and **D**). In both non-amyloglucosidase-treated (A and C) and amyloglucosidase-treated (B and D) samples, glucose was measured with commercially-available reagents. Results are reported as fold changes relative to vehicle control (i.e. sesame oil). Sample sizes (n) were ≥ 5 in all cases. Asterisks (*) indicate statistically significant differences (p≤0.05) between means indicated by brackets. Periodic acid-Schiff stain (PAS) was used to confirm differences in glycogen levels; a representative sample was chosen for each treatment group (**E**). Scale bars represents 20 μm.

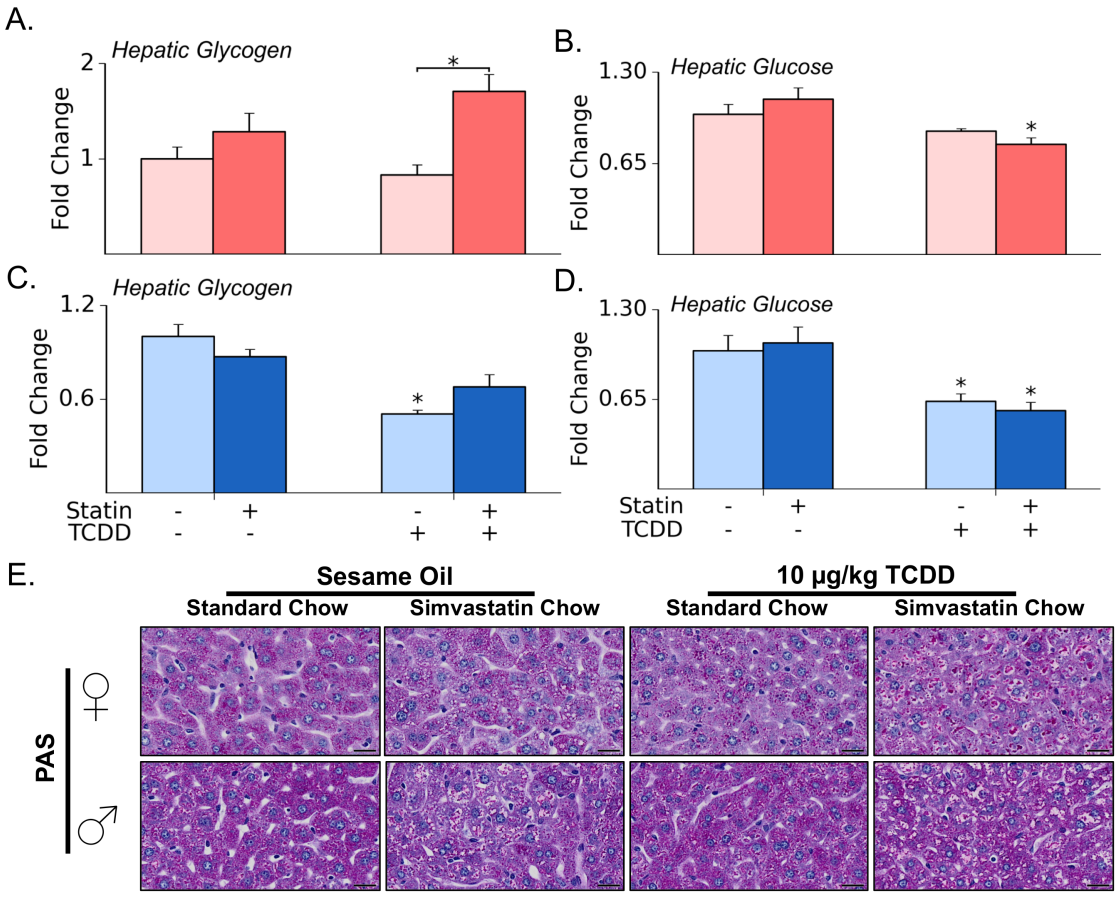

repressed by TCDD regardless of simvastatin treatment in males and females ($p<0.05$; Table 5.7). In comparing across TCDD treatments, S+T co-treated females, but not males, were found to have a lower level of *Gys2* expression as compared to TCDD alone ($p<0.05$; Table 5.7). Like *Gys2*, expression of the glycogen phosphorylase gene (*Pygl*) which is involved in regulating glycogen catabolism was significantly repressed by TCDD in males and females regardless of simvastatin exposure ($p<0.05$; Table 5.7). However, unlike *Gys2*, there were not differences in *Pygl* expression across TCDD treatments.

5.4. Discussion

Previous *in vitro* and rodent-based studies have indicated that exposures to AHR ligands repress expression of genes involved in cholesterol biosynthesis ultimately leading to reductions of circulating TC, HDL, and LDL in serum (Angrish et al. 2013; Tanos et al. 2012). Using the nationally-representative 2003-2004 NHANES data, regression analysis suggests that TCDD-mediated repression of cholesterol biosynthesis may be relevant in the human population and sex-specific. More specifically, regression models adjusted for age, BMI, and race estimate a male-specific 6.2% reduction in TC from T1 (*i.e.* low-TCDD) to T3 (*i.e.* high-TCDD) that was not present in the female-stratified or full cohort (Table 5.5; Figure 5.2A). Regression models also indicate that LDL levels are associated with serum TCDD with an estimated 13.0% reduction from T1 to T3 in the full-cohort, respectively ($p<0.05$; Table 5.5; Figure 5.2B). Estimations for male- and female-stratified cohorts were also negative and near statistical significance in comparing LDL from T3 to T1 ($p=0.08$ and $p=0.06$, respectively) suggesting that the reduction in LDL is not sex-specific (Table 5.5; Figure 5.2B). Lack of significance for the male- and female-stratified LDL dataset is likely due to smaller sample sizes relative to the full-cohort. Regression models indicate that HDL is not associated with TCDD. Overall, our statistical models suggest that AHR-mediated alteration in cholesterol homeostasis is relevant to humans. More importantly, the regression results suggest that environmentally-relevant TCDD exposure levels are altering cholesterol homeostasis in the American population.

To characterize the impact of TCDD-induced repression of cholesterol biosynthesis in TCDD-elicited liver pathology, C57BL/6 mice were gavaged with TCDD in the presence or absence of simvastatin, a competitive inhibitor of HMG-CoA reductase. While not statistically significant as seen in previous studies (Angrish et al. 2013; Tanos et al. 2012), TCDD-induced a consistent decrease in *Hmgcr* mRNA expression (Figure 5.3A and 5.3B). The decrease was confirmed at the protein level and was significant in males, but not females (Figure 5.3D and

5.3E). While the TCDD-induced repression of *Hmgcr* was modest, the TC and HDL levels were significantly lower in serum, which adheres to previous reports suggesting that TCDD alters cholesterol homeostasis in mice (Table 5.6)(Angrish et al. 2013). Unlike previous studies, however, LDL levels, were mostly unaffected in this study which is likely due to differences in study design (Angrish et al. 2013).

Simvastatin, while increasing *Hmgcr* mRNA expression, did not alter HMGCR protein levels (Figure 5.3D and 5.3E). Similarly, the level of serum TC and LDL was not impacted by simvastatin in serum at the time of sacrifice (Table 5.6). Notably, statins primarily reduce LDL levels in humans (Baigent et al. 2010). Previous studies have shown that statins are less effective in lower circulating LDL in mice since, unlike humans, HDL is their predominant lipoprotein (Schonewille et al. 2016). Along these lines, simvastatin was found to have a significant impact on serum HDL in females, but not males ($p<0.05$; Table 5.6). As the primary role of HDL is in reverse-cholesterol transport (RCT), these results suggest that simvastatin-treated female mice down-regulate transport of cholesterol from tissues to the liver. Gene expression of the scavenger receptor B1 (*Scarb1*) which serves as the HDL receptor was not impacted by simvastatin in the liver (Table 5.7). Expression of the apolipoprotein A1 gene (*Apoa1*), which is the primary lipoprotein component of HDL, was significantly increased in males, but not females, treated with simvastatin as compared vehicle mice ($p<0.05$; Table 5.7). Previous reports have established that APOA1 is essential for HDL formation and that *Apoa1*$^{-/-}$ mice have lower circulating levels of HDL (Plump et al. 1997). As such, a reduction in HDL found in females, but not males, could be due to discrepancies in the level of hepatic expression of APOA1 in response to simvastatin. Similarly, simvastatin-mediated repression of lecithin cholesterol acyltransferase (*Lcat*) was found to be near statistical significance in the females, but not males ($p=0.06$; Table 5.7). LCAT is primarily expressed by the liver and, once excreted, esterifies cholesterol and promotes HDL maturation (Zhou et al. 2015). LCAT deficiency is associated with decreased HDL and, ultimately, catabolism

of APOA1 (Simonelli et al. 2013). As such, lack of up-regulation of *Apoa1* and/or down-regulation of *Lcat* at the transcriptional level might play a mechanistic role in the simvastatin-mediated decrease in HDL in females.

Histological assessment and serum ALT levels suggest that the S+T co-treatment increases severity of TCDD-induced liver injury in males, but not females ($p<0.05$; Table 5.6; Figure 5.4A). As compared to TCDD alone, the S+T co-treated males have a greater-degree of AHR-mediated transcription as indicated by significant increases in expression of several AHR-battery genes, such as *Cyp1a1*, *Cyp1a2*, and *Cyp1b1* ($p<0.05$; Table 5.7). As TCDD-mediated liver injury is AHR-dependent (Fernandez-Salguero et al. 1996; Pierre et al. 2014), we hypothesize that the increase in liver damage in the male S+T co-treatment group is AHR-mediated. The mechanism behind increased AHR-mediated transcription which is unique to S+T co-treated males requires further research.

As seen in previous studies, TCDD exposure drove significant increases in hepatic cholesterol and lipid accumulation ($p<0.05$; Figure 5.4; Table 5.6)(Nault et al. 2017). S+T co-treatment, however, led to significantly-lower levels of hepatic cholesterol as compared to TCDD in both sexes (Table 5.6). These results correlate with lower-levels of lipid accumulation in the S+T co-treated group (Figure 5.4). Previous reports have associated NAFLD with higher-levels of HMGCR expression and accumulation of hepatic free cholesterol in humans (Min et al. 2012). Epidemiological studies have also suggested that statin-usage protects against hepatic steatosis (Dongiovanni et al. 2015). Collectively, these results suggest that AHR-mediated repression of *Hmgcr* and other genes involved in cholesterol biosynthesis might protect against TCDD-elicited steatosis. Our results confirm this hypothesis as simvastatin, an inhibitor of HMGCR, reduced hepatic cholesterol and lipid accumulation in mice that were treated with TCDD.

The simvastatin-mediated protection against TCDD-elicited hepatic lipid deposition appears to be somewhat sex-specific as it was more pronounced in females as compared to males (Figure 5.4). The decreased levels of FFAs in the serum of the S+T co-treated females suggest that S+T co-treated female mice have less mobilized lipids which may contribute to the lower-level of hepatic lipid accumulation ($p<0.05$; Table 5.6). Interestingly, S+T co-treated females have significantly lower levels of hepatic peroxisome proliferator-activator alpha (*Ppara*) gene expression, a master regulator of fatty acid oxidation, which coincides with decreases in exclusive PPAR-alpha target genes, such as *Cyp4a10* and *Cyp4a14* ($p<0.05$; Table 5.7)(Mandard et al. 2004). Furthermore, ketone bodies are also significantly lower in serum of S+T co-treated females as compared to the TCDD-treatment ($p<0.05$; Table 5.6). As such, the S+T co-treated females are likely not utilizing lipids as an energy source. These results suggest that the reduction in hepatic lipid as compared to TCDD-treated females is due to accumulation and not an increase in fatty acid metabolism. While having comparable levels of ORO and triglyceride levels in the liver as the females, male mice appear to be in a different metabolic state. Gene expression of *Ppara*, while not statistically significant, was slightly increased while PPAR-alpha target genes were significantly higher in S+T co-treated males as compared to TCDD alone ($p<0.05$; Table 5.7). As such, the gene expression results suggest that S+T co-treated males have less TCDD-mediated repression of fatty acid oxidation in the liver as compared to TCDD alone. While TCDD exposures are thought to repress beta-oxidation, male mice in our study had increases in the levels of ketone bodies in the serum suggesting that fatty acids are being utilized for energy production. However, while the hepatic gene expression suggests that S+T co-treated males have more PPAR-alpha-related activity, there is not a difference across TCDD treatments. As such, the increases in PPAR-alpha-related activity in the S+T co-treated males does not appear to be severe enough to induce a systemic increase in ketone body levels in the blood.

The most surprising phenotype was a significant increase in hepatic glycogen content found within the S+T co-treated females as compared to TCDD alone ($p<0.05$; Figure 5.5A and 5.5E). The phenotype coincides with an increase in liver weight ($p<0.05$; Table 5.6). While not as pronounced in females, the S+T co-treated males had a similar glycogen deposition and liver weight trend suggesting that the phenotype could also be present in males, but less severe (Figure 5.5B; Table 5.6). As previous reports have established that TCDD exposure depletes hepatic glycogen stores (Nault et al. 2016a), we hypothesize that the S+T co-treatment is driving a metabolic phenotype that is similar to a glycogen storage disease (GSD). GSDs are a diverse-set of autosomal recessively inherited metabolic disorders mediated through enzyme deficiencies (Ozen 2007). As the mice were fasted prior to sacrifice, we are hypothesizing that the greater level of glycogen content in S+T co-treated females as compared to TCDD-treatment is due to an impairment of glycogen catabolism. Gene expression of glycogen phosphorylase (*Pygl*), which is the rate-limiting enzyme of glycogenolysis, supports this hypothesis. While simvastatin treatment alone was found to decrease gene expression of *Pygl* ($p<0.05$), *Pygl* was repressed further in S+T co-treated females as compared to TCDD-treatment, but was not statistically significant ($p=0.27$; Table 5.7). Notably, much of the glycogen phosphorylase activity is regulated through post-translational modifications and allosteric interactions which we did not assay (Han et al. 2016). Glycogen synthase (*Gys2)* expression follows a similar pattern. *Gys2* expression was found to be lower in the S+T treated females, but not males, as compared to TCDD alone ($p<0.05$; Table 5.7). We hypothesize that reduction in *gys2* expression in the S+T-treated females may be a feedback mechanism due to the inability to catabolize hepatic glycogen. Notably, like glycogen phosphorylase, much of the glycogen synthase activity is regulated post-translationally (Han et al. 2016). Further studies are required to screen the expression and activity of enzymes involved glycogen catabolism in further detail to test our hypothesis and unravel the mechanism behind this phenotype.

In conclusion, the novelty of this study is two-fold. First, regression analysis of the NHANES 2003-2004 dataset suggests that environmentally-relevant TCDD exposures in the American population impact cholesterol homeostasis. Secondly, a functional mouse-based experiment characterized several roles of HMGCR in TCDD-mediated toxicity in the liver. Results suggest that TCDD-mediated repression of cholesterol biosynthesis protects against lipid accumulation in the liver of both sexes. While lipid accumulation is reduced, the S+T co-treatment appears to increase AHR-mediated liver injury in a male-specific manner. The S+T co-treatment resulted in greater levels of hepatic glycogen as compared to TCDD-treated mice in a female-specific manner. While further research is needed to better understand the mechanism and differences across sexes, our results suggest that human individuals who take statins may be protected from AHR-mediated steatosis, but more at risk for TCDD-mediated liver injury and alterations in glycogen metabolism in a sex-specific manner.

REFERENCES

REFERENCES

Angrish MM, Dominici CY, Zacharewski TR. 2013. Tcdd-elicited effects on liver, serum, and adipose lipid composition in c57bl/6 mice. Toxicol Sci 131:108-115.

Arguello G, Balboa E, Arrese M, Zanlungo S. 2015. Recent insights on the role of cholesterol in non-alcoholic fatty liver disease. Biochim Biophys Acta 1852:1765-1778.

Baigent C, Blackwell L, Emberson J, Holland LE, Reith C, Bhala N, et al. 2010. Efficacy and safety of more intensive lowering of ldl cholesterol: A meta-analysis of data from 170,000 participants in 26 randomised trials. Lancet 376:1670-1681.

Cave M, Appana S, Patel M, Falkner KC, McClain CJ, Brock G. 2010. Polychlorinated biphenyls, lead, and mercury are associated with liver disease in american adults: Nhanes 2003-2004. Environ Health Perspect 118:1735-1742.

Dongiovanni P, Petta S, Mannisto V, Mancina RM, Pipitone R, Karja V, et al. 2015. Statin use and non-alcoholic steatohepatitis in at risk individuals. J Hepatol 63:705-712.

Fader KA, Nault R, Zhang C, Kumagai K, Harkema JR, Zacharewski TR. 2017. 2,3,7,8-tetrachlorodibenzo-p-dioxin (tcdd)-elicited effects on bile acid homeostasis: Alterations in biosynthesis, enterohepatic circulation, and microbial metabolism. Sci Rep 7:5921.

Fernandez-Salguero PM, Hilbert DM, Rudikoff S, Ward JM, Gonzalez FJ. 1996. Aryl-hydrocarbon receptor-deficient mice are resistant to 2,3,7,8-tetrachlorodibenzo-p-dioxin-induced toxicity. Toxicol Appl Pharmacol 140:173-179.

Han HS, Kang G, Kim JS, Choi BH, Koo SH. 2016. Regulation of glucose metabolism from a liver-centric perspective. Exp Mol Med 48:e218.

Lee DH, Lee IK, Porta M, Steffes M, Jacobs DR, Jr. 2007. Relationship between serum concentrations of persistent organic pollutants and the prevalence of metabolic syndrome among non-diabetic adults: Results from the national health and nutrition examination survey 1999-2002. Diabetologia 50:1841-1851.

Mandard S, Muller M, Kersten S. 2004. Peroxisome proliferator-activated receptor alpha target genes. Cell Mol Life Sci 61:393-416.

Min HK, Kapoor A, Fuchs M, Mirshahi F, Zhou H, Maher J, et al. 2012. Increased hepatic synthesis and dysregulation of cholesterol metabolism is associated with the severity of nonalcoholic fatty liver disease. Cell Metab 15:665-674.

Nault R, Colbry D, Brandenberger C, Harkema JR, Zacharewski TR. 2015. Development of a computational high-throughput tool for the quantitative examination of dose-dependent histological features. Toxicol Pathol 43:366-375.

Nault R, Fader KA, Ammendolia DA, Dornbos P, Potter D, Sharratt B, et al. 2016a. Dose-dependent metabolic reprogramming and differential gene expression in tcdd-elicited hepatic fibrosis. Toxicol Sci 154:253-266.

Nault R, Fader KA, Kopec AK, Harkema JR, Zacharewski TR, Luyendyk JP. 2016b. From the cover: Coagulation-driven hepatic fibrosis requires protease activated receptor-1 (par-1) in a mouse model of tcdd-elicited steatohepatitis. Toxicol Sci 154:381-391.

Nault R, Fader KA, Lydic TA, Zacharewski TR. 2017. Lipidomic evaluation of aryl hydrocarbon receptor-mediated hepatic steatosis in male and female mice elicited by 2,3,7,8-tetrachlorodibenzo-p-dioxin. Chem Res Toxicol 30:1060-1075.

Ozen H. 2007. Glycogen storage diseases: New perspectives. World J Gastroenterol 13:2541-2553.

Pierre S, Chevallier A, Teixeira-Clerc F, Ambolet-Camoit A, Bui LC, Bats AS, et al. 2014. Aryl hydrocarbon receptor-dependent induction of liver fibrosis by dioxin. Toxicol Sci 137:114-124.

Plump AS, Azrolan N, Odaka H, Wu L, Jiang X, Tall A, et al. 1997. Apoa-i knockout mice: Characterization of hdl metabolism in homozygotes and identification of a post-rna mechanism of apoa-i up-regulation in heterozygotes. J Lipid Res 38:1033-1047.

Poland A, Palen D, Glover E. 1994. Analysis of the four alleles of the murine aryl hydrocarbon receptor. Mol Pharmacol 46:915-921.

Schonewille M, de Boer JF, Mele L, Wolters H, Bloks VW, Wolters JC, et al. 2016. Statins increase hepatic cholesterol synthesis and stimulate fecal cholesterol elimination in mice. J Lipid Res 57:1455-1464.

Simonelli S, Tinti C, Salvini L, Tinti L, Ossoli A, Vitali C, et al. 2013. Recombinant human lcat normalizes plasma lipoprotein profile in lcat deficiency. Biologicals 41:446-449.

Tanos R, Patel RD, Murray IA, Smith PB, Patterson AD, Perdew GH. 2012. Aryl hydrocarbon receptor regulates the cholesterol biosynthetic pathway in a dioxin response element-independent manner. Hepatology 55:1994-2004.

Zhou L, Li C, Gao L, Wang A. 2015. High-density lipoprotein synthesis and metabolism (review). Mol Med Rep 12:4015-4021.

Chapter 6: Conclusions and Future Directions

6.1. Overall Goal

The primary goal of this dissertation was to use a population-guided approach to characterize the impact of population-level heterogeneity in response to TCDD and identify novel modulators that impact susceptibility to TCDD-elicited adverse health outcomes. First, we confirmed the presence of profound interindividual variability in response to TCDD across human individuals. Second, a mouse panel was used to scan for genetic modifiers that may be involved in driving human interindividual variability in response to TCDD. Specific endpoints of focus were TCDD-mediated suppression of the B cell, hepatic sequestration of TCDD, and TCDD-mediated non-alcoholic fatty liver disease (NAFLD). Quantitative trait locus (QTL) analysis was used to identify regions of the genome that potentially modulate inter-strain differences in the responses to TCDD. Specific genes within these regions were chosen based on physiological processes and previous implications in AHR-mediated biology to characterize potential functional roles within TCDD-mediated toxicity.

6.2. Primary Findings and Future Directions

6.2.1. Specific Aim 1. Characterizing the impact of interindividual variability in TCDD-mediated suppression of the human B cell.

The primary novelty of this project was in the large number of individual human donors that were assayed. To our knowledge, this is the largest study of human primary leukocytes. B cells were isolated from 51 unique human donors, activated with CD40 ligand, and exposed to a TCDD dose-response for a total of 7 days. Following, we assayed the impact of TCDD on the number of B cells secreting IgM and the concentration of IgM secreted during the culture period.

First and foremost, results suggest that humans respond to TCDD to differing degrees. For example, there was ≥ 70 fold differences in the number of cells secreting IgM following exposure to 30 nM TCDD between individuals in our human B cell study. As the results suggest

that some individuals are more-susceptible to TCDD-mediated immunosuppression than others, the number of individuals assayed should be considered during chemical-based risk assessment of heterogeneous populations. Future work could entail a paradigm within risk-assessment that requires larger-scale studies to better encapsulate the response across heterogeneous populations. Larger studies would provide data that would better identify and protect individuals who are susceptible to chemical-induced toxicity, but would also ensure that exposure guidelines and required clean-up of contaminated sites is reasonable and based on empirical evidence.

Secondly, the data from the large number of human donors were used to assess the impact of population heterogeneity within the low-dose region of a TCDD-mediated dose-response relationship. Results suggest that the population of 51 donors do not have a linear low-dose relationship. Our results have direct implications within risk assessment as a recent report from the National Research Council (NRC) suggested that population-level dose-response curves would linearize for all non-cancer mediated endpoints (NRC 2009). Our data for TCDD-mediated repression of the human B cell does not support the NRC's hypothesis. However, future work would require a larger-scale study with > 51 human donors to empirically-disprove the low-dose no-threshold (LNT) hypothesis for our endpoints of interest. Future work is also required to test the LNT hypothesis for other TCDD-mediated endpoints and, beyond, other chemically-mediated adverse health outcomes. While ambitious, such results would ensure that exposure guidelines are set that are safe for the heterogeneous human population.

6.2.2. Specific Aim 2. Identifying and characterizing the impact of *Serpinb2* as modulator of TCDD-mediated suppression of the B cell.

The primary goal of this study was to use a genetics-based approach to screen for genetic modulators of TCDD-mediated suppression of CD40 ligand-activated B cells. B cells were isolated from 12 genetically-diverse strains and exposed to TCDD using the same model as used in our

previous human B cell study. QTL analysis of the number of cells secreting IgM from each strain at 30 nM was used to screen for potential genetic modulators of TCDD-mediated suppression of the B cell.

Results suggested that a region of chromosome 1 was associated with inter-strain differences in TCDD-mediated immunosuppression. A gene called *Serpinb2* that encodes for the serine peptidase inhibitor, clade B, member 2 was found to be within the genomic region of interest. Moreover, *Serpinb2* expression is altered upon TCDD exposures in mouse and human B cells (Kovalova et al. 2016). Our results suggest that TCDD-mediated dysregulation of *Serpinb2* is most-prominent in Ahr^{d} mice (i.e. strains less-sensitive to TCDD) and occurs in a time-dependent manner. Further downstream analysis suggested that $Serpinb2^{-/-}$ mice were significantly more sensitive to TCDD-mediated suppression of the number of cells secreting IgM. These results suggest that TCDD-mediated induction of *Serpinb2* activity is likely playing a protective role against TCDD-mediated suppression of the B cell.

Further work is required to better understand the role of *Serpinb2* in B cell biology. Our study is the first to link *Serpinb2*-related activity to B cell function. Immunological challenges of $Serpinb2^{-/-}$ mice have indicated a key role in immune function, but further work is needed to place more specific focus on the B cell (Schroder et al. 2010; Schroder et al. 2011). Furthermore, a more comprehensive study is required that can dissect the role of *Serpinb2* in TCDD-mediated suppression of IgM secretion. Given the time dependence of TCDD-mediated suppression, such a study would likely require a time-course over the 6-day period of culture. Such a study might elucidate whether *Serpinb2* activity is mitigating TCDD-mediated suppression of B cell activation or secretion of IgM.

The most pertinent future work is to translate our findings to human B cells to establish whether inhibition of *Serpinb2*-related activity increases the level of TCDD toxicity in humans. A viable method to translate would lie in a large-scale screen of the *Serpinb2* gene in human B cells which are exposed to TCDD. Such a study, while quite ambitious, might suggest whether *Serpinb2* polymorphisms that impact expression of functionality of plasminogen activator 2 (PAI2), the human ortholog of mouse SERPINB2, impacts susceptibility to TCDD-mediated immunosuppression. The results would have potential to identify individuals in the human population that may be more susceptible to TCDD-mediated immunosuppression.

6.2.3. Specific Aim 3. Characterizing the toxicodynamics of hepatic accumulation of TCDD and identifying *Tgfbr2* as a modulator of TCDD-mediated liver toxicity.

The primary goal of this study was to use a population-based approach to characterize the role of the AHR-mediated transcription in hepatic sequestration of TCDD. Mice from 14 genetically-diverse strains were exposed to TCDD over a 10-day period. The level of TCDD and the expression of 9 AHR-responsive genes were assessed in the liver following the exposure period. Furthermore, QTL analysis was used to scan for genetic modulators that potentially impact TCDD sequestration and AHR-mediated gene expression.

First and foremost, the level of TCDD in the livers were vastly-different across the 14 mouse strains with difference ≥ 30-fold. Heritability analysis suggests that genetic variability within our mouse panel drives ~15 times more of the observed variance as compared to environmental factors. As such, our results suggest that genetic background plays a strongly-influential role in the accumulation of TCDD. Overall, mice which carry sensitive *Ahr* alleles, such as the Ahr^{b1}, were found to have higher levels of hepatic TCDD sequestration suggesting an AHR-dependence in sequestration. Pearson correlation analysis of TCDD burden and hepatic expression further suggests that the TCDD sequestration is dependent on AHR-mediated transcription. Of the 9

genes assessed, the expression of classical AHR-battery genes, such as *Cyp1a1*, *Cyp1b1*, and *Cyp1a2*, were highly correlated with TCDD burden and adheres to previous studies (Diliberto et al. 1997; Hakk et al. 2009). Interestingly enough, we often found strains which were exceptions to the overall endpoint-specific findings. The most interesting discrepancy, however, were several strains (DBA1/J and BXD40) which appear to accumulate more TCDD than can be explain by the expression of the AHR-battery genes. We hypothesized, therefore, that other genomic factors beyond the inherited *Ahr* allele are likely impacting the hepatic sequestration of TCDD. Our QTL analysis supports this hypothesis as several areas of the genome were found to potentially modulate the accumulation of TCDD. Further research is needed to focus on these unique strains to establish whether genes or pathways associated with these QTLs explain discrepancies in TCDD burden. Such patterns may suggest why these strains fall away from the over-arching response of other strains and, furthermore, identify individuals that may be more susceptible to hepatic TCDD accumulation.

QTL analysis of the inter-strain differences in gene expression profiles pointed to several areas of the genome that may impact response to TCDD. Of these regions, we had particular interest in a significant association found in Chromosome 9 near the gene encoding transforming growth factor beta receptor type 2 (*Tgfbr2*). As the TGF-beta pathway had been previously implicated in TCDD-mediated liver toxicity by several groups (Nault et al. 2016; Pierre et al. 2014), we decided to conduct a study where TCDD-sensitive (i.e. Ahr^{b1}) mice were exposed to TCDD in the presence or absence of a TGFBR2-based antibody ligand trap. Results indicate that TCDD and TGFBR2-neutralizing antibody co-treatment led to increased hepatic steatosis and was most pronounced in males as compared to females. As male mice are known to be more sensitive to TCDD, we would suspect that a similar result in female mice would be found at a higher dose of TCDD. Previous reports have suggested that hepatocyte-specific $Tgfbr2^{-/-}$ mice fed a choline-deficient diet have decreased steatosis that corresponds with increased expression of genes

involved in beta-oxidation (Yang et al. 2014). As such, further research should investigate why TCDD treatment and choline-deficient diet, which both induce NAFLD, drive the opposite result in mouse models with reduced TGFBR2 activity. Notably, TCDD is well-known to reduce the expression of genes involved in beta-oxidation (Nault et al. 2016; Nault et al. 2017) that were found to increase in *Tgfbr2*$^{-/-}$ mice fed the choline-deficient diet (Yang et al. 2014) which might explain the discrepancy across models. A future experiment in which the hepatocyte-specific *Tgfbr2*$^{-/-}$ mice are treated with TCDD to confirm our results from the TGFBR2-neutralizing antibody co-treatment experiment might also be valuable.

The TCDD and TGFBR2-neutralizing antibody co-treatment was also found to decrease the level of infiltrating cells in the livers of males, but not females. These results coincide with previous reports in which NAFLD was induced in hepatocyte-specific *Tgfbr2*$^{-/-}$ mice (Yang et al. 2014). The expression of the *Tgfb1* gene along with several other pro-inflammatory RNAs which are primarily mediated through infiltrating cells were found to be lower in males treated with TCDD and TGFBR2-neutralizing antibody co-treatment compared to TCDD alone. As such, we hypothesize that intercepting ligands of TGFBR2 reduces the recruitment of inflammatory cells into the liver. Further experiments are needed to characterize the cell type where *Tgfb1* and *Tgfbr2* are being expressed within our experimental models (i.e. immune cells, hepatocytes, Kupffer cells, etc.). Such results may provide a means to treat individuals exposed to NAFLD-causing agents. However, while inflammation appears to be decreased in mice treated with TCDD, there is also an increase in steatosis which requires further mechanistic research prior to using the TGFBR2-neutralizing antibody as a viable treatment in humans.

6.2.4. Specific Aim 4. Identifying and characterizing the impact of TCDD-mediated repression of *Hmgcr* in modulating TCDD-mediated liver toxicity.

QTL analysis of the change in total body weight induced by TCDD across 14 genetically-diverse strains mapped to chromosome 13 near *Hmgcr.* Previous reports had suggested that TCDD represses genes involved in cholesterol biosynthesis, including *Hmgcr* which encodes HMG-CoA reductase that serves as the rate-limiting step (Angrish et al. 2013; Tanos et al. 2012). The TCDD-induced repression of these genes in mice coincides with lower levels of cholesterol in the blood (Angrish et al. 2013). As these previous reports have only focused on the mouse, we sought to test whether the phenotype was relevant in humans using epidemiological data from the Center for Disease Control's (CDC) National Health and Nutrition Examination Survey (NHANES)(Center for Disease Control 2005).

Results indicated that the phenotype is relevant within the human population. Males were found to have reduced total cholesterol in serum that were associated with increasing levels of lipid-adjusted TCDD following adjustment for confounding variables, such as race, age, and body mass index (BMI). Reductions in low-density lipoprotein (LDL) were associated with increasing lipid-adjusted TCDD levels in the full cohort (*i.e.* males and females) in a seemingly sex-independent manner. Overall, there is compelling evidence that TCDD is negatively associated with cholesterol levels in serum in the human population which coincides with previous rodent-based studies (Angrish et al. 2013; Tanos et al. 2012). Notably, cholesterol plays a wide-range of roles in physiology, such as a necessary component of cell membranes and precursor for sex-steroids, bile acid, and vitamin D. As cholesterol biosynthesis is highly-regulated, we hypothesize that reductions seen in the NHANES dataset will likely have an adverse effect in humans. However, future studies are required to focus on whether the reductions found within the NHANES dataset have physiological consequences.

To assess the potential role of *Hmgcr* in modulating TCDD-mediated toxicity, TCDD-sensitive (i.e. *Ahr*^{b1}) mice were exposed to TCDD in the presence or absence of simvastatin, a competitive inhibitor of HMG-CoA reductase. First, we found a reduction in lipid accumulation in the TCDD and simvastatin co-treatment as compared to TCDD treatment in both sexes. These results coincide with a simvastatin-mediated reduction in serum and liver total cholesterol in both sexes that were treated with TCDD. Such results coincide with several previous reports that have linked accumulation of cholesterol with severity of NAFLD (Arguello et al. 2015; Min et al. 2012). Future experiments should test whether simvastatin-mediated reduction in TCDD-elicited hepatic lipid accumulation carries across other statins. Furthermore, a *Hmgcr*$^{-/-}$ hepatic cell models might determine if the reduction in lipid accumulation is specific to HMG-CoA reductase activity in the liver or whether there are off-target effects of statins driving the phenotype.

While simvastatin appears to protect against TCDD-elicited steatosis, male, but not female, mice that were co-treated with simvastatin and TCDD were more susceptible to TCDD-mediated liver injury. Such results coincide with significantly more expression of AHR-battery genes which may indicate that, as TCDD-mediated liver injury is AHR-dependent (Pierre et al. 2014), increased AHR-mediated expression may be driving the increase in susceptibility. Future experiments could focus on genome-wide RNA expression and see if genes and pathways appear to different in the TCDD vs. TCDD and simvastatin co-treatment. Our results suggest that males who take statins may be at a greater-risk to TCDD-induced liver injury. Future research is needed to establish if the simvastatin and TCDD co-treatment is impacting expression and/or degradation of AHR which may explain the increase in liver injury. Other projects might focus on the transcriptomic and proteomic response to establish whether there are co-exposure-mediated gene expression profiles that recruit inflammatory cells to the liver in a male-specific manner. Finally, this phenotype needs to be confirmed in humans.

While simvastatin and TCDD co-treated males were more susceptible to liver injury, female mice that were co-treated were found to have significantly more hepatic glycogen as compared to TCDD alone. These results coincide with heavier livers and with a greater-degree of vacuolization in the simvastatin and TCDD co-treated females. While males appear to have a similar trend, the results were not statistically-significant or as severe. We are hypothesizing that the TCDD and simvastatin co-treatment is mimicking a glycogen storage disease that is much more prominent in females. Further research is needed to confirm our hypothesis and explore the sex-specific nature of the phenotype. Such a study would require screens for enzyme expression and activity that are involved in glycogen anabolism and catabolism. Further research is needed to establish whether this phenotype is present in humans as this may suggest that individuals who take statins may be more susceptible to TCDD-mediated disruption of glycogen metabolism.

6.3. Overall Conclusion

Overall, we hope that this thesis serves as an example of the power behind population-based approaches in understanding the variability and mechanisms behind chemical-induced toxicity. We have shown that responses are dependent on the individual or strain tested. Lack of data from genetically-diverse models that are used to assess risk of chemical exposures is destined to miss individuals that are most-susceptible to adverse health effects. Furthermore, homogenous models do not inform of the range in response across differing individuals. The current state of risk-assessment is to account for this variability with a generic 10-fold adjustment. The data in this thesis adds to a body of evidence suggesting that a 10-fold uncertainty factor is too conservative for some endpoints. As opposed to generic uncertainty factors, population-based approaches provide the means to more-accurately estimate the level of variability included in safe-exposure estimations with empirical evidence.

The results from these set of experiments not only serve as a proof of principle, but also adds to our understanding of the mechanisms behind TCDD-mediated toxicity. The data provided compliments a growing body of AHR-related literature as it provides links between genes and pathways that modulate AHR-mediated physiological processes. Such links provide a better understanding of AHR biology. We also speculate that information provided by this thesis work could be used to better understand how individuals exposed to TCDD may be treated to mitigate adverse health effects.

Beyond mechanistic toxicology, our results have the potential to impact real-world risk assessment. First, we have characterized the presence of a wide-degree of interindividual variability in response to TCDD using human primary cells. Such information can be used to better estimate safe-exposure limits of TCDD across heterogeneous populations. This aspect of the thesis is at the heart of the current-state of toxicology as it provides empirical data to keep populations safe from TCDD-mediated adverse health effects. Second, the mouse panel indicates that genetic background is playing a pivotal role in impacting the response to TCDD. While much of the aforementioned mouse work remains to be confirmed in humans, we have provided evidence that genetic background has profound impacts on susceptibility to TCDD-mediated toxicity. This aspect of the thesis, in my opinion, is at the heart of toxicology of the future. As we enter the age of personalized and precision medicine where characterizing individual's genetic background becomes more and more feasible, I speculate that genetic information can also be used for personalized risk assessment that will, ultimately, improve public health. Thus, individuals who are genetically-predisposed to TCDD-mediated toxicity can be forewarned prior to consumption of foods that may be high in TCDD and other AHR ligands.

REFERENCES

REFERENCES

Angrish MM, Dominici CY, Zacharewski TR. 2013. Tcdd-elicited effects on liver, serum, and adipose lipid composition in c57bl/6 mice. Toxicol Sci 131:108-115.

Arguello G, Balboa E, Arrese M, Zanlungo S. 2015. Recent insights on the role of cholesterol in non-alcoholic fatty liver disease. Biochim Biophys Acta 1852:1765-1778.

Center for Disease Control. 2005. National health and nutrition examination survey data. Nhanes 2003–2004. Available: https://wwwn.cdc.gov/nchs/nhanes/continuousnhanes/default.aspx?BeginYear=2003 [accessed August 21 2018].

Diliberto JJ, Burgin D, Birnbaum LS. 1997. Role of cyp1a2 in hepatic sequestration of dioxin: Studies using cyp1a2 knock-out mice. Biochem Biophys Res Commun 236:431-433.

Hakk H, Diliberto JJ, Birnbaum LS. 2009. The effect of dose on 2,3,7,8-tcdd tissue distribution, metabolism and elimination in cyp1a2 (-/-) knockout and c57bl/6n parental strains of mice. Toxicol Appl Pharmacol 241:119-126.

Kovalova N, Manzan M, Crawford R, Kaminski N. 2016. Role of aryl hydrocarbon receptor polymorphisms on tcdd-mediated cyp1b1 induction and igm suppression by human b cells. Toxicol Appl Pharmacol 309:15-23.

Min HK, Kapoor A, Fuchs M, Mirshahi F, Zhou H, Maher J, et al. 2012. Increased hepatic synthesis and dysregulation of cholesterol metabolism is associated with the severity of nonalcoholic fatty liver disease. Cell Metab 15:665-674.

Nault R, Fader KA, Ammendolia DA, Dornbos P, Potter D, Sharratt B, et al. 2016. Dose-dependent metabolic reprogramming and differential gene expression in tcdd-elicited hepatic fibrosis. Toxicol Sci 154:253-266.

Nault R, Fader KA, Lydic TA, Zacharewski TR. 2017. Lipidomic evaluation of aryl hydrocarbon receptor-mediated hepatic steatosis in male and female mice elicited by 2,3,7,8-tetrachlorodibenzo-p-dioxin. Chem Res Toxicol 30:1060-1075.

NRC. 2009. Science and decisions: Advancing risk assessment. In: Science and decisions: Advancing risk assessment. Washington DC:2009 by the National Academy of Sciences.

Pierre S, Chevallier A, Teixeira-Clerc F, Ambolet-Camoit A, Bui LC, Bats AS, et al. 2014. Aryl hydrocarbon receptor-dependent induction of liver fibrosis by dioxin. Toxicol Sci 137:114-124.

Schroder WA, Le TT, Major L, Street S, Gardner J, Lambley E, et al. 2010. A physiological function of inflammation-associated serpinb2 is regulation of adaptive immunity. J Immunol 184:2663-2670.

Schroder WA, Major L, Suhrbier A. 2011. The role of serpinb2 in immunity. Crit Rev Immunol 31:15-30.

Tanos R, Patel RD, Murray IA, Smith PB, Patterson AD, Perdew GH. 2012. Aryl hydrocarbon receptor regulates the cholesterol biosynthetic pathway in a dioxin response element-independent manner. Hepatology 55:1994-2004.

Yang L, Roh YS, Song J, Zhang B, Liu C, Loomba R, et al. 2014. Transforming growth factor beta signaling in hepatocytes participates in steatohepatitis through regulation of cell death and lipid metabolism in mice. Hepatology 59:483-495.

Chapter 7: Materials and Methods

7.1. Human Leukocyte Packs

Human leukocytes packs from 51 unique, anonymous non-smoking human donors were acquired from the Gulf Coast Regional Blood Center (Houston, TX). Blood was screened for human immunodeficiency virus and hepatitis prior to shipment. Sex and age were not controlled. Given the anonymity of blood donation, institutional review board (IRB) approval was not necessary.

7.2. Single Cell Splenocyte Suspension

Twelve inbred mouse strains were assessed: 1) C57BL/6J (n=6), 2) 129S1/SvlmJ (n=3), 3) NOD/ShiLtJ (n=6), 4) A/J (n=6), 5) NZO/HILTJ (n=5), 6) C3HeB/FeJ (n=5), 7) CBA/J (n=3), 8) DBA/1J (n=5), 9) FVB/NJ (n=5), 10) BALB/CJ (n=6), 11) CC019 (n=4), and 12) CC041 (n=5). Ages ranged between 2 and 5 months at the time when spleens were processed. Technical replicates contain pools of splenocytes from male and female mice in all cases with the exception of C3HeB/FeJ and CBA/J which only contained male mice. A replicate was considered a biological replicate (i.e. n=1) following isolation of B cells from the splenocyte pools. Table 7.1 outlines the total number of male and female mice used for each strain. In all cases, mice were anesthetized with 2,2,2-tribromoethanol (225 mg/kg of bodyweight) and euthanized via CO_2 asphyxiation at Texas A&M. Spleens were sent to Michigan State University overnight on wet ice for B cell isolation. Spleens were mashed in a culture dish to create a single cell suspension. The single cell suspension was washed with 10 mL of Hank's Balanced Salt Solution (HBSS) and resuspended in 1 mL of HBSS per mouse spleen included in the pool. The number of cells were quantified with an automated cell counter (Beckman Coulter Inc., Brea, CA) following treatment with 2 drops of Zapaglobin to lyse red blood cells (Beckman Coulter Inc).

Table 7.1. Sample sizes of males and females from each mouse strain used in B cell pools.

Strain	Number of Females	Number of Males
A/J	8	24
BALB/cJ	5	5
C3HeB/FeJ	0	18
C57BL/6J	16	14
CBA/J	0	10
CC019	10	9
CC041	9	7
DBA/1J	5	10
FVB/NJ	5	5
NOD/ShiLtJ	4	22
NZO/HILTJ	4	15

7.3. B Cell Isolation

7.3.1. Human B Cell Study

Human naïve B cells were isolated from the peripheral blood mononuclear cells (PBMCs) acquired via density gradient centrifugation of the blood in the presence of Ficoll-Paque Plus (GE Healthcare, Piscatawy, NJ). The PBMCs were subjected to negative selection of naïve B cells using magnetic-activated cell sorting (MACS) Naïve human B cell II isolation kits per the manufacturer's instructions (MiltenyiBiotec, Auburn, CA). Naïve B cell purity was measured via flow cytometry following staining for CD19+ cells; B cell purity averaged ~90%. Following isolation, B cells were cultured in RPMI 1640 supplemented with 10% human AB Serum (Atlantic Biologicals, Atlanta, GA), 100 U/ml of penicillin, 100 µg/ml of streptomycin, and 50 µM of 2-mercaptoethanol.

7.3.2. Mouse B Cell Study

B cells were subject to negative selection using the magnetic-activated cell sorting (MACS) mouse B cell II isolation kits per the manufacturer's instructions (MiltenyiBiotec, Auburn, CA). B cell purity for all samples included in this study (i.e. percentage of $CD19^+$ cells) averaged 98.08% ± standard deviation of 2.25. Following isolation, B cells were cultured at $1x10^6$ cells/mL in RPMI 1640, supplemented with 10% HyClone Cosmic Calf Serum (CCS; GE Healthcare, Piscatawy, NJ), 100 U/ml of penicillin, 100 µg/ml of streptomycin, and 50 µM of 2-mercaptoethanol.

7.4. TCDD Exposure for Primary B Cells

TCDD (99.1% pure) was purchased from AccuStandard, Incorporated (New Have, CT). Isolated naïve B cells (10^6 cells/mL) were then left untreated (control), exposed to DMSO (0.04%, vehicle control), or TCDD (0.0001, 0.001, 0.01, 0.1, 0.3, 1, 3, 10, and 30 nM). This dose-response provides environmentally relevance as the concentration range overlaps serum lipid-adjusted

TEQ values for TCDD and dioxin-like compounds that were reported across the human population (Nault et al. 2016a).

7.5. CD40 Ligand Activation

Naïve human primary B cells and mouse primary B cells were activated via co-culture in the presence of a mouse fibroblast cell line that expresses membrane-bound human CD154/CD40-ligand (CD40L-L). CD40L-L cells were maintained in Dulbecco's Modified Eagle Medium (DMEM) as previously described (Lu et al. 2009). In all cases, culture conditions were maintained at 37°C and 5% CO_2.

7.5.1. Human B Cell Study

For the human B cells, CD40L cells were irradiated and seeded on 48 well dishes at 10^4 cells/mL for the human study for a minimum of 24 hours. Immediately following TCDD treatment, the naïve human B cell culture was supplemented with recombinant human interleukin-2 (IL-2, 0.2 U/mL; Roche Applied Sciences, Indianapolis, IN), interleukin-6 (1 U/mL; Roche Applied Sciences, Indianapolis, IN), interleukin-10 (0.2 ng/mL; Bender Medsystems, Burlingame, CA), and co-cultured for 4 days with irradiated CD40L-expressing cells and an additional 3 days without CD40L-expressing cells (*i.e.* 7 days).

7.5.2. Mouse B Cell Study

For the mouse study, CD40L cells were plated on 96-well plates at a concentration of $5x10^4$ cells/mL for a minimum of 24 hours. Primary mouse B cells were supplemented with recombinant interleukin 2 (5 ng/mL, Cell Signaling Technologies, Danver, MA), interleukin 6 (0.0375 ng/mL, Biolegend, San Diego, CA), and interleukin 10 (2 ng/mL, Cell Signaling Technologies). Mouse B cells were co-cultured with the CD40L cells for 3 days and then an additional 3 days (*i.e.* 6 days) in the absence of the CD40L cells.

7.6. Enzyme-Linked ImmunoSpot (ELISPOT) Assay

The number of IgM secreting cells were assessed with an ELISPOT as previously described (Lu *et al.,* 2009). Briefly, 96-well multiscreen filter plates (Millipore, Billerica, MA) were coated with anti-human IgM antibody (5 µg/mL; Sigma Aldrich, St. Louis, MO) or anti-mouse IgM antibody (5 µg/mL; Sigma Aldrich, St. Louis, MO) overnight at 4°C. The plates were washed 3X with phosphate-buffered saline with 0.1% Tween-20 (0.1% PBST; Sigma), 3X with nanopure H_2O, and blocked with 5% bovine serum albumin (Sigma). Plates were then washed 3X with PBST and 3X with nanopure H_2O. The treated B cells were washed 2X in RPMI 1640 and resuspended in RPMI 1640 supplemented with 10% CCS (GE Healthcare) and incubated over the primary antibody overnight at 37°C and 5% CO_2. The culture plates were then washed 6X with 0.1% PBST, 3X with nanopure H_2O, and coated with biotin-conjugated antihuman IgM antibody (Sigma) or anti-mouse IgM antibody (Sigma) for a 1-hour incubation at 37°C and 5% CO_2. The culture plates were then washed 3x with 0.1% PBST, 3X with nanopure H_2O, and coated with ultrasensitive streptavidin-conjugated horseradish peroxidase (Sigma) for 1 hour at 37°C and 5% CO_2. The culture plates were washed 3X with 0.1% PBST, 3X with nanopure H_2O, and spots were developed with an aminoethylcarbazole staining kit (Sigma) per the manufacturer's instructions. Spots were enumerated with Immunospot Software (Cellular Technology, Ltd, Shaker Heights, OH). Each biological replicate (i.e. n of 1) consisted of 4 experimental replicates at each dose of TCDD and, in all cases, the datasets analyzed are complete and balanced at each concentration of TCDD tested. The number of spots were normalized to the total number of cells plated in each well of the ELISPOT plate which was quantified with an automated cell counter (Beckman Coulter Inc.).

7.7. Enzyme-Linked Immunosorbant Assay (ELISA)

The amount of IgM secreted into the culture media was analyzed via a sandwich ELISA. Briefly, Immulon 4 HBX 96-well microtiter plates (VWR International, Radnor, PA) were coated with anti-human IgM antibody (1 µg/mL; Sigma Aldrich, St. Louis, MO) overnight. Culture media was incubated over primary antibody coated plates (1 hour, 37°C) and was followed by exposure to an anti-human IgM-horseradish peroxidase conjugate (Sigma, 1 hour, 37°C). Incubations were followed with 3 washes with phosphate-buffered saline (pH 7.4) containing 0.05% Tween-20 (Sigma) and one wash with nanopure H_2O. 2,2'-azino-bis(3-ethylbenzothiazoline-6-sulphonic acid) (ABTS, Roche Diagnostics, Indianapolis, IN) was then added as a colorimetric substrate for the HRP. The rate of colorimetric change was quantified with a Synergy HT microplate reader (BioTek, Winooski, VT) at 405 nM for 1 hour. Concentration of IgM in media was calculated based on a standard curve created in each plate.

7.8. Statistical Modeling in the Human B Cell Study

7.8.1 Individual Human DRRs

All dose-response endpoints from the 51 donors were fit to statistical models at the individual (i.e. 1 biological replicate) level. A series of models were fit using the BMD Software (U.S. Environmental Protection Agency or EPA) including the Hill, Exponential 1, Exponential 2, Exponential 3, Exponential 4, Exponential 5, polynomial 2°, power, and a linear model (Table 7.2). Model fit and statistical assumptions were assessed to ensure adherence to recommendations outlined by the EPA (Davis et al. 2011). All data was log-transformed to achieve a normal distribution and equal variance across dose groups prior to statistical analyses. All best fit model coefficients acquired from the BMD software were validated with maximum-likelihood estimation using code developed in-lab with the version 1.0.17 of the bbmle package in R (Bolker 2010; R Core Team 2015).

Table 7.2. Models available in the BMD software. Table indicates the model type, model equation, and coefficients associated with each model.

Model Type	Parameters	Equation
Exponential 2	Dose (x) Intercept (a) Direction of Change ($sign$) Slope (b)	$\boldsymbol{f(x) = a * (e^{(sign*(b*x))})}$
Exponential 3	Dose (x) Intercept (a) Direction of Change ($sign$) Slope (b) Power (d)	$\boldsymbol{f(x) = a * (e^{(sign*(b*x))^d})}$
Exponential 4	Dose (x) Intercept (a) Direction of Change ($sign$) Slope (b) Power (d)	$\boldsymbol{f(x) = a * (c - (c-1)(e^{(sign*(b*x))})}$
Exponential 5	Dose (x) Intercept (a) Direction of Change ($sign$) Slope (b) Asymptote (c) Power (d)	$\boldsymbol{f(x) = a * (c - (c-1)(e^{(sign*(b*x))^d})}$
Hill	Dose (x) Intercept (y) Slope (v) ED50 (k) Power (n)	$\boldsymbol{f(x) = y + \frac{v * x^n}{k^n + x^n}}$
Linear	Dose (x) Intercept (β_0) Slope (β_1)	$\boldsymbol{f(x) = \beta_0 + (\beta_1 * x)}$
Polynomial 2	Dose (x) Intercept (β_0) Slope (β_1)	$\boldsymbol{f(x) = \beta_0 + (\beta_1 * x) + (\beta_2 * x)^2 + (\beta_n * x)^n}$
Power	Dose (x) Intercept (β_0) Slope (β_1) Power (n)	$\boldsymbol{f(x) = \beta_0 + (\beta_1 * x^n)}$

7.8.2. Statistical Modeling of the Low-dose Region of the Human Dose-response

The mean values for each dose group of each individual were combined (*i.e.* 51 biological replicates) and used for assessing the shape of the low-dose region of a DRR. First, the half-maximal inhibitory concentrations (IC_{50}) for the all DRRs was determined with maximum-likelihood estimations of the coefficients in a 4-parameter logistic model using code developed in-lab using bbmle package in R (Bolker 2010; R Core Team 2015). IC_{50} values were confirmed with hill model coefficients that were acquired with the BMD software. Low-dose region of the dose-response were defined as those below the established IC_{50} values. The BMD software was then used to identify the best fitting model for the low-dose region of the DRRs. In all instances, statistical assumptions and model fit were assessed via the previously mentioned recommendations of the EPA (Davis et al. 2011). All coefficients acquired from the BMD software were validated with maximum-likelihood estimation using the bbmle package in R (Bolker 2010; R Core Team 2015)

7.9. Phylogenetic Analysis

Genomes which were freely-available were downloaded from the Collaborative Cross website (http://csbio.unc.edu/). For the BXD strains, C3HeB/FeJ strain, and DBA/1J strain, sequenced or imputed genomes have not been reported. As the BXD panel is a cross between C57BL/6J and DBA/1J, genetic sequences were inferred for the BXD mice based on single nucleotide polymorphism (SNP) data reported on the University of Tennessee's GeneNetwork website (http://www.genenetwork.org/genotypes/BXD.geno). A region of Chromosome 1 of BXD100 near the location of *Etnk2*, *Kiss1*, and *Adipor1* was found to be hetereozygous and, thus, the strain was removed prior to the phylogenetic analysis of these genes. For DBA/1J and C3HeB/FeJ, SNP and INDEL data was used to compare the genetic regions of interest with closely-related strains that have been sequenced (i.e. DBA/2J and C3H/HeJ) using the Sanger SNP querying tool (Keane et al. 2011; Yalcin et al. 2011). In all cases, no differing SNPs or indels between DBA/1J vs. DBA/2J or C3Heb/FeJ vs. C3H/HeJ and, thus, the sequenced genome of the closely-related

strains was used for genetic analysis. Gene sequences were extracted from genomes by flanking the coordinates based on the reference mouse genome (C57BL/6J mm10) using a custom python script (https://github.com/PeterDornbos/Extracting_Gene_Sequences). The extracted sequences were then processed manually to remove the flanking sequences around the gene of interest. The extracted gene sequence was then aligned to the cDNA sequence of the gene of interest using EMBOSS Stretcher. The alignment output was used to extract the exons of the gene and remove intronic regions (i.e. predict the cDNA sequence for each individual strain). The predicted cDNA sequence was translated into the protein sequence using EMBOSS Transeq software. The predicted protein sequences were manually trimmed to remove untranslated amino acids. Predicted protein sequences from all strains were aligned via Multiple Alignment using Fast Fourier Transform (MAFFT) software (Katoh et al. 2005). Phylogenetic trees were built based on MAFFT outputs using FigTree v1.4.2. In all cases, custom python scripts were written in-lab using Python version 2.7.10. Statistical differences between allelic category phenotypes were assess with an ANOVA with a Tukey's posthoc.

7.10. Heritability Analysis

As the R^2 of a linear regression model reflects the proportion of experimental variance in the dependent variable that is attributed to the variability within the independent variable replicates, the heritability (h^2) estimate of 1) percent inhibition of the IgM response of primary mouse B cells induced at 30 nM of TCDD and 2) hepatic accumulation of TCDD at the high-dose (100 ng/kg/day).

7.10.1. Mouse B Cell Regression Model

The multiple R^2 of the following regression model was used to estimated the heritability (h^2) of percent inhibition in the IgM response of the mouse B cell at 30 nM TCDD:

$$\text{Percent inhibition at the high dose of TCDD} = \beta_0 + \beta_1*x_1 + \beta_2*x_2 + \beta_3*x_3 + \beta_4*x_4 + \beta_5*x_5 + \beta_6*x_6 + \beta_7*x_7 + \beta_8*x_8 + \beta_9*x_9 + \beta_{10}*x_{10} + \beta_{11}*x_{11} + \varepsilon_i$$

In this regression model, β_0 is the intercept while the remaining coefficients reflect the response seen within each strain set as categorical variables. The regression coefficient estimates are relative to the 129S1/SvlmJ (i.e. the least responsive strain to TCDD): β_1 = A/J, β_2 = BALB/CJ, β_3 = C3HeB/FeJ, β_4 = C57BL/6J, β_5 = CBA/J, β_6 = CC019, β_7 = CC041, β_8 = DBA/1J, β_9 = FVB/NJ, β_{10} = NOD/ShiLtJ, and β_{11} = NZO/HILTJ. The 95% confidence intervals associated with multiple R^2 of the regression model were calculated via bootstrapping with 1,000 replications using bias corrected and accelerated method in the boot library in R (Canty and Ripley 2017).

7.10.2. Hepatic Accumulation of TCDD Regression Model

The multiple R^2 of the following regression model was used to estimated the heritability (h^2) associated with TCDD accumulation at the high dose of TCDD (100 ng/kg/day):

$$\text{TCDD Accumulation (ng/kg)} = \beta_0 + \beta_1*x_1 + \beta_2*x_2 + \beta_3*x_3 + \beta_4*x_4 + \beta_5*x_5 + \beta_6*x_6 + \beta_7*x_7 + \beta_8*x_8 + \beta_9*x_9 + \beta_{10}*x_{10} + \beta_{11}*x_{11} + \beta_{12}*x_{12} + \beta_{13}*x_{13}\ \varepsilon_i$$

In the model, the coefficient estimates are relative to the NOD/ShiLtJ (i.e. the strain with the lowest level of TCDD): β_1 = 129S1/SvlmJ, β_2 = A/J, β_3 = BALB/CJ, β_4 = BXD100, β_5 = BXD40, β_6 = BXD91, β_7 = C3HeB/FeJ, β_8 = C57BL/6J, β_9 = CBA/J, β_{10} = CC019, β_{11} = DBA/1J, β_{12} = FVB/NJ, and β_{13} = NZO/HILTJ. β_0 represent the model intercept. The 95% confidence intervals of the multiple R^2 from the regression model were calculated with bias corrected and accelerated method via the boot library in R (Canty and Ripley 2017).

7.11. Quantitative Trait Locus Analysis (QTL)

QTL analysis was performed using Gene Network's online-based WebQTL program (http://www.genenetwork.org/webqtl/main.py)(Wang et al. 2003). Scans for QTLs were performed using several differing endpoints:

A) percent inhibition in the number of cells secreting IgM (i.e. ELISPOT data) at the high dose (30 nM) of TCDD (mouse B cells study).

B) mean level of TCDD accumulation in the liver (Toxicodynamics of TCDD accumulation study)

C) mean fold change in hepatic gene expression of AHR-responsive genes (Toxicodynamics of TCDD accumulation study)

D) mean change in total body weight (HMGCR functional study)

The mapping was performed using the data from the 10 strains that are members of the Mouse Diversity Panel: 1) C57BL/6J, 2) 129S1/SvlmJ, 3) NOD/ShiLtJ, 4) A/J, 5) NZO/HILTJ, 6) C3HeB/FeJ, 7) CBA/J, 8) DBA/1J, 9) FVB/nJ, 10) BALB/cJ. The whole-genome interval mapping was performed using the default settings of 2000 bootstrap tests. The threshold of significance was determined via permutation test (n=10,000). In all cases, log of the odds (LOD) ratio is reported which was calculated as outlined in the WebQTL glossary of terms (i.e. LRS/4.61).

7.12. RNA Isolation

7.12.1. Mouse B Cells

Total RNA was extracted from B cells isolated from male C57BL/6J (n=3) and DBA/1J (n=3) mice that were treated with DMSO (0.01%) or TCDD (30 nm) for 0.33, 1, 2, 3, 4, 5, or 6 days. Isolated B cells were diluted to $1X10^6$ cells/mL, supplemented with cytokines, and activated using CD40L cell co-culture scheme as previously outlined with the exception that 6 well dishes were used in this exposure (i.e. larger volumes of cells at the same density). RNA was extracted with Qiagen

RNeasy Mini Kits per the manufacturer's instructions. RNA quality (i.e. A260/A280 ratio) and quantity was assessed with a NanoDrop 1000 spectrophotometer.

7.12.1. Mouse Liver

Frozen liver (~50 mg) was homogenized in 1 mL of TriZOL with chrome-steel beads using a Mixer Mill 300 (Life Sciences, Carlsbad, CA) for 4 minutes. Following, total RNA was extracted per the manufacturer's instructions with an additional 5:1 phenol:chloroform extraction step (Sigma Aldrich, St. Louis, MO). The quantity and quality (260/280 ratio) of RNA was analyzed with a NanoDrop 1000 spectrophotometer prior to cDNA conversion. The quantity of total RNA was assessed using the Quant-iT RNA Assay Kit prior to gene expression analysis with the Nanostring nCounter.

7.13. Quantitative Real-Time Polymerase Chain Reation (QRTPCR)

In all cases, Oligo dT primers and reverse transcriptase superscript III were used for the cDNA conversion. QRTPCR was performed using a DNA Engine Opticon 2 (Bio-Rad, Hercules CA). Expression was normalized to housekeeping genes and, following, a vehicle control group. Fold changes were calculated using the $2^{-\Delta\Delta CT}$ method.

7.13.1. Mouse B Cells

500 ng of total RNA was used for the cDNA conversion. SYBR green Mastermix (Life Technologies) was used for all QRTPCR in the mouse B cell study. Primer sequences are located in Table 7.3. Expression was normalized to *Hprt.*

7.13.2. Mouse Liver

For hepatic gene expression analysis, 2 µg of total RNA was used for cDNA conversion. TaqMan Mastermix (Thermo Fisher) and FAM-based probe for *Cyp1a1*

Table 7.3. Primer Sequences used for SYBR green-based QRTPCR.

Gene ID	Official Gene ID	Forward Sequence (5' to 3')	Reverse Sequence (5' to 3')
Actb	11461	TGTTACCAACTGGGACGACA	GGGGTGTTGAAGGTCTCAAA
Apoa1	11806	GTGGCTCTGGTCTTCCTGAC	ACGGTTGAACCCAGAGTGTC
Ccl2	20296	CAGGTCCCTGTCATGCTTCT	TCTGGACCCATTCCTTCTTG
Cyp1a1	13076	AAGTGCAGATGCGGTCTTCT	AAAGTAGGAGGCAGGCACAA
Cyp1a2	13077	CACTAACGGCAAGAGCATGA	AGCTTGCTGACGAGATGGTT
Cyp1b1	13078	TGCTTTTGTTTCTGCCACAG	GGGGCATGAATTCTTGTGAT
Cyp4a10	13117	ACCACAATGTGCATCAAGGA	CTGAGAAGGGCAGGAATGAG
Cyp4a14	13119	ACCTGTCACCTTCCCAGATG	AGCAAACTGTTTCCCAATGC
Gusb	110006	GAGGATCAACAGTGCCCATT	AGGTAAGGCCACCAGAGGTT
Gys2	232493	GGGACACTGTGCATTGTTTG	CCGATTCGTCTAATGGTGCT
Hprt	15452	GCTTACCTCACTGCTTTCCG	ATCGCTAATCACGACGCTGG
Il1b	111343	GTACAAGGAGAACCAAGCAACG	TGGGATCCACACTCTCCAGC
Il6	16193	TCCTCTCTGCAAGAGACTTCCATCC	ACAGGTCTGTTGGGAGTGGTATCC
Lcat	16816	GCTCCTCAATGTGCTCTTCC	AATCCAGCCAGATGGTGAAG
Ldlr	16835	TCCTGGAGATGTGATGGACA	GAGCCATCTAGGCAATCTCG
Ppara	19013	GAGGGTTGAGCTCAGTCAGG	GGTCACCTACGAGTGGCATT
Pygl	110095	ACCAAATCGACAATGGCTTC	CCATTGTGTTCCAGGCTTTT
Scarb1	20778	CAGGCTGTGGGAACTCTAGC	GAAAAAGCGCCAGATACAGC
Serpinb2	20778	CTGCTACCCGAAGGTTCTG	GGAAGCAACAGGAGCATGC
Tgfb1	21803	TGCGCTTGCAGAGATTAAAA	CTGCCGTACAACTCCAGTGA
Tgfb3	21809	CTGGGAGTCCTGAAGCTCAC	TGGTGCAAGTGGACAGAGAG
Tgfbr2	21813	CCAGAACCCACGACAAAAGT	GTTCCCAGAACAGGGTGAAA
Tnf	21926	CCACGTCGTAGCAAACCACC	ACAAGGTACAACCCATCGGC

(Mm00487218_m1; Thermo Fisher) and VIC-based probe for eukaryotic *Rn18s* (Thermo Fisher) were used to verify Nanostring Plexset-based expression levels. SYBR green Mastermix (Life Technologies) was used for all other SYBR-based gene expression analysis. Primer sequences used in the SYBR green analysis can be found in Table 7.3. Expression was normalized to an intra-well *Rn18s* for the TaqMan-based analysis or the geometric mean of *Hprt*, *Actb*, and *Gusb* for the SYBR green-based analysis.

7.14. Intracellular Protein Expression Analysis

For flow cytometry analysis, B cells, isolated from C57BL/6J (n=4) and DBA/1J (n=4) mice and were activated with cytokines and CD40L cells as previously outlined with the exception that 12 well dishes were used for this exposure. Activation was performed in the presence of DMSO (0.01%) or TCDD (30 nm) for 0, 2, 3, 4, and 5 days. Following exposure, cells were washed with HBSS and treated with Fc Block (BD Pharminogen, San Diego, CA) and unlabeled anti-mouse IgM (BD Pharminogen) for 15 minutes at 4°C to ensure surface receptors were blocked. Following 3 washes with FACS buffer, cells were fixed with Cytofix (BD Pharminogen) for 20 minutes at room temperature. Cells were washed 2X with FACS buffer and then treated with Perm/Wash (BD Pharminogen) for 10 minutes. Intracellular SERPINB2 and IgM were stained simultaneously with anti-mouse SERPINB2 conjugated to biotin (LS Bioscience, Seattle, WA) and anti-mouse IgM conjugated to FITC (BD Pharminogen), respectively for 20 minutes at 4°C. Cells were then washed 4X with 3mL of Perm/Wash and treated with streptavidin-conjugated Alexa Fluor 647 (AF647) for 20 minutes at 4°C. Cells were then washed 4X with 3 mL of Perm/Wash and resuspended in FACS buffer and analyzed with a BD FACSCanto II. Data was analyzed with FlowJo Software version 10.2 (Treestar Software, Ashland, OR). Gates were created to isolate singlets and B cells (Figure 7.1). In all cases, a 1:1 mixture of vehicle and TCDD treated cells that were stained with an isotype control including streptavidin-conjugated AF647 to determine AF647

Figure 7.1. Overview of B cell gates. Figure indicates a visual representation of how B cells were gated in flow cytometry data analysis. Gates were drawn for singlets and, following for B cells within the singlet gate.

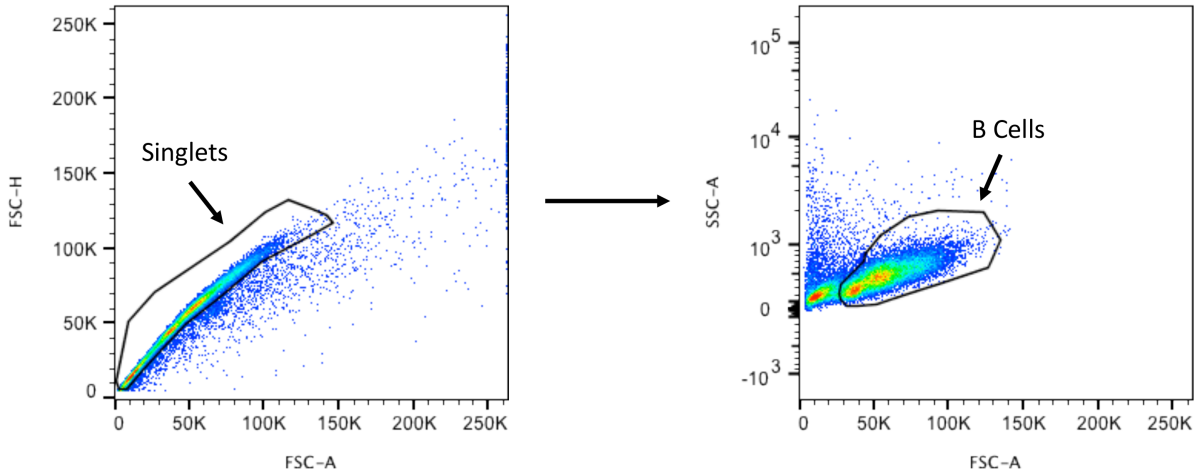

and FITC background levels. Potential statistical differences for each time-point were assessed with an ANOVA and a Tukey's posthoc.

7.15. *Serpinb2*$^{-/-}$ and *Serpine1*$^{-/-}$ Mouse Studies

The *Serpinb2*-null (*Serpinb2*$^{-/-}$) mice and wildtype controls were graciously provided by the lab of Dr. Toni Antalis (University of Maryland School of Medicine, Baltimore, MA). The mice were originally developed by the lab of Dr. David Ginsburg (University of Michigan Medical School, Ann Arbor, MI) and have been further backcrossed onto C57BL/6 background for a total of 13 generations (Dougherty et al. 1999; Siefert et al. 2014). The *Serpine1*-null (*Serpine1*$^{-/-}$) mice were graciously provided by the lab of Dr. Jim Luyendyk (Michigan State University, East Lansing, MI). The mice were originally donated to Jackson Labs (JAX stock #002507) by Dr. Peter Carmeliet (University of Leuvin, Leuvin, Belgium)(Carmeliet et al. 1993). The mice were backcrossed onto C57BL/6J background until congenic. All mice included in knockout studies were male ranging from 14 and 17 weeks of age. All mice were anesthetized with isoflurane and euthanized via cervical dislocation. Statistical differences were calculated with an ANOVA and Tukey's posthoc.

7.16. Mouse Panel and TCDD Exposure

All animal handling was in accordance with Texas A&M University's Institutional Animal Care and Use Committee (IACUC). Fourteen mouse strains were used: 1) C57BL/6J, 2) A/J, 3) BALB/cJ, 4) FVB/nJ, 5) C3HeB/FeJ, 6) CBA/J, 7) DBA/1J, 8) NOD/ShilTJ, 9) NZO/HilTj, 10) 129S1/SvlmJ, 11) BXD40, 12) BXD91, 13) BXD100, 14) CC019/TauUNC. Animals were obtained from Jackson Laboratory (Bar Harbor, Maine) and mated in plastic cages at 6-8 weeks of age. Females were checked daily for vaginal plugs. If plug was present, mice were separated, weighed, and randomly placed into a TCDD dose group: vehicle control, 1, or 100 ng/kg/day. TCDD was administered to mice using peanut butter as the vehicle. Administration of daily gavage was found to result in spontaneous abortion of embryos, regardless of TCDD. Mice were treated with vehicle or TCDD

daily for 10 days. On day 11, mice were anesthetized with avertin, euthanized via cervical dislocation, and tissues were snap frozen in liquid nitrogen. Pregnancy success was assessed by the presence of absorption sites or embryos within the uterus under a dissection microscope; only pregnant mice were included in downstream analysis. Standard mouse chow and water was provided *ad libitum* during mating and throughout the TCDD treatment. Mice were exposed to constant 12-hour light/dark cycles, temperature, and humidity during mating and TCDD treatment.

7.17. TCDD Burden Analysis

TCDD accumulation was measured in liver tissue via gas chromatography-mass spectrometry (GC/MS). TCDD was measured in the livers of all 14 strains of the mouse panel that were treated with 1 ng/kg/day (n=3) or 100 n/gkg/day (n=3) of TCDD. A subset of strains (n=9) were randomly chosen to assess the level of TCDD in the vehicle control groups. Sample extraction and purification procedure were developed in-house based on U.S. Environmental Protection Agency method 8290. Briefly, 50 ml of 5% benzene in a hexane solution, 10 ng of ^{13}C-TCDD (Wellington, Lot# MD0480912), and 30 ml of concentrated HCl (trace metal grade) were added to each sample in sequence. Lab control spike (LCS) sample, which contains 10 ng of native TCDD (Wellington, Lot #90STN1013) and 0.5 g of corn oil, and method blank (MB) sample (0.5 g of corn oil) were analyzed along with each set of samples. All samples were shaken for 1 hour on a shaking bed, vented to release pressure, and then shaken overnight. After shaking, the organic layer was transferred to new bottle for subsequent sample purification (column clean-up). Acid/base silica column and alumina column were utilized for sample purification. The samples extracts were then purged to dryness and reconstituted with 20 µl of ^{13}C-1,2,7,8-TCDF (Wellington, Lot# 020701), which was treated as the injection standard to account for the recovery of internal standard (^{13}C-TCDD). All samples were quantified using either gas chromatograph/high efficiency triple-quadrupole system (GC/MS/MS, Agilent 7000 series) or low-resolution single-quadrupole GC/MS (HP 5973/6890), depending on the dosing level of TCDD. Both instruments were equipped with

30 m × 0.25 mm DB-5ms column and data were quantified via isotopic dilution approach using either chemstation (Agilent) or masshunter (Agilent) software. Results of all quality control samples (MB and LCS) have passed method criteria indicating satisfying analytical quality. The average level of TCDD in the vehicle control group was 2.8 ng/kg liver and, in comparing strains, does not appear be genotype-dependent.

7.18. Gene Expression Profiling with NanoString nCounter Technology

Per manufacturer's instructions, an RNA titration was performed prior to running the PlexSet assay. Briefly, RNA was pooled into two treatments: 1) three C57BL/6J mice that were treated with TCDD and 2) three C57BL/6J mice that were treated with the vehicle control. RNA was titrated to assess optimum concentration needed for this customized probe set. 500 ng of total RNA was found to provide detection for all probes in the two treatment pools. The customized probe-set was designed by Nanostring technicians to target nine AHR-target genes and three housekeeping (HK) genes: 1) *Cyp1a1*, 2) *Cyp1a2*, 3) *Cyp1b1*, 4) *Ahrr*, 5) *Gpnmb*, 6) *Pmm1*, 7) *Mt2*, 8) *Slc15a2*, 9) *Serpinb2*, 10) *Hprt* (HK), 11) *Gusb* (HK), and 12) *Eef1g* (HK). A list of the putative DREs (pDREs) with matrix similarity scores ≥ 0.856 (Nault et al. 2016b) and hepatic AHR ChIP-Seq peaks (Fader et al. 2017) from previous reports along with citations of AHR-mediated gene dysregulation can be found for each of the 9 AHR-target genes in Table 7.4. In short, the NanoString PlexSet assay uses a hybridization-based technology were two probes (probe A and probe B) target an RNA sequence of interest. Sequences used for probe A can be found within Table 7.5 and sequence for probe B are found within Table 7.6. The nCounter workstation digitizes an image of the SPRINT cartridge. In all cases, a 555 field of vision was chosen for each cartridge to analyze the number of individual reporter tags detected (i.e. one reporter tag detected is equivalent to one transcript for the respective target RNA). Intra-codeset probe variability was calibrated using a reference sample across the differing codesets using nSolver 3.0 software. The transcript numbers were normalized to the geometric mean of the three housekeeping genes. The

Table 7.4. Presence of pDRES, AHR ChIP peaks, and previous reports that identified AHR-mediated gene dyresgulation of the 9 genes analyzed in this study. DREs and AHR ChIP Peaks are reported if found within gene or within 10 Kb upstream of the transcription start site.

Official Gene Symbol	Putative DREs?	AHR Chip Peaks?	Previous Reports showing TCDD-induced Dysregulation
Ahrr	Yes	Yes	(Brauze et al. 2006; Harrill et al. 2013)
Cyp1a1	Yes	Yes	(Boutros et al. 2008; Hao et al. 2012; Nault et al. 2016a)
Cyp1a2	Yes	Yes	(Boutros et al. 2008; Harrill et al. 2013)
Cyp1b1	Yes	Yes	(Hao et al. 2012; Harrill et al. 2013; Nault et al. 2016a)
Gpnmb	Yes	Yes	(Nault et al. 2016a)
Mt2	Yes	Yes	(Frueh et al. 2001; Nishimura et al. 2001)
Pmm1	Yes	Yes	(Boutros et al. 2008)
SerpinB2	No	No	(Brauze et al. 2017; Hao et al. 2012)
Slc15a2	Yes	No	GEO: GSE87519

Table 7.5. Primer sequences used for probe set A in toxicodynamics and TGFBR2 inhibition study.

Official Gene Symbol	Official Gene ID	Accession	Target Sequence A
Cyp1a1	13076	NM_009992.3	AACAATCGTGATGACCTTATCATCTGACAGCTGGACATTGGCATTCTCGTCCTCAAGACCTAAGCGACAGCGTGACCTTGTTTCA
Cyp1a2	13077	NM_009993.3	TGTGGTGACTGTGTCAAAGCCAGCTCCAAAGATGTCATTGACAATGTTGACATCCTCTTCTTTTCTTGGTGTTGAGAAGATGCTC
Cyp1b1	13078	NM_009994.1	CGCATTGATTCATAAAGAAAAGCCATGACATATGGCAGGTTGGGCTGGTCCACAATTCTGCGGGTTAGCAGGAAGGTTAGGGAAC
Ahrr	11624	NM_009644.3	GTCCAGCAGGCAGCGAACACGACAAATGAAGCAGCGTGTCAAGAAGGCCGCTGTTGAGATTATTGAGCTTCATCATGACCAGAAG
Gpnmb	93695	NM_053110.4	CATCTTTCACCTTCGAGATGGGAATGTATGCCCGGCCGTATCTTCGAAAGCAAAGACGCCTATCTTCCAGTTTGATCGGGAAACT
Pmm1	29858	NM_013872.4	GGATCTTCTCCTTCTTGTCCAGTTCCGAGAACTCGCGAACCTAACTCCTCGCTACATTCCTATTGTTTTC
Mt2	17750	NM_008630.2	CGCGGAGCGCGACCTTTATAGCGGAGAGTATTGGGTCGAGCGCAAAAGCCAATTTGGTTTTACTCCCCTCGATTATGCGGAGT
Slc15a2	57738	NM_001145899.1	GCATTTTTCCTCCCAGTATTGGTATGGCACCCAAAGACTTGAATACATGGCTTTCGGGTTATATCTATCATTTACTTGACACCCT
SerpinB2	18788	NM_001174170.1	TCTGGACAGGTATGCTCTCATGCGAGTTCACACGGAAAGGATAAAGCCCACAACAGCCACTTTTTTTCCAAATTTTGCAAGAGCC
Hprt	15452	NM_013556.2	CTCCGGAAAGCAGTGAGGTAAGCCCAACGCTCTCCCACCGTGTGGACGGCAACTCAGAGATAACGCATAT
GusB	110006	NM_010368.1	GTTCGTCATGAAGTCGGCGAAATTCCAGATGAGCTCTCCGACCACGTATTCCTGGAGTTTATGTATTGCCAACGAGTTTGTCTTT
Eef1g	67160	NM_026007.4	CTCTCAAACACACAGAATCCATCATCACCCTCAAATGCTGGAACCTTGCCCAGATAAGGTTGTTATTGTGGAGGATGTTACTACA

Table 7.6. Primer sequences used for probe set B in toxicodynamics and TGFBR2 inhibition study.

Official Gene Symbol	Official Gene ID	Accession	Target Sequence B
Cyp1a1	13076	NM_009992.3	CGAAAGCCATGACCTCCGATCACTCCACGAGATAGCAGTTGTGACTGTGTCAAACCCAGCTCCAAAGAGGTCCAA
Cyp1a2	13077	NM_009993.3	CGAAAGCCATGACCTCCGATCACTCCACGTTAGGCCATGTCACAAGTAGCAAAATGCTCCAGGTGATGGC
Cyp1b1	13078	NM_009994.1	CGAAAGCCATGACCTCCGATCACTCTGTTGGCGGTGGTGGCGTGTGGAATGGTGACAGGCAAAAAGCTGGAGAAT
Ahrr	11624	NM_009644.3	CGAAAGCCATGACCTCCGATCACTCAGGAATTTTAGTTTTCCTTGGAACTGCATGGTCAGAAAGCCAGAGGTGCT
Gpnmb	93695	NM_053110.4	CGAAAGCCATGACCTCCGATCACTCCTTCTGGGACATGGTCACGAATACAGGGATCTGATCTGTTATCACATACA
Pmm1	29858	NM_013872.4	CGAAAGCCATGACCTCCGATCACTCCCAGCAAACTCTGTCTTCAAGGCTTCCACAAACTTCTCCC
Mt2	17750	NM_008630.2	CGAAAGCCATGACCTCCGATCACTCTCGACGAGAGATCGGTTTGAAGAGTTCTAGGAGCGTGATGGAGAGAAGCA
Slc15a2	57738	NM_001145899.1	CGAAAGCCATGACCTCCGATCACTCTGTTCCCAGAGCTATGAGACTCAGGCCAACCAATGATAAGATTGTATGTA
SerpinB2	18788	NM_001174170.1	CGAAAGCCATGACCTCCGATCACTCCAGGTCCTTTATGTATCCAATGTTCAGCTTTGCATGGAGGAACATCA
Hprt	15452	NM_013556.2	CGAAAGCCATGACCTCCGATCACTCCAAAAAGCGGTCTGAGGAGGAAGCCGGCGGAGGAGGTGCTACCG
GusB	110006	NM_010368.1	CGAAAGCCATGACCTCCGATCACTCTGGCGAGTGAAGATCCCCTTCTTGTTTCCGATTACTCTCAGCGGTGACTG
Eef1g	67160	NM_026007.4	CGAAAGCCATGACCTCCGATCACTCTACTTCCTCGCAGCTCCTCATTGCTTACATAATAGGCAATGGCATTG

transcript levels were normalized to vehicle control group for that respective gene and mouse strain to calculate fold changes. A ≥ 1.5 fold change cutoff was used to define dysregulated gene transcription.

7.19. TGFBR2 Mouse Study

All animal handling was in accordance with Michigan State University's Committee on Animal Use and Care guidelines. Male and female C57BL/6 mice were ordered from Charles River Laboratories (Kingston, NY). Mice were delivered on postnatal day 25 (PND25) and acclimated for 7 days prior to treatment. Mice were housed in Innocages (Innovive, San Diego, CA) containing ALPHA-dri bedding (Shepherd Specialty Papers, Chicago, IL) with constant 12-hour light/dark cycles, temperature, and humidity. Standard mouse chow (Harlan Teklad Rodent Diet 8940) and Aquavive water (Innovive) were provided *ad libitum* throughout the period of acclimatization and treatment. Following acclimation, mice were treated with a daily oral gavage of sesame oil (i.e. vehicle control) or 10 μg/kg of TCDD daily for 10 consecutive days. During the TCDD treatment regime, mice were given an intraperitoneal (IP) injection of phosphate-buffered saline or 15 mg/kg of a TGFBR2-Fc fusion protein (i.e. a TGFBR2 ligand trap) dissolved in phosphate-buffered saline every 3 days based on previous reports (days 1, 4, and 7)(Yung et al. 2016). Mice were sacrificed on day 11. Tissues were either fixed in 10% phosphate-buffered formalin (Thermo Fisher) or snap frozen in liquid nitrogen.

7.20. Histological Analyses

Histological processing and staining was performed by the Michigan State University Investigative HistoPathology Laboratory. Fixed liver was processed and vacuum infiltrated with paraffin using a Tissue-Tek VIP 2000 (Sakura) and embedded with the HistoCentre III Embedding Center (Thermo Fisher). Blocks were sectioned at 4-5 μm with a Rechert Jung 2030 rotary microtome (Reichert, Depew NY). Sections from fixed tissues were dried for 2-24 h at 56°C on slides. Liver

sections were stained with hematoxylin and eosin (H&E) for general morphometric analysis and and with periodic acid–Schiff (PAS) to detect glycogen. Frozen tissues were sectioned at 6 μm and stained for presence of neutral lipids with oil red O (ORO) as previously described (Kopec et al. 2010). Slides were digitized at 20x magnification using an Olympus Virtual Slide System VS110 (Olympus, Center Valley, PA). Virtual slides were sampled (100% coverage) using the Visiomorph Microimager (Visiopharm, Denmark). ORO staining was quantified (i.e percent area of tissue positive for ORO) using the Quantitative Histological Analysis Tool (QuHAnT) as previously described (Nault et al. 2015). Using ImageJ (https://imagej.nih.gov/ij/), optimal hue, saturation, and value (HSV) image segmentation thresholds for feature (ORO) extraction were determined to be 0 to 50 and 225 to 255 (hue), 30 to 255 (saturation), and 0 to 255 (value), while optimal total tissue feature extraction thresholds were 0 to 255 (hue), 20 to 255 (saturation), and 0 to 255 (value).

7.21. General Statistical Analyses

With the exception of the NHANES analysis, all statistical analyses were performed using version 3.0.2 in R (R Core Team 2015). Histograms and q-q plots were used to assess distributions prior to all statistical analyses. In all cases, a p-value ≤ 0.05 was considered statistically significant.

7.21.1. Dose-Response Analysis

Analysis of Variance (ANOVA) with Dunnett's two-tailed post hoc was used to assess the potential differences between dose groups and the vehicle controls. All dose-response data was log-transformed to achieve a normal distribution prior to statistical analyses for the human and mouse B cell study.

7.21.2. T test and Analysis of Variance (ANOVA)

Outliers within dose-groups were assessed with a Grubbs' test; significant outliers (i.e. $p<0.05$) were removed prior to downstream analysis. Potential significant differences across dose groups and strains were calculated with a t-test or ANOVA where appropriate.

7.21.3. Pearson Correlation Analysis

Potential associations between gene expression (housekeeper-normalized transcript numbers) and TCDD burden were assessed via Pearson correlation analysis. Pearson's correlation coefficient (r) and p-values are reported in Figure 4.5 for all genes of which expression was assessed.

7.22. National Health and Nutrition Examination Survey (NHANES) Study Design

Human survey and laboratory data were acquired from the 2003-2004 nationally-representative and cross-sectional U.S. National Health and Nutrition Examination Survey (NHANES)(Center for Disease Control 2005a). The NHANES laboratory examination data were used to assess the body mass index (BMI; weight in kg / height in m^2) and serum levels of lipid-adjusted TCDD (pg/g), total cholesterol (TC; mg/dL), high-density lipoprotein (HDL; mg/dL), and low-density lipoprotein (LDL; mg/dL). In all cases, the CDC outlines detailed methodology of these analyses. Briefly, serum TCDD was measured with high resolution gas chromatography-high resolution mass spectrometry (Center for Disease Control 2008). Total serum cholesterol and high-density lipoprotein (HDL) levels were measured using an enzymatic assay and direct immunoassay, respectively, at Johns Hopkins University Lipoprotein Analytical Laboratory (Center for Disease Control 2006b). Low-density lipoprotein levels (LDL) were inferred via the Friedewald calculation [LDL = Total Cholesterol – (triglyceride level / 5)]; triglyceride levels were measured enzymatically at Johns Hopkins University Lipoprotein Analytical Laboratory (Center for Disease Control 2006a). Survey data were used to acquire demographic data including sex, race, and age for each sample

included in the analyses (Center for Disease Control 2005b). Statin usage was determined based on self-reporting of study participants (Center for Disease Control 2016); all statin users (included statin combination medicines) were identified based on reported generic drug codes (Table 7.7.) and removed prior to analysis. Ethnicity/race was divided into four categories: 1) Caucasian, 2) African American, 3) Mexican American, or 4) Other Race. Only adults ≥ 20 years of age were included in the dataset. Samples with missing data were removed prior to analysis to create a complete and balanced dataset for each variables of interest. Three independent datasets were created to test for an association of lipid-adjusted TCDD with 1) LDL (n=520), 2) HDL (n=1,094), and 3) TC (n=1,094). Detection limits (DLs) for serum TCDD were variable across the analysis. For samples that were below DL, the CDC-reported imputed serum lipid-adjusted TCDD value was used (DL/$\sqrt{2}$)(Center for Disease Control 2008). Prior to all statistical analyses, histograms and normal q-q plots were used to assess distributions of the continuous variables. Lipid-adjusted TCDD levels were log transformed ($\log_{10}$) prior to downstream statistical analyses to adjust for a extreme right-skew. In all cases, data was merged, transformed, and analyzed using SAS version 9.4 (SAS Institute Inc., Cary, NC). As recommended by the documentation, all statistical analyses were performed using sample weights reported in the dioxin dataset.

7.23. NHANES Demographic Statistics

Demographic statistics were calculated with the SAS SURVEYMEANS or SURVEYFREQ function. As the detection frequency was ~50% for serum TCDD, the log-transformed lipid-adjusted TCDD levels were used to divide samples into sample-weighted tertiles. The SAS PROC SURVEYREG function was used to compare demographic across the TCDD tertiles with a one-way Kruskal Wallis test followed by a Dwass-Steel-Crichtlow-Fligner pair-wise posthoc and to compare frequencies with chi-squared test. Each dataset was stratified by sex. The SAS PROC

Table 7.7. Generic drug codes used to identify statin-users in NHANES.

Statin	Generic Drug Code
atorvastatin + amlodipine	d05048
atorvastatin	d04105
cerivastatin	d04140
ezetimibe + simvastatin	d05348
fluvastatin	d03183
lovastatin	d00280
lovastatin + niacin	d04787
niacin + simvastatin	d07110
pitavastatin	d07537
pravastatin	d00348
rosuvastatin	d04851
simvastatin	d00746
simvastatin + sitagliptin	d07850

SURVEYREG function was used to compare across the sexes with a t-test. In all cases, a $p \leq 0.05$ was considered significant.

7.24. NHANES Multiple Linear Regression Modeling

Multiple linear regression models were fit using the SAS PROC SURVEYREG function. Crude regression models were made during primary analyses (i.e. no adjustments) to assess whether TCDD tertiles were associated with TC, HDL, and LDL. Subsequent final regression models were adjusted for age, BMI, and race. Regression estimates are reported for the full cohort and sex-stratified cohorts for each dataset. In all cases, sample weights were derived from the dioxin dataset and a $p \leq 0.05$ was considered significant.

7.25. Statin and TCDD Co-Treatment Study

Age-matched C57BL/6 mice were ordered from Charles River Laboratories (Kingston, NY) and delivered to Michigan State University on postnatal day 25 (PND25) and acclimated to the Michigan State University facility for 7 days prior to treatment. Mice were housed in Innovive Innocages (Innovive, Sand Diego, CA) with ALPHA-dri bedding (Shepherd Specialty Papers, Chicago, IL) under constant 12-hour light/dark cycles, temperature, and humidity. Mice were provided either standard mouse chow (Harlan Teklad Rodent Diet 8940) or standard mouse chow (Harlan Teklad Rodent Diet 8940) containing 500 mg of simvastatin per kg of food (Sigma Aldrich, St. Louis, MO) *ad libitum*. The simvastatin-laced chow was prepared at Envigo (Huntingdon, UK). Mice were acclimated to the simvastatin-laced chow for 3 days prior to treatment with TCDD. The average (mg/kg body weight) and standard deviation of simvastatin exposure for females and males over the 13-day period was 77.2 ± 2.8 and 73.6 ± 1.2, respectively. Sesame oil (vehicle control) or TCDD (10 μg/kg) treatment was administered with a daily oral gavage for 10 consecutive days. TCDD treatment did not impact consumption of simvastatin-laced chow.

Following the dosing regime, the mice were sacrificed on day 11 following a 6 hour fasting-period. Tissues were either frozen in liquid nitrogen or fixed in 10% phosphate-buffered formalin (Thermo Fisher, Waltham, MA).

7.26. Western Blot Analysis

Frozen liver was homogenized in radioimmunoprecipitation assay (RIPA) buffer using a Mixer Mill 300 (Life Sciences, Carlsbad, CA). The protein concentration in the supernatant was determined with a Bradford Assay following a 10 min centrifugation (16,000 x g)(Lowry et al. 1951). Sodium dodecyl sulfate-polyacrylamide gel electrophoresis (SDS-PAGE) was used to separate 15 µg of total protein which was subsequently transferred to a nitrocellulose membrane. The membrane was blocked with 5% non-fat dry milk dissolved in Tris-Buffered Saline with 0.05% tween 20 (TBST) and probed with monoclonal anti-mouse HMGCR antibody (1:1000; Abcam, Cambridge, MA) or a monoclonal Beta-actin antibody (1:3000; Santa Cruz Biotechnology, Dallas, TX) overnight at 4°C. Following 3x5-minute washes with TBST, the membrane was exposed to a monoclonal mouse anti-rabbit IgG-HRP (1:1000; Santa Cruz Biotechnology, Dallas, TX) or a mouse IgG kappa binding protein-HRP (1:3000; Santa Cruz Biotechnology, Dallas, TX). Following 3x5-minute washes with TBST, the blots were developed using the Pierce enhanced chemiluminescence (ECL) Western Blotting Substrate (Thermo Fisher, Waltham, MA. The Image Studio Lite software (LI-COR, Lincoln, NE) was used for the densitometry analysis. HMGCR expression was normalized to ACTB prior to statistical analysis.

7.27. Serum Clinical Chemistry

Serum total cholesterol, low-density lipoprotein (LDL), alanine aminotransferase (ALT) and glucose levels were measured using commercially-available reagents (FUJIFILM Wako Diagnostics, Richmond, VA). Serum triglycerides were measured with commercially-available reagents (Pointe Scientific, Canton, MI). Serum high-density lipoprotein (HDL) was quantified with

a commercially-available kit (Crystal Chemical, Houston, TX). Serum free fatty acids and ketone bodies (i.e. beta hydroxybutyrate) were measured using commercially-available kits (Cayman Chemical, Ann Arbor, MI). In all cases, a SpectraMax M2 microplate reader was used (Molecular Devices, San Jose, CA).

7.28. Hepatic Lipid Extraction

Hepatic lipids were extracted as previously described (Luyendyk et al. 2010). Frozen liver was homogenized in 10x volume of extraction buffer (18 mM Tris (pH 7.5), 300 mM D-Mannitol, 50 mM EGTA, and 0.1 mM phenylmethylsulfonyl fluoride) using a Mixer Mill 300 (Life Sciences, Carlsbad, CA). 500 µL of homogenate was added to 4 mL of 2:1 chloroform:methanol and mixed end-over-end shaking overnight at room temperature. Following, 800 mL of H_20 was added with vortexing and spun at 3000 x g for 5 min. 2 mL of the organic phase was transferred to a new tube and evaporated over nitrogen to dryness. Following an incubation at 45°C for 5 min, the lipid residue was dissolved in 300 uL of isopropyl alcohol with 10% Triton X-100. Commercially-available reagents were used to analyze triglycerides (Pointe Scientific, Canton, MI) and total cholesterol (FUJIFILM Wako Diagnostics, Richmond, VA) with a SpectraMax M2 microplate reader (Molecular Devices, San Jose, CA).

7.29. Hepatic Glycogen and Glucose Assay

The level of glycogen and free glucose were determined as previously described (Nault et al. 2016a). Frozen liver (~50 mg) was homogenized in 250 µL of 6% perchloric acid using a Polytron PT21000 (Kinematica AG, Luzern, Switzerland). A subset of homogenate was used to measure background glucose while another subset of homogenate (50 µL) was combined with 25 µL of 1M NaHCO3 and 125 µL of amyloglucosidase solution (2 mg/mL; Sigma Aldrich, St. Louis, MO). The mixtures were incubated with shaking at 37°C for 2 hours. Background-corrected glucose levels were used to infer hepatic glycogen levels. Glucose was assessed using commercially-available

reagents (FUJIFILM Wako Diagnostics, Richmond, VA) and a SpectraMax M2 microplate reader (Molecular Devices, San Jose, CA).

REFERENCES

REFERENCES

Bolker B. 2010. Bbmle: Tools for general maximum likelihood estimation.R package version 0.9.

Boutros PC, Yan R, Moffat ID, Pohjanvirta R, Okey AB. 2008. Transcriptomic responses to 2,3,7,8-tetrachlorodibenzo-p-dioxin (tcdd) in liver: Comparison of rat and mouse. BMC Genomics 9:419.

Brauze D, Widerak M, Cwykiel J, Szyfter K, Baer-Dubowska W. 2006. The effect of aryl hydrocarbon receptor ligands on the expression of ahr, ahrr, arnt, hif1alpha, cyp1a1 and nqo1 genes in rat liver. Toxicol Lett 167:212-220.

Brauze D, Zawierucha P, Kiwerska K, Bednarek K, Oleszak M, Rydzanicz M, et al. 2017. Induction of expression of aryl hydrocarbon receptor-dependent genes in human heparg cell line modified by shrna and treated with beta-naphthoflavone. Mol Cell Biochem 425:59-75.

Canty A, Ripley B. 2017. Boot: Bootstrap r (s-plus) functions. R package version 13-20.

Carmeliet P, Kieckens L, Schoonjans L, Ream B, van Nuffelen A, Prendergast G, et al. 1993. Plasminogen activator inhibitor-1 gene-deficient mice. I. Generation by homologous recombination and characterization. J Clin Invest 92:2746-2755.

Center for Disease Control. 2005a. National health and nutrition examination survey data. Nhanes 2003–2004. Available: https://wwwn.cdc.gov/nchs/nhanes/continuousnhanes/default.aspx?BeginYear=2003 [accessed August 21 2018].

Center for Disease Control. 2005b. National health and examination survey: 2003-2004 data documentation, codebook, and frequencies: Demographic variables & sample weights Available: https://wwwn.cdc.gov/Nchs/Nhanes/2003-2004/DEMO_C.htm [accessed August 21 2018].

Center for Disease Control. 2006a. National health and examination survey: 2003-2004 data documentation, codebook, and frequencies: Triglycerides and ldl. Available: https://wwwn.cdc.gov/Nchs/Nhanes/2003-2004/L13AM_C.htm [accessed August 21 2018].

Center for Disease Control. 2006b. National health and examination survey: 2003-2004 data documentation, codebook, and frequencies: Total cholesterol and hdl. Available: https://wwwn.cdc.gov/Nchs/Nhanes/2003-2004/L13_C.htm [accessed August 21 2018].

Center for Disease Control. 2008. Health and examination survey: 2003-2004 data documentation, codebook, and frequencies: Dioxins, furans, and coplanar pcbs. Available: https://wwwn.cdc.gov/Nchs/Nhanes/2003-2004/L28DFP_C.htm [accessed August 21 2018].

Center for Disease Control. 2016. National health and examination survey: 1988-2016 data documentation:
prescription medications - drug information. Available: https://wwwn.cdc.gov/Nchs/Nhanes/1999-2000/RXQ_DRUG.htm [accessed August 21 2018].

Davis JA, Gift JS, Zhao QJ. 2011. Introduction to benchmark dose methods and u.S. Epa's benchmark dose software (bmds) version 2.1.1. Toxicol Appl Pharmacol 254:181-191.

Dougherty KM, Pearson JM, Yang AY, Westrick RJ, Baker MS, Ginsburg D. 1999. The plasminogen activator inhibitor-2 gene is not required for normal murine development or survival. Proc Natl Acad Sci U S A 96:686-691.

Fader KA, Nault R, Kirby MP, Markous G, Matthews J, Zacharewski TR. 2017. Convergence of hepcidin deficiency, systemic iron overloading, heme accumulation, and rev-erbalpha/beta activation in aryl hydrocarbon receptor-elicited hepatotoxicity. Toxicol Appl Pharmacol 321:1-17.

Frueh FW, Hayashibara KC, Brown PO, Whitlock JP, Jr. 2001. Use of cdna microarrays to analyze dioxin-induced changes in human liver gene expression. Toxicol Lett 122:189-203.

Hao N, Lee KL, Furness SG, Bosdotter C, Poellinger L, Whitelaw ML. 2012. Xenobiotics and loss of cell adhesion drive distinct transcriptional outcomes by aryl hydrocarbon receptor signaling. Mol Pharmacol 82:1082-1093.

Harrill JA, Hukkanen RR, Lawson M, Martin G, Gilger B, Soldatow V, et al. 2013. Knockout of the aryl hydrocarbon receptor results in distinct hepatic and renal phenotypes in rats and mice. Toxicol Appl Pharmacol 272:503-518.

Katoh K, Kuma K, Toh H, Miyata T. 2005. Mafft version 5: Improvement in accuracy of multiple sequence alignment. Nucleic Acids Res 33:511-518.

Keane TM, Goodstadt L, Danecek P, White MA, Wong K, Yalcin B, et al. 2011. Mouse genomic variation and its effect on phenotypes and gene regulation. Nature 477:289-294.

Kopec AK, Burgoon LD, Ibrahim-Aibo D, Mets BD, Tashiro C, Potter D, et al. 2010. Pcb153-elicited hepatic responses in the immature, ovariectomized c57bl/6 mice: Comparative toxicogenomic effects of dioxin and non-dioxin-like ligands. Toxicol Appl Pharmacol 243:359-371.

Lowry OH, Rosebrough NJ, Farr AL, Randall RJ. 1951. Protein measurement with the folin phenol reagent. J Biol Chem 193:265-275.

Lu H, Crawford RB, North CM, Kaplan BL, Kaminski NE. 2009. Establishment of an immunoglobulin m antibody-forming cell response model for characterizing immunotoxicity in primary human b cells. Toxicol Sci 112:363-373.

Luyendyk JP, Sullivan BP, Guo GL, Wang R. 2010. Tissue factor-deficiency and protease activated receptor-1-deficiency reduce inflammation elicited by diet-induced steatohepatitis in mice. Am J Pathol 176:177-186.

Nault R, Colbry D, Brandenberger C, Harkema JR, Zacharewski TR. 2015. Development of a computational high-throughput tool for the quantitative examination of dose-dependent histological features. Toxicol Pathol 43:366-375.

Nault R, Fader KA, Ammendolia DA, Dornbos P, Potter D, Sharratt B, et al. 2016a. Dose-dependent metabolic reprogramming and differential gene expression in tcdd-elicited hepatic fibrosis. Toxicol Sci 154:253-266.

Nault R, Fader KA, Kirby MP, Ahmed S, Matthews J, Jones AD, et al. 2016b. Pyruvate kinase isoform switching and hepatic metabolic reprogramming by the environmental contaminant 2,3,7,8-tetrachlorodibenzo-p-dioxin. Toxicol Sci 149:358-371.

Nishimura N, Miyabara Y, Suzuki JS, Sato M, Aoki Y, Satoh M, et al. 2001. Induction of metallothionein in the livers of female sprague-dawley rats treated with 2,3,7 ,8-tetrachlorodibenzo-p-dioxin. Life Sci 69:1291-1303.

R Core Team. 2015. R: A language and environment for statistical computing [internet]. Vienna, austria: R foundation for statistical computing; 2013. Document freely available on the internet at: http://wwwr-projectorg/.

Siefert SA, Chabasse C, Mukhopadhyay S, Hoofnagle MH, Strickland DK, Sarkar R, et al. 2014. Enhanced venous thrombus resolution in plasminogen activator inhibitor type-2 deficient mice. J Thromb Haemost 12:1706-1716.

Wang J, Williams RW, Manly KF. 2003. Webqtl: Web-based complex trait analysis. Neuroinformatics 1:299-308.

Yalcin B, Wong K, Agam A, Goodson M, Keane TM, Gan X, et al. 2011. Sequence-based characterization of structural variation in the mouse genome. Nature 477:326-329.

Yung LM, Nikolic I, Paskin-Flerlage SD, Pearsall RS, Kumar R, Yu PB. 2016. A selective transforming growth factor-beta ligand trap attenuates pulmonary hypertension. Am J Respir Crit Care Med 194:1140-1151.